dortmund university

CHEMICAL GENOMICS CENTRE
OF THE MAX PLANCK SOCIETY

MAX PLANCK INSTITUTE
OF MOLECULAR PHYSIOLOGY

Discovery of USP53 and USP54 deubiquitinase activities

Dissertation

for achievement of the academic degree of
Doctor in Natural Sciences
(Dr. rer. nat.)

Submitted to the
Department of Chemistry and Chemical Biology
TU Dortmund University

by

Kim Solveig Wendrich

Dortmund 2025

The work for this dissertation was performed from March 2019 until May 2024 under the supervision of Dr. Malte Gersch at the Chemical Genomics Centre of the Max-Planck Society, the Max Planck Institute of Molecular Physiology, and the Faculty of Chemistry and Chemical Biology of the TU Dortmund University in Dortmund, Germany.

Supervisor	Dr. Malte Gersch
1st Examiner:	Dr. Malte Gersch
2nd Examiner:	Prof. Dr. Dr. h.c. Herbert Waldmann

Disclaimer

The results detailed in this thesis have contributed to the following publications:

Wendrich K[#], Gallant K[#], Recknagel S, Petroulia S, Kazi N, Hane J, Führer S, Bezstarosti K, O'Dea R, Demmers J, Gersch M, Discovery and mechanism of K63 linkage-directed deubiquitinase activity in USP53, *Nat Chem Biol,* 2025, 21(5):746-757, [#]Co-first authors

Zhao Z, O'Dea R, **Wendrich K**, Kazi N, Gersch M, Native Semisynthesis of Isopeptide-Linked Substrates for Specificity Analysis of Deubiquitinases and Ubl Proteases, *J Am Chem Soc*, 2023, 145(38):20801-20812

O'Dea R, Kazi N, Hoffmann-Benito, A. Zhao, Z, Recknagel S, **Wendrich K**, Janning P, Gersch M, Molecular basis for ubiquitin/Fubi cross-reactivity in USP16 and USP36, *Nat Chem Biol*, 2023, 19(11):1394-1405

Experimental results obtained by Sarah Recknagel or Jan André Hane, and included in this dissertation, are annotated in the respective figure captions. These results are also included in the corresponding master's and bachelor's theses:

Sarah Recknagel, 'Biochemical Characterization of the Deubiquitinases USP53 and USP54', Master thesis, 2022, TU Dortmund University

Jan André Hane, 'Biochemical characterization and inhibition of deubiquitinases', Bachelor thesis, 2022, TU Dortmund University

Dr. Zhou Zhao contributed to this thesis through developing methodology for probe generation as well as providing the diUb(K63)-2Br probe and other chemical molecules. Chemical reagents provided by Dr. Zhou Zhao or Dr. Christian Grethe are indicated in the figure captions or in the text. Dr. Nafizul Haque Kazi purified and Jan André Hane assayed USP53 G31S, USP53 C303Y and USP53 H132Y.

Acknowledgments

My heartfelt gratitude goes out to all those who accompanied me on this journey, and joined me on emotional highs and lows, a good share of frustration and disappointment, hard-earned successes, as well as many moments of joy and excitement. I learned so much along the way, and this experience would have been far less enjoyable and simply not the same without the support of so many wonderful people. Thank you.

The first person to mention in name is my supervisor, Dr. Malte Gersch, who never doubted my abilities, even when things did not go smoothly at the start of my PhD. Thank you for your scientific guidance, for your unwavering support of my project, and for providing an environment to succeed. I am especially grateful for the times you shared your expertise and ideas, and also for stepping into the lab when needed, for example to ensure crystals could be grown in time for shipment.

I sincerely thank Prof. Dr. Dr. h.c. Herbert Waldmann for his commitment to the CGC, providing multiple generations of PhD students, such as myself, with the chance to pursue their scientific research. I also appreciate his willingness to take on the role of second examiner for my thesis.

I gratefully acknowledge the Max Planck Research School for Living Matter for financial support to attend conferences, the opportunity to organize a student symposium, and for providing workshops that helped me grow personally and professionally. I am also thankful to Prof. Dr. Andrea Musacchio and Prof. Dr. Hemmo Meyer for their time and suggestions as part of my thesis advisory committee, especially for recommending to discontinue my first project, which proved to be the right decision. Thank you, Lucia and Christa, for organizing the research school and for your kindness. I always enjoyed meeting both of you and appreciated your continued interest in my writing progress even after my contract ended.
I greatly benefited from the excellent facilities and staff at the MPI. Thank you to the PCF team for providing fluorophores, proteases, and what must have been half a ton of 2YT media. I would also like to thank Dr. Raphael Gasper and Petra Geue for their support with biophysical methods, as well as Dr. Philipp Lampe and Dr. Sonja Sievers from COMAS for their assistance with assay transfer, inhibitor screening, and valuable discussions. A special thanks goes to the LC-MS team at CGC for fixing the machine whenever needed, and to Jens Warmers for keeping the LC-MS at MPI running and for getting the program working after me crashing it.

To all current and former members of the Gersch group: thank you for being the kind of team I wish everyone could have. Your questions, feedback, and knowledge shaped my scientific thinking and improved my experimental work and presentations. I valued the genuine joy we

shared in each other's successes, and the support when things went wrong. From puzzling over data to coffee breaks and shared laughter, you made this time truly special. Thank you, Christian, Evie, Jan, Kai, Lucy, Mirko, Niko, Rachel, Sarah, Siska and Zhou.
I especially want to thank Kai, with whom I shared the USP53 and USP54 project. I am grateful for every discussion we had, as well as for your help proofreading my thesis. You and Rachel brought warmth, humor and cohesion to the group. I am so thankful you both joined, and even more so that I get to call you friends. To my favorite chemist, Zhou, I greatly appreciate your generosity with both your time and expertise, as well as and your 80 mg compound batches, which made a profound impact on my research.

To my Bachelor and Master students, Jan and Sarah, I truly count myself lucky to have worked with you. Your perspectives, drive, and curiosity not only enriched the USP53 and USP54 project but also made our time together genuinely enjoyable. Sarah, I am delighted to tell you that your Monstera cutting is thriving, its newest leaf just unfurled with six perfect windows. Just like the plant, I hope you both continue to grow and flourish wherever your paths take you.

At the CGC and MPI, many more people crossed my path. I especially want to thank Aylin, Elisabeth, Jen-Yao, Kim, Lydia, Julia K., Julia S., and Stefan. You made this journey more than a scientific one. Aylin, thank you for introducing me to yoga, helping us loosen our shoulders on Friday evenings, and for being my little refugium at the MPI. Lydia, Julia K. and Julia S., thank you for the evenings filled with food, fun, and easy friendship. Thank you also, Lydia, for your organizational brilliance, which made our symposium planning a breeze. To my phenomenal office neighbor Stefan, thank you for being not only a fountain of knowledge, but also my favorite source of lab gossip. And special thanks for the old PMSF stock.

I cannot express enough how thankful I am to my focus session group for the motivation and the supportive atmosphere. It played a crucial role in getting this thesis over the finish line. To the word wizard Anne, I am especially grateful for your steady presence, your encouragement, and for calling be back after breaks. And to Anja, your commitment to staying until the end truly meant a lot. I deeply appreciate your understanding, non-judgmental nature, and the friendship and mental support you both offered throughout. Thank you for being such amazing friends. I am looking forward to more memories like our rooftop swim in Bath.

Last but not least, love and thanks to my partner and my family. Marius, thank you for standing by me in the scariest times. Your support has made an immeasurable impact and I am endlessly grateful to have you at my side. My deepest gratitude goes to my parents, for their unwavering support not just throughout the PhD but long before that. Thank you for believing in me and for always being my safety net.

Abstract

Ubiquitin is a small protein that can be conjugated to substrates and to itself in a process called ubiquitination, which affects numerous cellular activities. The signaling function depends on the length and linkage type of the ubiquitin chains. These chains are regulated by deubiquitinating enzymes (DUBs) due to their ability to cleave the isopeptide bonds within ubiquitin chains or between ubiquitin and substrates. Despite their classification as members of the USP DUB family, USP53 and USP54 have been reported to be catalytically inactive. Biallelic mutations in *USP53* cause familial intrahepatic cholestasis, an inherited liver disease in children, by an unknown mechanism. Additionally, while reports on the cellular functions of both proteins are beginning to emerge, a comprehensive analysis of their catalytic activities is lacking.

In this study, the catalytic activity of USP53 and USP54 was investigated through an *in vitro* approach involving the expression, purification, and biochemical and structural characterization of their catalytic domains. Initial assays using specifically linked ubiquitin chains as substrates reveal a surprisingly specific activity of both enzymes on K63-linked ubiquitin chains with a preference for longer chains. This length specificity is mediated by a cryptic S2 ubiquitin binding site in both enzymes, visualized for USP54~diUb(K63)-PA in a crystal structure. The structure revealed a common USP fold of USP54, but also unique features that are present in both enzymes and are relevant for their activities. Generating and assaying complex customized substrates led to the identification of two different activity profiles for USP53 and USP54. The latter displays a K63 linkage-specific deubiquitination activity with a strong dependence on ubiquitin binding in the S1' site. Conversely, USP53 exhibits a novel DUB cleavage activity. This K63 linkage-directed deubiquitination activity is mediated by a promiscuous catalytic center under the control of a K63 linkage-specific S2 site. Importantly, introducing reported cholestasis patient mutations into USP53 renders the enzyme inactive, correlating for the first time the catalytic activity with the disease phenotype.

Collectively, I have made the surprising discovery that USP53 and USP54 are active enzymes with distinct molecular mechanisms for the length-dependent decoding of K63-linked ubiquitin chains. These findings will guide the cellular analysis of USP53 and USP54 to identify their substrates and to understand the role of their activities for cellular functions.

Zusammenfassung

Das kleine Protein Ubiquitin kann in einem als Ubiquitinierung bezeichneten Prozess kovalent mit Substraten und mit sich selbst verknüpft werden und reguliert dadurch zahlreiche zelluläre Prozesse. Die Signalfunktion hängt dabei von der Länge und der Verknüpfung der Ubiquitinketten ab. Deubiquitinasen (DUBs) sind in der Lage, die Isopeptidbindungen in Ubiquitinketten oder zwischen Ubiquitin und Substraten wieder zu spalten und damit die genaue Form dieser Ketten zu bestimmen. Die beiden Proteine USP53 und USP54 gehören zu der USP-DUB-Familie, werden aber in der Literatur als katalytisch inaktiv beschrieben. Mutationen in *USP53* verursachen über einen unbekannten Mechanismus familiäre intrahepatische Cholestase, eine erbliche Lebererkrankung bei Kindern. Darüber hinaus gibt es erste Berichte über zelluläre Funktionen beider Proteine. Eine umfassende Untersuchung ihrer katalytischen Aktivitäten steht jedoch noch aus.

In dieser Arbeit wurde die katalytische Aktivität und die Struktur von USP53 und USP54 in einem *in vitro* Ansatz mit bakteriell exprimierten und gereinigten katalytischen Domänen untersucht. Spaltungstests mit spezifisch verknüpften Ubiquitinketten als Substrate zeigen überraschenderweise eine Aktivität beider Enzyme für K63-verknüpfte Ubiquitinketten und zusätzlich eine Präferenz für längere Ketten, vermittelt durch S2-Bindungsstellen für Ubiquitin. Die Kristallstruktur von USP54 im Komplex mit einer K63-verknüpften Diubiquitinsonde zeigt die zusätzliche S2-Bindungsstelle eingebettet in eine typische katalytische USP-Domäne, aber auch einzigartige Strukturmotive, die ebenfalls in USP53 vorhanden und für die Aktivität wichtig sind. Spaltungstests mit komplexen und speziell hergestellten Substraten zeigen, dass USP53 und USP54 unterschiedliche Aktivitätsprofile aufweisen. USP54 schneidet spezifisch K63-Bindungen und die Aktivität hängt stark von der Bindung von Ubiquitin in der S1'-Bindungsstelle ab. Im Gegensatz dazu zeigt USP53 eine neuartige K63-Bindung gesteuerte Spaltungsaktivität. Diese ist durch ein nicht-selektives katalytisches Zentrum gekennzeichnet, das unter der Kontrolle einer für K63-Bindungen spezifischen S2-Bindungsstelle steht. Die Untersuchung der Aktivität von USP53 mit Cholestase-Mutationen zeigen, dass USP53 durch diese Patientenmutationen inaktiviert wird. Damit konnte erstmals die katalytische Aktivität mit dem Krankheitsphänotyp korreliert werden.

Insgesamt habe ich die überraschende Entdeckung gemacht, dass USP53 und USP54 aktive Enzyme mit unterschiedlichen molekularen Mechanismen sind, um K63-verknüpfte Ubiquitinketten zu entschlüsseln. Diese Erkenntnisse werden die zelluläre Erforschung von USP53 und USP54 unterstützen, um ihre zelluläre Rolle zu verstehen und um Substrate zu identifizieren.

Table of Contents

1 Introduction

The human body is a remarkable and intricate system, from its organs and specialized tissues down to each individual cell. Each cell contains 46 chromosomes, organized into 23 pairs. Chromosomes are composed of proteins and deoxyribonucleic acid (DNA). A complete set of DNA is an organism's genome. DNA itself is the carrier molecule of all information needed for an organism to develop and function and is made up of two polynucleotide chains that form a double helix, with four nucleotides as the building blocks. The sequence of these nucleotides encodes for our genetic makeup.[1] A global scientific effort launched in 1990 aimed to sequence the entire human genome in order to identify all human genes and their genomic location. Two initial drafts covering about 90 % of the human genome were published in 2001, and gaps were filled in the following years.[2-4] A major finding was that the human genome contains around 20,000 protein-coding genes, a much smaller number than expected.[4] Of the remaining 98% of non-coding DNA, approximately three-quarters are transcribed into non-coding RNA, which is important for gene regulation.[5,6] DNA encoding for proteins is transcribed into messenger RNA (mRNA). Subsequently, these mRNA transcripts then serve as templates for protein synthesis. However, the complexity of the proteome is not limited to the number of protein-coding genes (Figure 1).[7] Due to alternative promoter usage, as well as alternative splicing and mRNA editing, the complexity of the transcriptome increases from 20,000 DNA-encoded genes to ~100,000 different mRNA transcripts that are translated into an amino acid sequence providing the primary structure of proteins.[8-10] Proteins act as major functional units of the cell and can be post-translationally modified by covalent conjugation of chemical groups or even small proteins to amino acid side chains and termini.[11,12] Over 200 different post-translational modifications (PTMs) have been identified by mass spectrometry and prominent examples are phosphorylation, acetylation, methylation, glycosylation and ubiquitination.[13] PTMs expand the chemical environment on proteins, are mostly reversible and affect protein stability, activity, localization, function, structure and interactions, thereby dramatically increasing proteome complexity to a number of over one million different protein species in eukaryotic cells (Figure 1).[7,12,14]

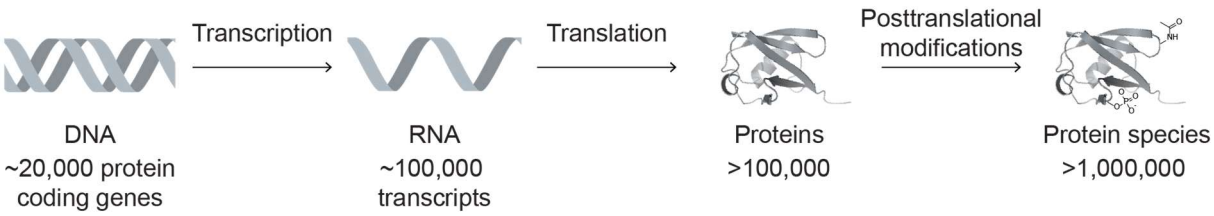

Figure 1: Posttranslational modifications increase the proteome complexity. DNA is transcribed into RNA. From mRNA transcripts, proteins are generated by translation. These can be further modified by a multitude of posttranslational modifications. Acetylation and phosphorylation are shown as two examples. The cartoon representation of ubiquitin is shown as exemplary protein (PDB: 1ubq).

1.1 The ubiquitin system

The ubiquitin system regulates almost all physiological processes, including the cell cycle, DNA repair, and developmental processes.[15-17] The system's key molecule is ubiquitin, a small protein of 76 amino acids with a molecular weight of 8.5 kDa that is present in all eukaryotic cells. The majority of ubiquitin adopts a compact β-grasp fold and only the six-residue C-terminal tail is unstructured and flexible (Figure 2A).[18] In a process termed ubiquitination, the C-terminal tail of ubiquitin is covalently linked to other proteins or to itself as a PTM by the coordinated action of E1, E2, and E3 enzymes. These are collectively referred to as the writers of the ubiquitin code because serial conjugation of ubiquitin to itself allows the formation of a wide variety of ubiquitin chains that provide distinct cellular signals (Figure 2B).[19,20] The first identified and most prominent outcome of ubiquitination is proteasomal degradation of the target protein, but non-proteolytic signaling functions are also mediated.[19,21] These cellular effects are mediated by reader proteins that contain ubiquitin-binding domains (UBDs) that enable them to specifically recognize and bind to ubiquitin and ubiquitin chains.[19,22] Deubiquitinating enzymes (DUBs) as the erasers of the ubiquitin code are another integral part of the ubiquitin system (Figure 2B). They remove or edit ubiquitin chains, thereby finetune the ubiquitination status of proteins which then alters the final cellular outcome.[23]

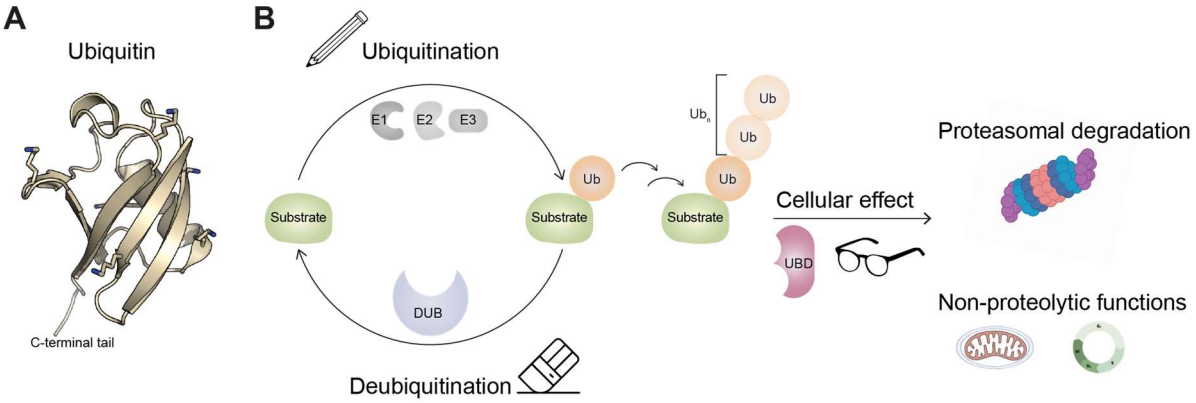

Figure 2: The ubiquitin system. A) Cartoon representation of ubiquitin (PDB:1ubq). Lysine residues are shown as sticks. B) E1, E2 and E3 enzymes are the writers of the ubiquitin system and catalyze the covalent conjugation of ubiquitin to substrate proteins or to itself, a process termed ubiquitination. The readers, proteins that contain ubiquitin binding domains (UBDs), recognize ubiquitin and mediate the cellular outcome. DUBs are the erasers of the ubiquitin system and can remove ubiquitin chains from substrates.

1.2 The ubiquitin code

The ubiquitin code encompasses all types of ubiquitin modifications, including ubiquitin chains of various lengths and linkages, and the signaling information they encode.[19] The attachment of ubiquitin as a monomer to one or several lysine residues of a substrate protein results in monoubiquitination or multimonoubiquitination, respectively (Figure 3). More than 10,000 ubiquitination sites have been identified on proteins.[24,25] The addition of further ubiquitin molecules to one or more of the seven lysine residues (K6, K11, K27, K29, K33, K48, K63) or to the amino group of the N-terminal methionine (M1) of ubiquitin itself leads to the formation of polyubiquitin chains. These are classified as homotypic or heterotypic, depending on the type of linkage between the ubiquitin moieties. Homotypic ubiquitin chains are linear chains in which all ubiquitin moieties are connected through the same lysine residue. In heterotypic chains, the ubiquitin moieties are linked through different lysine residues. A linear chain with alternating linkage sites is referred to as mixed, whereas in branched ubiquitin chains, at least two lysine residues of one ubiquitin molecule are modified with ubiquitin (Figure 3).[20,26] The ubiquitin code is further extended by the existence of ubiquitin-like proteins (Ubls), which are evolutionarily related to ubiquitin. The sequence similarity to ubiquitin varies among Ubls, but they all share the ß-grasp fold of ubiquitin.[27] Type I Ubls contain a C-terminal glycine or diglycine and can be conjugated to substrate proteins or, in one instance, to lipids. In contrast, for type II Ubls, the Ubl domain is not conjugated but is instead part of larger multidomain proteins.[28] Human conjugatable Ubls include small ubiquitin-like modifier (SUMO) proteins, neural precursor cell expressed and developmentally down-regulated 8 (NEDD8), interferon-stimulated gene 15 (ISG15), ubiquitin-fold modifier 1 (UFM1), FAU-encoded ubiquitin-like protein (FUBI), human leukocyte antigen F locus adjacent transcript 10 (FAT10), ubiquitin-related modifier 1 (URM1), autophagy-related protein family 8 (ATG8) proteins, and ATG12.[27,29] The number of substrates identified for each conjugatable Ubl varies and the effects of Ubl modifications on the substrates are diverse.[27,28] Crosstalk between ubiquitination and Ubl modifications can occur in several ways, including targeting of the same lysine residue in substrate proteins, parallel modification of the same substrate, or the formation of hybrid chains (Figure 3).[30,31] In addition, ubiquitin itself can undergo chemical modifications, such as phosphorylation or acetylation, which result in structural changes, influence protein interactions, and consequently alter its cellular signaling function (Figure 3).[25,26,32,33]

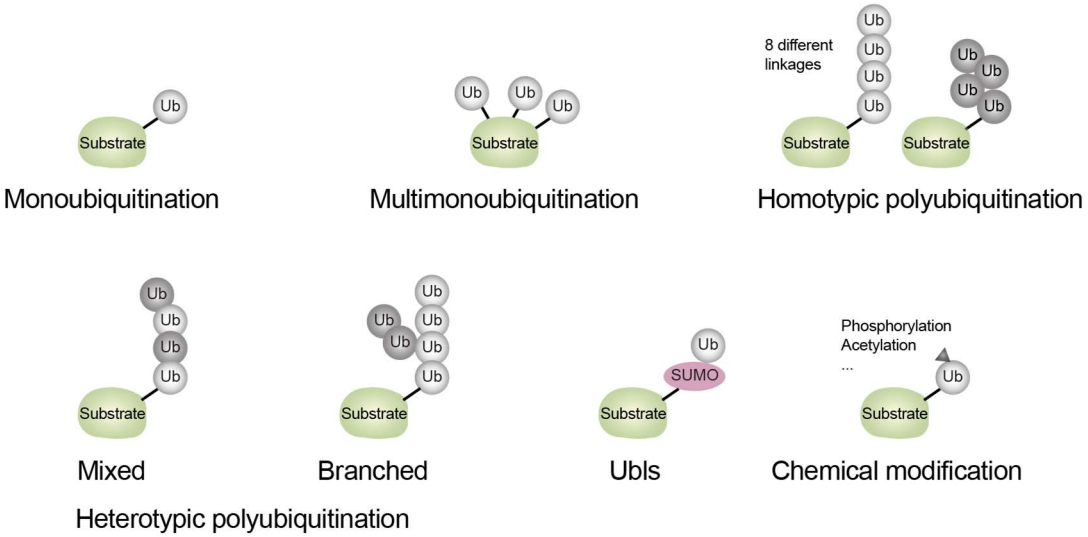

Figure 3: The ubiquitin code. Representation of possible ubiquitination types that enable the formation of a huge variety of structures. Different linkages between ubiquitin moieties are illustrated through two different shades of grey. The incorporation of Ubls is exemplified by SUMO. Additional PTMs on ubiquitin are shown as a triangle.

Canonical ubiquitination is the process by which ubiquitin is attached via its C-terminal carboxyl group to the ε-amino group of a lysine residue of a substrate protein through the formation of an isopeptide bond.[34] The process itself is orchestrated and requires sequential activity of ubiquitin-activating enzymes (E1s), ubiquitin-conjugating enzymes (E2s), and ubiquitin ligases (E3s) with a similar but distinct cascade of E1, E2 and E3 enzymes for most Ubls.[29,35] The human genome encodes two E1s, 35 E2s, and over 600 E3s.[28,29,36-40] The function of E1 enzymes is to initiate the ATP-hydrolysis dependent activation of the C-terminus of ubiquitin. Subsequently, its catalytic cysteine attacks the adenylated ubiquitin (Ub-AMP), initially forming a tetrahedral intermediate (Ub-AMP~E1, '~' denotes a covalent bond), which then leads to the formation of a thioester bond (Ub~E1) and release of AMP.[29] A second adenylation reaction and ubiquitin binding event goes hand in hand with the transfer of the thioester-bound ubiquitin to the catalytic cysteine of the E2 via transthiolation (Figure 4A).[29,41] E2s are characterized by a highly conserved catalytic ubiquitin-conjugating domain that mediates the interactions with the E1 and E3s, of which only one can be bound at a time, due to overlapping interaction sites.[42] Most ubiquitin-charged E2s (E2~Ub) are able to directly transfer ubiquitin to lysines.[43] However, the efficiency of this reaction is strongly increased by E3 ligases that catalyze the transfer.[44-47] The diverse group of E3 ligases is classified into three main families based on the structure of the catalytic domain and the employed mechanism to catalyze ubiquitin transfer to substrates: RING-, HECT- and RBR-E3 ligases (Figure 4B).[48]

Really interesting new gene (RING)-type E3s represent the majority of all E3s and contain either a RING or U-box catalytic domain. They serve as a scaffold by simultaneously binding the E2~Ub and the substrate, bringing them into close proximity to catalyze the direct transfer of ubiquitin from the E2 to the substrate.[49] RING-type E3s exist as monomers or dimers, but

also as multi subunit protein complexes which include the Cullin RING ligases (CRL) that use interchangeable adaptor proteins for specific substrate recognition.[50,51]

The second main class with around 30 members in humans are the homologous to E6AP C-terminus (HECT)-E3 ligases.[47] The HECT catalytic domain contains an N-lobe for E2 binding and a C-lobe with a catalytic cysteine that initially forms a thioester bond with ubiquitin prior to transferring it to the target substrate.[47,52]

RING-in-between-RING (RBR) ligases with 14 members in humans contain one RING domain for E2 engagement but employ a HECT-like mechanism using a catalytic cysteine in the second RING domain.[44,47]

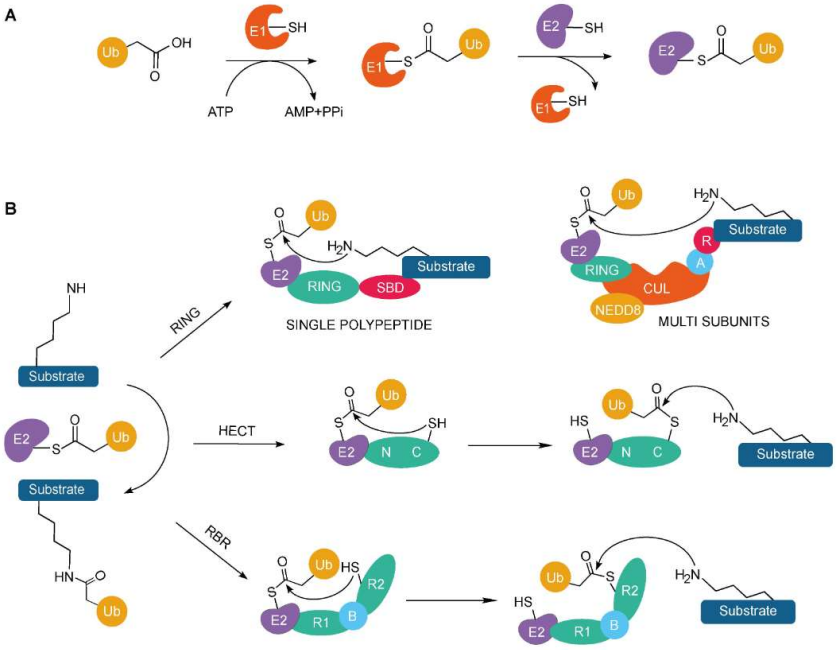

Figure 4: Ubiquitination is mediated by the consecutive action of E1, E2 and E3 enzymes. A) E1 enzymes activate ubiquitin in an ATP-hydrolysis-dependent reaction, leading to the formation of a thioester bond of the catalytic cysteine with the carboxy terminus of ubiquitin. Then, ubiquitin is transferred to the catalytic cysteine of the E2 enzyme via transthiolation. B) E3 ligases catalyze the last step of ubiquitination in which ubiquitin is covalently conjugated to a substrate's lysine. The different mechanisms of RING, HECT and RBR E3 ligases are shown. Ubiquitin is either transferred directly from the E2 (RING E3s) or via an E3~Ub thioester (HECT, RBR E3s) to the substrate lysine. SBD: substrate binding domain, CUL: cullin protein, A: adaptor, R: substrate-receptor, C: C-terminal domain, N: N-terminal domain, R1: RING domain 1, B: in-between domain, R2: RING domain 2. The figure is taken from D'Amico *et al.*[53]

Substrate specificity, reaction efficiency, processivity, and the type of ubiquitination are determined by the combined actions of E2 and E3 enzymes during ubiquitination. While most E2s lack substrate specificity, they influence the type of ubiquitination by collaborating with various E3 ligases, which typically confer substrate specificity.[47,51,54] The attachment of the first ubiquitin molecule to a substrate can serve either as a monoubiquitin signal or as an initiation step for chain elongation or branching. In RING E3 ligases, the decision between monoubiquitination and chain elongation is typically determined by the interacting E2 enzyme, often requiring an exchange of the E2 enzyme for the different activities.[55] For instance, the APC/cyclosome-associated E2 enzyme UBE2S requires a correctly positioned acceptor

ubiquitin and only mediates K11 linkage assembly.[56] In contrast, HECT and RBR E3 ligases directly determine ubiquitin chain topology and linkage.[19]

The ubiquitin code is deciphered by proteins containing ubiquitin binding domains (UBDs), which mediate downstream cellular events.[19] These effector proteins recognize specific surfaces on ubiquitin, with the hydrophobic Ile44 patch (I44, L8, V70, H68) being a primary interaction site. Additional key binding surfaces include the Ile36 patch (I36, L71, L73), the Phe4 patch (Q2, F4, T12), and the hydrophilic TEK-box (K6, K11, T12, T14, E34).[19] The importance of the surface of ubiquitin to mediate protein interactions is underscored by its exceptional conservation across eukaryotes. Importantly, differently linked ubiquitin chains adopt distinct conformations: K48-linked ubiquitin chains form compact structures, whereas K63- and M1-linked ubiquitin chains adopt more extended conformations, exposing different interaction surfaces for recognition.[19,57] Branched ubiquitin chains further increase the local ubiquitin density, creating unique binding surfaces.[58] Interactome studies of various K48- and K63-linked ubiquitin chains, as well as shorter versus longer chains, revealed branch- and length-specific ubiquitin interactors illustrating how chain length and linkage-type can influence cellular outcomes.[20,59,60]

In cells, all ubiquitin linkage types coexist.[61] Monoubiquitination is the most prevalent modification, with histone H2A being a major contributor as ~15% are monoubiquitinated in mammalian cells, except during mitosis.[62,63] Monoubiquitination plays key roles in chromatin remodeling and DNA repair.[64] Among polyubiquitin chains, K48 linkages are the most abundant, followed by K63 and K11 linkages.[65] Recently, branched ubiquitin chains have been shown to be quite common, constituting up to 5-20% of the cellular polyubiquitin pool.[66,67]

The first cellular function attributed to ubiquitination was protein degradation by the ubiquitin-proteasome system, a discovery recognized with the Nobel prize.[68] While K48-linked chains are the primary signal for proteasomal degradation, other modifications including multiple modifications by short ubiquitin chains of various linkages, monoubiquitination, and branched chains, also promote degradation.[69-72] K63-linked chains are mainly associated with non-degradative signaling such as DNA repair, trafficking, autophagy, although they also serve as degradative signal by seeding branched K48/K63 ubiquitin chains.[19,73-76] Other, less common linkages (K6, K11, K27, K29, K33) have been linked to both degradative and non-degradative functions.[19,20] Specific signaling functions have been attributed to more complex ubiquitin modifications. For example, mixed K11/K63 chains play a role in endocytosis, M1/K63 hybrid chains function in immune signaling, and K48/K63 branched chains play a role in NF-κB activation.[77-79]

Beyond lysine ubiquitination of protein substrates, novel forms of ubiquitination with alternative chemical linkages and corresponding ligase activities have recently been identified.[16] These include ester linkages between the C-terminal carboxy group of ubiquitin and the hydroxyl groups of serine/threonine or phosphoribosyl linkages between R42 of ubiquitin and substrate serines, which are catalyzed by E1- and E2-independent effector enzymes of the bacterial pathogen *Legionella pneumophilia*.[80-82] In addition, non-protein ubiquitination targets have emerged, including lipopolysaccharides of *Salmonella* during bacterial infection, phosphatidylethanolamine, saccharides and ADP-ribose.[83-86] Given the increasing complexity of the ubiquitin code and its recently discovered extensions, it is clear that our understanding of this system remains incomplete. Advancing this field will require new tools, methodologies and experiments to uncover further exciting aspects of ubiquitin signaling.[87]

1.3 Deubiquitinating enzymes (DUBs)

Deubiquitination, mediated by deubiquitinating enzymes (DUBs) is as important as ubiquitination for regulating cellular processes.[23] This is evident from the transient nature of ubiquitination, as a recent study found its global half-life to be short and independent of proteasome activity.[88] DUBs cleave the isopeptide bond between the C-terminus of ubiquitin and typically the ε-amino group of a lysine or the peptide bond in linear ubiquitin chains, playing multiple functional roles (Figure 5).[23] As erasers of the ubiquitin code, DUBs can rescue proteins from degradation or modify ubiquitin signaling function by removing or editing ubiquitin chains. Additionally, they maintain free ubiquitin levels by recycling ubiquitin at the proteasome where the DUB PSMD14/RPN11 acts on substrates committed to degradation, while USP14 and UCH37/UCHL5 function prior to commitment, as well as by disassembling free unanchored chains.[89] USP5 is able to specifically recognize the free C-terminus of ubiquitin via its zinc-finger ubiquitin-binding domain, a feature shared by other USP DUBs.[90] DUBs also generate ubiquitin monomers from newly expressed ubiquitin precursors encoded by *UBA52, UBA80, UBB* and *UBC*, with UCHL3, USP9X, USP9X, USP7, USP5 and OTULIN being the most active DUBs in this process.[91]

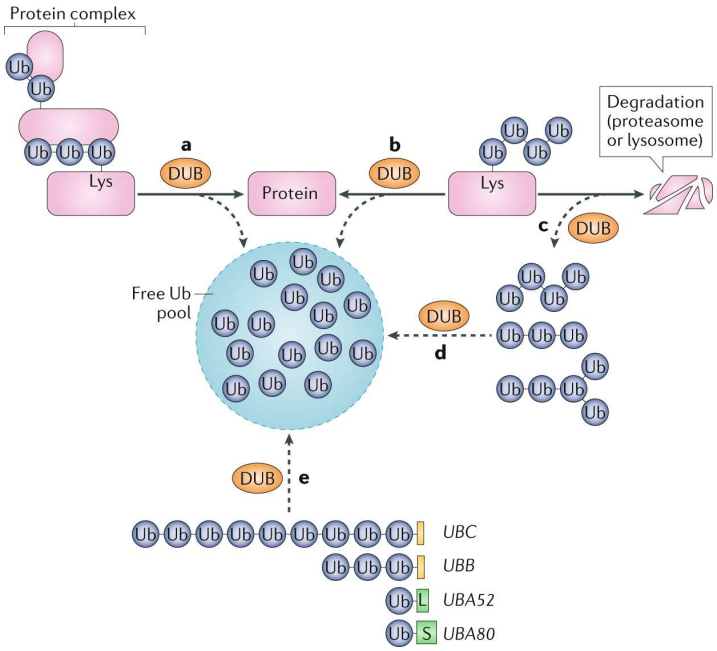

Figure 5: DUBs have multiple cellular functions. They remove ubiquitin or and ubiquitin chains from substrates and thereby regulate signaling functions of non-degradative ubiquitination (a) or rescue proteins from degradation (b). Another cellular role is replenishing of the free Ub pool mediated by the recycling of ubiquitin at the proteasome (c), disassembly of unanchored ubiquitin chains (d), and cleavage of expressed ubiquitin precursors (e). The figure is taken from Clague *et al.*[23]

DUBs play essential roles in numerous cellular processes including DNA repair, inflammation, apoptosis and cell-cycle progression. Their dysregulation or dysfunction is linked to various diseases, such as cancer by affecting the stability and function of tumor suppressors and oncogenes, as well as neurodegenerative disorders and immune dysfunction.[92] For example, the DUB activity of A20 is important for its anti-inflammatory functions, and mutations in its encoding gene have been associated with autoimmune disorders.[93] The activity, localization and abundance of DUBs is tightly controlled, restricting their function to the right substrate and the right time. Mechanisms to modulate the catalytic activity include posttranslational modification, redox-regulation, protein binding, and allosteric activation.[23,94] DUBs can recruit their substrates through direct interaction with the ubiquitinated protein, as part of macromolecular assemblies that facilitate substrate binding, or by specifically recognizing certain ubiquitin chain types, such as those with defined linkages.[95] This topic will be explored in more detail in the following section (1.4).

The human genome contains approximately 100 DUBs that are classified into seven families according to sequence and structure similarity of their catalytic domains. Members of the Jab1/Mov34/MPN (JAMM) family are zinc-dependent metalloproteases. The USP (ubiquitin-specific protease), OTU (ovarian tumor), MJD (Machado-Josephin domain-containing protease), UCH (ubiquitin C-terminal hydrolase), MINDY (motif interacting with Ub-containing novel DUB family, and ZUFSP (zinc finger with the UFM1-specific peptidase domain protein) families comprise cysteine proteases.[23] Not all DUB family members have deubiquitinase

activity. Some members, particularly common in the JAMM family, are considered to be inactive pseudoenzymes and some members, particularly common in the USP family, are Ubl proteases or cross-reactive DUBs and Ubl proteases.[96-100] Interestingly, threonine and esterase activities have been identified as functions of MJD family members.[101]

The catalytic activity of cysteine protease DUBs is mediated by a core catalytic domain containing a papain-like catalytic triad of the highly conserved residues cysteine and histidine, often together with a third residue (D, N, E, S).[94,102,103] The third acidic residue polarizes the basic histidine, which in turn deprotonates the thiol group of the catalytic cysteine, increasing its nucleophilicity and facilitating its attack on the carbonyl carbon of the ubiquitin-substrate or ubiquitin-ubiquitin bond. This results in the formation of a tetrahedral intermediate where the negatively charged oxyanion is stabilized by hydrogen-bond interactions within the oxyanion hole of the active site. Following the release of the substrate with a free lysine, the acyl enzyme intermediate is hydrolyzed by a water molecule. Release of ubiquitin with a free C-terminus recovers the enzyme for another catalytic cycle.[95,104] While the catalytic mechanism is conserved across cysteine DUBs, some only possess a catalytic dyad or use different mechanisms to substitute the role of the acidic residue for polarization of the catalytic histidine.[94]

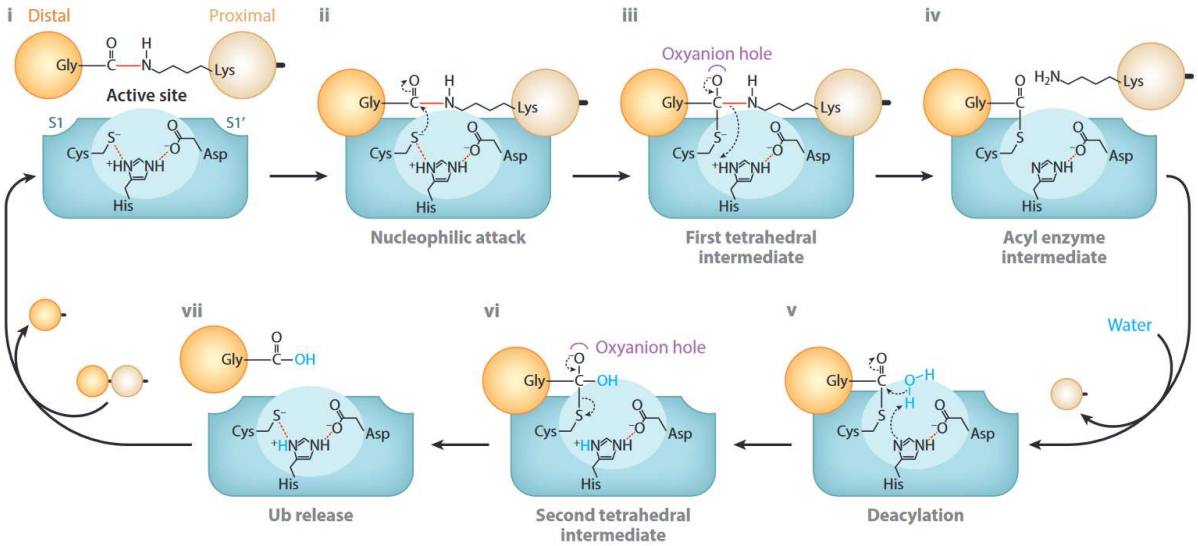

Figure 6: Catalytic mechanism of cysteine protease DUBs. Cysteine protease DUBs generally contain a catalytic triad of cysteine, histidine and an acidic residue in a formation to increase the nucleophilicity of the thiol group that catalyzes the hydrolysis of the isopeptide bond. The figure is taken from Mevissen and Komander.[95]

1.4 Substrate recognition and specificity in DUBs

The specificity of DUBs for both substrates and ubiquitin chain types is determined by precise recognition mechanisms.[105] The nomenclature for DUB binding sites follows a convention similar to that of other proteases, where sites are named relative to the scissile bond within the substrate.[106] In a diubiquitin chain, the ubiquitin with a free C-terminus is referred to as the

proximal ubiquitin, while the conjugated ubiquitin is the distal ubiquitin. When the scissile bond of diubiquitin is positioned in the active site, the S1 site binds the distal ubiquitin, while the S1' site binds the proximal ubiquitin. Additional ubiquitin-binding sites are numbered sequentially in both directions (Figure 7A). In longer ubiquitin chains, the proximal ubiquitin remains the one with the free C-terminus, whereas the distal ubiquitin is the one that is conjugated but not further modified. In ubiquitin chains conjugated to substrate proteins, the proximal ubiquitin is the one directly linked to the substrate lysine (Figure 7B). Based on their binding site interactions, DUBs exhibit different modes of cleavage: *endo*, where cleavage occurs within a chain; *exo*, where ubiquitin is removed stepwise from one end; and *en-bloc*, where an entire ubiquitin chain is removed at once (Figure 7B).[94]

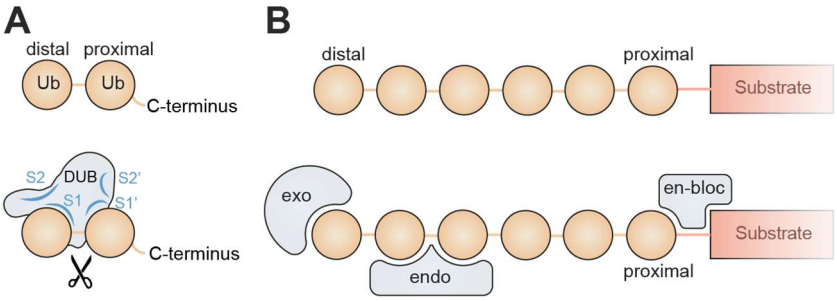

Figure 7: Nomenclature of ubiquitin binding sites and cleavage activities of DUBs. The figure is adapted from Mevissen and Komander.[95]

Every DUB contains an S1 site which binds the ubiquitin moiety contributing its C-terminus to the targeted scissile bond. This site forms extensive interactions with ubiquitin, covering 20-40% of its surface, significantly more than other UBDs.[105] Key recognition elements include the hydrophobic Ile44, Ile36 and Phe4 patches, and the extended C-terminal tail, which is guided into the active center through various hydrogen bonds.[107,108] The specific interaction between the S1 site and ubiquitin, particularly its C-terminal tail, allow DUBs to distinguish ubiquitin from Ubls as these differ in the hydrophobic surface patches and except for ISG15 vary in their C-terminal tails (Figure 8A).[108] It has been shown that cross-reactive DUBs such as USP36 that cleaves ubiquitin, FUBI and ISG15, are able to accommodate the differences.[109] Sole ubiquitin binding in the S1 site can lead to promiscuous cleavage, targeting any linkage, whether between two ubiquitin molecules or between ubiquitin and a substrate (Figure 8B). This applies to many USP DUBs, which exhibit broad substrate and linkage specificity due to strong S1 and limited S1' site interactions with ubiquitin.[95,98,110,111]

Conversely, DUBs with substrate-specific S1' sites can directly engage ubiquitinated substrates, enabling site-specific cleavage activity (Figure 8C). The yeast DUB Ubp8 is proposed to have a histone-specific S1' site, as structural analysis of the SAGA DUB module bound to monoubiquitinated nucleosome revealed direct interactions between the catalytic domain of Ubp8 and the substrate.[112]

Linkage specificity in DUBs is often mediated by ubiquitin chain engagement in the S1 and S1' sites, where the S1' site positions the proximal ubiquitin in a defined orientation, restricting cleavage to specific linkages (Figure 8D). Especially the structural elucidation of DUBs in complex with diubiquitin substrates or probes has shed light on their linkage-specificity mechanisms (Figure 9).

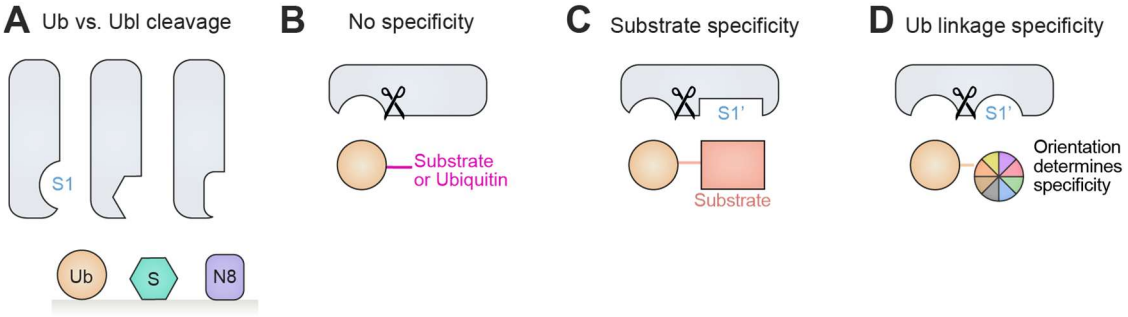

Figure 8: Principles of substrate recognition and linkage specificity. A) DUB S1 site discrimination between ubiquitin and Ubls. B) Promiscuous cleavage activity of DUBs mediated by S1 site binding. C-D) Substrate or linkage-specific cleavage activity of DUBs mediated by S1' sites. The figure is adapted from Mevissen and Komander.[95]

Examples of length- and linkage-specific DUBs

The different families of DUBs exhibit varying degrees of ubiquitin chain linkage-specificity. Members of the OTU, JAMM and MINDY families as well as ZUP1 of the ZUFSP family are highly linkage-specific, while most USP DUBs display limited specificity in this regard.[110,111,113-115] Two exceptions among USP DUBs are USP30 and CYLD. USP30 exhibits selectivity for K6-linked ubiquitin chains and CYLD specifically cleaves M1- and K63-linked ubiquitin chains.[116,117] In USP30, engagement of K6-modified ubiquitin in the S1' site supports the weakened ubiquitin binding in the S1 site to enhance catalytic activity.[116] Structural analysis of the JAMM family member AMSH-LP in complex with K63-linked diubiquitin reveals that both the S1 and S1' sites are part of the catalytic domain (Figure 9). The S1' site specifically interacts with the amino acids surrounding K63 as well as I44 in the proximal ubiquitin, thereby restricting its activity to K63 linkages.[118] The mechanism of OTULIN is an example for a substrate-assisted linkage-specificity mechanism. Upon binding of linear ubiquitin chains, inhibitory interactions present in the apo form are released.[119] Domains outside of the catalytic domains can also contribute to S1' site formation, as seen in CYLD. Its specificity relies on an insertion within the catalytic domain that extends into a ß-sheet forming the S1' site for selective binding of M1- and K63-linked ubiquitin (Figure 9).[117]

More complex linkage-specificity mechanisms involve additional ubiquitin-binding sites apart from S1 and S1' (Figure 9). The catalytic domain of OTUD2 contains K11 linkage-specific S1' and S2 binding sites, facilitating *endo*-cleavage of longer K11-linked chains.[120] A similar S2 site has been identified in SARS-CoV-1 PLpro mediating its specificity for K48-linked ubiquitin chains.[121,122] ZUP1 specifically cleaves long K63-linked ubiquitin chains, with its S1' site likely

formed by tandem UBD's located outside of the catalytic domain.[115] Their structure and ubiquitin interactions remain uncharacterized.

On top of these described mechanism, many DUBs possess additional UBDs outside of their catalytic domains, further fine-tuning substrate recruitment and specificity.[94]

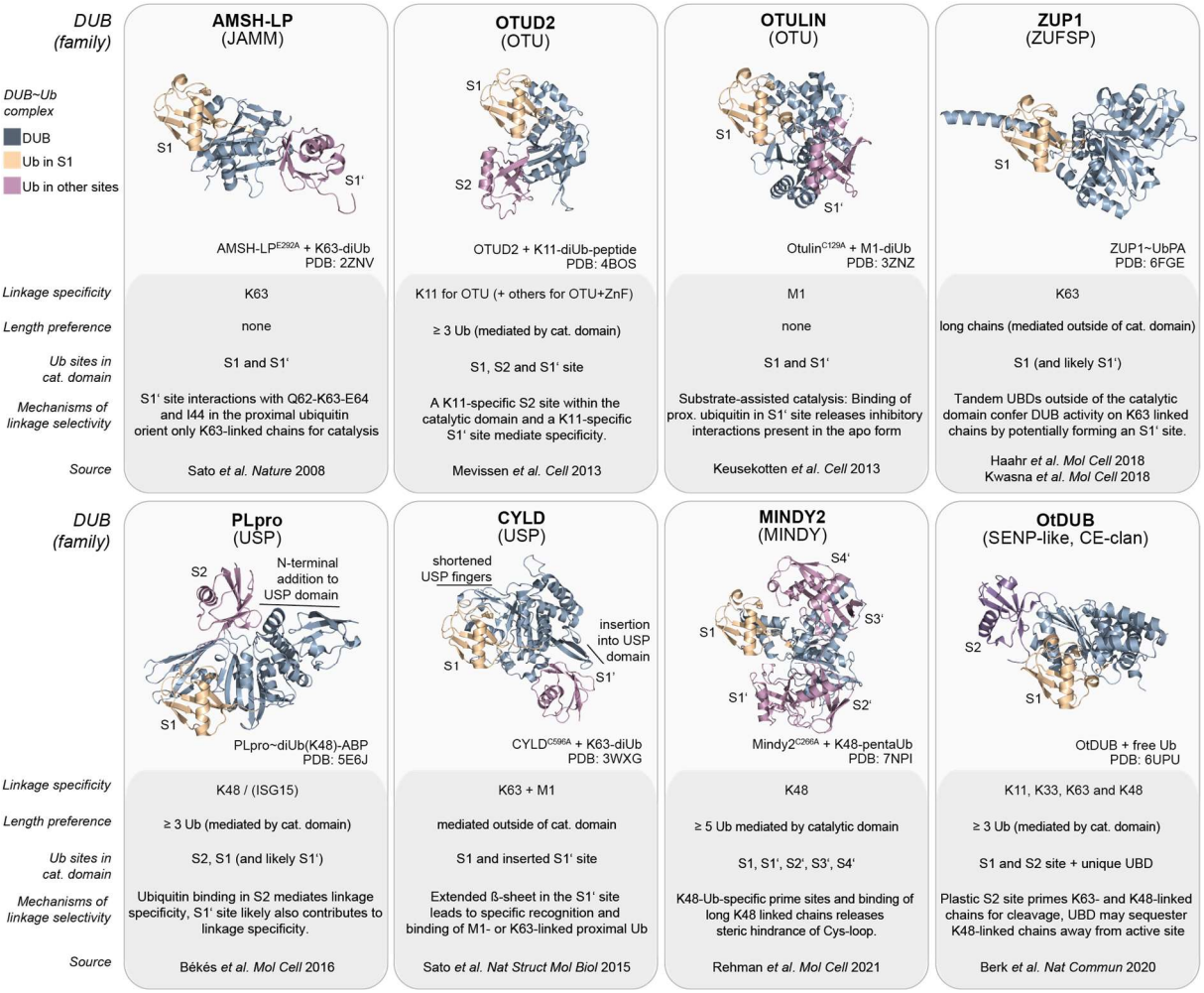

Figure 9: Information cards for linkage- and/or length-specific DUBs. Cartoon representations of members of different DUB families are shown in dark grey. Ubiquitin bound in the S1 site is shown in gold, while ubiquitin moieties bound in other binding sites are illustrated in violet. Additionally, characteristics of the mechanisms are presented.

1.5 The USP DUB family

The USP DUB family contains over 50 members which regulate diverse physiological functions.[23] Sequence alignments of USP DUBs reveal six conserved boxes that together cover ~350 amino acids across all members, show high sequence similarity, contain the catalytic dyad/triad and relate to the core catalytic domains.[123] These domains can be extended by insertions between conserved boxes as well as by N-terminal and C-terminal extensions which vary among individual USP DUBs.[105] Structurally, the core catalytic domains adopt a hand-like architecture with thumb, fingers and palm subdomains, a classification based on the structure of USP7, the first crystallized human DUB.[124] The primary ubiquitin-binding site (S1)

is located between the fingers, palm, and thumb domains with ubiquitin positioned on top of the fingers domain. The C-terminus of ubiquitin extends into a narrow catalytic cleft formed by the palm and thumb domains.

Two homologous proteins of the USP DUB family, USP53 and USP54 are phylogenetically distinct from other USP DUBs, and are most closely related to USPL1, a SUMO protease (Figure 10A).[23,123] Their canonical protein sequences consist of 1073 and 1684 amino acids, respectively (Figure 10B).[125] Both proteins feature an N-terminal catalytic domain and an extended C-terminal tail, with USP53 containing a predicted Src-homology 3 (SH3) binding domain and USP54 harboring a microtubule interacting and transport (MIT) domain (Figure 10B).[126] According to the Human Protein Atlas, USP53 and USP54 are expressed in a tissue-unspecific manner.[127] They have been annotated as catalytically inactive, due to sequence differences in highly conserved regions of the USP catalytic domain, lack of *in vitro* cleavage activity on a Ub-ß-galactosidase fusion protein and the absence of ubiquitin probe labeling of cellular USP53.[128,129] However, recent studies have increasingly linked USP53 and USP54 to various cellular processes and disease phenotypes. Reports on potential substrates suggest that USP53 and USP54 are active deubiquitinases.[130-133] Despite this, definitive proof of their catalytic activity remains elusive.

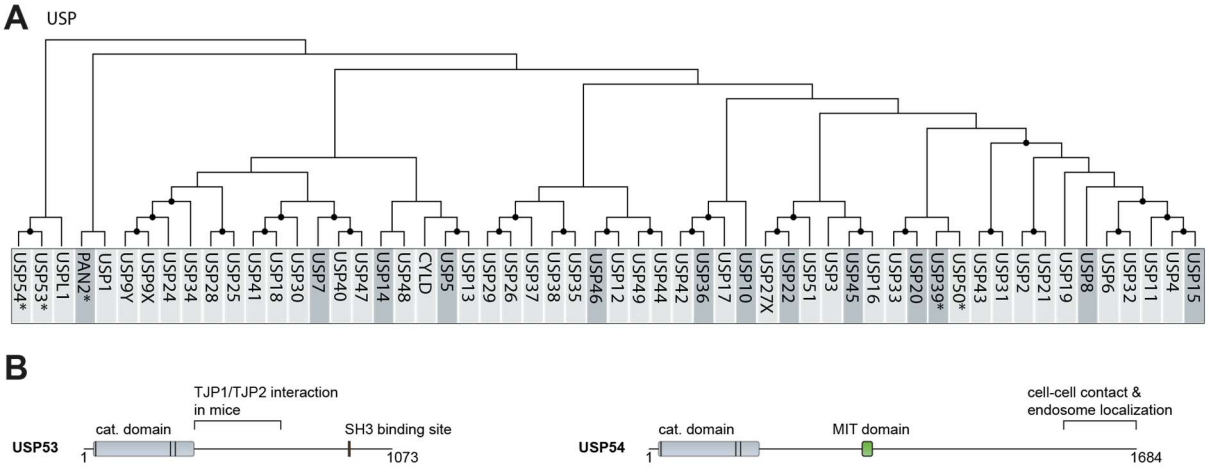

Figure 10: USP53 and USP54. A) Phylogenetic tree of the catalytic domains of human USP DUBs. The stars denote assumed inactive DUBs.[23] B) Schematic depiction of the protein sequences of USP53 and USP54. Identified or predicted structural elements are annotated.

1.5.1 USP53

Biallelic loss or mutation of *USP53* have been found as a novel genetic factor for familial intrahepatic cholestasis, a hereditary liver disorder affecting primarily children and occasionally associated with deafness.[134-138] These genetic mutations result in no protein expression, truncated proteins, or proteins with a single point mutation which cluster in the catalytic domain of USP53 (Table S1). Histopathological analysis of liver biopsy samples from affected patients has revealed abnormalities such as fibrosis, elongated tight junctions (TJs) and giant-cell

change of hepatocytes.[136] Another common genetic cause of cholestasis are pathogenic variants of *TJP2*, which are also associated with elongated TJs and deafness. *TJP2* encodes tight junction protein 2 (TJP2), a scaffolding protein present in tight junctions and adherens junctions.[139,140] Similarly, biallelic loss or missense mutation of *USP53* has been linked to deafness in mice.[129,141] The missense mutation (C228S) causes outer hair cell degeneration, progressive hearing loss and reduced endocochlear potential in mice.[129] The mutated residue C228, located at the tip of the fingers domain within the unusual CXXXC motif of USP53, is likely important for zinc binding. Notably, this same mutation has been identified in a cholestasis patient as well as in two patients diagnosed with psychosis.[142,143]

Co-immunoprecipitation (Co-IP) experiments suggest an interaction between the C-terminal tail of mouse USP53 and endogenous TJP1 and TJP2 in HEK293T cells (Figure 10B).[129] In Madin-Darby canine kidney (MDCK) cells, which form a polarized epithelium at high densities, transfection with GFP-USP53 resulted in colocalization with TJP2, indicating recruitment of USP53 to TJs in epithelial cells.[129] TJs typically connect the apical cell border in epithelial cells. In mouse hair and supporting cells transfected with GFP-USP53, as well as in dissected wild-type mouse organs of Corti, USP53 localizes to the apical cell borders and to cell-cell contacts between hair cells and Deiters' cell, respectively.[129] These observations suggest that USP53 plays a critical role in maintaining functional cell-cell barriers necessary for bile secretion in the liver and cochlear fluid homeostasis in the inner ear. This makes USP53 one of the very few DUBs whose mutations in the catalytic domain are linked to disease phenotypes.[144-147]

Beyond its role in cholestasis, USP53 has been attributed additional cellular roles. In triple negative breast cancer (TNBC), USP53 exhibits oncogenic properties.[131] Elevated levels of USP53 correlate with enhanced cell proliferation, metastasis and reduced survival in TNBC patients, while USP53 knockout suppresses cell growth and tumor formation in immunocompromised mice.[131] This effect is mediated by Crk-like protein (CRKL), an adaptor protein involved in multiple biological processes and frequently overexpressed in cancers.[148] USP53 appears to deubiquitinate CRKL as demonstrated by Co-IP experiments, partial stabilization of CRKL upon overexpression of USP53, and cellular DUB assays.[131]

In contrast, USP53 has been associated with tumor-suppressive roles in other cancer types, by promoting apoptosis or inhibiting cancer progression. These include breast cancer; esophageal carcinoma; hepatocellular cancer presumably through deubiquitination of cytochrome c, renal cell carcinoma through inactivation of the nuclear factor kappa B (NF-κB) pathway, as well as lung adenocarcinoma through inhibition of the protein kinase B (AKT) signaling pathway by stabilization and possible deubiquitination of FK506-binding protein 51 (FKBP51).[130,149-152] In the context of FKBP51, USP53 has been implicated in the FKBP51/RhoA/ROCK pathway, which is involved in chronic constriction injury-induced neuropathic pain.[153]

USP53 has also been recognized for its role in mesenchymal cell differentiation, skeletal development and bone homeostasis.[141,154,155] Mesenchymal stem cells (MSCs) can differentiate into a variety of cell types, including adipocytes and osteoblasts.[156] In osteoblasts, *USP53* is a transcriptional target of parathyroid hormone (PTH) signaling, a regulation pathway of bone remodeling.[155] In mouse bone marrow-derived mesenchymal stem cells (BMSCs), knockdown of USP53 promotes osteogenesis while decreasing adipogenesis.[155] In contrast, USP53 promotes osteogenic differentiation of human BMSCs *in vitro* with lower USP53 expression observed in BMCs of osteoporosis patients.[154] USP53 knockout mice exhibit low bone mass and increased bone marrow adipose tissue volume,[141] consistent with a case study of a patient with a duplication of *USP53* and adjacent genes who presented with bone deformities and severe obesity.[157] Furthermore, another study found a correlation between USP53 gene expression in adipose tissue and effective weight control in obese subjects.[158] Overall, these findings highlight the multifaceted role of USP53 in diverse biological processes.

1.5.2 USP54

USP54 has been implicated in tumor progression across various cancers, making it a potential target for anti-cancer therapies, although its precise oncogenic mechanisms remain largely unclear.[132,159,160] In prostate cancer, USP54 expression increases during the transition from hormone-sensitive prostate cancer to castration-resistant prostate cancer (CRPC), with elevated USP54 mRNA and protein levels observed in tumor cells compared to normal prostate cells. USP54 knockdown inhibits CRPC cell proliferation *in vitro* and *in vivo*, potentially through androgen receptor signaling, highlighting its role in CRPC pathogenesis.[159]

USP54 has also been linked to colon cancer progression.[160] In colorectal carcinoma cells, USP54 downregulation impedes their tumorigenesis and USP54-deficient mice develop fewer adenocarcinomas following chemical induction of colon carcinoma than control mice. In humans, adenomas show higher USP54 expression than adjacent cells.[160] Similarly, USP54 knockdown in melanoma cells reduces lung metastasis formation in immunodeficient mice, further supporting its pro-tumorigenic role.[160]

In gastric cancer, USP54 expression and centrosome aggregation have been shown to be promoted by centrosomal protein 120 (CEP120).[132] CEP120 and polo-like kinase 4 (PLK4) function in centrosome replication, and both proteins have been linked to tumorigenesis when dysregulated.[132,161] USP54 is proposed to deubiquitinate and stabilize PLK4 upon recruitment by CEP120, supporting its involvement in centrosome function.[132] Further evidence for this role include the identification of USP54 as a proximity-interaction partner of CEP135 and PLK4, as well as the partial rescue of centriole duplication effects upon its knockdown.[162,163] Additionally,

USP54 negatively regulates ciliogenesis with centrioles being part of the basal bodies of primary cilia.[163,164]

Beyond its role in cancer, USP54 has been identified as a hit in an RNAi screen aimed at identifying novel DUB regulators of the endocytic pathway and has been proposed to regulate the integrity of cell-cell contact sites and endocytic trafficking.[165] In the same study, full-length USP54 localized to areas of actin filaments, cell-cell contacts, and endosomes, fitting its identified interaction partners: tight and adherens junctions associated proteins, components of the HOPS complex which is important for endosome fusion and maturation, actin-based motor proteins, and cilia proteins.[165] Loss of USP54 in MelJuSo cells disrupts mitosis and leads to a strong clustering of organelles, including endocytic vesicles and mitochondria, at the microtubule-organizing center. These defects may be attributed to the effect of USP54 on microtubule dynamics and the endocytic network, suggesting a role for USP54 in cytoskeletal organization. The expression of a catalytically inactive variant of USP54 in HeLa cells led to a microtubule defect that was similar to that observed in USP54-deficient cells. Additionally, USP54 expressed in HEK293T cells reacted with a ubiquitin-based probe.[165] All of the above findings indicate that the DUB activity of USP54 exists and is functionally relevant.

1.6 Tools to study DUBs

To discover novel DUBs, explore new activities in known DUBs, and better understand their activities, specificities and biological functions under normal and pathological conditions, the development of innovative tools and methods has been essential.[94,95,166,167] Recent advances in this field include, but are not limited to, cell-permeable small molecule probes, the development of selective and potent small molecule inhibitors for DUBs, and proteomics studies combined with probe treatment, tandem-repeated Ub-binding entity (TUBE) reagents, Ub-clipping or trypsin treatment/di-Gly antibodies.[24,67,167-170] Beyond studying DUBs in a cellular context, researchers have established a growing number of methods to generate ubiquitin-based probes, ubiquitin-based substrates, and ubiquitinated proteins.[171,172] These tools are particularly useful for investigating DUB activity, specificity and structures *in vitro*.

1.6.1 Substrates for *in vitro* DUB assays

A direct way to study DUB activity is to use substrates whose hydrolysis can be quantified by techniques such as fluorescence measurements or analyzed by SDS-PAGE and protein band staining. This approach enables the correlation of DUB activity with substrate hydrolysis, making it particularly useful for studying purified DUBs or those isolated from cell lysates by immunoprecipitation or pulldown.

Ubiquitin-based substrates

Fluorogenic substrates such as Ub-7-amino-4-methylcoumarin (Ub-AMC) or Ub-rhodamineG (Ub-RhoG) feature ubiquitin covalently conjugated to fluorophores via an aryl amide bond. Cleavage by DUBs releases and unquenches the fluorophore, allowing quantification of DUB activity through fluorescence measurements.[173,174] The simple measurement facilitates high-throughput screening for DUB inhibitors and these substrates have been used for several DUBs including USP7, USP14 USP28 and the protease PLpro from SARS-CoV-2.[175-178] An advanced substrate, Ub-KG-TAMRA, incorporates an isopeptide bond between the C-terminus of ubiquitin and the lysine of the TAMRA-labeled KG peptide.[179] Due to the isopeptide bond, cleavage of Ub-KG-TAMRA, detected by the decrease in fluorescence anisotropy, more accurately represents DUB activity than cleavage of Ub-AMC or Ub-RhoG. Similar substrates with Ubls as the recognition modules have been developed to quantify the activity of Ubl proteases and to compare cross-reactive enzyme activities. Recent semi-native ligation procedures have, in contrast to earlier methods, the advantage that the Ub/Ubl substrates remain folded during the entire generation process.[99,180]

A limitation of monoubiquitin-based substrates is that they only interact with the S1 site of DUBs. However, various DUBs recognize specific polyubiquitin chain types and contain additional ubiquitin and substrate binding sites.[113,181] To address and study these specificities, ubiquitin chains of defined length, linkage and topology, and ubiquitinated substrates serve as great tools.[116,172,182] The enzymatic assembly of specific polyubiquitin chains depends on the knowledge about E2 and E3s specificities.[182,183] To date, homotypic K6-, K11-, K29-, K33-, K48- and K63-linked polyubiquitin chains can be enzymatically assembled from single ubiquitin moieties.[183] Native linkages of all types, including K27 linkages, can also be obtained by other strategies.[184] For instance, solid-phase peptide synthesis (SPPS) of ubiquitin mutants with an incorporated thiolysine, followed by native chemical ligation with an Ub-thioester and desulfurization enables the synthesis of K27-linked diubiquitin.[185,186] Additionally, strategies for the generation of more complex ubiquitin chains such as mixed, branched or hybrid chains with native, non-native isopeptide bonds or non-hydrolyzable bonds have been developed.[172,184,187-192]

Site-specific ubiquitination of target proteins

DUBs can have three distinct cleavage modes: *endo*, *exo* and *en bloc* cleavage. To distinguish between these activities *in vitro*, it is necessary to assay ubiquitinated substrates. One approach to generate these substrates in a completely native manner is enzymatic ubiquitination using the appropriate E1, E2 and E3 enzymes. For example, PCNA is efficiently monoubiquitinated by an E1 enzyme and the E2 enzyme UbcH5c.[182] However, many ubiquitinated proteins lack well-characterized corresponding E1, E2, and E3 enzymes, making

in vitro assembly challenging. To overcome this, enzymatic, native chemical ligation, and bioorthogonal protein labeling strategies have been developed for site-specific ubiquitination of substrate proteins.[193] Since the isopeptide bond is relevant for recognition by ubiquitin-binding proteins and DUBs, it is essential to generate bonds that closely resemble the native linkages. Site-specific native ubiquitination can be achieved by incorporating specific unnatural amino acids into the substrate protein, followed by native chemical ligation and desulfurization.[194] The generation of an isopeptide bond under native conditions, thus obviating the need for refolding, is possible by sortylation. This chemoenzymatic approach relies on the genetic incorporation of the unnatural amino acid GGK into the substrate protein, which is then labeled by sortase with a ubiquitin that contains a C-terminal sortase recognition motif that is similar but not identical to its native C-terminus.[195] Consequently, the final ubiquitinated substrate contains two mutations (R72A, R74A) in the C-terminus of ubiquitin, which may hinder its recognition by DUBs. Further development of this method has allowed the generation of polyubiquitinated substrates, but with the same limitation.[191] An alternative, lysine acylation using conjugating enzymes (LACE), enables site-specific monoubiquitination of substrates in a native manner without ubiquitin truncation. Here, Ub-sodium 2-mercaptoethanesulfonate (Ub-MesNa) serves as a SUMO1-E1 thioester mimic and can be conjugated to a LACE-tagged target protein by Ubc9, the E2 conjugation enzyme for sumoylation.[196] The development of a chimeric E1-activating enzyme that cooperates with Ubc9 further improved this method and allows direct conjugation of ubiquitin and polyubiquitin chains to the LACE tag in purified proteins. Additionally, co-expression of all components in bacterial cells enables direct expression of monoubiquitinated proteins in cells.[197]

1.6.2 Probes

Activity-based probes (ABPs) have emerged as powerful tools for studying enzyme activities. Instead of serving as a substrate and being turned over, ABPs covalently react with the active site of enzymes.[198,199] Typically, ABPs consist of three key components: 1) a recognition module that is specific for the target enzyme, 2) a reactive group, also termed warhead, that covalently reacts with the catalytic active residue, and 3) an optional reporter tag such as HA, biotin, or a fluorophore for detection (Figure 11A).[199] Since most DUBs are cysteine proteases, they can be selectively targeted by probes that contain ubiquitin as the recognition module and an electrophilic warhead that covalently reacts with the catalytic cysteine. Importantly, to ensure effective enzyme labeling, the warhead replaces the C-terminal glycine of ubiquitin, positioning the electrophile precisely where the carbonyl C-atom of the isopeptide bond would normally reside (Figure 12). Applications of Ub probes include the discovery and cellular profiling of DUB activities as the formed covalent complexes can be enriched and detected by

the reporter tag, allowing their identification as well as the differentiation between expression levels and the activity of DUBs.[114,200] Additionally, Ub-based probes have been instrumental in determining DUB structures, performing *in vitro* activity assays with purified DUBs, and developing DUB inhibitors.[122,124,175]

Semi-synthesis and total synthesis approaches have been developed to generate ubiquitin with functionalized C-termini.[184,201,202] A common semi-synthesis approach is intein-based chemical ligation. Taking advantage of the ability of protein splicing elements (inteins) to self-splice and to form a thioester as an intermediate by N-S acyl shift, first reactive Ub-thioesters are generated (Figure 14).[203] During splicing, the N-terminal and C-terminal peptides upstream and downstream of the intein are normally linked.[204] However, expression of ubiquitin fused N-terminally to an intein in which the C-terminal Asp is mutated to Ala allows the cleavage of the thioester intermediate by transthioesterification upon addition of thiol-containing nucleophiles, such as DTT or MesNa, resulting in a thioester bond at the C-terminus of ubiquitin and release of the intein with a free N-terminus. The Ub-thioester can then be efficiently lysed by the addition of high concentrations of small molecule amines to form a stable amide bond. As a result, a variety of electrophiles that differ in chemical structure and reactivity can be incorporated into Ub probes.[184] Depending on their reaction with the catalytic cysteine of DUBs, these electrophiles can be classified into three distinct mechanisms: direct addition, conjugate addition, and nucleophilic substitution (Figure 11B).[205]

Direct addition mechanism (1,2 addition)

The earliest developed probes ubiquitin-aldehyde (UbaI) and Ub-nitrile (Ub-CN) react with DUBs via direct addition, forming unstable complexes through hemithioacetal and thioimidate bonds, respectively.[206] Among these, UbaI has been widely used in structural studies, with USP7~UbaI being the first resolved human DUB structure.[124] A more recently developed and now in Ub probes widely used warhead, propargylamide (PA), contains an alkyne group that reacts covalently with DUBs to form a stable vinyl thioether bond (Figure 11B).[166] This probe led to the discovery of two new DUB families.[115,181,207]

Conjugate addition mechanism (1,4 addition)

Ub probes with Michael acceptors as electrophiles react with DUBs via conjugate addition. Ub-vinyl methyl sulfone (Ub-VS) (Figure 11B) and Ub-vinyl methyl ester (Ub-VME) fall into this category and have been used in proteomics, structural and activity-based studies.[202,203,208,209] Notably, Ub-VS was the first developed probe to form a stable complex with DUBs.[198]

Nucleophilic substitution mechanism

Ub probes featuring alkyl halides, such as Ub-2Br (Figure 11B) and Ub-Cl, react with DUBs via nucleophilic substitution. This reaction results in a stable thioester bond while releasing the

halogen as a leaving group. Their use has contributed to the discovery of members of the OTU DUB family.[203] Acycloxymethyl ketones as highly reactive warheads are suitable for capturing not only DUBs but also many E1, E2, and E3 enzymes.[210]

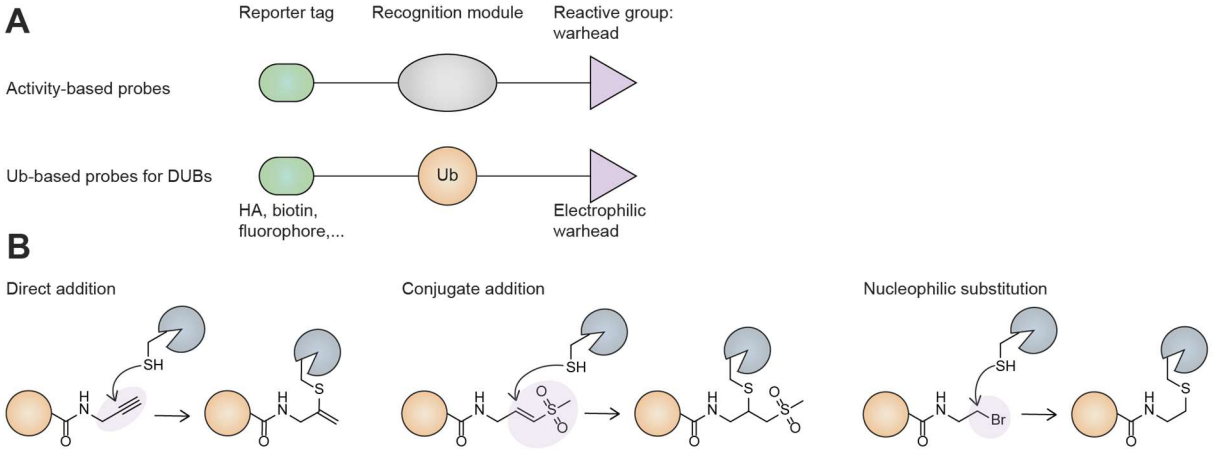

Figure 11: Composition and reaction mechanisms of Ub-based probes. A) Activity-based probes consist of three elements: the reactive group, also called the warhead (blue triangle), the recognition module (grey) and the reporter tag (purple). B) Different electrophiles used as warheads in Ub-based probes react by three different mechanisms with the catalytic cysteine of DUBs.

In general, ubiquitin-based probes are unselective and react with a variety of DUBs. However, different warheads show different engagement profiles during DUB profiling. Consequently, for individual warheads, different sets of DUBs are detected after enrichment and mass spectrometry detection after cell lysate probe treatment of cell lysate.[203,211] A method to generate more selective Ub-based probes is to engineer ubiquitin to contain unnatural amino acids, especially located at the C-terminus.[212]

Monoubiquitin probes provide insights into ubiquitin binding in the S1 site of DUBs, but offer limited information on specificity for ubiquitin chain linkage and length (Figure 12A). To address this, more complex ubiquitin-based probes have been developed to characterize DUB activity and obtain structural information about ubiquitin interactions at multiple binding sites.[199,213-216] Diubiquitin-based probes, in which two ubiquitin moieties are linked by a molecule containing an electrophilic warhead, allow for studying DUB linkage specificity by engaging both the S1 and S1' sites (Figure 12B). While the alkyne warhead used in Ub-PA is unsuitable for internal use, Michael acceptors (MA) serve as effective electrophiles between ubiquitin moieties. Specifically-linked diUb probes with Michael acceptor-based internal warheads, that differ in the chemistry and length of the linker have been generated by semi-synthesis and total synthesis approaches (Figure 12B). Generally, their generation follows a step-wise strategy: 1) Generation of a modified proximal ubiquitin whose relevant lysine is replaced with a reactive group that serves as an anchor for linkage formation. 2) Functionalization of the C-terminus of the distal ubiquitin with a linker that incorporates the reactive group and a handle for

conjugation. 3) Ligation of the two ubiquitin moieties and if needed further reactions (e.g. thiol elimination) to obtain the Michael acceptor electrophile.[214,215,217] Exemplary, a K11 linkage mimicking covalent amide-linked diUb probe has been used to resolve the structure of Cezanne with occupied S1 and S1' sites, informing on its mechanism of linkage specificity.[215,218] An alternative warhead is incorporated in the dehydroalanine (Dha)-based diUb probe.[219]

To investigate DUBs that recognize polyubiquitin via additional S2 binding sites, such as OTUD2 and the SARS-CoV-1 protease PLpro, diUb probes have been designed with warheads at the C-terminus of the proximal ubiquitin (Figure 12C). Consequently, interaction with both the S1 and S2 sites, but not with the S1 and S1' sites, enable the reaction with DUBs.[120,208,213] One approach utilized a linear diubiquitin aldehyde probe, while another generated and employed non-hydrolyzable triazole-linked diUb probes, applicable to all linkages (Figure 12C).[98,213] The structural characterization of SARS-CoV-1 PLpro in complex with such a triazole-linked K48 linkage mimicking diUb probe revealed the molecular basis of ubiquitin recognition in the S1 and S2 sites.[122]

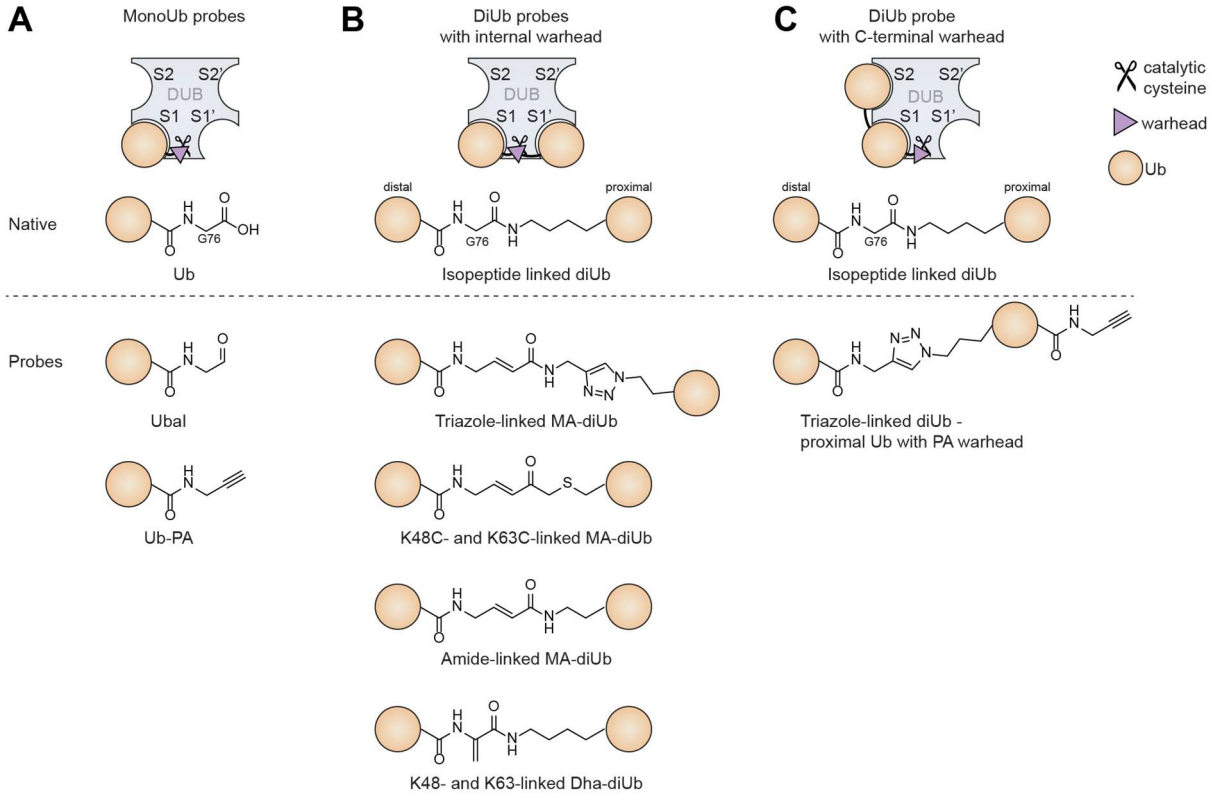

Figure 12: Overview of ubiquitin-based probes. A) Probes featuring a single ubiquitin moiety with a C-terminal warhead reacting with the catalytic cysteine of DUBs upon interacting with the S1 binding site of DUBs. B) Diubiquitin-based probes with an in-between warhead to probe for DUB activity upon binding of the S1 and S1' sites of DUBs. C) Diubiquitin-based probes with a C-terminal warhead on the proximal ubiquitin moiety. Binding in the S1 and S2 sites of DUBs leads to DUB~probe complex formation. The figure is adapted from Mulder *et al*.[184]

2 Aim

Dysregulation of deubiquitinating enzymes (DUBs) has been implicated in a variety of diseases, including cancer and developmental disorders.[220,221] A prerequisite for the development of novel therapeutic approaches is to investigate the biochemical activities of DUBs at the molecular level and to understand their cellular functions and roles.[94] This work focuses on two DUBs: USP53 and USP54. Although mutations in *USP53* have been associated with pediatric cholestasis, and both proteins have been implicated in different cancer types, their cellular and pathophysiological functions remain largely unexplored as both enzymes are assumed to be catalytically inactive.[128,131,132,136,149,160] Strikingly, a conclusive analysis of their activities remains elusive to date.

The aim of this work is to characterize the potential catalytic activities of USP53 and USP54 by analyzing their substrate specificity, possibly for ubiquitin and/or another Ubl. An *in vitro* approach will be used to achieve this goal. Generation of a panel of ubiquitin- and Ubl-based probes and substrates will allow the specificity analysis of bacterially expressed and purified catalytic constructs. Once established, the substrate specificity will be further explored to uncover the mechanisms and molecular details of substrate recognition of USP53 and USP54. To this end, a suite of specifically designed substrates and ubiquitin-based probes will be generated and used in *in vitro* DUB assays and structural studies.
Finally, to bridge the gap between the activity of USP53 and the observed cholestasis phenotype, identified mutations in *USP53* in patients, will be tested at the protein level with *in vitro* DUB activity assays.

The collective impact of this work has the potential to change the way we think about USP53 and USP54 and facilitate a mechanistic understanding of their catalytic activities. This, in turn, will pave the way to uncovering their cellular roles and the mechanistic basis of their involvement in disease pathogenesis.

3 Material and Methods

3.1 Material

3.1.1 Commercially available material, enzymes and kits

Table 1: Commercially available material, enzymes and kits

Name	Source
Cloning	
10x HF Phusion polymerase buffer	NEB
10x T4 DNA ligase buffer	NEB
Deoxynucleotide solution mix (dNTPs)	NEB
In-Fusion cloning mix	TaKaRa
Phusion HF DNA polymerase	NEB
QIAprep Spin Miniprep Kit	Qiagen
QIAquick Gel Extraction Kit	Qiagen
QIAquick PCR Purification Kit	Qiagen
Restriction enzymes	
DpnI	NEB
HindIII-HF	NEB
KpnI-HF	NEB
NdeI	NEB
SapI	NEB
T4 DNA ligase	NEB
DUB substrates	
Ubiquitin-Rhodamine110Gly	UbiQ
SUMO1-Rhodamine110Gly	UbiQ
SUMO2-Rhodamine110Gly	UbiQ
NEDD8-Rhodamine110Gly	UbiQ
ISG15-Rhodamine110Gly	UbiQ
Diubiquitin panel of all 8 linkages	UbiQ
K29-linked tetraubiquitin	Bio-techne
K33-linked tetraubiquitin	Bio-techne

Name	Source
Protein purification	
20x NuPAGE MES SDS Running Buffer	Thermo Fisher Scientific
4x NuPAGE LDS Sample Buffer	Thermo Fisher Scientific
Chitin resin	NEB
Complete, EDTA-free Protease inhibitor cocktail tablets (PIC)	Roche Diagnostics
DnaseI	AppliChem
Glutathione Sepharose 4B	GE Healthcare
InstantBlue™	Abcam
Lysozyme	Roth
NuPAGE 4-12%, Bis-Tris Gels, 15 well/26 well	Thermo Fisher Scientific
NuPAGE 3-8% Tris-Acetate Gels	Thermo Fisher Scientific
SeeBlue™ Plus2 Pre-stained Protein Standard	Thermo Fisher Scientific
Silver Stain Plus kit	BioRad
SYPRO Orange protein gel stain	Sigma-Aldrich
Screening plates	
Core I, II, III, IV, Classics I, PEGs I, II, JCSG+, PACT, Cryos	Qiagen
Memgold I & II, Morpheus screening plates	Molecular Dimensions

3.1.2 Laboratory equipment and consumables

Table 2: Laboratory equipment

Name	Manufacturer
Agilent 1260 II Infinity system	Agilent
Äkta pure protein purification system	GE Healthcare
Cell density meter, Biowave, CO 8000	Biochrom
CFX Connect Real-Time PCR System	Bio-Rad
Chemidoc MP Imaging System	Bio-Rad
Centrifuges	
Avanti J-25	Beckman Coulter
Avanti J-26 XP	Beckman Coulter
5415R, 5417, 5415D, 5804R	Eppendorf
Crystallization	
Mosquito LCP robot	TTP Labtech
DragonFly	TTP Labtech
RockImager	Formulatrix
Drying and heating chamber ED53	BINDER

Name	Manufacturer
Econo-Column Chromatography Columns	Bio-Rad
Heating and stirring plate IKA RCT classic	IKA
Incubator shaker Innova 42, Innova 4430	New Brunswick Scientific
Isotemp water bath, GPD 02	Fisher scientific
PCR Thermal Cycler	BioRad
Peristaltic pump LA-900	Landgraf Laborsysteme
Pipettes (2 µl, 10 µl, 20 µl, 100 µl 200 µl, 1000 µl)	Gilson
Power Supply (Power Pac™ HC, Power Pac™ Basic)	Bio-Rad
Thermomixer compact	Eppendorf
Sonicator with probe, 700 W	Fisherbrand
Spectrophotometer, NanoDrop 2000c	Peqlab
SureLock Tandem Midi Gel Tank	Thermo Fisher Scientific
XCell SureLock Mini-Cell	Thermo Fisher Scientific

Table 3: Consumables

Name	Manufacturer
96 deepwell blocks	Greiner
96-well PCR plates (white)	Bio-Rad
384-well assay plates (black)	Greiner
Amicon Ultra-15 (MWCO 3kDa, MWCO 10 kDa)	Merck
Amicon Ultra-4 (MWCO 3kDa, MWCO 10 kDA)	Merck
CryoPure tubes (1.8 ml)	Sarstedt
Microcentrifuge tubes (1.5 ml, 2 ml)	Sarstedt
MRC 96-well crystallization plates (2-Drop, 3-Drop)	Molecular Dimensions
PCR tubes, PCR 8-well strip tubes & lids	Axygen
Pipette tips (10 µL, 20 µL, 200 µl, 1000 µL)	Sarstedt
Serological pipettes (2 mL, 5 mL, 10 ml, 25 ml, 50 ml)	Sarstedt
Snake Skin Dialysis Tubing (MWCO 3.5 kDa)	Thermo Scientific
Sticky aluminium seals	Thermo Fisher Scientific
Syringe filter, Filtropur S, pore size: 0.2 µm/0.45 µm	Sarstedt
Transparent sealing films	Bio-Rad
Tubes (15 ml, 50 ml)	Sarstedt

3.1.3 Buffers

Table 4: Buffers

Name	Composition
Buffer D	20 mM Na_2HPO_4, 100 mM NaCl, pH 6.0
Buffer M	20 mM 2-(*N*-morpholino)ethanesulfonic acid (MES) pH 8.0
Buffer N	50 mM NaH_2PO_4, 300 mM NaCl, 20 mM imidazole, 4 mM 2-mercaptoethanol (ß-ME), pH 8.0
Buffer S	50 mM NaOAc, pH 4.5
Buffer T	20 mM tris(hydroxymethyl)-aminomethane (Tris), 100 mM NaCl, 5 mM dithiothreitol (DTT), pH 8.0
Cleavage buffer	20 mM Tris, 100 mM NaCl, 5 mM DTT, 0.5 mg/ml bovine serum albumin (BSA), pH 8.0
Conjugation buffer	40 mM Tris, 10 mM $MgCl_2$, 10 mM adenosine triphosphate (ATP), pH 8.5
DUB buffer	20 mM Tris, 100 mM NaCl, 4 mM ß-ME, 5% (v/v) glycerol, pH 8.0
GST HS buffer	20 mM Tris, 500 mM NaCl, 10 mM ß-ME, pH 8.0
GST LS buffer	20 mM Tris, 150 mM NaCl, 10 mM ß-ME, pH 8.0
GST lysis buffer	50 mM Tris, 500 mM NaCl, 1 mM ethylenediaminetetraacetic acid (EDTA), 10% (v/v) glycerol,10 mM ß-ME, pH 8.0
K48 linkage assembly buffer	40 mM Tris, 10 mM $MgCl_2$, 10 mM ATP, 1 µM E1, 25 µM Ube2R, pH 8.5
K63 linkage assembly buffer	40 mM Tris, 10 mM $MgCl_2$, 10 mM ATP, 1 µM E1, 8 µM Ube2N, 8 µM Ube2V, pH 8.5
Labeling buffer	1x PBS,1 mM tris(2-carboxyethyl)phosphine (TCEP)
LACE reaction buffer	50 mM 4-(2-hydroxyethyl)-1-piperazineethanesulfonic acid (HEPES), 50 mM KCl, pH 7.6
Low salt (LS) buffer	25 mM Tris, 50 mM NaCl, 4 mM ß-ME, pH 8.5
Lysis buffer	50 mM Tris, 1 mM EDTA, pH 7.4
Phosphate-buffered saline (PBS)	0.137 M NaCl, 2.7 mM KCl, 10 mM Na_2HPO_4, 1.8 mM KH_2PO_4, pH 7.4
Reaction buffer	20 mM Tris, 100 mM NaCl, 5 mM DTT, pH 7.7
Storage buffer	20 mM Tris, 100 mM NaCl, 4 mM DTT, 5% (v/v) glycerol, pH 8.0
Tris-acetate running buffer	50 mM *N*-(tris-hydroxymethyl)methylglycine (Tricine), 50 mM Tris, 0.1% (w/v) sodium dodecyl sulfate (SDS), pH 8.24
TSA buffer	20 mM HEPES, 100 mM NaCl, 5 mM DTT, pH 7.5
Ubiquitin lysis buffer	20 mM Tris, 2 mM EDTA, pH 7.4

3.1.4 Cultivation media

The ingredients for media used for *Escherichia coli* (*E. coli)* cultivation are listed in Table 5. All media were autoclaved. For plasmid selection and amplification, ampicillin was added to a final concentration of 100 µg/ml, kanamycin to a final concentration of 50 µg/ml and chloramphenicol to a final concentration of 34 µg/ml to LB agar plates, LB medium or 2YT medium.

Table 5: Ingredients of media for the cultivation of *E. coli.*

Name	Composition
Lysogeny broth (LB) medium	10 g/l tryptone/peptone 5 g/l yeast extract, 10 g/l NaCl, pH 7.4
LB agar plates	1.5 % (w/v) bacto agar in LB medium
2x yeast extract-tryptone medium (2YT)	16 g/l tryptone, 10 g/l yeast extract, 5 g/l NaCl, pH 7.4

3.1.5 Organisms

Two *E. coli* strains were used in this study and are listed with their genotypes in Table 6. The Top10F' strain was used for the amplification and selection of plasmids, the Rosetta 2 strain for protein expression.

Table 6: Used *E. coli* strains

Name	Genotype
Top10F'	F'*mcr*A Δ(*mrr-hsd*RMS-*mcr*BC) φ80*lac*ZΔM15 Δ*lac*X74 *rec*A1 *ara*D139 Δ(*ara-leu*) 7697 *gal*U *gal*K *rps*L *end*A1 *nup*G
Rosetta 2 (DE3)pLacI	F^- *ompT hsdS*$_B$(r_B^- m_B^-) *gal dcm* (DE3) pLacIRARE2 (Cam^R)

3.1.6 Oligonucleotides

Oligonucleotides used in this work are listed in Table 7. They were ordered from Sigma-Aldrich and were used for insert amplification, InFusion cloning, SOE-PCR or site-directed mutagenesis.

Table 7: List of oligonucleotides used in this study

Name	Sequence (5' --> 3')	Purpose
K123	TGAACCGGGTCAGAATAGCTCGTTTCTGAA TAGCGCAGTT	Introduction of C41S into *USP53* (fwd)
K124	AACTGCGCTATTCAGAAACGAGCTATTCTG ACCCGGTTCA	Introduction of C41S into *USP53* (rev)
K125	CCGAGCGATAATATTTCTCATGCACTGGCA G	Introduction of R99S into *USP53* (fwd)
K126	CTGCCAGTGCATGAGAAATATTATCGCTCG G	Introduction of R99S into *USP53* (rev)
K129	TGAACCGGGTCAGAATAGCTCGTTTCTGAA TAGCGCACTG	Introduction of C42S into *USP54* (fwd)
K130	CAGTGCGCTATTCAGAAACGAGCTATTCTG ACCCGGTTCA	Introduction of C42S into *USP54* (rev)
K168	GGTTGATCTTTGCTGGGAGGCAGCTGGAA GATGGACGC	Introduction of K48R into *Ubiquitin* (fwd)
K169	GCGTCCATCTTCCAGCTGCCTCCCAGCAAA GATCAACC	Introduction of K48R into *ubiquitin* (rev)
K178	CTGACTACAACATCCAGAGGGAGTCCACCC TGCACCTG	Introduction of K63R into *Ubiquitin* (fwd)
K179	CAGGTGCAGGGTGGACTCCCTCTGGATGT TGTAGTCAG	Introduction of K63R into *Ubiquitin* (rev)
K180	AAGTTCTGTTTCAGGGCCCGGGATCCGCC GGGCTGC	Amplification of *UBE2N* for pOPINK from aa 1 (fwd)
K181	ATGGTCTAGAAAGCTTTAAATATTATTCATG GCATATAGCCTAGTCCATGCTC	Amplification of *UBE2N* for pOPINK from aa 252 (rev)
K192	ATGGTCTAGAAAGCTTTATGACCAGCTGAT GACCTGCCTG	Amplification of *USP53* for pOPINK from aa 368 (rev)
K193	ATGGTCTAGAAAGCTTTACTGAAATTCGGC CTGCGGAGG	Amplification of *USP54* for pOPINK from aa 369 (rev)
K204	GAAGGAGATATACATATGCAGATCTTCGTG AAGAC	Amplification of *Ubiquitin* for pET17b from aa 1 (for)
K206	TAAGAATTCTGCAGATATCCATCACACTGG C	Amplification of pET17B backbone (fwd)
K207	ATGTATATCTCCTTCTTAAAGTTAAACAAAA TTATTTCTAGAGGGAAACC	Amplification of pET17B backbone (rev)
K208	TCTGCAGAATTCTTATCAAGCGCAACCTCT GAGACGGAGGACCAG	Amplification of *Ubiquitin* for pET17b from aa 75 with a C-terminal CA extension (rev)

Name	Sequence (5' --> 3')	Purpose
K209	TCTGCAGAATTCTTATTAGCAACAGCCAGGACAACAGGACCAACCTCTGAGACGGAGGACCAG	Amplification of *Ubiquitin* for pET17b from aa 75 with C-terminal WSCCPGCC extension (rev)
K213	GTCTGACTACAACATCCAGTGCGAGTCCACCCTGCACCTGG	Introduction of K63C into *Ubiquitin* (fwd)
K214	CCAGGTGCAGGGTGGACTCGCACTGGATGTTGTAGTCAGAC	Introduction of K63C into *Ubiquitin* (rev)
K215	GAGGTTGATCTTTGCTGGGTGCCAGCTGGAAGATGGACGCA	Introduction of K48C into *Ubiquitin* (fwd)
K216	TGCGTCCATCTTCCAGCTGGCACCCAGCAAAGATCAACCTC	Introduction of K48C into *Ubiquitin* (rev)
K221	AAGTTCTGTTTCAGGGCCCGATGAACTCCAACGTGGAGAACCTACCC	Amplification of *UBE2S* for pOPINK from aa 2 (fwd)
K222	ATGGTCTAGAAAGCTTTAAGCCATGGGACCCTCAGCCCC	Amplification of *UBE2S* for pOPINK from aa 196 (rev)
K225	AAGTTCTGTTTCAGGGCCCGCTGGGATCCATGTCGGGGATCG	Amplification of *UBC9* for pOPINB from aa 1 (fwd)
K226	ATGGTCTAGAAAGCTTTATGAGGGCGCAAACTTCTTGGCTTG	Amplification of *UBC9* for pOPINB from aa 158 (rev)
K227	AAGTTCTGTTTCAGGGCCCGATGAGCAAAGGTGAAGAACTGTTTACCG	Amplification of emGFP for pOPINB from aa 1 (fwd)
K230	ATGGTCTAGAAAGCTTTATTCTTCGCTTTCCATTTTAATCACTTTGCGCGGGCCGCTGCCTTTGTACAGTTCATCCATACCATGGGTAATACC	Amplification of *emGFP* for pOPINB from aa 238 with C-terminal LACEtag GSGPRKVIKMESEE (rev)
K247	CTGAGCAATCTGGGCAATACCTGTTTTCTGAATAGCGCACTGCAGG	Amplification of *USP54* for pOPINK with internal LGNT sequence (fwd)
K248	CAGAAAACAGGTATTGCCCAGATTGCTCAGACCTTTGCTCGGTG	Amplification of *USP54* for pOPINK with internal LGNT sequence (rev)
K253	CTGCTGAATCTGGGCAATACCTGTTTTCTGAATAGCGCAGTTCAGGTTC	Amplification of *USP53* for pOPINK with internal LGNT sequence (fwd)
K254	CAGAAAACAGGTATTGCCCAGATTCAGCAGACCTTTGGTCGGTG	Amplification of *USP53* for pOPINK with internal LGNT sequence (rev)
K257	CATGCTATATACTTGCTGGATTTCAAGTACTTATCAATTTG	Amplification of pOPINK backbone (rev)

Name	Sequence (5' --> 3')	Purpose
K258	AGCTTTCTAGACCATTTAAACACCACCAC	Amplification of pOPINK backbone (fwd)
K259	CAAGTATATAGCATGGCCTTTGCAGGG	Amplification of any pOPINK insert compatible with amplified pOPINK backbone (fwd)
K260	TGGTATGATTTGCTATTACGGCAAACGCGA TAGCACCTTTTTCTTTCAGACCAAG	Introduction of H302A into *USP54* (fwd)
K261	CTTGGTCTGAAAGAAAAAGGTGCTATCGCG TTTGCCGTAATAGCAAATCATACCA	Introduction of H302A into *USP54* (rev)
K264	TGCCGAGCGATACCCTGGCGAGTGCACTG GCAAAAAC	Introduction of R100A into *USP54* (fwd)
K265	GTTTTTGCCAGTGCACTCGCCAGGGTATCG CTCGGCA	Introduction of R100A into *USP54* (rev)
K266	GCATGATTTGTTATACCAGCCAGGCGTATT GTGCCTTTGCCTTTCATAC	Introduction of H301A into *USP53* (fwd)
K267	GTATGAAAGGCAAAGGCACAATACGCCTG GCTGGTATAACAAATCATGC	Introduction of H301A into *USP53* (rev)
K274	TGTCTGACTACAACATCGCGAAAGCGTCCA CCCTGCACCTGG	Introduction of Q62A and E64A into *Ubiquitin* (fwd)
K275	CCAGGTGCAGGGTGGACGCTTTCGCGATG TTGTAGTCAGACA	Introduction of Q62A and E64A into *Ubiquitin* (rev)
M#1-A1	AAGTTCTGTTTCAGGGCCCGGGTAGCATGC TGAGCCTGGC	Amplification of *USP53* for pOPINK from aa 20 (fwd)
M#1-A4	ATGGTCTAGAAAGCTTTACGGTTTTTCACAA CCCATGTTTTCGG	Amplification of *USP53* for pOPINK from aa 383 (rev)
M#1-A5	AAGTTCTGTTTCAGGGCCCGCGTAGCAGCA CCAGCATTGCAC	Amplification of *USP54* for pOPINK from aa 21 (fwd)
M#1-E12	GGTGGTCATATGTACCCATACGATGTTCCA GATTACGCTGGATCCATGGCCAATGAAAAA CCGACCGAAGAAG	Amplification of *SUMO4* for pTXB1 from aa 1 with N-terminal HA tag (fwd)
M#1-F1	GGTGGTTGCTCTTCCGCAACCGGTCGGCT GCTGAAAAACATC	Amplification of *SUMO4* for pTXB1 from aa 92 (rev)
M#1-F3	GGTGGTCATATGTACCCATACGATGTTCCA GATTACGCTGGATCCATGAGCGATCTGGAA GCAAAACCGAGC	Amplification of *SUMO5* for pTXB1 from aa 1 with N-terminal HA tag (fwd)
M#1-F4	GGTGGTTGCTCTTCCGCAACCAATCTGCTC TTGATAAACTTCGATAACG	Amplification of *SUMO5* for pTXB1 from aa 96 (rev)
M#1-F6	GGTGGTCATATGTACCCATACGATGTTCCA GATTACGCTGGATCCATGGCAGCACCGCT GTCAGTTGAAG	Amplification of *URM1* for pTXB1 from aa 1 with N-terminal HA tag (fwd)

Name	Sequence (5' --> 3')	Purpose
M#1-F7	GGTGGTTGCTCTTCCGCAACCATGCAGGG TGCTAATAAACAGAACG	Amplification of *URM1* for pTXB1 from aa 100 (rev)
M#1-F9	GGTGGTCATATGTACCCATACGATGTTCCA GATTACGCTGGATCCATGAGCAAAGTTAGC TTCAAAATTACCCTGAC	Amplification of *UFM1* for pTXB1 from aa 1 with N-terminal HA tag (fwd)
M#1-F10	GGTGGTTGCTCTTCCGCAAACACGATCACG CGGAATAATACGCAG	Amplification of *UFM1* for pTXB1 from aa 82 (rev)
M#2-A8	GGTGGTCATATGTACCCATACGATGTTCCA GATTACGCTGGATCCATGAGCTGTGTTCAT TACAAATTCAGCAGC	Amplification of *DWNN* for pTXB1 from aa 1 with N-terminal HA tag (fwd)
M#2-A9	GGTGGTTGCTCTTCCGCAACCAATCGGAAT ACGACGAACAATAACGC	Amplification of *DWNN* for pTXB1 from aa 78 (rev)

3.1.7 Plasmids

Table 8: List of plasmids used in this study

Identifier	Insert	Backbone	Source
MG1-6	Ub^{1-74}-CCPGCC	pET17b	Komander lab
MG1-7	2xUb^{1-76} (M1)	pET17b	Komander lab
MG1-11	Ub^{1-75} intein	pTXB1	Komander lab
MG1-13	Mouse E1, UBA1	pET21d	Addgene #34965
MG1-18	UBE2S-UBD	pGEX-6P1	Komander lab
MG1-19	AREL1	pOPINS	Komander lab
MG1-20	UBE3C	pOPINS	Komander lab
MG1-24	OTUB1*, UBE2D2 fused to an inactive E2	pOPINB	Komander lab
MG1-28	OTULIN	pOPINB	Komander lab
MG1-31	AMSH*, mSTAM2 VHS-UIM	pOPINB	Komander lab
MG1-77	UBE2L3	pGEX-6P1	Dundee
MG1-78	UBE2N	pGEX-6P1	Dundee
MG1-79	UBE2R1	pGEX-6P1	Dundee
MG1-80	UBE2V1A	pGEX-6P1	Dundee
MG1-81	UBE2I, UBC9	pGEX-6P1	Dundee
MG1-82	Ub^{1-75}	pET17b	Komander lab
MG2-45	Ub K48R	pET17b	Komander lab
MG2-46	Ub K63R	pET17b	Komander lab
MG2-50	Ub WT	pET17b	MG lab
MG2-53	HA-$SUMO1^{1-96}$ intein	pTXB1	MG lab
MG2-54	HA-$SUMO2^{1-92}$ intein	pTXB1	MG lab
MG2-56	HA-$ISG15^{1-156}$ intein	pTXB1	MG lab
MG3-2	$USP53^{20-383}$	pOPINK	MG lab
MG3-6	$USP54^{21-385}$	pOPINK	MG lab
MG3-27	$USP53^{20-383}$ C41A	pOPINK	MG lab
MG3-29	$USP54^{21-283}$ C42A	pOPINK	MG lab
MG3-41	HA-$SUMO4^{1-92}$ intein	pTXB1	This study
MG3-43	HA-$SUMO5^{1-96}$ intein	pTXB1	This study
MG3-45	HA-$URM1^{1-100}$ intein	pTXB1	This study
MG3-47	HA-$UFM1^{1-82}$ intein	pTXB1	This study
MG3-75	HA-$DWNN^{1-78}$ intein	pTXB1	This study
MG5-12	Ub^{1-76} intein	pTXB1	MG lab
MG6-23	His-GST-3C-HA-$FUBI^{1-73}$ C57L intein	pTXB1	MG lab

Identifier	Insert	Backbone	Source
MG7-2	USP53$^{20-383}$ C41S	pOPINK	This study
MG7-3	USP53$^{20-383}$ R99S	pOPINK	This study
MG7-5	USP54$^{21-283}$ C42S	pOPINK	This study
MG7-44	Ub$^{1-75}$-CA	pET17b	This study
MG7-45	Ub$^{1-75}$-WSCCPGCC	pET17b	This study
MG7-48	Ub K63C	pET17b	This study
MG7-49	Ub K48C	pET17b	This study
MG7-54	USP54$^{21-369}$	pOPINK	This study
MG7-55	Ub K63R I44A	pET17b	MG lab
MG7-56	Ub K63R F4R	pET17b	MG lab
MG7-57	Ub K63R V70A	pET17b	MG lab
MG7-58	Ub K63R R42E	pET17b	MG lab
MG7-59	Ub K63R H68R	pET17b	MG lab
MG7-60	Ub I44A	pET17b	MG lab
MG7-61	Ub K6E	pET17b	MG lab
MG7-62	Ub$^{1-75}$ I44A	pET17b	MG lab
MG7-63	Ub$^{1-75}$ F4R	pET17b	MG lab
MG7-64	Ub$^{1-75}$ F4A	pET17b	MG lab
MG7-65	USP54$^{21-369}$ F161K	pOPINK	MG lab
MG7-75	UBE2S	pOPINK	This study
MG7-77	UBE2I, Ubc9	pOPINB	This study
MG7-81	GFP-C-LACEtag	pOPINB	This study
MG7-84	USP54$^{21-35}$-LGNT-$^{42-369}$	pOPINK	This study
MG7-87	USP53$^{20-34}$-LGNT-$^{41-383}$	pOPINK	This study
MG7-89	USP54$^{21-369}$ H302A	pOPINK	This study
MG7-91	USP54$^{21-369}$ R100A	pOPINK	This study
MG7-92	USP53$^{20-383}$ H301A	pOPINK	This study
MG11-3	Ub$^{1-75}$ Q62A E64A	pET17b	This study
MG11-4	USP53$^{20-383}$ Y160K	pOPINK	MG lab
MG11-11	USP53$^{20-368}$	pOPINK	This study
MG11-16	USP53$^{20-383}$ N34A	pOPINK	This study
MG11-17	USP54$^{21-369}$ N35A	pOPINK	This study
MG11-22	Ub$^{1-75}$ K48R	pET17b	This study
MG11-23	Ub$^{1-75}$ K63R	pET17b	This study

3.1.8 Software

Table 9: List of software used in this study

Name	Description	Supplier
Adobe Illustrator 2023	Vector graphics	Adobe
Aimless 1.12.10	Data analysis	Bio-Rad
ASTRA 7.3.2.21	Data collection and analysis	Wyatt Technology
CFX Maestro 4.1.2433.1219	Data collection and analysis	Bio-Rad
ChemDraw	Chemical structure visualization	PerkinElmer Inc.
Coot 0.7.1	Protein modelling	[222]
CRANK2 2.9.281	X-ray structure solution	[223]
Dials 3.5.0	Data analysis	[224]
Excel	Data analysis	Microsoft Corporation
ImageJ 1.53	Image analysis	[225]
ImageLab 2.4.0.03	Imaging	Bio-Rad
MR Phaser 2.8.3	Data analysis	[226]
OpenLab CDS 2.4	Data collection and analysis	Agilent
Origin 2019b	Data analysis and visualization	OriginLab Corporation
Phenix.Refine 1.19.2	Protein structure refinement	[227]
PISA webserver	Interface are calculation	[228]
Prism 9	Data analysis and visualization	GraphPad Software
Promass 3.Orev12	Mass spectra deconvolution	Enovatia
PyMOL 2.5.5	Protein structure analysis and visualization	Schrödinger LLC
Rock Maker 3.10	Protein crystallization	Formulatrix
SparkControl 2.3	Data collection and analysis	Tecan
SwissModel webserver 4.0	Homology model building	[229]

3.2 Methods

3.2.1 General procedures

3.2.1.1 Restriction/ligation cloning

Restriction/ligation cloning was used to integrate ubiquitin or ubiquitin like protein encoding DNA fragments into the pTXB1 vector in front of the intein and the chitin binding domain encoding sequences.

Inserts were amplified by polymerase chain reaction (PCR) in a solution containing 1 µl of a 1:1000 dilution of template DNA (50-100 ng/µl), 1x HF Phusion polymerase buffer (NEB), 200 nM dNTPs (NEB), 5 nM of the forward and reverse primers, 0.5 µl Phusion polymerase (NEB) and ddH_2O in a reaction volume of 50 µl according to Table 10. Purification of the PCR reactions was conducted in two ways: directly using the QIAquick PCR Purification Kit (Qiagen) and after agarose gel electrophoresis by using the QIAquick Gel Extraction Kit (Qiagen).

Table 10: Temperature cycling PCR program for insert amplification

Step	Temperature	Duration	
Initial denaturation	98 °C	60 s	
Denaturation	98 °C	10 s	35x
Primer annealing	55-58 °C	20 s	
Elongation	72 °C	30 s per 1 kbp	
Elongation	72 °C	360 s	
	12 °C	∞	

The purified amplified inserts and the pTXB1 expression vector were cleaved with the restriction enzymes *SapI* and *NdeI* and then purified using the QIAquick PCR Purification Kit (Quiagen). Importantly, water was used for elution. The ligation reaction was performed using 100 ng of the cut vector and 50 ng of the insert, 1x T4 DNA ligase buffer (NEB), and 1 µl T4 DNA ligase (NEB) in a total volume of 20 µl in ddH_2O for 20 min at room temperature. Subsequently, the mixture was used for bacterial transformation (3.2.1.5).

3.2.1.2 In-Fusion cloning

In-Fusion reactions were conducted with amplified inserts and linearized vectors exhibiting a 15-base pair (bp) overlap at their ends. Generally, *KpnI-HF* and *HindIII-HF* linearized pOPINB and pOPINK vectors were used as backbones. The inserts were first amplified by PCR using primers that contained 15 bp extensions that were complementary to the linearized pOPINB and pOPINK vectors and then purified as detailed in section 3.2.1.1. 50-100 ng of linearized

vector and 50-100 ng of inserts were combined with 0.5 µl of In-Fusion cloning mix (TaKaRa) and ddH_20 in 5 µl reactions. These were then incubated at 50 °C for 15 min and subsequently then used for bacterial transformation (3.2.1.5).

3.2.1.3 Splicing by overlap extension-PCR

Splicing by overlap extension (SOE)-PCR enables the combination of two DNA fragments into one fragment and the introduction of additional DNA base pairs into an existing DNA sequence. Here, SOE-PCR was employed to replace the DNA sequence coding for EPGQNS with LGNT in USP53 and USP54. Two DNA fragments were amplified as described in section 3.2.1.1. Fragment 1 corresponded to $USP53^{20-34}$ or $USP54^{21-35}$, while fragment 2 corresponded to $USP53^{41-383}$ or $USP54^{42-369}$. The reverse primer for fragment 1 and the forward primer for fragment 2 were designed to encode the LGNT sequence and also to create an overlap between the two DNA fragments. Following agarose gel purification, 1 µl of each 1:200 dilution of fragment 1 and fragment 2, were used as templates in the same PCR, which was performed as described in section 3.2.1.1 using the forward primer for fragment 1 and the reverse primer for fragment 2. The resulting combined DNA insert was purified by agarose gel electrophoresis and by using the QIAquick Gel Extraction Kit (Qiagen), and subsequently used for InFusion cloning (3.2.1.2).

3.2.1.4 Site-directed mutagenesis

The QuikChange method was used for site-directed mutagenesis. The reverse and forward primers (Table 7) were complementary to opposite strands of the template plasmid, and contained the desired mutations. The primers were designed using the QuikChange Primer Design webtool from Agilent. A total of 50 ng of template plasmid DNA was combined with 1x HF Phusion polymerase buffer, 200 nM deoxynucleotides, 5 nM of the reverse and forward primers and ddH_2O in a reaction volume of 20 µl. Lastly, 0.2 µl of Phusion polymerase was added to the mixture, which was subjected to a three-set temperature cycling program (Table 11).

Table 11: Temperature cycling PCR program for site-directed mutagenesis

Step	Temperature	Duration	
Initial denaturation	95 °C	30 s	
Denaturation	95 °C	10 s	18x
Primer Annealing	55 °C	20 s	
Elongation	72 °C	30 s per 1 kbp	
	12 °C	∞	

Following PCR, 1 µl *DpnI* was added to digest the methylated template DNA. After incubation for 3 h at 37 °C or overnight at 22 °C, the reaction mixtures were used for the transformation of competent *E. coli* cells (3.2.1.5).

3.2.1.5 Transformation of chemically competent E. coli and plasmid isolation

A volume of 50-100 µl of chemically competent TOP10 cells was transformed with 1-3 µl of DNA or plasmids obtained by cloning methods described in sections 3.2.1.1-3.2.1.4. The mixture was incubated for 30 minutes on ice, subjected to a heat shock at 42 °C for 45 seconds. and cooled down on ice for 2 min. Subsequently, 1 ml LB medium was added, and the cells were incubated at 37 °C for 45 min while shaking at 800 rpm. Following centrifugation (10,000xg, 1min, room temperature), the supernatant was discarded, and the cells were resuspended in approximately 50 µl residual liquid. The suspension was then spread out on a selective LB agar plate and incubated overnight at 37 °C. Single clones were picked and cultivated overnight at 37 °C in 5 ml of LB medium containing the respective antibiotic. Plasmid DNA was extracted from TOP10 cells using the QIAprep Spin Miniprep Kit (Qiagen). Successful cloning or the correct insertion of the mutation was verified by Sanger sequencing by Eurofins or Seqlab.

3.2.1.6 Sodium dodecylsulphate polyacrylamide gel electrophoresis (SDS-PAGE)

SDS-PAGE was used to separate proteins according to their respective molecular weights. Samples were prepared by the addition of 1.3x NuPAGE LDS sample buffer to protein solutions which served to denature the proteins. The protein samples were loaded onto NuPAGE Bis-Tris or Tris-Acetate gradient gels (Invitrogen) and proteins were separated at a constant voltage of 160 V for ~40 min – in NuPAGE MES SDS running buffer or Tris-acetate running buffer, respectively. For protein band detection, the gels were either imaged directly, stained with InstantBlue solution while gently shaking and then washed with deionized water, or silver stained using the Silver Stain Plus kit (Bio-Rad) according to the instructions provided. Imaging was done using a Chemidoc MP Imaging System (BioRad).

3.2.1.7 Heterologous protein expression in E. coli

Proteins were expressed using Rosetta 2(DE3)pLacI cells. The main expression cultures were inoculated in a 1:100 ratio from an overnight preculture of *E. coli* cells, transformed with the appropriate plasmid encoding the protein of interest in 2YT medium, and cultured at 37 °C with constant shaking (180 rpm). Upon reaching an OD_{600} of approximately 0.8, the cultures were cooled at 18 °C for a period of 30 min. Protein expression was then induced by the addition of 0.5 mM IPTG and conducted at 18 °C overnight. Bacterial cells were harvested by centrifugation and the cell pellets were stored at -80 °C until further use.

3.2.1.8 DNA and protein concentration determination

The concentrations of DNA and proteins were determined by absorbance measurements with a NanoDrop 2000 spectrophotometer. Protein concentrations were determined by absorbance measurements at 280 nm, while plasmid DNA concentration was determined at 260 nm. The extinction coefficient and the molecular weight of proteins were determined from their sequence using the program Protparam on the Expasy server.[230]

3.2.1.9 Thermal shift assay

Thermal shift assays (TSA) were employed to determine the stabilities of proteins and protein complexes. In general, protein samples were assayed at a concentration of 3 µM in TSA buffer (20 mM HEPES pH 7.5, 100 mM NaCl, 5 mM DTT) with 3x SYPRO Orange dye. To obtain probe-labeled samples for TSA measurement, 6 µM apo protein solutions were incubated with 18 µM probe solutions overnight at 4 °C. Prior to measurement, the protein-probe mixture was mixed in a 1:1 ratio with SYPRO Orange dye solution (6x SYPRO Orange dye in TSA buffer). For the comparative measurement of USP54 F161K, USP54 F161K~Ub-PA and USP54 F161K~diUb-PA, samples underwent purification and were assayed in a PBS/Tris pH 8.0 buffer solution. Samples were added to white, 96 well PCR plates and measured in triplicate or in quadruplicate. A temperature gradient was applied, ranging from 20 to 90 °C, with an increment 0.3 °C and a hold time of 5 s before reading. Following each incremental temperature change, the fluorescence intensity was measured in the FRET channel (excitation: 450-490 nm, emission: 560-580 nm) using a CFX connect Real-Time PCR System (Bio-Rad). The data were analyzed automatically by the software CFX Maestro (Bio-Rad), which yielded the first derivative and the melting temperature as the inflection point of the melting curve.

3.2.1.10 SEC-MALS

Size exclusion chromatography with multi-angle light scattering (SEC-MALS) was conducted using an Agilent Infinity II HPLC system. This system was equipped with a Wyatt DAWN NEON 8 angle detector, an Optilab online refractive index detector, and an Agilent VWD UV detector. Protein solutions (60 µl at a concentration of 2 mg/ml) were injected and separated on a Superdex 75 Increase 10/300 column (Cytiva) with a flow rate of 0.5 mL/min in 20 mM Tris pH 8.0, 100 mM NaCl. Masses were determined using the Astra software (Wyatt Technology), which was calibrated with bovine serum albumin (BSA).

3.2.1.11 Intact protein mass spectrometry

For protein mass determination, protein samples were diluted to approximately 0.5-1 mg/ml in PBS and desalted on an AdvanceBioDesaltingRP 2.1x12.5 mm cartridge (Agilent) using a

gradient of 5-80% solvent B (solvent A = HPLC-grade water + 0.1% trifluoracetic acid; solvent B = HPLC-grade acetonitrile + 0.1% trifluoracetic acid). The desalting process was conducted at a flow rate of 0.4 ml/min, a runtime of 6 min, and a column temperature of 32 °C. The analysis was performed on an Agilent 1260 II Infinity system (Agilent), which was equipped with an electrospray ion source in positive mode. The capillary voltage was set at 4 kV, the desolvation gas flow was 80 L/min, and the temperature was 350 °C. The ProMass program (Enovatia) was used to deconvolute mass spectra.

3.2.2 Protein purification

Protein solutions were maintained at a temperature of 4 °C and all protein purification steps were conducted at this temperature unless otherwise specified. Following purification, concentrated protein samples were aliquoted, snap frozen in liquid nitrogen, and stored at -80 °C. The purity and identity of proteins were assessed by intact protein mass spectrometry (3.2.1.11). His-3C, GST-3C and His-TEV proteases used for tag cleavage during protein purification were obtained from Dortmund Protein Facility. If not indicated otherwise, all purification steps were performed on an ÄKTA pure protein purification system (GE Healthcare/Cytiva).

3.2.2.1 Ubiquitin and ubiquitin variants

Acidic precipitation, cation exchange chromatography and size exclusion chromatography were employed to obtain pure ubiquitin species.[231] These included ubiquitin, M1-linked diubiquitin, M1-linked tetraubiquitin and ubiquitin variants, including Ub^{1-74}-CCPGCC, Ub^{1-75}-CA, Ub K63R, Ub K6E, Ub I44A, Ub K63R/R42A, Ub K63R/I44A, Ub K63R/H68R, Ub K63R/V70A, Ub K63R/F4R, Ub^{1-75}, Ub^{1-75} F4A, Ub^{1-75} F4R, Ub^{1-75} I44A and Ub^{1-75} Q62A/E64A. Following protein expression, the cell pellets were resuspended in ubiquitin lysis buffer (20 mM Tris pH 7.4, 2 mM EDTA) supplemented with lysozyme and DNAseI, and lysed by sonication (55% amplitude, 10''on/10''off) on ice. The lysate was then clarified by centrifugation, after which the supernatant was brought to 0.5% (v/v) perchloric acid, while being cooled on ice. The remaining soluble protein was subsequently dialyzed against buffer S (50 mM NaOAc, pH 4.5). Cation exchange chromatography using a HiPrep SP FF 16/10 column (GE Healthcare), with an elution gradient ranging from 0 to 1000 mM NaCl in buffer S and SEC using a HiLoad 16/600 Superdex 75 pg column in phosphate buffered saline (PBS) resulted in the isolation of pure ubiquitin species.

3.2.2.2 Purification of ubiquitin or ubiquitin-like protein (Ubl)-thioesters

To obtain ubiquitin or Ubl species with a thioester functionalized C-terminus as precursors for probe generation, their DNA sequences were cloned from codon-optimized gene strings into

the pTXB1 vector upstream of the intein and chitin-binding domain sequence. The purification procedure was conducted as reported previously, with intein-mediated cleavage induction by the addition of MesNa.[109] The Ub^{1-76}-MesNa as building block for ubiquitinating GFP was generated in an identical procedure to that used for Ub^{1-75}-MesNa.

3.2.2.3 Purification of the catalytic domains of USP53 and USP54

The catalytic domains of USP53 and USP54 were expressed as fusion proteins with N-terminal polyhistidine-GST tags. Their purification process involved multiple steps, including nickel NTA affinity purification (Ni-NTA), reverse Ni-NTA, anion exchange chromatography and size exclusion chromatography (SEC). The same purification procedure was performed for all variants including USP53 C41A, USP54 C42A, USP53 C41S, USP54 C42S, USP53 H301A, USP54 H302A, USP54 LGNT, USP53 LGNT, USP53 N34A, USP54 N35A, USP53 Y160K, USP54 F161K, USP53 R99S, and USP54 R100A. First, the corresponding bacterial cells were resuspended in buffer N (20 mM NaH_2PO_4 pH 8.0, 300 mM NaCl, 20 mM imidazole, 4 mM ß-ME) supplemented with DNAseI, lysozyme, EDTA-free protease inhibitor cocktail (1 tablet/100 mL, Roche) and 1 mM phenylmethylsulfonyl fluoride (PMSF). The cell suspension was subjected to sonication (55% amplitude, 5''on/10''off) while being kept cool in a water-ice bath. Following sonification, the mixture was centrifuged, and the cleared lysate was filtered through a 45 µm filter. Next, the filtered lysate was applied to a Ni-NTA FF column (Cytiva) preequilibrated with buffer N. Bound proteins were eluted using buffer N supplemented with 500 mM imidazole. Elution fractions containing USP53 or USP54 were combined. After addition of His-3C protease to cleave off the 6x-GST tag, the protein solution was dialyzed overnight against buffer N supplemented with 4 mM ß-ME. The subsequent purification step involved a reverse Ni-NTA. For this, the protein solution was manually passed through a preequilibrated Ni-NTA FF column (Cytiva) using a peristaltic pump (Bio-Rad). The flow-through was dialyzed against low salt (LS) buffer (25 mM Tris pH 8.5, 50 mM NaCl, 4 mM ß-ME). Subsequently, the sample was subjected to anion exchange chromatography on a Resource Q (ResQ) column (GE Healthcare). After column loading and washing using LS buffer, bound proteins were eluted with a salt gradient ranging from 50 to 500 mM NaCl in LS buffer. Fractions containing the target protein were combined, concentrated, and subjected to SEC using DUB buffer (20 mM Tris pH 8.0, 100 mM NaCl, 4 mM ß-ME, 5 % glycerol) or storage buffer (20 mM Tris pH 8.0, 100 mM NaCl, 4 mM DTT, 5% glycerol) on a HiLoad 16/600 Superdex 75 pg column (GE Healthcare). Alternatively, the anion-exchange chromatography fractions were buffer exchanged into storage buffer.

3.2.2.4 Ubiquitin chain conjugating enzymes

The mouse E1 enzyme was purified by Ni-NTA and ResQ as described for USP53 and USP54 (3.2.2.3). Subsequent SEC was performed on a HiLoad 16/600 Superdex 200 pg column (GE Healthcare) in storage buffer. UBE2N and UBE2S were purified by Ni-NTA, reverse Ni-NTA and SEC as described for USP53 and USP54 (3.2.2.3), except that SEC was performed in storage buffer.

UBE2R, UBE2V, UBE2S-UBD and UBE2L were expressed as GST fusion proteins and purified by the Dortmund Protein Facility using GST affinity chromatography, on-column cleavage with GST-3C and SEC on a HiLoad 16/600 Superdex 75 pg column in storage buffer that contained 1mM TCEP instead of 4 mM DTT as reducing agent. The DUBs OTUB1* and AMSH* were expressed as polyhistidine tag fusion proteins and purified by the Dortmund Protein Facility using Ni-NTA, on-column cleavage with His-3C protease and SEC on a HiLoad 16/600 Superdex 75 pg column in storage buffer that contained 1mM TCEP instead of 4 mM DTT as reducing agent.

NleL was expressed as GST fusion protein and purified by GST affinity purification. After cell resuspension in GST lysis buffer (50 mM Tris pH 8.0, 500 mM NaCl, 1 mM EDTA, 10% glycerol, 10 mM ß-ME) and lysis by sonication, the cleared lysate was filtered and incubated for 1 h at 4 °C with GSH beads equilibrated in lysis buffer. The GSH beads with bound protein were first washed with GST high salt (HS) buffer (50 mM Tris pH 8.0, 500 mM NaCl, 10 mM ß-ME) and then with GST LS buffer (50 mM Tris pH 8.0, 150 mM NaCl, 10 mM ß-ME) in a gravity flow column. On-bead cleavage was performed with His-TEV protease overnight at 4 °C. The flow-through and the wash with GST LS buffer of the beads containing the protein of interest were combined, concentrated, aliquoted, and directly snap-frozen in liquid nitrogen.

3.2.2.5 Additional proteins

ULP1 was obtained from the Dortmund protein facility. USP2 and USP8 were purified by Dr. Malte Gersch. GFP-C-LACE-tag was expressed with a cleavable N-terminal polyhistidine tag. The used GFP sequence has been reported previously[232] and the sequence of the C-terminal LACE tag was adopted from the literature.[196]

Ubc9 was expressed with an N-terminal polyhistidine tag that was not cleaved during purification. Pure His-Ubc9 was obtained by Ni-NTA and SEC as described for USP53 and USP54 (3.2.2.3) except that SEC was performed in storage buffer.

3.2.3 DUB substrate generation

3.2.3.1 Generation of di, tri, tetra, and polyubiquitin chains of specific linkages

Ubiquitin chains of defined linkages were enzymatically generated at 37 °C from single ubiquitin moieties using specific E1, E2, E3 and DUB combinations in conjugation buffer (40 mM Tris pH 8.5, 10 mM $MgCl_2$, 10 mM ATP). Assembly reactions were conducted at 37 °C, the progress was monitored by intact protein mass spectrometry (3.2.1.11), and the reactions were stopped by the addition of 10 mM DTT. Concentrations and identities of the used enzymes and assembly reactions times are given in Table 12 and were used based on reported conditions.[183] K11-linked diubiquitin chains were obtained by using the E2 fusion protein UBE2S-UBD. To obtain K11-linked tetraubiquitin chains, UBE2S was used instead as the E2 enzyme and K11-linked diubiquitin chains were used as building blocks.

Table 12: Combinations and concentrations of enzymes to assemble specifically linked ubiquitin chains

	K6	K11	K48	K63
Ubiquitin	2.5 mM	2.5 mM/0.5 mM	2.5 mM	1.5 mM
mE1	200 nM	250 nM	1 µM	1 µM
E2	600 nM UBE2L3	20 µM UBE2S-UBD/ 10 µM UBE2S	25 µM UBE2R	8 µM UBE2V2 8 µM UBE2N
E3	10 µM NleL	-	-	-
Reaction time	3 h	8 h/48 h	3 h	3 h
DUB	2 µM OTUB1*, 16 h	2 µM AMSH*, 16 h	-	-

The reaction mixtures containing specifically linked chains of different lengths were first diluted in buffer S, then subjected to cation exchange chromatography on a ResS column, and eluted with a gradient of 0 to 1000 mM NaCl in buffer S to separate the ubiquitin chains according to their length. Fractions containing diubiquitin, triubiquitin, tetraubiquitin, or polyubiquitin with chains of at least five ubiquitins were individually combined. Subsequently, the chains of a specific length were further purified by SEC using a HiLoad 16/600 Superdex 75 pg column in PBS.

M1-linked diubiquitin and tetraubiquitin chains were expressed in *E. coli* and purified as described for ubiquitin (3.2.2.1).

Enzymatically assembled K29- and K33-linked tetraubiquitin chains were obtained from commercial sources.

3.2.3.2 Ub-KG-TAMRA

Ub-KG-TAMRA was prepared using a methodology developed by Dr. Zhou Zhao.[99] However, slightly modified reactions times, a higher concentration of KG-TAMRA and a streamlined purification procedure were used. Ub^{1-76}-hydrazide was obtained from Ub-MesNa as described.[99] To a precooled solution of 250 µl of 1.8 mM Ub^{1-76}-hydrazide, precooled solutions of 125 µl of 1 M $NaNO_2$ and 125 µl of 200 mM citric acid were added and incubated in a sodium chloride-ice-water bath at -10 °C for 20 min. Then, 500 µl of 20 mM KG-TAMRA (molecule provided by Dr. Zhou Zhao) in 1.5 M HEPES pH 8.0 was added and incubated at 30 °C for 1 hour. Unreacted KG-TAMRA and diubiquitin by-products were removed by SEC in buffer M (20 mM MES pH 8.0). Ub-KG-TAMRA containing fractions were combined, diluted in buffer S and subjected to cation exchange chromatography on a ResS column. Elution was performed with a gradient ranging from 0 to 300 mM NaCl in buffer S and pure Ub-KG-TAMRA was obtained by combining fractions containing the correct protein species.

3.2.3.3 Generation of TAMRA-maleimide labeled K63-linked ubiquitin chains

The introduction of a C-terminal cysteine and alanine to a truncated ubiquitin (Ub^{1-75}-CA) allowed fluorescent labeling of the proximal ubiquitin in polyubiquitin chains with tetramethylrhodamine (TAMRA)-maleimide. All samples were protected from light during and after the labeling reactions.

K63-linked diubiquitin chains containing Ub^{1-75}-CA as proximal ubiquitin (Ub K63R-Ub^{1-75}-CA) were generated enzymatically by incubating 900 µM Ub K63R with 1.3 mM Ub^{1-75}-CA in K63 linkage assembly buffer (40 mM Tris, pH 8.5, 10 mM $MgCl_2$, 1 µM E1, 8 µM UbeV1, 8 µM Ube2N, 10 mM ATP) for 3 h at 37 °C.

K63-linked triubiquitin chains containing Ub^{1-75}-CA as proximal ubiquitin (Ub_2-Ub^{1-75}-CA) were generated by incubating 180 µM K63-linked diubiquitin with 1800 µM Ub^{1-75}-CA in K63 linkage assembly buffer at 37 °C until all diubiquitin was consumed. The 1:10 ratio was used to favor formation of triubiquitin over tetraubiquitin species.

K63-linked tetraubiquitin chains containing Ub^{1-75}-CA as proximal ubiquitin (Ub_3-Ub^{1-75}-CA) were generated by incubating 80 µM Ub_2-Ub^{1-75}-CA with 500 µM Ub K63R in K63 linkage assembly buffer for 2 h at 37 °C.

The protein mixtures were diluted in buffer S, loaded on a ResS column, and eluted with a gradient ranging from 0 to 1000 mM NaCl in buffer S. The purified products Ub K63R-Ub^{1-75}-CA, Ub_2-Ub^{1-75}-CA and Ub K63R-Ub_2-Ub^{1-75}-CA were then buffer exchanged into labeling buffer (1xPBS, 1 mM TCEP) and labeled with a 1.1 molar equivalent of TAMRA maleimide. The reaction was terminated after 1 h incubation at RT and stopped by the addition of 5 mM DTT. Extensive dialysis against PBS removed excess dye and subsequent SEC on a HiLoad 16/600 Superdex 75 pg column in PBS provided pure labeled K63-linked ubiquitin chains.

3.2.3.4 Generation of monoubiquitinated GFP

The model substrate GFP-C-LACE-tag (GFP-LT) was monoubiquitinated via lysine acylation using conjugating enzymes (LACE) adapted from Hofmann et al.[196] For this, 60 µM GFP-LT, 60 µM His-Ubc9, 150 µM Ub^{1-76}-MesNa and 1 mM Ac-Cys-NHMe (generated by Dr. Christian Grethe, CG263) were combined in LACE reaction buffer (50 mM HEPES pH 7.6, 50 mM KCl) and incubated for 24 h at 30 °C. After dilution in buffer N, reverse Ni-NTA was performed on a Ni-NTA FF column (Cytiva) equilibrated in binding buffer. The flow-through was dialyzed into LS buffer and anion exchange chromatography was performed using a ResQ column. Proteins were eluted with a gradient from 50 to 125 mM NaCl in LS buffer. Fractions containing GFP-LT monoubiquitinated at its LACE-tag (GFP-mUb) were combined and further purified by SEC on a HiLoad 16/600 Superdex 75 pg column in PBS.

3.2.3.5 Generation of ubiquitin building blocks

K63-linked Ub K63R – Ub and Ub K63R – Ub – Ub were generated by setting up 0.6 mM Ub with 3 mM Ub K63R or 160 µM K63-linked diUb with 1.2 mM Ub K63R in K63 linkage assembly buffer (40 mM Tris, pH 8.5, 10 mM $MgCl_2$, 1 µM mE1, 8 µM UbeV1, 8 µM Ube2N, 10 mM ATP), respectively.

K48-linked Ub K48R – Ub was generated by mixing 2.5 mM Ub K48R with 250 µM Ub (10:1 ratio) in K48 linkage assembly buffer (40 mM Tris, pH 8.5, 10 mM $MgCl_2$, 1 µM mE1, 25 µM Ube2R, 10 mM ATP).

Assembly reactions were monitored by intact protein LC-MS and stopped after 6-16 h incubation at 37 °C by addition of 10 mM DTT. For purification, reaction mixtures were diluted in buffer S and subjected to cation exchange chromatography on a ResS column (GE Healthcare) with a gradient ranging from 0 to 1000 mM NaCl in buffer S, followed by SEC on a HiLoad 16/600 Superdex 75 pg column in PBS.

3.2.3.6 Generation of polyubiquitinated GFP

GFP-mUb was further ubiquitinated by enzymatic assembly reactions at 37 °C for 6-16 h using ubiquitin variants or previously assembled and purified ubiquitin building blocks. Samples were protected from light during the reactions and subsequent purification steps.

To obtain GFP-LT modified with K63-linked diubiquitin, triubiquitin or tetraubiquitin, 50 µM GFP-mUb was mixed with either 200 µM Ub K63R or 100 µM K63-linked diUb (Ub K63R – Ub) or 100 µM K63-linked triUb (Ub K63R – Ub – Ub), respectively. All reactions were set up in K63 linkage assembly buffer.

GFP-LT modified with K48-linked diubiquitin and triubiquitin was obtained by combining 50 µM GFP-mUb with 200 µM Ub K48R or 100 µM K48-linked diUb (Ub K48R – Ub) in K48 linkage assembly buffer.

GFP-Ub_n containing reaction mixtures were diluted in LS buffer (20 mM Tris pH 8.5, 50 mM NaCl), loaded onto a ResQ column (GE Healthcare) and eluted by a gradient of 50 to 500 mM NaCl in LS buffer. Protein fractions containing pure K63-linked polyubiquitinated GFP species were combined and buffer exchanged into PBS. Fractions containing K48-linked polyubiquitinated GFP species were further purified by SEC on a HiLoad 16/600 Superdex 75 pg column in PBS.

3.2.3.7 Generation of triubiquitin chains of mixed linkages

Triubiquitin chains containing mixed K48 and K63 linkages were generated by two consecutive conjugation reactions from specific ubiquitin moieties to ensure that only defined linkages can be generated. This also meant that each ubiquitin building block had a different mass enabling the differentiation of cleavage products in mass spectrometry-based cleavage assays. For the comparison of cleavage of mixed triubiquitin chains with homotypic triubiquitin chains, additionally K63-linked and K48-linked triubiquitin chains of the same ubiquitin moieties as building blocks were generated. The annotation K63-K48-linked triubiquitin chains labels a K63 linkage between the distal and middle ubiquitin and a K48 linkage between the middle and proximal ubiquitin in the triubiquitin chain. The same notation was applied to all generated mixed triubiquitin chains. Triubiquitin chains containing mixed M1 and K63 linkages were generated by a single conjugation reaction using M1-linked diubiquitin chains and either Ub K63R or Ub^{1-75} as building blocks. All reactions were performed at 37 °C, progress was monitored by intact protein mass spectrometry (3.2.1.11), and reactions were stopped after 3-12 h incubation by addition of 10 mM DTT. Each conjugation reaction product was purified as described for wild-type ubiquitin chains (3.2.2.1) prior to use in another assembly reaction or in cleavage assays. The used ubiquitin variants and their concentrations are detailed in Table 13. K63 linkage assembly buffer included 40 mM Tris pH 8.5, 10 mM MgCl2, 1 µM mE1, 8 µM UbeV1, 8 µM Ube2N and 10 mM ATP, while K48 linkage assembly buffer included 40 mM Tris pH 8.5, 10 mM MgCl2, 1 µM mE1, 25 µM Ube2R and 10 mM ATP. The homotypic K63-linked triubiquitin chains generated in this way were also used for the co-crystallization attempt with USP53 C41S and USP54 C42S (4.3.2).

Table 13: Concentrations of ubiquitin building blocks used in assembly reactions to generate mixed triubiquitin chains

Reaction product	Reaction 1	Reaction 2
K63-K48 mixed triUb: Ub K63R – Ub – Ub^{1-75} K63R	0.5 mM Ub, 3 mM Ub^{1-75} K63R, K48 linkage assembly buffer	440 µM Ub K63R, 220 µM reaction 1 product, K63 linkage assembly buffer
K48-K63 mixed triUb: Ub K48R – Ub – Ub^{1-75} K48R	0.5 mM Ub, 3 mM Ub^{1-75} K48R, K63 linkage assembly buffer	550 µM Ub K48R, 275 µM reaction 1 product, K48 linkage assembly buffer
K63-K63 triUb: Ub K63R – Ub – Ub^{1-75}	0.6 mM Ub, 3 mM Ub^{1-75} K63 linkage assembly buffer	5 mM Ub K63R, 528 µM reaction 1 product, K63 linkage assembly buffer
K48-K48 triUb: Ub K48R – Ub – Ub^{1-75}	0.5 mM Ub, 3 mM Ub^{1-75} K48 linkage assembly buffer	450 µM Ub K48R, 204 µM reaction 1 product K48 linkage assembly buffer
M1-K63 mixed triUb: Ub – Ub – Ub^{1-75}	500 µM M1-linked diUb, 3 mM Ub^{1-75}, K63 linkage assembly buffer	
K63-M1 mixed triUb: Ub K63R – Ub – Ub	150 µM M1-linked diUb, 1.5 mM Ub K63R, K63 linkage assembly buffer	

3.2.3.8 Generation of K63-linked triubiquitin chains with mutations in specific ubiquitin moieties

Similar to the generation of mixed-linked triubiquitin chains, K63-linked triubiquitin chains with mutations in specific ubiquitin moieties were generated by two consecutive conjugation reactions from specific ubiquitin moieties as building blocks. In general, shortened Ub^{1-75} was used as the building block for the proximal ubiquitin in the chain, wild-type ubiquitin as the middle ubiquitin and Ub K63R as the distal ubiquitin. To test the effect of mutations at specific positions in the K63-linked triubiquitin chain on the cleavage activity of DUBs, these were introduced only into the respective ubiquitin building block according to the intended position of the mutation. The mutations are indicated by an X. Reactions were performed at 37 °C in K63 linkage assembly buffer, progress was monitored by intact protein mass spectrometry (3.2.1.11), and reactions were stopped after between 3 h up to 3 days of incubation by addition of 10 mM DTT. Purification was performed after each conjugation reaction as previously described for wild-type ubiquitin chains (3.2.3.1). The purified diubiquitin species obtained after

the first reaction step served as one building block in the second conjugation reaction. The concentrations of the ubiquitin building blocks for each conjugation step are detailed in Table 14.

Table 14: Concentrations of ubiquitin building blocks used in K63 linkage assembly reactions

Position of additional mutation	Reaction 1	Reaction 2
Distal ubiquitin	0.6 mM Ub, 3 mM Ub^{1-75}	0.5 mM Ub K63R/X, 180 mM reaction 1 product
Middle ubiquitin	0.6 mM Ub X, 3 mM Ub^{1-75}	1 mM Ub K63R, 250-300 µM reaction 1 product
Proximal ubiquitin	3 mM Ub K63R, 0.6 mM Ub	175 µM reaction 1 product, 175 µM Ub^{1-75} X

3.2.4 Generation of ubiquitin- and ubiquitin like protein-based probes

3.2.4.1 Ubiquitin or Ubl with a propargylamide warhead or a VS warhead

Ub/Ubl probes with C-terminal propargylamine (PA) and vinyl sulfone (VS) warheads were prepared as previously described through direct conversion of C-terminal protein thioesters with small molecule amines.[99,109] The vinyl sulfone-containing molecule was provided by Dr. Zhou Zhao.

3.2.4.2 K63-linked diUb-PA

High amounts of K63-linked diubiquitin-PA were obtained by combining 750 µM Ub-PA with 800 µM Ub K63R for 16 hours at room temperature in K63 linkage assembly buffer. After stopping the reaction by adding 10 mM DTT, the reaction mixture was diluted in buffer S, loaded onto a ResS column, and eluted with a gradient from 0 to 1000 mM NaCl in buffer S. Subsequent SEC using a HiLoad 16/600 Superdex 75 pg column in reaction buffer (20 mM Tris pH 7.7, 100 mM NaCl, 5 mM DTT) yielded pure diUb(K63)-PA.

3.2.4.3 Diubiquitin probes with in-between warheads

K48 and K63 linkage mimicking diUb probes with an in-between Michael acceptor warhead were generated according to reported methodology[217] with slight variations.

350 µM of Ub^{1-75}-MesNa, 40 mM *N*-hydroxysuccinimide, and 30 mM compound ZH107 were mixed, titrated to a pH of ~7-7.3 with 4 M NaOH and incubated for 24 h at room temperature to yield C-terminal modified ubiquitin. Deprotection was performed at a low pH of 1.3-1.6 reached by stepwise addition of 10% perchloric acid solution. Upon completion of deprotection after 7 days of incubation at room temperature, the protein mixture was extensively dialyzed against buffer D (20 mM Na_2HPO_4, 100 mM NaCl, pH 6.0). Coupling reactions were performed by mixing 1900 µl of the reaction mixture with a concentration of approximately 1.5 mg/ml with

either 408 µl of 10.1 mg/ml Ub K48C to obtain a K48 linkage mimicking diUb probe or with 594 µl of 14.7 mg/ml Ub K63C to obtain a K63 linkage mimicking diUb probe. Both diUb probes were purified by cation-exchange chromatography using a ResS column and a gradient from 0 to 1000 mM NaCl in buffer S and a subsequent SEC using a HiLoad 16/600 Superdex 75 pg column in buffer containing 20 mM MES pH 6.0 and 1 mM TCEP.
The diUb(K63)-2Br probe was generated by Dr. Zhou Zhao.

3.2.5 Crystallization

3.2.5.1 Generation of protein complexes used for crystallization

Purification of probe-labeled USP54 and USP53 complexes was performed as described in the protocol for the apo proteins, with the exception of an additional labeling step incorporated after reverse Ni-NTA chromatography. For this, the flow-through solution after reverse Ni-NTA chromatography containing USP53 or USP54 was buffer exchanged into buffer T (20 mM Tris pH 8.0, 100 mM NaCl, 5 mM DTT) using Amicons with a cutoff of 10 kDa and then concentrated to approximately 3-5 mg/ml total protein concentration, including any remaining impurities. Then, Ub-PA or diUb(K63)-PA probes were added in a 1.5-fold excess to the total DUB amount, and labeling was conducted overnight at 4 °C. Subsequent purification by anion exchange chromatography and SEC in buffer T was performed as described for unlabeled USP53 and USP53 (3.2.2.3), yielding the protein complexes used for crystallization (3.2.5.2). The following complexes were generated for coarse screening: USP54$^{21-385}$~mUb-PA at a concentration of 6.5 mg/ml, USP54$^{21-369}$~diUb(K63)-PA at a concentration of 13.4 mg/ml, USP53$^{20-383}$~mUb-PA at a concentration of 6 mg/ml, a mixture of USP53$^{20-383}$~diUb(K63)-PA and USP53$^{20-383}$ (70%/30%) at a concentration of 5 mg/ml, and USP53$^{20-368}$~diUb(K63)-PA at a concentration of 2.8 mg/ml. Two samples were prepared for finescreening of crystallization conditions for USP54 in complex with diUb(K63)-PA. The USP54$^{21-369}$~diUb(K63)-PA sample for finescreening of the initial K/Na-tartrate condition was concentrated to 11.8 mg/ml. Finescreening of the initial PeG400 condition was performed with a sample of a concentration of 13 mg/ml.
USP53$^{20-385}$ C41S and USP54$^{21-369}$ C42S used for co-crystallization with K63-linked triUb chains were purified as described above (3.2.2.3). K63-linked triUb chains were added in a molar ratio of 1.1:1 to not yet concentrated USP53 and USP54 solutions, obtained after SEC. Subsequently, both protein mixtures were concentrated to a final concentration of 8 mg/ml.

3.2.5.2 Crystallization conditions

Crystallization screens were set up using a Mosquito LCP robot (TTP Labtech) in 96 well sitting drop vapor diffusion plates (MRC format, Molecular Dimensions), incubated at 20 °C and

imaged according to a Fibonacci imaging schedule using a RockImager (Formulatrix). Coarse screening of prepared protein complexes (3.2.5.1) was performed with commercially available screening plates to identify initial crystallization conditions. Generally, crystallization drops for coarse screening were set up in a 1:1 ratio of protein solution to reservoir solution (200+200 µl or 150+150 µl). Fine screening plates were prepared with a Dragonfly robot (TTP Labtech) based on two initial conditions for which crystal growth of USP54~diUb(K63)-PA was observed. Based on the PEG400 condition, plates were prepared in which the concentration of $CaCl_2$ in the reservoir solutions was kept constant at 200 µM, while PEG400 was varied from 20% to 35% (w/v) and the pH of the HEPES buffer was varied from 6.8 to 8.0. Furthermore, a K/Na-tartrate-based fine screening plate was prepared in which the K/Na-tartrate concentration was varied from 0.6 to 1.1 M and the HEPES buffer was varied in pH from 6.8 to 8.0. 100 mM NaCl was added as a salt component to half of the plate. Drop ratios of 1:1, 1:2 and 2:1 were tested for the fine screening of USP54~diUb(K63)-PA. The crystal used for structure determination was obtained from a 500 + 500 nl drop of a 13 mg/ml USP54~diUb(K63)-PA solution in 20 mM Tris pH 8.0, 100 mM NaCl and 4 mM DTT and a reservoir solution containing 100 mM HEPES pH 6.8, 27.2% (v/v) PEG400 and 200 mM of $CaCl_2$. After fishing, the crystal was cryoprotected by soaking it briefly in a solution of 100 mM HEPES pH 7.3, 30% (v/v) PEG400 and 200 mM $CaCl_2$. Subsequently, the loop was immersed in liquid nitrogen, resulting in vitrification of the crystal.

3.2.5.3 Data collection, structure solution and refinement

Data on USP54~diUb(K63)-PA crystals were collected at 100 K at the Swiss Light Source (SLS, Villingen PSI, Switzerland) on beamline PX2. Anomalous datasets (collected at a wavelength of 1.2823 Å) and native datasets (collected at a wavelength of 1.000 Å) were obtained. The software DIALS[224] and AIMLESS[233] were used to integrate and scale the obtained diffraction data, respectively. The anomalous dataset of a well-diffracting USP54~diUb(K63)-PA crystal and the CRANK2 software[223] were employed to determine the positions and identities of the zinc atoms along with all protein chains. This information was used to generate a search model containing four truncated Alphafold models of USP54 (AF-Q70EL1-F1) and eight times the structure of free free ubiquitin (PDB: 1UBQ) in the correct orientation. Molecular replacement was performed with MR Phaser[226] on the native dataset using the search model, which solved the structure. Subsequent performance of multiple cycles of structure building in Coot[234] and refinement with Phenix.Refine[235] yielded the final USP54~diUb-PA model. The data collection and refinement statistics are presented in Table 15, and the data are available in the protein data bank under accession number 8C61. The PISA webserver was employed to calculate values characterizing the interfaces between USP54 and the ubiquitin moieties (https://www.ebi.ac.uk/pdbe/pisa/).

3.2.6 DUB reactivity and cleavage assays

3.2.6.1 Probe reactivity assay

To assess the reactivity of DUB and Ubl proteases with probes, the enzymes and probes were typically mixed in a 1:3 ratio in either PBS (pH 7.7) or in reaction buffer (20 mM Tris pH 7.7, 100 mM NaCl, 5 mM DTT). The final concentrations of DUBs ranged from 2 to 3.5 µM, while probe concentrations varied from 6 to 10.5 µM. Following a 60 min incubation at room temperature, the protein mixtures were subjected to SDS-PAGE and Coomassie-staining (3.2.1.6) to analyze labeling.

3.2.6.2 Ub/Ubl-RhodamineG cleavage assay

Fluorogenic Ub/Ubl-RhodamineG (Ub/Ubl-RhoG) substrate cleavage assays were performed in black 384 well low volume non-binding surface plates (Greiner). All samples were measured in triplicate and protein solutions were prepared in cleavage buffer (20 mM Tris pH 7.7, 100 mM NaCl, 5 mM DTT, 0.5 mg/ml BSA). Immediately following the addition of 10 µl of 2x Ub/Ubl-RhoG solution (final concentration of 50 nM) to 10 µl of 2x enzyme solution (final concentrations of 2 nM-4 µM), the fluorescence measurement (excitation: 492 nm, emission: 525 nm) was initiated and monitored for 1 h at 25 °C using a TECAN Spark plate reader.

3.2.6.3 Fluorescence polarization cleavage assay

Fluorescence polarization measurements were performed to monitor the cleavage of fluorescent Ub-KG-TAMRA, K63-linked diUb-TAMRA, and K63-linked triUb-TAMRA. All samples were measured in triplicate in black 384-well low volume non-binding surface plates (Greiner). Protein solutions were prepared in cleavage buffer (20 mM Tris pH 7.7, 100 mM NaCl, 5 mM DTT, 0.5 mg/ml BSA). 10 µl of the 2x substrate solution (final concentration of 50 nM) were added to the plates and incubated for 10 min. Subsequently, 10 µl of 2x enzyme solution (final concentrations of 0.0625 µM to 4 µM) were added to each well, and the fluorescence measurement (monochromator mode, 50 flashes, excitation wavelength: 533 nm, excitation bandwidth: 25 nm, emission wavelength: 595 nm, emission bandwidth: 20 nm) was initiated and monitored for 2 h at 25 °C using a TECAN Spark plate reader. The average anisotropy of technical triplicates was plotted against the reaction time in Prism, and the function ‘Plateau followed by one phase decay’ was applied to determine observed rate constants (k_{obs}) for each enzyme concentration. The catalytic efficiencies for each substrate were calculated as the slope of the linear fit of k_{obs} plotted against the respective enzyme concentration.

3.2.6.4 Fluorescence polarization binding assay

The binding of K63-linked triUb-TAMRA to inactive USP53 and USP54 variants was assessed by fluorescence polarization measurements in black 384 well low volume non-binding surface plates (Greiner) on a TECAN Spark plate reader at 25 °C (excitation: 535 nm, emission: 595 nm). Solutions of 2x triUb-TAMRA (final concentration of 50 nM) and 2x dilution series of USP53 C41A, USP53 C41S, USP54 C42A and USP54 C42S (final concentrations of 0.3125 µM to 40 µM) were prepared in cleavage buffer and mixed in a 1:1 ratio. 20 µl of the mixtures were added to each well in triplicate. Following a 15 min incubation in the dark for equilibration, the static fluorescence polarization values were measured.

3.2.6.5 Gel-based cleavage assays

Gel-based cleavage assays were performed using diubiquitin, triubiquitin, tetraubiquitin, polyubiquitin chains as well as ubiquitin chain variants as substrates. For these experiments, 2x substrate dilutions (final concentration: 2 – 4 µM) and 2x enzyme solutions (final concentration: 0.3 µM for USP54, 2-3 µM for USP53) were prepared in either PBS or in reaction buffer (20 mM Tris pH 7.7, 100 mM NaCl, 5 mM DTT). The substrate and enzyme solutions were brought to reaction temperature and subsequently combined in a 1:1 ratio, initiating the reaction. Following the designated incubation periods at either 37 °C or at room temperature, samples were collected and analyzed for substrate cleavage via SDS-PAGE on NuPAGE Bis-Tris gradient gels (4-12%, Invitrogen). Protein bands were typically visualized by Coomassie-staining. In the case of fluorescent TAMRA-labeled ubiquitin chain substrates, additionally, in-gel fluorescence was visualized using the Alexa546 channel (602/50 emission filter) on a Chemidoc MP Imaging System (Bio-Rad).

Protein levels were quantified by densitometry using the ImageJ software. To assess DUB cleavage activity in a quantitative manner, the intensities of the remaining substrate protein bands were normalized to initial substrate protein bands. The mean ratios and standard deviations were calculated from three to four independent cleavage assays.

Gel-based cleavage assays were also conducted with purified GFP-species modified with K48- or K63-linked ubiquitin chains of specific length as substrates in the same way as described above, with the exception of the following details. The final concentration of the GFP substrates was 1 µM. The final concentration of USP54 was 0.3 µM. The final concentration of USP53 was varied, with 0.5 µM and 2 µM being assayed. Samples were analyzed by SDS-PAGE with NuPAGE Bis-tris gradient gels (4-12%) and with NuPAGE Tris-acetate gels (3-8%). Proteins bands were visualized by in-gel fluorescence using the Alexa 488 channel (532/28 emission filter) and by Coomassie-staining. In the gel-based stability assay of the GFP substrates, no enzymes were added prior to incubation at 37 °C and analysis.

Gel-based cleavage assays were also performed for triubiquitin chains of mixed linkages. In addition to SDS-PAGE analysis of the cleavage activity (3.2.6.5), 15 µl of the same sample were mixed with 2 µl of 2 M HCl instead of LDS sample buffer to stop the cleavage reaction. Subsequently, the masses of the obtained cleavage products were determined by intact protein mass spectrometry (3.2.1.11).

4 Results

USP53 and USP54 have widely been presumed to be catalytically inactive based on sequence considerations as both proteins lack glycine and histidine residues in front of the catalytic histidine, which are otherwise highly conserved in the USP family (Table S2).[123] Within the phylogenetic tree of the catalytic domains of USP DUBs, USP53 and USP54 are most closely related to one another and, beyond that, to the deSUMOylase USPL1 (Figure 13A).[23] In addition, the aforementioned conserved histidine and glycine residues are also absent in CYLD, an active USP DUB with a specificity for K63- and M1-linked ubiquitin chains refuting the necessity of these residues for cleavage activity.[117,123] These two observations, together with the clustering of cholestasis-causing mutations in USP53 in its catalytic domain, led to the hypothesis that both proteins are active enzymes, either for one of the many Ubls or for a specific ubiquitin chain type.

In order to directly test USP53 and USP54 activity *in vitro*, catalytic domain constructs of USP53 (20-383) and USP54 (21-385) were expressed with an N-terminal 6xHis-GST tag in *E. coli* (Figure 13B). Their purifications included multiple steps including nickel-nitrilotriacetic acid (Ni-NTA) affinity chromatography, reverse Ni-NTA chromatography after tag removal, anion-exchange chromatography, and, for most purifications, size exclusion chromatography (SEC). One expression and a representative purification, performed by Jan André Hane, are shown for USP53$^{20-383}$ (Figure 13C-D). Addition of IPTG induced USP53 expression, as evidenced by the appearance of an additional strong protein band after 18 hours of incubation (Figure 13C). The supernatant of the pelleted cell lysate was subjected to Ni-NTA chromatography, resulting in a strong enrichment of His_6-GST-USP53 in the elution fractions. After addition of His-3C protease, partial tag cleavage was observed after 10 min and complete tag cleavage after overnight incubation. The His3C-protease and the cleaved His_6-GST-tag were removed by reverse Ni-NTA chromatography. Remaining impurities were further removed by ion-exchange chromatography (IEX) (Figure 13D). In general, pure USP53 and USP54 proteins were obtained in rather low yields of ~0.1-0.6 mg per liter of expression culture (Figure 13E). During lysis, USP54$^{21-385}$ was partly C-terminally truncated yielding two proteins of different mass separable by IEX (Figure 13F). One protein corresponded to amino acids 21-385 and the other to amino acids 21-369 (Figure 13G). Subsequently, USP53 and USP54 were also directly expressed as shorter versions. Information on the used construct is given in the figure captions for each experiment. USP53$^{20-383}$ and USP54$^{21-369}$ were used in most of the experiments. An attempt to obtain the full-length proteins by expression in insect cells did not yield any soluble protein, as all the protein was found in the pellet fraction after cell lysis.

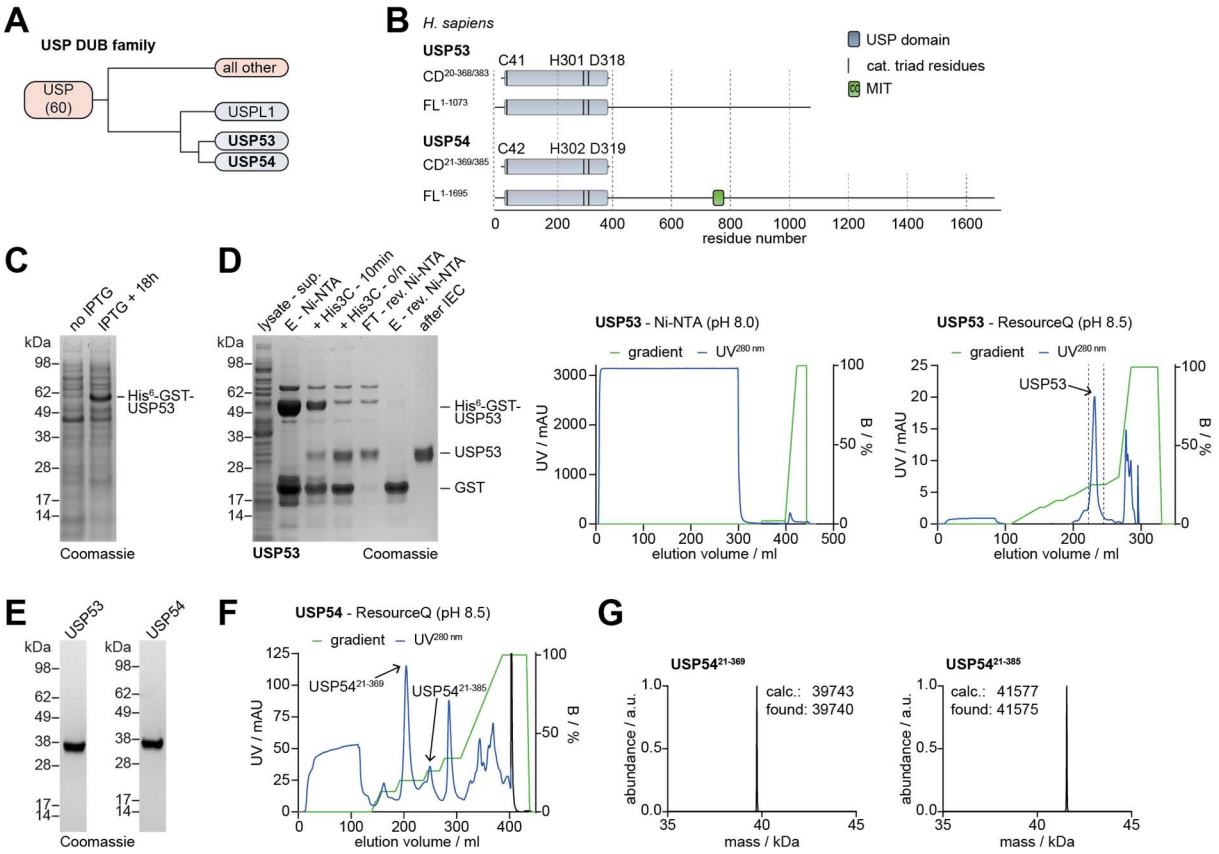

Figure 13: Expression and purification of USP53 and USP54. A) Phylogenetic tree of the catalytic domains of members of the USP DUB family.[23] B) Schematic representation of the full-length amino acid sequence of USP53 and USP54 and the catalytic domain constructs used in the experiments presented in this work. C) SDS-PAGE and Coomassie-staining of *E. coli* lysate before and 18 h after IPTG induced protein expression of USP53$^{20-383}$. D) Representative purification of USP53$^{20-383}$ using Ni-NTA, reverse Ni-NTA and IEX. Samples were taken throughout the purification and analyzed by SDS-PAGE and Coomassie-staining (*left*). The chromatograms of the Ni-NTA and IEX chromatography are shown (*right*). The purification shown in panels C and D was performed by Jan André Hane as part of his bachelor's thesis. E) The purity of USP54$^{21-369}$ and USP53$^{20-383}$ was assessed by SDS-PAGE and Coomassie-staining. F) Separation of USP54$^{21-369}$ and USP54$^{21-385}$ by IEX. G) Deconvoluted mass spectra of USP54$^{21-369}$ and USP54$^{21-385}$.

The results obtained in this thesis on USP53 and USP54 are presented in three parts including i) the functional analysis of USP53 and USP54 ii) the structural analysis of USP53 and USP54 and iii) the analysis of the effect of cholestasis mutations in USP53 on its activity.

4.1 Discovery of USP53 and USP54 activity

The first results chapter of this thesis focuses on the biochemical characterization and the understanding of the catalytic activity of USP53 and USP54 by performing various activity assays. Many of the used substrates were specifically designed and generated to allow analysis of linkage and length specificity in both DUBs.

4.1.1 Ub/Ubl specificity analysis

USP53 and USP54 are closest related to USPL1, a protease for the Ubl SUMO.[236] To test for potential cross-reactivity of USP53 and USP54, a panel of HA-tagged probes was generated

containing ubiquitin or one of the Ubls (SUMO1/2/4/5, ISG15, UFM1, FUBI, URM1, DWNN) as recognition modules.[237] After expression of the Ubl proteins as intein fusion proteins and their immobilization on chitin beads through the C-terminal chitin-binding domain (CBD), cleavage was induced by addition of MesNa. Obtained Ub/Ubl-MesNa species were purified by size exclusion purification and then functionalized with propargylamine (PA) yielding a panel of pure Ub-PA/Ubl-PA probes (Figure 14A-B). The panel was created in collaboration with Dr. Rachel O'Dea. The corresponding masses can be found in the appendix (Figure S1). The C-terminal PA warhead reacts via a direct addition mechanism with catalytic cysteines of active enzymes , to form a vinyl thioether bond (Figure 14C).[205] Notably, labeling of USP53 and USP54, visible by the appearance of a higher molecular weight band, was observed with HA-Ub-PA but not with any other Ubl-based probe (Figure 14D-E). The reactivity depended on the presence of the catalytic cysteines, as catalytically inactive USP53 C41S and USP54 C42S did not react with HA-Ub-PA (Figure 14D-E).

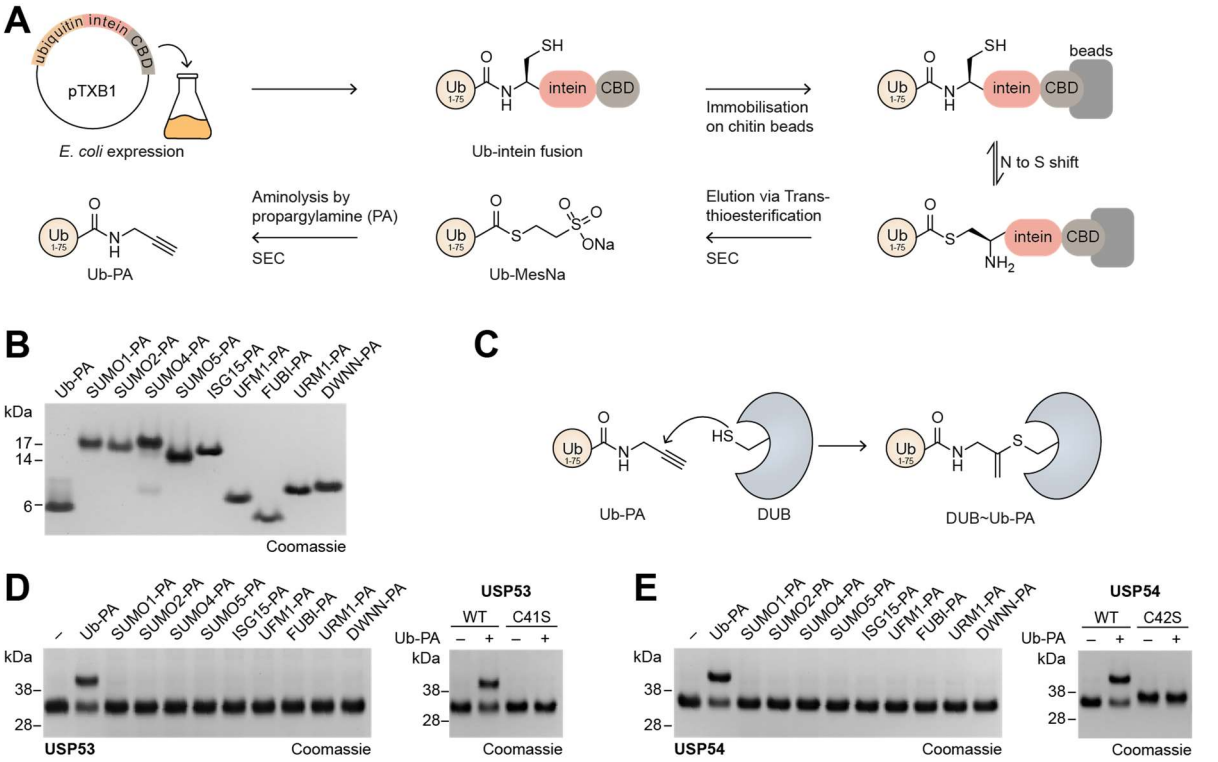

Figure 14: Probe panel and probe reactivity assays. A) All probes of the panel were generated using the IMPACT (Intein Mediated Purification with an Affinity Chitin-binding TAG) system as illustrated for ubiquitin. After expression as an HA-tagged intein fusion protein, addition of the thiol reagent MesNa leads to self-cleavage of the intein tag and release of ubiquitin with a C-terminal thioester. The thioester can then be lysed by primary amines. Propargylamine (PA) was used to obtain probes with a C-terminal PA warhead. HA-tag: hemagglutinin-tag. B) The purity of the probe panel of HA- tagged probes was analyzed by SDS-PAGE and Coomassie-staining. The probe panel was generated in collaboration with Dr. Rachel O'Dea. C) Schematic of the addition of the PA warhead to a cysteine DUB, forming a covalent vinyl thioether bond. D) Probe reactivity assays with USP53. The probe panel was incubated with USP53$^{20-383}$. HA-Ub-PA was additionally incubated with USP53$^{20-383}$ and the catalytically inactive USP53$^{20-383}$ C41S. Labeling was analyzed by SDS-PAGE and Coomassie-staining. E) Probe reactivity assays with USP54. The same assays as described in panel D were performed for USP54$^{21-369}$ and USP54$^{21-385}$ C42S.

Having demonstrated the recognition of a ubiquitin-based probe by USP53 and USP54, the next step was to directly assess their hydrolase activities using a commercially available fluorogenic substrate panel consisting of ubiquitin-RhodamineG (Ub-RhoG), SUMO1-RhoG, SUMO2-RhoG, NEDD8-RhoG and ISG15-RhoG. When conjugated to Ub/Ubl, the fluorescence of RhoG is quenched. The respective hydrolases bind these substrates with their S1 binding sites and cleave the amide bond between ubiquitin/Ubl and RhoG. The cleavage activity can be quantified by fluorescence measurements as the released RhoG exhibits strongly increased fluorescence (Figure 15A). Incubation of the substrate panel with USP53 and USP54 revealed specific hydrolase activity towards ubiquitin since an increase in fluorescence was detected for Ub-RhoG, but not for any other substrate (Figure 15B). Testing a range of concentrations of USP53 and USP54 showed that the turnover of Ub-RhoG increased for higher enzyme concentrations (Figure 15C). No increase in fluorescence was observed when no enzyme was added or when the corresponding catalytic cysteine mutants were added at a high concentration showing that the turnover was indeed facilitated by the enzyme activity mediated by the catalytic cysteine (Figure 15C). ULP1 and USP2 were used as control enzymes for the substrate panel. As expected, ULP1, a yeast deSUMOylase with a preference for Sumo1[99,238], cleaved S1-RhoG and S2-RhoG substrates and the DUB USP2 efficiently cleaved Ub-RhoG but not the Ubl-RhoG substrates (Figure 15D).

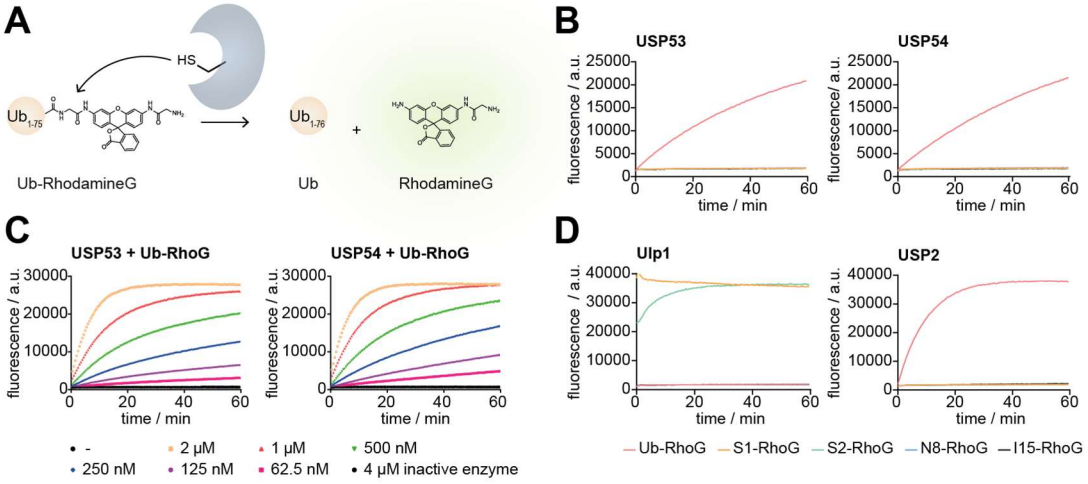

Figure 15: Fluorescence-based cleavage assays. A) Upon cleavage of Ub-RhodamineG (Ub-RhoG) by DUBs, free ubiquitin and fluorescent RhoG are released. B) A panel of Ub/Ubl-RhoG substrates was incubated with USP53[20-383] and USP54[21-369]. The fluorescence intensity was measured over time. C) Concentration-dependent cleavage of Ub-RhoG by USP53[20-383] and USP54[21-369] and corresponding catalytically inactive mutants. D) The same assay as in panel B was performed with ULP1 and USP2.

4.1.2 Analysis of linkage and length specificity

So far, the probe reactivity and fluorescence intensity assays revealed that USP53 and USP54 recognize ubiquitin and cleave a ubiquitin-based activated substrate. For both activities, the catalytic cysteines were essential and cross-reactivity on tested Ubls could be excluded. Typically, USP DUBs show limited selectivity and can cleave ubiquitin chains of different

lengths and linkages.[110] An exception is the USP DUB CYLD, which is specific for M1 and K63 linkages.[117] In order to test the activity of USP53 and USP54 on isopeptide linkages, a commercially available panel of diubiquitin (diUb) chains (UbiQ) covering all possible linkages was used. USP53 and USP54 cleaved K11-, K48- and K63-linked diUb chains to a limited extent at very high concentrations of 10 µM (Figure 16). While the highest activity for USP53 was detected on K48-linked diUb chains, a preferential cleavage of K63-linked diUb chains was observed for USP54.

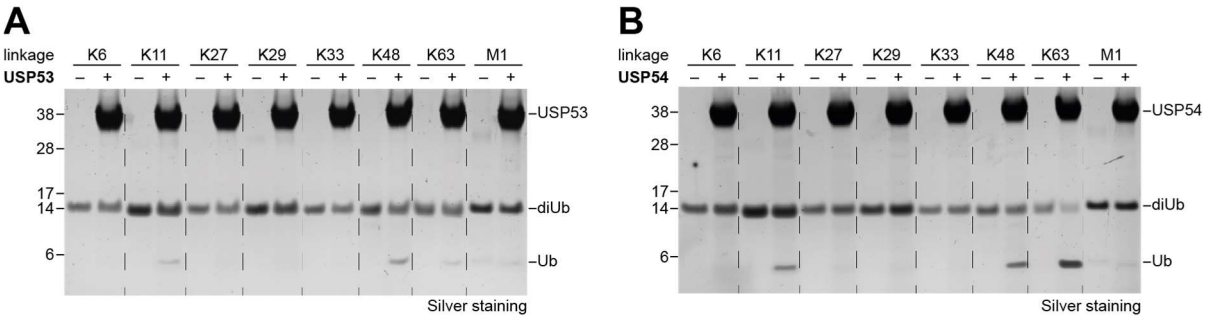

Figure 16: Gel-based cleavage assays of a diubiquitin chain panel. A/B) A panel of eight differently linked and synthetically generated diUb chains were incubated with USP53$^{20-383}$ (A) or USP54$^{21-369}$ (B) for 120 min. Samples were analyzed by SDS-PAGE and protein bands visualized by silver staining.

High concentrations of USP53 and USP54 were required to detect diUb chain processing (Figure 16). To further test the linkage and length specificity of USP53 and USP54, an enzymatically assembled tetraubiquitin (tetraUb) panel was compiled, rather than the previously used synthetically generated diUb panel. The advantage of the enzymatic approach is the improved substrate quality due to the absence of harsh conditions during substrate generation and purification making refolding unnecessary. TetraUb chains of four different linkages (K48, K63, K11, K6) were generated *in vitro* using single ubiquitin moieties as building blocks and the required conjugating and deubiquitinating enzymes according to reported methodology.[183] M1-linked tetraUb chains were directly expressed as tetramers. To extend the panel, enzymatically assembled K29- and K33-linked tetraUb chains were obtained commercially. K27-linked tetraUb chains are not included in the panel because they cannot yet be generated enzymatically *in vitro*.

In a first step, the protein levels of the differently linked tetraUb chains were equalized and then used in a gel-based cleavage assay with USP53 and USP54. Notably, both enzymes specifically cleaved K63-linked tetraUb chains (Figure 17). USP53 concentrations of 2 µM were required for efficient K63-linked cleavage. At this concentration, slight cleavage of K11- and K48-linked tetraUb chains was observed. On the other hand, USP54 exclusively cleaved K63-linked tetraUb chains at the used concentration of 300 nM. Another striking observation was the accumulation of K63-linked diUb chains suggesting a preferential cleavage of longer K63-linked chains by USP53 and USP54 (Figure 17).

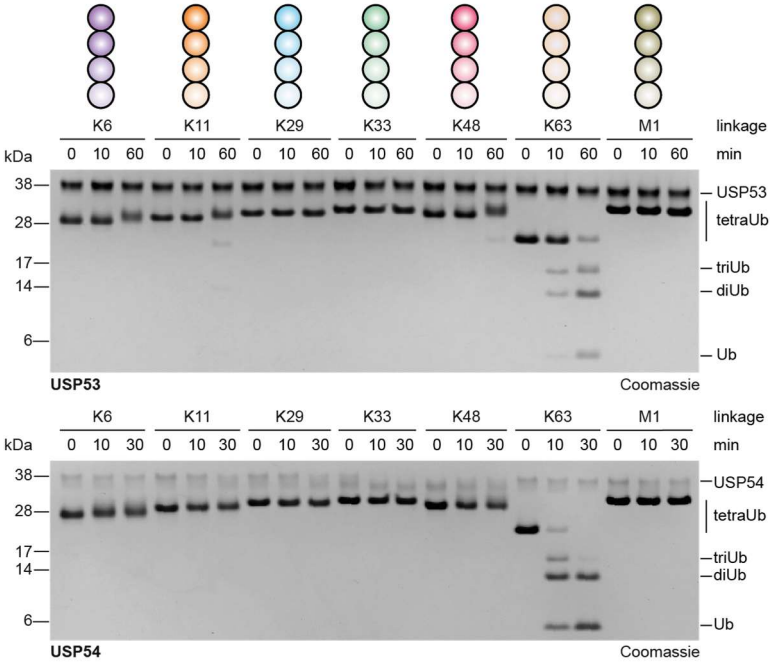

Figure 17. Gel-based cleavage assay of a tetraubiquitin chain panel. A panel of seven differently linked and enzymatically assembled tetraUb chains were incubated with USP53$^{20-383}$ and USP54$^{21-369}$ for annotated time points. Samples were analyzed by SDS-PAGE and Coomassie-staining.

To further assess the length preference, K63-linked diUb, triubiquitin (triUb) or tetraUb chains were incubated with USP53 and USP54. K63-linked diUb chains were not a good substrate for USP53 and significant cleavage activity was only observed for longer K63-linked triUb and tetraUb chains (Figure 18A). As with the diUb panel, USP54 cleaved K63-linked diUb chains. However, a preference for triUb and tetraUb chains was observed, as both were efficiently cleaved, whereas K63-linked diUb chains accumulated as cleavage products (Figure 18B). In time-resolved cleavage assays with enzymatically assembled K48-linked diUb, triUb or tetraUb chains, these were not cleaved by either USP53 or USP54 (Figure 18C-D). Next, a mixture of longer K63- or K48-linked polyubiquitin chains of at least five ubiquitin moieties was tested in the gel-based cleavage assays with USP53 and USP54. USP53 efficiently cleaved K63-linked polyubiquitin, as evidenced by the formation of shorter ubiquitin chains. These were further processed with the exception of K63-linked diUb (Figure 18E). Longer K48-linked polyubiquitin was processed by USP53, but to a lesser extent than K63-linked polyubiquitin, suggesting a selectivity but not a specificity of USP53 for K63 linkages in longer ubiquitin chains (Figure 18E). In the case of USP54, the polyubiquitin smear corresponding to longer K63-linked ubiquitin chains rapidly collapsed, nascent shorter cleavage products were further cleaved to mUb species, and only diUb chains accumulated (Figure 18F). In contrast to USP53, USP54 barely cleaved K48-linked polyubiquitin, underlining its specificity for K63 linkages also in longer ubiquitin chains (Figure 18F).

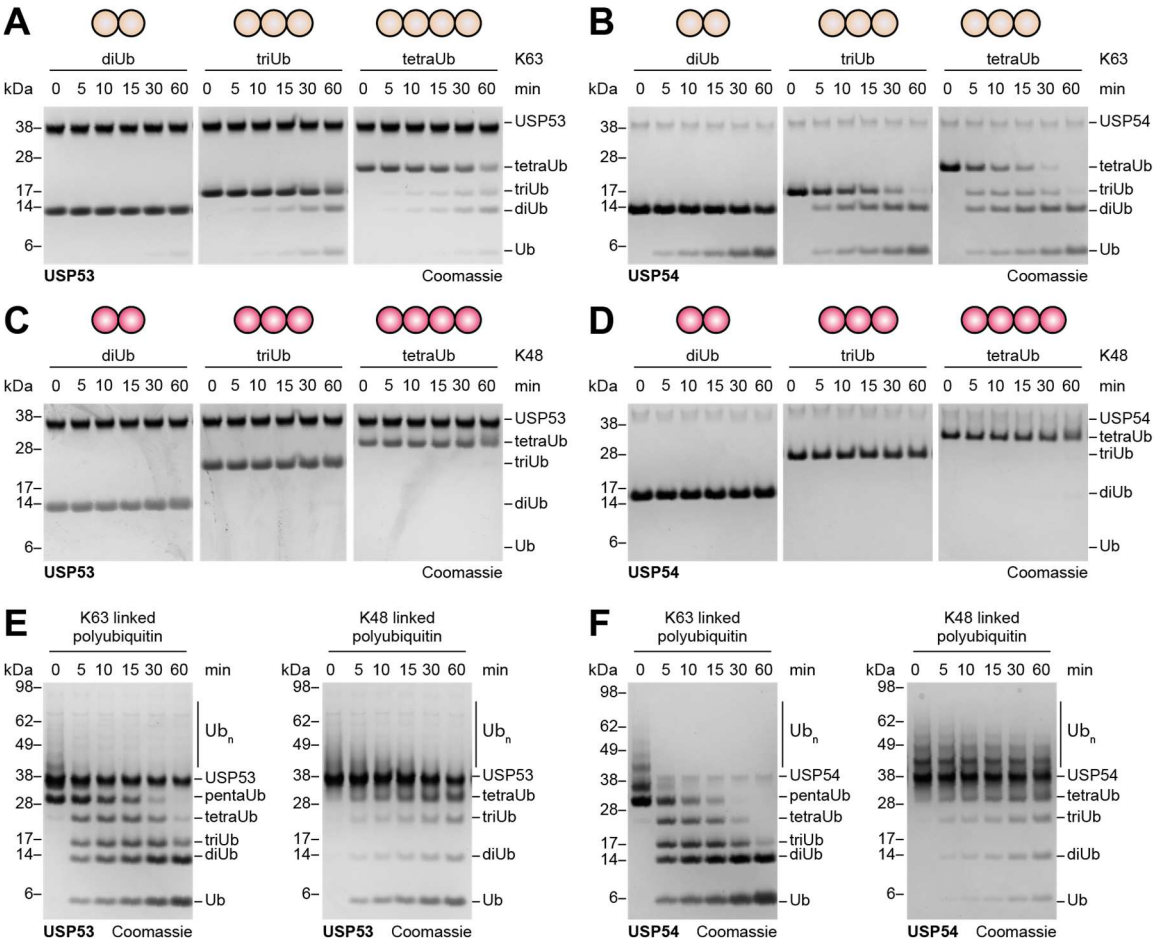

Figure 18: Time-resolved cleavage assays of K48- and K63-linked polyubiquitin chains. A) K63-linked di-, tri- and tetraUb chains were incubated with USP53$^{20-383}$ for indicated time points. B) The same assay as in panel A was performed for USP54$^{21-369}$. C) K48-linked di-, tri- or tetraUb chains were incubated with USP53$^{20-383}$ for indicated time points. D) The same assay as in panel C was performed for USP54$^{21-369}$ E) USP53$^{20-383}$ was incubated with K63- (left) or K48- (right) linked polyubiquitin for indicated time points. F) The same assays as in panel E were performed for USP54$^{21-269}$. All samples were analyzed by SDS-PAGE and Coomassie-staining.

The linkage-specific cleavage of diUb chains is mediated by ubiquitin binding in the S1 and S1' sites of DUBs. For USP53 and USP54, however, their preferential cleavage of K63-linked ubiquitin chains of at least three ubiquitin suggests that both proteins contain an additional third ubiquitin-binding site. This could either be an S2 or an S2' site. Fluorescent labeling of ubiquitin chains at one end allows the study of where exactly the ubiquitin chain is cleaved. Therefore, K63-linked triUb chains with a labeled proximal ubiquitin were used to identify the nature of the third ubiquitin-binding site of USP53 and USP54 depending on the cleavage products. The generation of fluorescent monoUb would indicate an S2 site, while fluorescent diUb would indicate an S2' site (Figure 19A). In line with previously used diUb-FlAsH substrates,[98,116,239] a K63-linked triUb-FlAsH substrate was generated by conjugating K63-linked diUb to ubiquitin with a C-terminal FlAsH tag. By-products were removed by cation exchange chromatography. The FlAsH tag was subsequently fluorescently labeled by adding FlAsH-EDT$_2$ (Figure 19B). However, the triUb-FlAsH substrate was not further used because the FlAsH dye interfered with USP54 activity (Figure 19C). This interference fits the

observation that ubiquitin probes with the fluorophores Cy5 or fluorescein at the C-terminus are less reactive than the unmodified probe.[240] Instead, a K63-linked triUb-TAMRA was generated from K63-linked diUb and a truncated ubiquitin containing a single cysteine at the C-terminus (Ub^{1-75}-CA), which was labeled with maleimide-TAMRA in a second step (Figure 19D). Possible by-products such as tetraUb or pentaUb were removed by cation-exchange chromatography. The corresponding deconvoluted mass spectrum of the final substrate proved its purity (Figure S2). USP54 cleaved K63-linked triUb-TAMRA and wild-type K63-linked triUb equally demonstrating that TAMRA as fluorescent label did not affect cleavage (Figure 19E). Addition of USP53 and USP54 to the triUb-TAMRA reagent resulted in the appearance of fluorescent Ub-TAMRA and non-fluorescent diUb, suggesting the presence of an S2 ubiquitin binding site in both enzymes (Figure 19F-G).

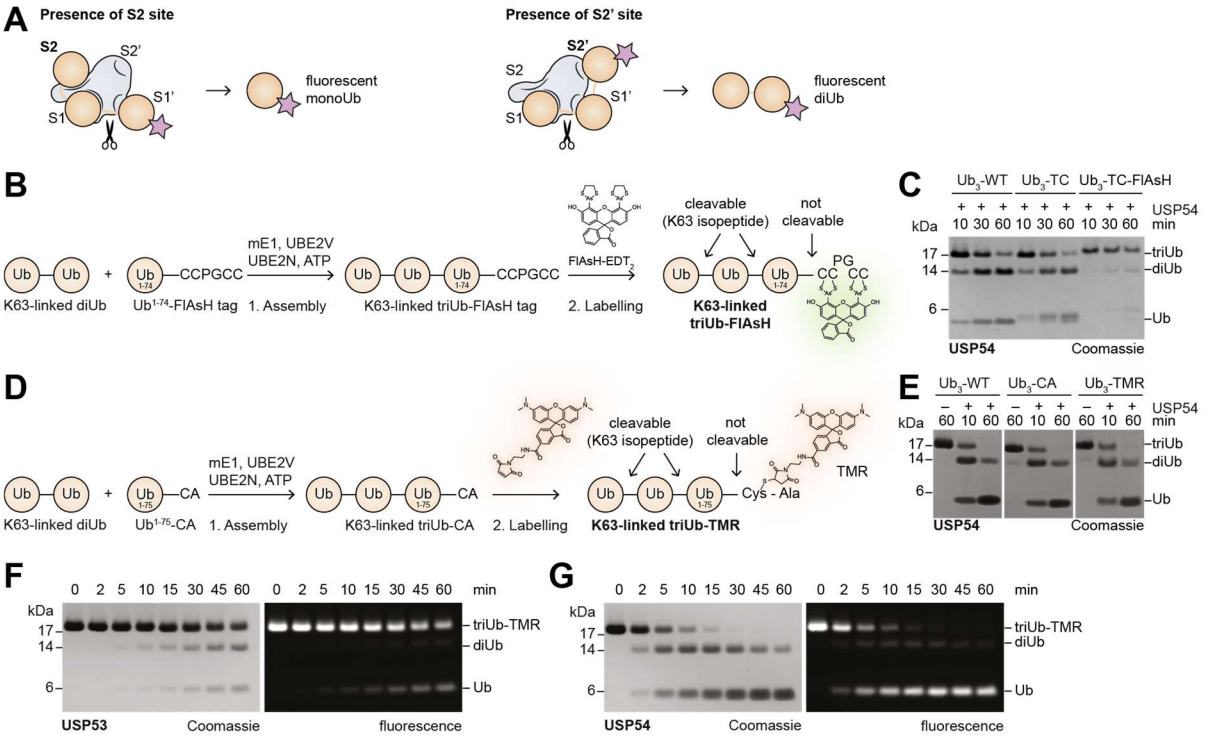

Figure 19: Generation of fluorescent K63-linked triUb chains and cleavage assays with USP53 and USP54. A) Illustration of the possible cleavage events of labeled triUb chains depending on the nature of the third ubiquitin binding site in DUBs. The presence of an S2 site would preferentially lead to fluorescent monoUb, whereas the presence of an S2' site would lead to fluorescent diUb species. B) Schematic of the assembly and labeling reactions to generate K63-linked triUb-FlAsH. C) Test cleavage assay of WT triUb, tetracysteine-tagged triUb (triUb-TC), or FlAsH labeled triUb by USP54. D) Schematic of the assembly and labeling reactions to obtain K63-linked triUb-TAMRA. E) Cleavage assay of wild-type K63-linked triUb, K63-linked triUb containing a CA truncation at the C-terminus of the proximal Ub and K63-linked and TAMRA-labeled triUb-TAMRA. F-G) Cleavage of K63-linked triUb-TAMRA by $USP53^{20-383}$ (F) or $USP54^{21-369}$ (G). Samples were collected at the indicated time points and analyzed by SDS-PAGE, fluorescence scanning and Coomassie-staining. TMR, TAMRA

To test for an additional fourth ubiquitin binding site, a K63-linked tetraUb-TAMRA reagent was assembled from ubiquitin containing a K63R mutation (Ub^{K63R}) and unlabeled K63-linked triUb-CA generated as described above (Figure 19D and Figure 20A). After purification and maleimide-TAMRA coupling to the cysteine, the substrate identity and purity were verified with mass spectrometry (Figure S2) and then the substrate was incubated with USP53 and USP54.

At the earliest time points, K63-linked tetraUb-TAMRA was cleaved by USP53 and USP54 into equal amounts of fluorescent Ub-TAMRA and diUb-TAMRA (Figure 20B-C). These results suggest that both enzymes contain S1, S1' and S2 sites without an additional fourth ubiquitin binding site.

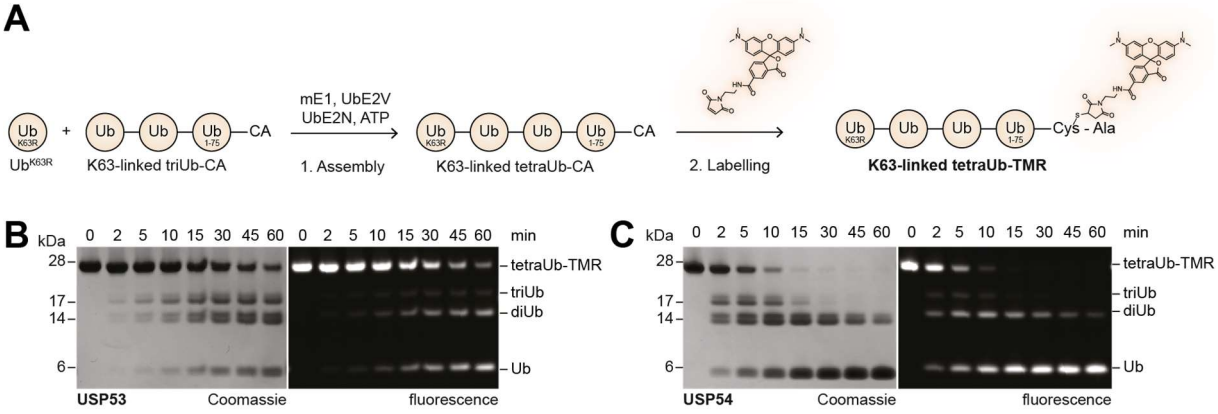

Figure 20: Generation and cleavage of fluorescent K63-linked tetraUb chains. A) Schematic depiction of the assembly and labeling steps to obtain K63-linked tetraUb-TAMRA. B-C) K63-linked tetraUb-TAMRA was incubated with USP53$^{20-383}$ (B) and USP54$^{21-369}$ (C) for indicated time points. Samples were analyzed by SDS-PAGE and visualized by fluorescence scanning and Coomassie-staining. TMR, TAMRA

4.1.3 Effect of ubiquitin binding in S1, S1' and S2 sites of USP53 and USP54

Having determined the nature of the third ubiquitin site in USP53 and USP54, the contribution of each of their ubiquitin binding sites to cleavage activity was quantified using fluorescence polarization assays with a substrate panel consisting of Ub-KG-TAMRA, K63-linked diUb-TAMRA and K63-linked triUb-TAMRA (Figure 21A). Measurement of the decrease in anisotropy over time after addition of DUBs allows quantification of their cleavage activity (Figure 21B). Ub-KG-TAMRA was generated using a semi-synthetic method developed by Dr. Zhou Zhao in the lab who also provided the KG-TAMRA molecule.[99] Briefly, Ub-hydrazide was first activated to an acyl azide, followed by functionalization with KG-TAMRA. Pure Ub-KG-TAMRA was obtained by cation exchange chromatography and its mass was verified by mass spectrometry (Figure 21C, Figure S2). In contrast to the Ub-RhoG substrate, in Ub-KG-TAMRA the C-terminus of ubiquitin is conjugated via an isopeptide bond to a dipeptide consisting of lysine and glycine. The lysine is further conjugated to a fluorescent TAMRA. Ub-KG-TAMRA is cleaved upon binding to the S1 site of DUBs (Figure 21A). K63-linked diUb-TAMRA was generated similarly to triUb- and tetraUb-TAMRA by an *in vitro* enzymatic assembly reaction. Ub^{K63R} was conjugated to K63 of ubiquitin containing a C-terminal cysteine, which was then fluorescently labeled (Figure 21D). In order for the isopeptide bond in K63-linked diUb-TAMRA to be cleaved, it must be bound by the S1 and S1' ubiquitin binding sites of DUBs (Figure 21A). The third substrate, K63-linked triUb-TAMRA, contained two cleavable isopeptide bonds. However, as previously tested, USP53 and USP54 cleave preferentially between the middle and proximal ubiquitin (Figure 21A). Therefore triUb-TAMRA allowed quantification of the

contribution of additional binding in the S2 sites of USP53 and USP54 in addition to the S1 and S1' binding sites.

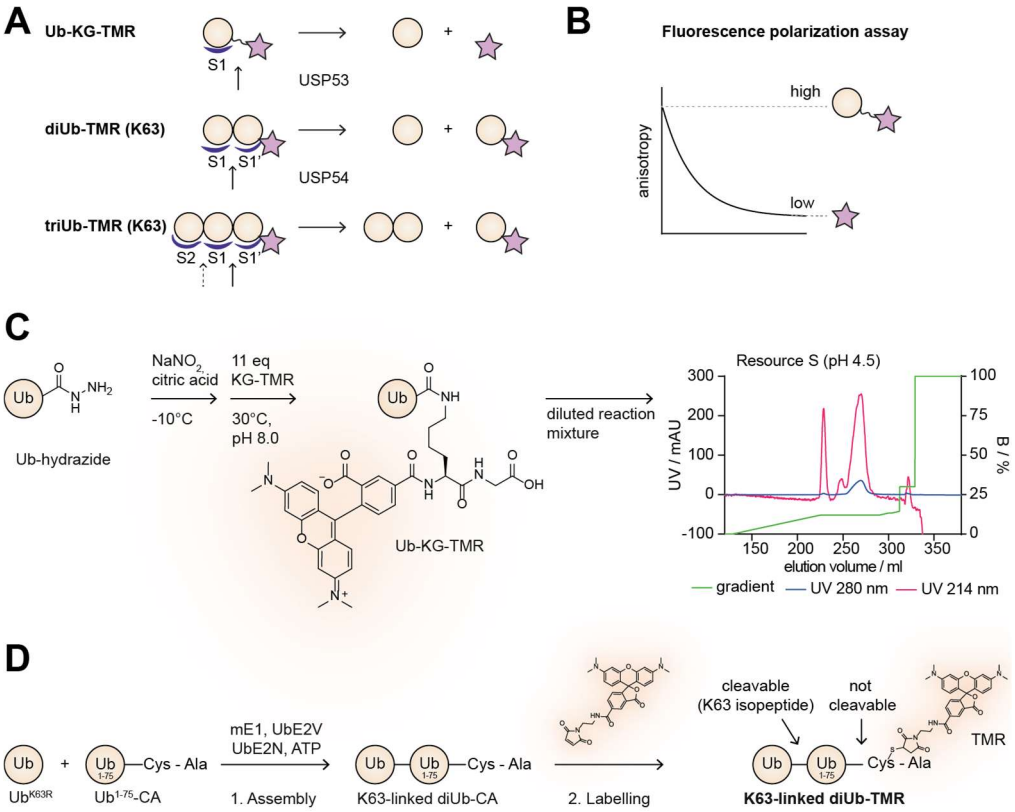

Figure 21: Substrate panel generation for a fluorescence polarization assay. A) Schematic depiction of the three used substrates Ub-KG-TAMRA, diUb-TAMRA (K63) and triUb-TAMRA (K63). Possible cleavage events are illustrated with black arrows and recognition of the ubiquitin species by the different ubiquitin binding sites in USP53 and USP54 is indicated. B) Assay principle of the fluorescence polarization assay. C) Schematic depiction of the generation of Ub-KG-TAMRA by the semi-synthetic method developed by Zhou Zhao. The chromatogram of the purification by cation exchange chromatography is shown. D) Schematic of the assembly and labeling steps to obtain K63-linked diUb-TAMRA.

All three substrates were incubated with USP53 or USP54 and fitting of the measured decrease in anisotropy over time yielded rate constants for each tested enzyme concentration (Figure 22A, C). Subsequently, the rate constants were plotted against the corresponding enzyme concentrations to obtain the catalytic efficiencies for the different substrates as the slopes of the linear regression lines (Figure 22B, D). USP53 poorly cleaved Ub-KG-TAMRA and a further decrease in the catalytic efficiency was observed for diUb-TAMRA. However, USP53 cleaved triUb-TAMRA with a 6-fold increase in the catalytic efficiency compared to Ub-KG-TAMRA (Figure 22B). USP54 showed similarly low catalytic efficiencies for Ub-KG-TAMRA. In contrast to USP53, the catalytic efficiency of USP54 for diUb-TAMRA increased 20-fold relative to Ub-KG-TAMRA, highlighting the importance of the S1' site in USP54. Additional binding of ubiquitin to the S2 site of USP54 by triUb-TAMRA resulted in a further 3-fold increase in catalytic efficiency compared to diUb-TAMRA (Figure 22D). These results suggest two distinct cleavage mechanisms for USP53 and USP54. USP54 was highly dependent on its S1' ubiquitin-binding site for enhanced cleavage activity and the S2 ubiquitin-

binding site further increased efficiency. On the other hand, USP53 contains a strong S2 ubiquitin binding site, which enhanced cleavage activity and probably sequestered K63-linked diUb-TMR away from the catalytic active site by unproductive binding in its S1 and S2 ubiquitin binding sites.

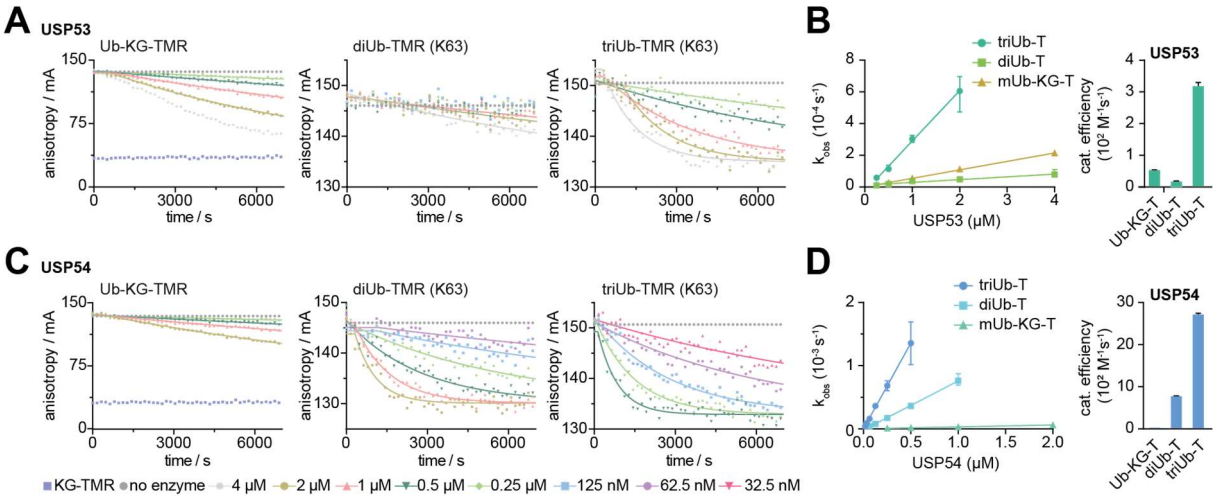

Figure 22: Quantification of the contribution of the S1, S1' and S2 ubiquitin binding sites in USP53 and USP54 to their cleavage activity A/C) Fluorescence polarization assays. The anisotropy of each the three substrates upon addition of USP54$^{21-369}$ (C) or USP53$^{20-383}$ (A) was measured over time. B/D): Observed rate constants (k_{obs}) were calculated using the function 'Plateau followed by one-phase decay' in GraphPad Prism for different concentration of USP53 and USP54. k_{obs} values were then plotted against the corresponding enzyme concentration and the catalytic efficiencies for each substrate were obtained as the slope of the linear regression line after linear fitting.

4.1.4 Generation and cleavage of ubiquitinated GFP

DUBs can either cleave isopeptide bonds at the distal end of ubiquitin chains, in between ubiquitin chains or directly between ubiquitin and the lysine of a substrate protein. These activities are referred to as *exo*-, *endo*- and *en bloc* cleavage activity, respectively.[94] So far, USP53 and USP54 have only been tested for their activity on ubiquitin chains. Given the differences in the ubiquitin binding between USP53 and USP54, the next step was to test their activity on protein-bound ubiquitin chains. To produce a model substrate modified with specifically linked ubiquitin chains of a given length, all necessary building blocks were first prepared (Figure 23). Monoubiquitinated GFP was used as the base for further attachment of ubiquitin moieties and was generated with a recently published method called lysine acylation using conjugating enzymes (LACE).[196] In this method, a specificity tag, derived from the consensus SUMOylation motif (LACE tag: PRKVIKMESEE) is incorporated into the substrate protein. In a first step, Ub-MesNa is activated by the small molecule Ac-Cys-NHMe to form an E1 thioester mimic. The SUMO-conjugating enzyme Ubc9 then catalyzes the site-specific attachment of the activated Ub-MesNa to the lysine in the tag through the formation of an isopeptide bond.[196] Here, the previously reported LACE reaction for the production of monoubiquitinated GFP was scaled up and the native purification of GFP-mUb established.

The small molecule Ac-Cys-NHMe was provided by Dr. Christian Grethe. The required proteins including Ub$^{1-76}$-MesNa, His-Ubc9 and GFP with a C-terminal LACE tag, were expressed and successfully purified (Figure 23A, Figure S3). In a large-scale LACE reaction with optimized protein concentrations, approximately half of the initial GFP was ubiquitinated after 24 hours (Figure 23B). The first step in the purification process included the removal of His-Ubc9 from the reaction mixture by reverse Ni-NTA affinity chromatography. The flow-through was then subjected to anion-exchange chromatography to separate free and monoubiquitinated GFP. The separation worked and pure GFP-mUb was obtained as shown by the uniformity of the SEC elution peak and the corresponding Coomassie-stained gel (Figure 23C-D). Accordingly, the measured mass of GFP-mUb matched the calculated mass (Figure S3). Next, K63-linked or K48-linked ubiquitin chains were generated as secondary building blocks. These chains contained a distal ubiquitin with a K63R or a K48R mutation, respectively (Figure 23E). Thus, they can only act as donors, but not as acceptors, in respective K63 or K48 linkage assembly reactions with GFP-mUb.

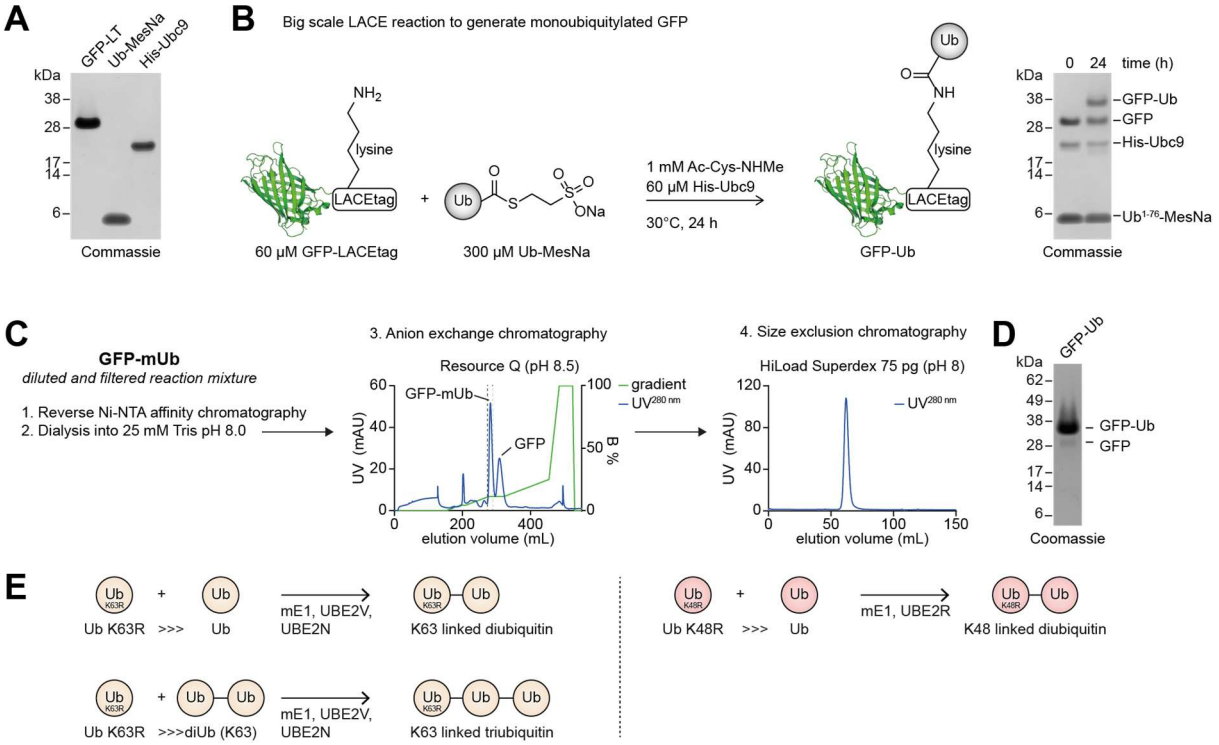

Figure 23: Generation of building blocks for the generation of specifically ubiquitinated GFP-species. A) Purified proteins to be used in the LACE reaction were analyzed by SDS-PAGE and Coomassie-staining. B) Large scale LACE reaction. The small molecule Ac-Cys-NHMe was synthesized by Dr. Christian Grethe. Samples were taken immediately after the start of the reaction and after 24h incubation at 37 °C and analyzed by SDS-PAGE and Coomassie-staining C) Purification of GFP-mUb obtained after the LACE reaction shown in panel B. His-Ubc9 was removed by reverse Ni-NTA. GFP and GFP-mUb were separated by anion-exchange chromatography. SEC was performed as the final purification step. D) The purity of GFP-mUb was verified by SDS-PAGE and Coomassie-staining. E) Schematic of the enzymatic assembly of K63-linked (*left*) or K48-linked (*right*) ubiquitin chains in which the distal ubiquitin contains a K63R (*left*) or a K48R (*right*) mutation, respectively.

To obtain ubiquitinated GFP modified with chains of a specific length and linkage, Ub K63R, Ub K48R and each of the premade K63-linked or K48-linked ubiquitin chains with a mutated

distal ubiquitin were conjugated to GFP-mUb in respective K63- (Figure 24A) and K48- (Figure 24B) linkage assembly reactions. These combinations allow for exactly one possible conjugation reaction and thus the exact length of the ubiquitin chains was obtained.

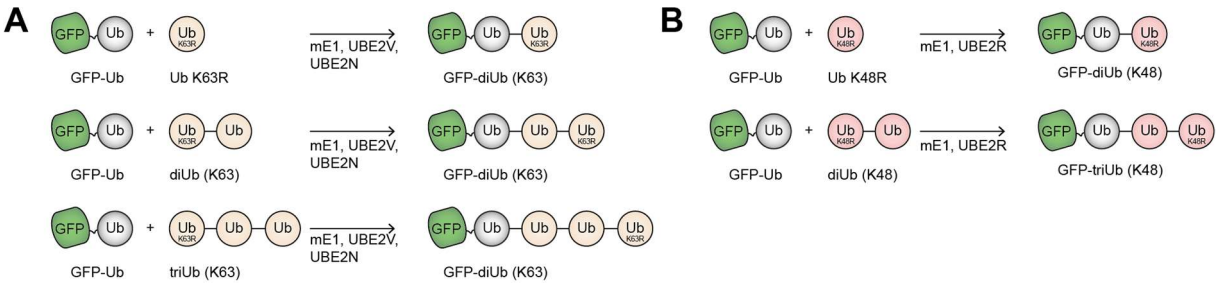

Figure 24: *In vitro* assembly reactions for GFP modified with K48- or K63-linked ubiquitin chains of a specific length. A) K63 linkage assembly reactions for the conjugation of GFP-mUb with Ub K63R or K63-linked diUb or K63-linked triUb chains. B) K48 linkage assembly reactions for the conjugation of GFP-mUb with Ub K48R or K48-linked diUb or K48-linked triUb chains.

To monitor reaction progress, protein mixtures after *in vitro* K63 linkage assembly reactions, performed as shown in Figure 24A, were separated by SDS-PAGE and visualized by Coomassie-staining. Ub K63R, diUb (K63) and triUb (K63) were used in excess of GFP-mUb and were therefore still detected (Figure 25A). Limited amounts of residual GFP-mUb and strong protein bands corresponding to K63-linked polyubiquitinated GFP species were visible, indicating that GFP-mUb was efficiently further ubiquitinated (Figure 25A). K63 linkage assembly enzymes, unconjugated ubiquitin or ubiquitin chains and incompletely transformed GFP-mUb were separated by IEC to yield GFP-diub (K63), GFP-triUb (K63) and GFP-tetraUb (K63) (Figure 25B). The K48 linkage assembly reactions were not as efficient as the reactions for K63 linkage assembly (Figure 25C). The remaining GFP-mUb was not separated from GFP-diUb (K48) or GFP-triUb (K48) by IEC as GFP-mUb eluted together with GFP-diUb (K48) or GFP-triUb (K48) in single elution peaks (Figure 25C). Therefore, SEC was performed as a second purification step and fractions containing only polyubiquitinated GFP were combined as indicated by the dashed lines (Figure 25C). Masses of all created ubiquitinated GFP-species were verified by mass spectrometry (Figure S3). To test whether the differently ubiquitinated GFP species can be distinguished by SDS-PAGE, two different gel systems were tested. On Bis-Tris gradient gels (4-12%), GFP and GFP-mUb ran at different heights, while GFP-diUb (K63) and GFP-triUb (K63) ran close together (Figure 25D). Using Tris-acetate gradient gels (3-8%) gave very good separation of GFPs modified with ubiquitin chains of different lengths but GFP and GFP-mUb ran at similar heights. (Figure 25D). The Coomassie-stained Bis-Tris gel showed the high purity of all substrates, with only the GFP-triUb (K48) preparation containing low levels of unmodified GFP (Figure 25D). Generally, the fluorescence of GFP survived the conditions of sample preparation and SDS-PAGE-based separation (Figure 25D) enabling reaction analysis by in-gel fluorescence measurement.

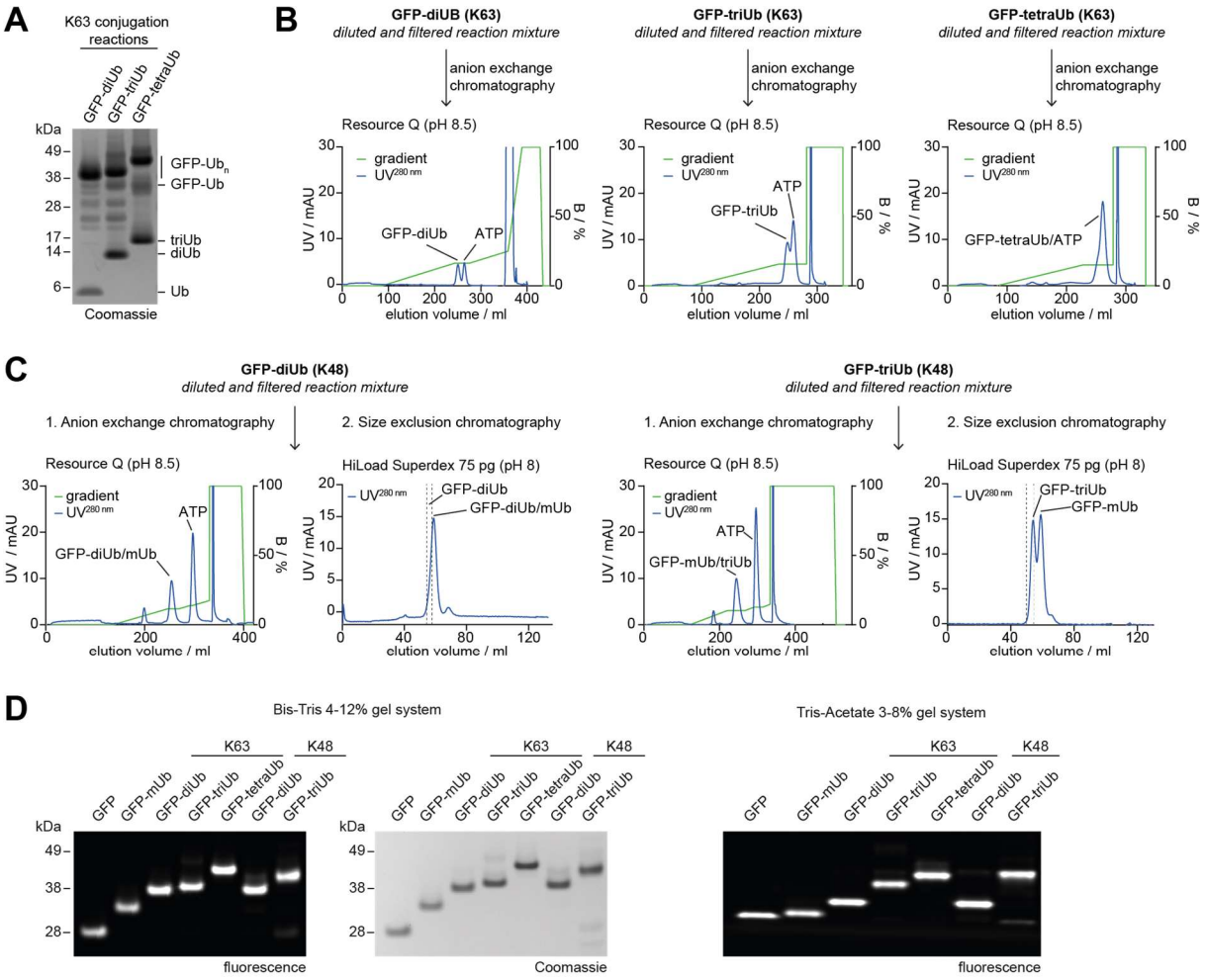

Figure 25: Generation of GFP modified with K48-linked or K63-linked ubiquitin chains of a specific length. A) Samples of K63 linkage assembly reactions were taken and analyzed by SDS-PAGE and Coomassie-staining. B) GFP-diUb (K63), GFP-triUb (K63) and GFP-tetraUb (K63) obtained by assembly reactions shown in panel A were purified by IEX and the corresponding chromatograms are shown. Absorption at 280 nm was shown in blue, the gradient of buffer B as the elution buffer is shown in green. C) GFP-diUb (K48) and GFP-triUb (K48) were purified after the assembly reaction by IEX and SEC. The dashed lines illustrate the combined elution fractions after SEC. D) GFP and GFP-Ub$_n$-species were analyzed by SDS-PAGE using two different gel system and protein bands were visualized by Coomassie-staining and fluorescence scanning.

The stability of the GFP substrates modified with ubiquitin chains of different linkage and length (GFP-Ub$_n$) was assessed by gel-based visualization after incubation at the reaction temperature of 37 °C. While 30 min incubation was well tolerated, longer incubation times of 120 min resulted in some loss of detected fluorescence after SDS-PAGE and separation of the GFP-Ub$_n$ bands into two distinct bands, presumably corresponding to different folding states of GFP or the attached ubiquitin moieties (Figure 26A). Even after 120 min incubation, no free ubiquitin species appeared, indicating that no arbitrary cleavage of the isopeptide bonds was taking place (Figure 26A). Concluding, the appearance of cleaved ubiquitin or ubiquitin chains is easier to interpret than the disappearance of GFP fluorescence at longer incubation times. To avoid this, superfolder GFP, a robust and stable GFP variant, could be used to generate future ubiquitinated GFP species.

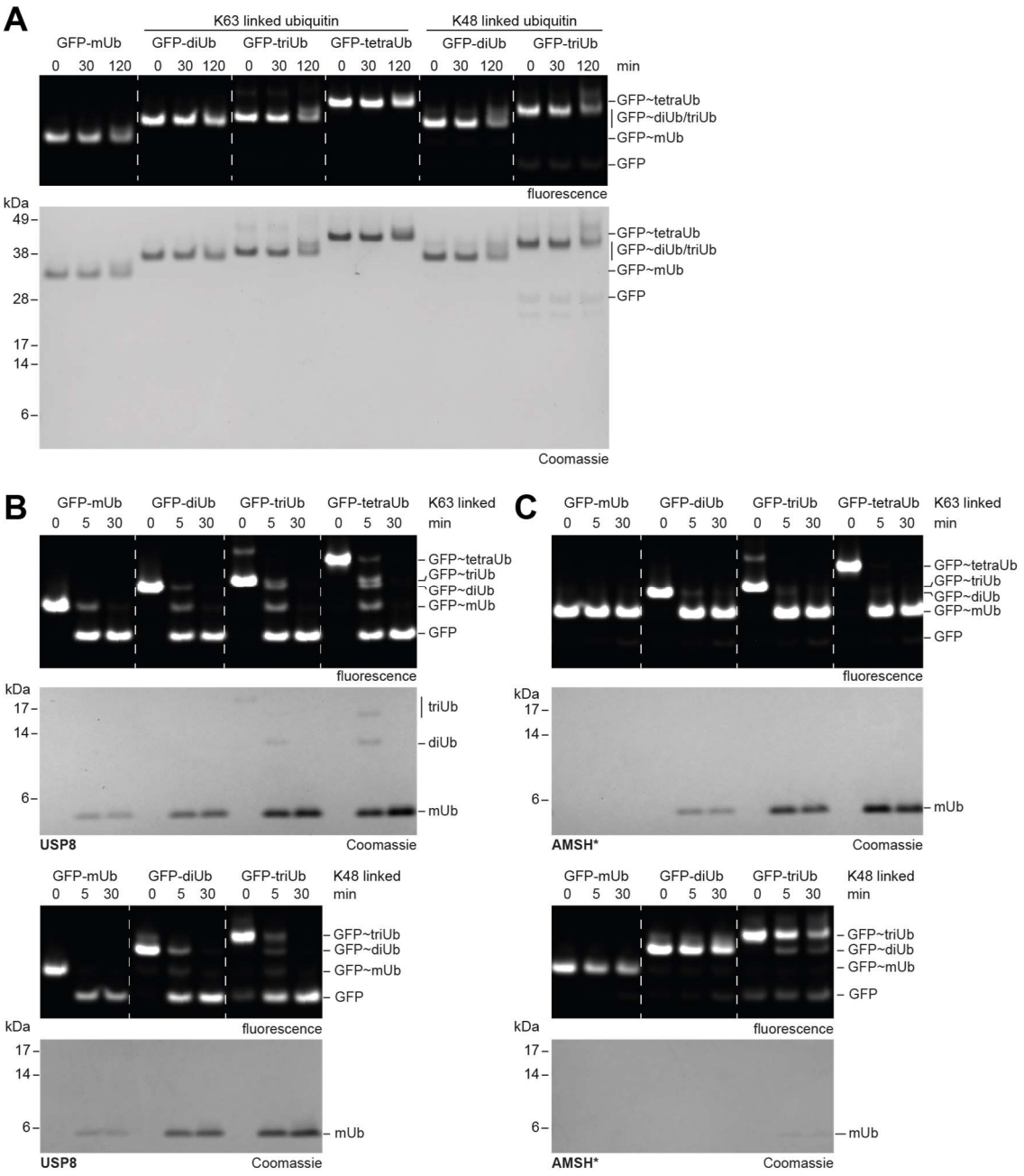

Figure 26: Quality control of GFP-Ub$_n$ substrates. A) The substrates were incubated at 37 °C. Samples taken at indicated time points were analyzed by SDS-PAGE, fluorescence-scanning and Coomassie-staining. B-C) GFP substrates were incubated with 80 nM USP8 (B) or 200 nM AMSH* (C). Samples taken at indicated time-points were analyzed by SDS-PAGE, followed by fluorescence-scanning and Coomassie-staining.

To verify the linkage type, the correct folding of the ubiquitin chains and the accessibility of the isopeptide bonds for DUB cleavage, the non-specific DUB USP8 and the K63 linkage-specific DUB AMSH* were incubated with the ubiquitinated GFP substrates. USP8 completely cleaved all isopeptide bonds including K63-, K48- and ubiquitin substrate bonds. After 30 min incubation, only GFP and monoubiquitin were detected (Figure 26B). AMSH* rapidly cleaved all K63-linked isopeptide bonds but not those directly between ubiquitin and GFP, as only monoubiquitin species and GFP-mUb were detected after 5 min incubation of AMSH* with GFPs modified with K63-linked ubiquitin chains. GFP-mUb or GFP modified with K48-linked

ubiquitin chains were not processed by AMSH*. For these substrates, no ubiquitin bands or a very weak monoubiquitin band for the GFP-triUb (K48) substrate appeared on the gel after Coomassie-staining (Figure 26C). These experiments proved the cleavability of all isopeptide bonds present in the GFP-Ub_n substrates, as well as the composition of the K63-linked ubiquitin chains conjugated to GFP.

Following substrate verification, the activity of USP53 and USP54 was tested on the differently polyubiquitinated GFP substrates to learn about their cleavage preferences in a more complex substrate setting. Here, isopeptide bonds between ubiquitin moieties compete for cleavage with isopeptide bonds between ubiquitin and the model substrate GFP. Surprisingly, USP53 preferentially cleaved K63-linked ubiquitin chains *en bloc* from GFP at both tested concentrations of 0.5 µM and 2 µM, as shown by the preferential release of unprocessed substrate-free ubiquitin chains, especially at early timepoints (Figure 27A-B). At the higher concentration, USP53 also cleaved K48-linked ubiquitin chains attached to GFP as well as monoubiquitin from GFP, albeit less efficiently than the GFP substrates modified with K63-linked ubiquitin chains and without preferential cleavage of the isopeptide bond between ubiquitin and GFP (Figure 27A). At a lower concentration of 500 nM, USP53 specifically recognized and cleaved K63-linked ubiquitin chains on GFP whereas K48-linked ubiquitin chains and monoubiquitin were not removed from GFP (Figure 27B). In contrast to USP53, USP54 showed a different cleavage pattern. K63-linked ubiquitin chains were efficiently cleaved by USP54, with the efficiency increasing with the length of the ubiquitin chain (Figure 27C). However, like for AMSH*, a monoubiquitin residue remained attached to GFP in the cleavage reactions with GFP modified with K63-linked ubiquitin chains. Consequently, USP54 also did not cleave GFP-mUb illustrating the importance of the S1' ubiquitin binding site of USP54 for its cleavage activity (Figure 27C). GFP modified with K48-linked ubiquitin chains was not cleaved by USP54, demonstrating its specificity for K63-linked ubiquitin chains (Figure 27C).

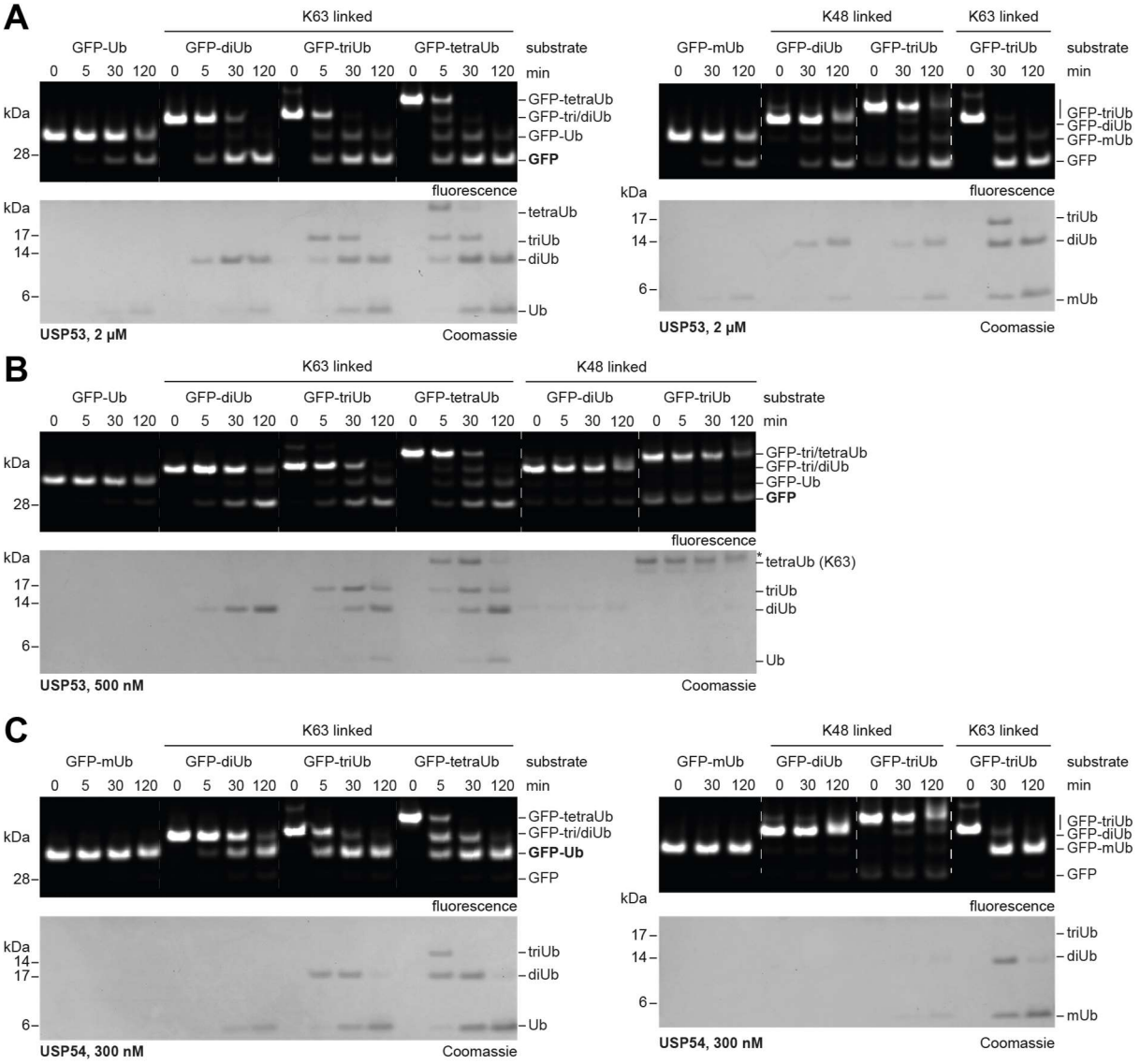

Figure 27: Gel-based cleavage assays of GFP-Ub$_n$ substrates. Differently ubiquitinated GFP species were incubated with specified concentrations of USP53$^{20-383}$ (A-B) or USP54$^{21-369}$(C). Samples taken at the indicated time points were analyzed by SDS-PAGE, fluorescence scanning and Coomassie-staining. (*): Likely K48-linked triUb contaminant present in the GFP-triUb (K48) preparation.

4.1.5 Generation and cleavage of heterotypic triUb chain substrates

To further analyze the different cleavage mechanisms of USP53 and USP54, homotypic triUb chains and heterotypic triUb chains containing mixed K63/K48 linkages were generated (Figure 28). In these chains, each ubiquitin moiety contained a different mass allowing the differential analysis of the two possible cleavage events in a triUb chain by mass analysis. Thus, the linkage dependence of the cleavage between the middle and proximal ubiquitin bound in the S1 and S1' binding sites of USP53 and USP54 can be analyzed with the heterotypic chains. In order to generate K48 and K63 linkages at the specific positions between the ubiquitin moieties, the known *in vitro* methodology for the assembly of K63 and K48 chain linkages was refined (Figure 28): A ubiquitin with a truncated C-terminus (Ub$^{1-75}$) and, for the

heterotypic triUb substrates, either a K48R or K63R mutation, was used as the proximal ubiquitin because it cannot be conjugated via its C-terminus and serves only as an acceptor ubiquitin. In assembly reactions with wild-type ubiquitin, the truncated ubiquitin species were used in a tenfold excess to strongly favor the formation of non-conjugatable K48- or K63-linked diUb over wild-type diUb. In the secondary reaction steps, the distal ubiquitin containing a K48R mutation for K48 linkage assembly or a K63R mutation for K63 linkage assembly was conjugated to the respective K48- or K63-linked diUb species yielding homotypic or mixed K63/K48 triUb chains. To illustrate the chain compositions, the proximal ubiquitin with the free C-terminus is shown as grey sphere, ubiquitin moieties conjugated to K48 as red spheres and ubiquitin moieties conjugated to K63 as yellow spheres. The deconvoluted mass spectra of the generated homotypic and heterotypic triUb chains showed both their purity and composition, as the identified masses correlated with the calculated masses (Figure 28).

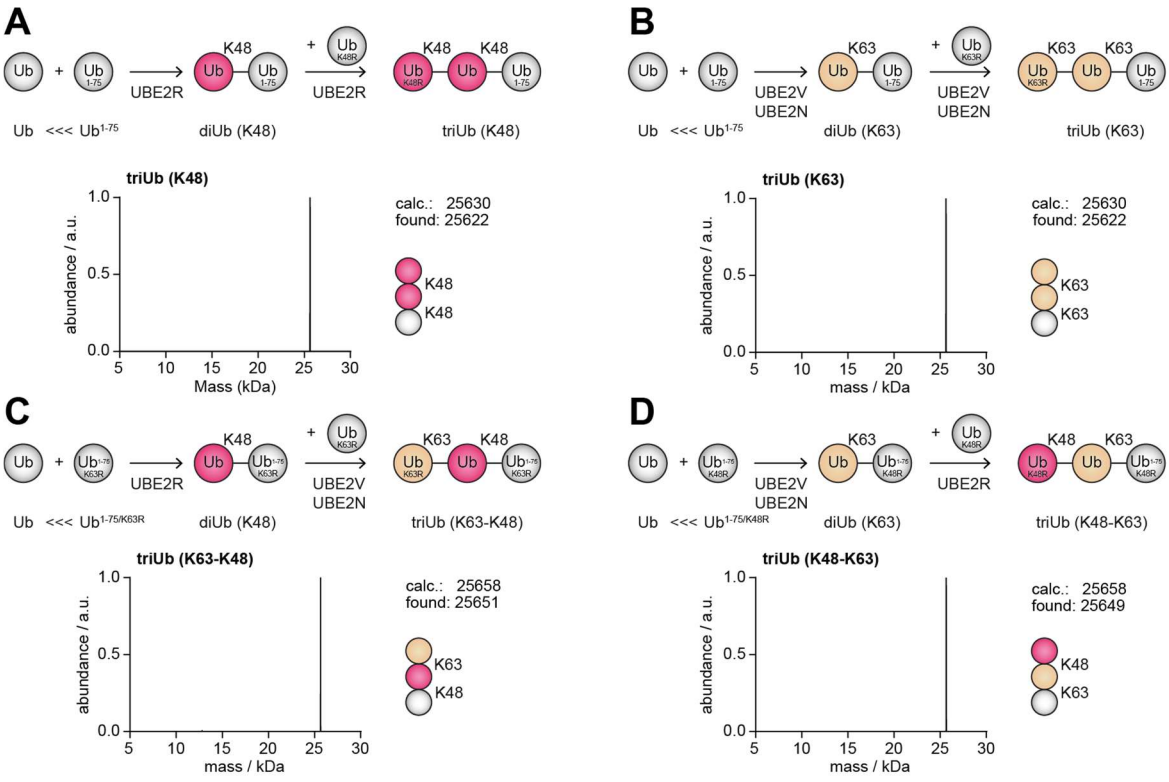

Figure 28: Assembly of homotypic and mixed K63/K48-linked triUb chains. A-D) Schematic depiction of the building blocks and the enzymatic assembly steps to generate K63-linked triUb (A), K48-linked triUb (B), heterotypically linked triUb (K63-K48) (C) or triUb (K48-K63) (D). Each assembly step was performed using the mE1 enzyme and the specific E2 enzymes annotated for each reaction step. Ubiquitin with a free C-terminus is depicted in white, ubiquitin conjugated to K48 in red and ubiquitin conjugated to K63 in yellow. Deconvoluted mass spectra are shown for each of the final triUb chain substrates.

After generation of the homotypic and heterotypic K63/K48-linked triUb substrates, these were used in cleavage assays with USP53 and USP54 (Figure 29, Figure 30). SDS-PAGE analysis and Coomassie-staining revealed efficient cleavage of K63-linked triUb and of mixed K63-K48-linked triUb chains into mUb and diUb species by USP53 (Figure 29A). In contrast, the inversely mixed K48-K63-linked triUb chains were significantly less cleaved, comparable to

K63-linked diUb chains (Figure 29A). USP53 slightly cleaved K48-linked diUb and triUb chains (Figure 29A). To identify the cleavage position and thus the cleaved linkage, the mass of the mUb and diUb species formed after incubation of the triUb substrates with USP53 was determined by intact mass spectrometry. Identified cleavage products of K63-linked triUb and of mixed K63-K48-linked triUb chains corresponded to cleavage between the proximal and middle ubiquitin consistent with occupancy of the S1 and S2 sites by two ubiquitin moieties linked by a K63 isopeptide bond (Figure 29B). The cleaved linkage type varied between the two substrates, implying that USP53 activity is primarily based on S1 and S2 site occupancy and that then different isopeptide linkages between ubiquitin chains can be cleaved. For the mixed K48-K63-linked triUb substrate, the masses of cleavage products determined after incubation with USP53 corresponded to the proximal ubiquitin and the diUb species consisting of the middle and distal ubiquitin (Figure 29B). In conclusion, the K63 linkage was cleaved preferentially over the K48 linkage, demonstrating that K48-linked distal and middle ubiquitin, which are unlikely to bind to the S1 and S2 sites, did not enhance USP53 activity on the K63 linkage between the middle and proximal ubiquitin.

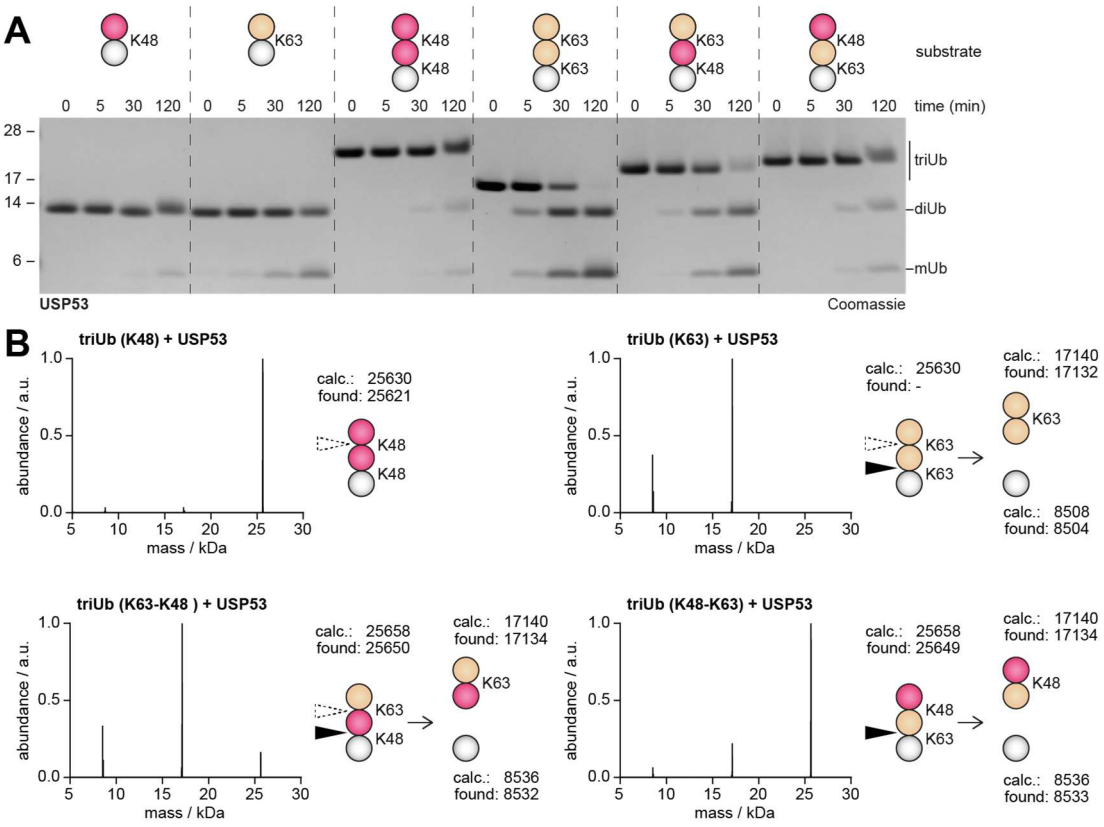

Figure 29: Mass- and gel-based cleavage assay of differently linked diUb and triUb substrates by USP53. A) The diUb and triUb substrates were incubated with USP53$^{20-368}$. Samples were taken at indicated time points and analyzed by SDS-PAGE and Coomassie-staining. B) Samples corresponding to the 120 min time point in panel A were further analyzed by intact mass spectrometry and the corresponding deconvoluted mass spectra are shown for the triUb substrates. Major cleavage events are shown schematically and the cleavage sites are indicated by black arrows. Dashed arrows indicate limited cleavage events. The same color code as in Figure 28 was used to illustrate linkages in the ubiquitin chains.

Performing the same triUb cleavage assays with USP54 gave a different result. Homotypic K63-linked triUb chains were rapidly cleaved into their three monoubiquitin species and all three masses were identified by mass spectrometry (Figure 30A and B). The mixed K48/K63-linked triUb substrates were completely cleaved into diUb chains and monoubiquitin, comparably efficient as the cleavage of K63-linked diUb chains (Figure 30A). Identification of the resulting masses of the mUb and diUb species showed that specifically K63 linkages were cleaved by USP54 while the K48 linkages were retained, irrespective of their position in the triUb chains (Figure 30B). For K48-linked substrates minimal cleavage was detected at longer time points (Figure 30A).

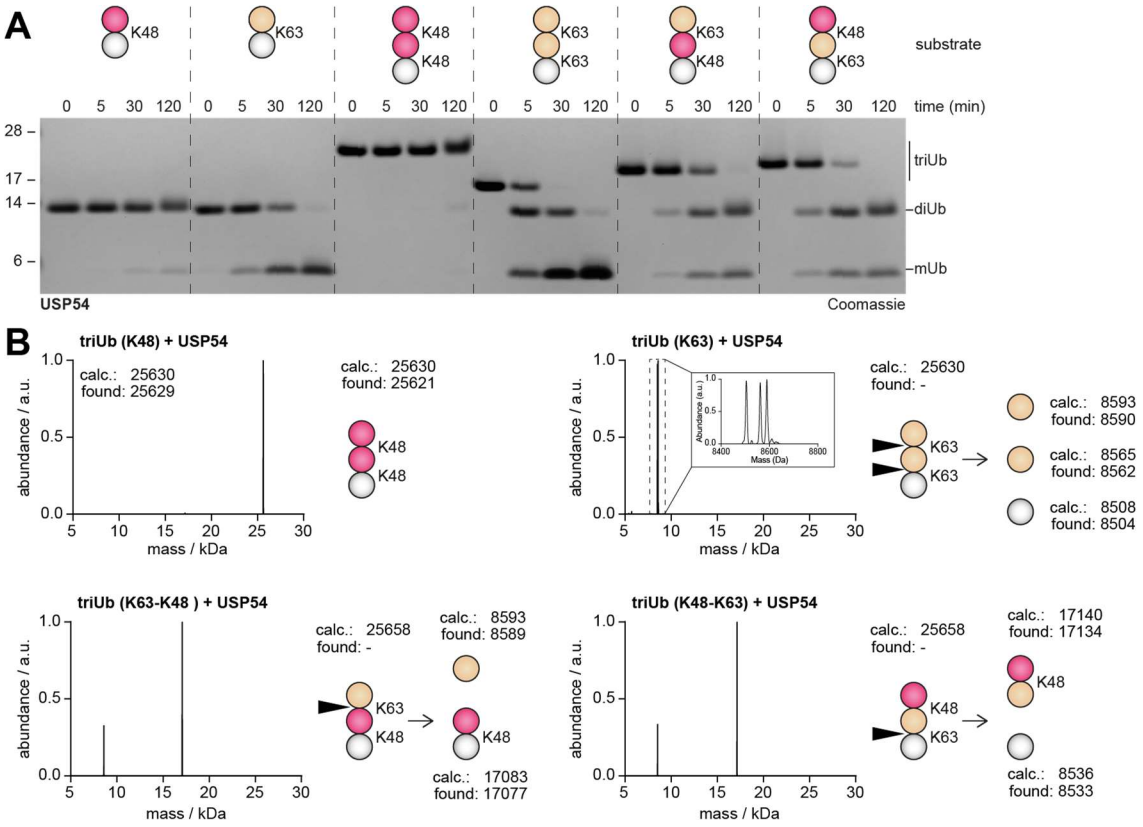

Figure 30: Mass and gel-based cleavage assay of differently linked diUb and triUb substrates by USP54. A) The diUb and triUb substrates were incubated with USP54$^{21-369}$. Samples were taken at indicated time points and analyzed by SDS-PAGE and Coomassie-staining. B) Samples corresponding to the 120 min time point in panel A were further analyzed by intact mass spectrometry and the corresponding deconvoluted mass spectra are shown for the triUb substrates. Major cleavage events are shown schematically and the cleavage sites are indicated by black arrows. Dashes arrows indicate limited cleavage events. The same color code as in Figure 28 was used to illustrate linkages in the ubiquitin chains.

USP DUBs are most often non-specific.[110] However, several USP DUBs show some selectivity between ubiquitin linkages and often no or little activity on M1-linked ubiquitin chains.[110,116,241] In ubiquitin, the N-terminus and K63 are in close proximity and both, M1 and K63 linkages result in extended ubiquitin chains with similar surfaces being assessible for protein interactions.[242] However, M1 linkages are formed by peptide bonds connecting ubiquitin molecules head to tail, whereas K63 linkages are formed by isopeptide bonds between the C-terminus of one ubiquitin molecule and the epsilon amino group of the lysine side chain of

another ubiquitin. This leads to different degrees of flexibility which affect binding by DUBs.[214] To test for the ability of USP54 and especially of USP53 to cleave M1 linkages in mixed chains, heterotypic triUb chains containing mixed K63/M1 linkages were generated in one-step *in vitro* assembly reactions.

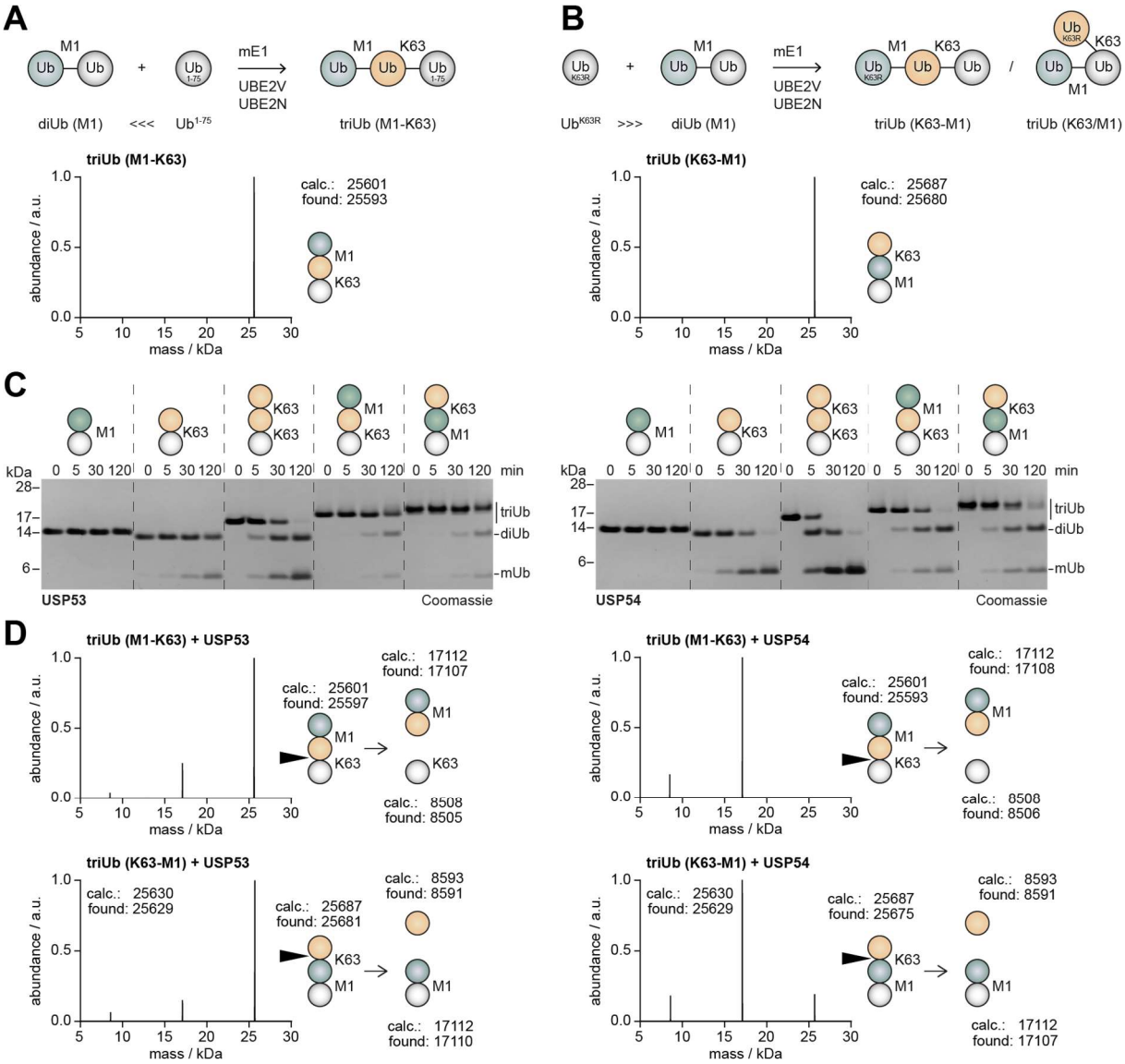

Figure 31: Generation and cleavage assay of heterotypic triUb chains containing M1 and K63 linkages. A-B) Schematic depiction of the building blocks and enzymatic assembly steps for triUb (M1-K63) (A) or triUb (K63-M1 (B). Ubiquitin with a free C-terminus is depicted in white, ubiquitin conjugated to the N-terminus (M1 linkage) in green and ubiquitin conjugated to K63 in yellow. Deconvoluted mass spectra are shown for both final triUb chain substrates. C) Differently linked diUb and triUb chain substrates were incubated with USP53$^{20-368}$ or USP54$^{21-369}$. Samples were taken at indicated time points and analyzed by SDS-PAGE and Coomassie-staining. D) Samples corresponding to the 120 min time point in panel C were further analyzed by intact mass spectrometry and the corresponding deconvoluted mass spectra are shown for the heterotypic triUb substrates. Major cleavage events are shown schematically and the cleavage sites are indicated by black arrows.

M1-linked diUb was conjugated to K63 of ubiquitin with a truncated C-terminus (Ub$^{1-75}$) (Figure 31A). Ub$^{1-75}$ cannot be further conjugated and was used in excess to favor the formation of mixed M1-K63-linked triUb chains over the formation of potential by-products. After purification, pure mixed M1-K63-linked triUb chains were obtained (Figure 31A). To generate

mixed K63-M1-linked triUb chains, Ub K63R was assembled to M1-linked diUb (Figure 31B). The purified substrate mixture may contain branched M1/K63-linked triUb chains, as these can be formed with the used building blocks and are indistinguishable from mixed K63-M1-linked triUb chains by mass spectrometry (Figure 31B).

Cleavage assays with the mixed M1/K63-linked triUb chains showed that both heterotypic substrates were cleaved as efficiently as K63-linked diUb chains and less efficiently than K63-linked triUb chains by USP53 and USP54 (Figure 31C). The masses of the cleavage products indicated that both enzymes cleaved only the K63 linkages, while the M1 linkages were not cleaved (Figure 31D).

In conclusion, the functional analysis revealed USP53 and USP54 to be active DUBs. A specificity for K63 linkages with a preference for longer chains, which is unusual for USP DUBs, has been observed for USP54. USP53, on the other hand, depends on the recognition of K63-linked diUb in its S1 and S2 sites for efficient cleavage of isopeptide bonds in ubiquitin chains or between ubiquitin and substrate proteins.

4.2 Structural characterization of USP53 and USP54

To understand the molecular basis of the two distinct cleavage mechanisms of USP53 and USP54 and to visualize ubiquitin recognition, the second aim of this work was the structural elucidation of USP53 and USP54 in complex with ubiquitin using crystallography. There are several strategies to help crystallize the catalytic domains of DUBs.[116,218,243] Many USP DUBs contain large insertions or extended loops between the six main boxes that form the common catalytic core consisting of the fingers, palm and thumb domains. Trimming these extensions or replacing them with crystallization tags makes crystallization more likely.[243] Catalytic inactivation of DUBs can convert them into ubiquitin traps, allowing co-crystallization with ubiquitin or substrate mimetics.[244] This strategy has proven useful for linkage-specific DUBs. Their co-crystallization with the corresponding linked polyubiquitin substrates allowed the visualization of their additional ubiquitin binding sites.[113,116,118,119] A common strategy for the crystallization of DUBs is the use of ubiquitin-based probes with different warheads. Upon covalent bond formation, DUBs are stabilized and for USP DUBs, the stabilization of the flexible fingers domains makes crystallization more likely.[115,116] Another strategy involves crystallization of DUBs in complex with stabilizing cellular binding partners, for example of USP1 in complex with its cofactor UAF1.[245]

As part of the work for her bachelor's thesis in 2020, Lucia-Maria Kaps purified catalytic domain constructs of USP53 and USP54. However, both apo forms were resistant to crystallization, which may in part be due to the low enzyme concentration, as both enzymes tend to aggregate at concentrations above 3 mg/ml and low temperatures.

The second part of the results section describes the structural characterization of USP53 and USP54 by X-ray crystallography. Many of the approaches summarized above have been attempted to obtain crystals for USP53 and USP54. Crystallization studies of USP53 and USP54 were carried out for both enzymes in complex with mUb-PA and K63-linked diUb-PA. Additionally, crystallization trials were performed with catalytically inactive USP53 and USP54 with K63-linked-triUb chains.

4.2.1 Crystallization trials of USP53 and USP54 with Ub-PA or diUb(K63)-PA

In order to obtain USP53 and USP54 in complex with Ub-PA or K63-linked diUb-PA, the first objective was to generate large quantities of the probes. Ub-PA was generated using the intein-chemistry method described above (Figure 14A, Figure 32D). Previously, a protease-resistant triazole-based K48-linked diUb probe was used to label the SARS-CoV-1 enzyme PLpro. Structure determination of the complex allowed the visualization of the PLpro S2 site.[122] However, instead of using the triazole linkage, a simple way to produce large quantities of K63-linked diUb-PA was to enzymatically assemble the second ubiquitin moiety to Ub-PA. This

approach depended on the compatibility of Ub-PA or its precursor Ub-MesNa with the enzymes required for *in vitro* synthesis of K63-linked ubiquitin chains and was tested by co-incubation and SDS-PAGE analysis. While Ub-MesNa formed covalent adducts with the assembly enzymes, Ub-PA did not react with mE1, UBE2R and UBE2V, suggesting that Ub-PA does not interfere with their enzymatic activity and can be used as acceptor ubiquitin in K63 and K48 linkage conjugation reactions (Figure 32A). In a test assembly, a diubiquitin species formed upon incubation of Ub-PA and Ub K63R with mE1, UBE2V and UBE2V (Figure 32B). Adding the complete reaction mixture to USP53 and USP54 resulted in them being labeled by Ub-PA but also by diUb-PA, demonstrating that a diUb probe with a functional PA warhead was produced (Figure 32B).

Large quantities of K63-linked diUb-PA were obtained by a large-scale assembly reaction in which Ub K63R was conjugated to K63 of Ub-PA (Figure 32C). The use of Ub K63R prevented side reactions, as it cannot be conjugated to itself in K63 linkage assembly reactions. Conjugating enzymes and unreacted mUb species were removed by IEX and SEC, yielding pure K63-linked diUb-PA (Figure 32D, Figure S4). The effect of Ub-PA or diUb-PA labeling, and thus occupancy of the S1 or S1 and S2 ubiquitin binding sites of USP53 and USP54 (Figure 32E), was then tested by thermal stability assays to determine the melting temperatures of the resulting complexes. USP53 and USP54 were stabilized by Ub-PA labeling and a further increase in melting temperatures was observed upon binding of diUb(K63)-PA (Figure 32F-G). USP54~diUb-PA was the most stable complex with a melting temperature of 65 °C (Figure 32G).

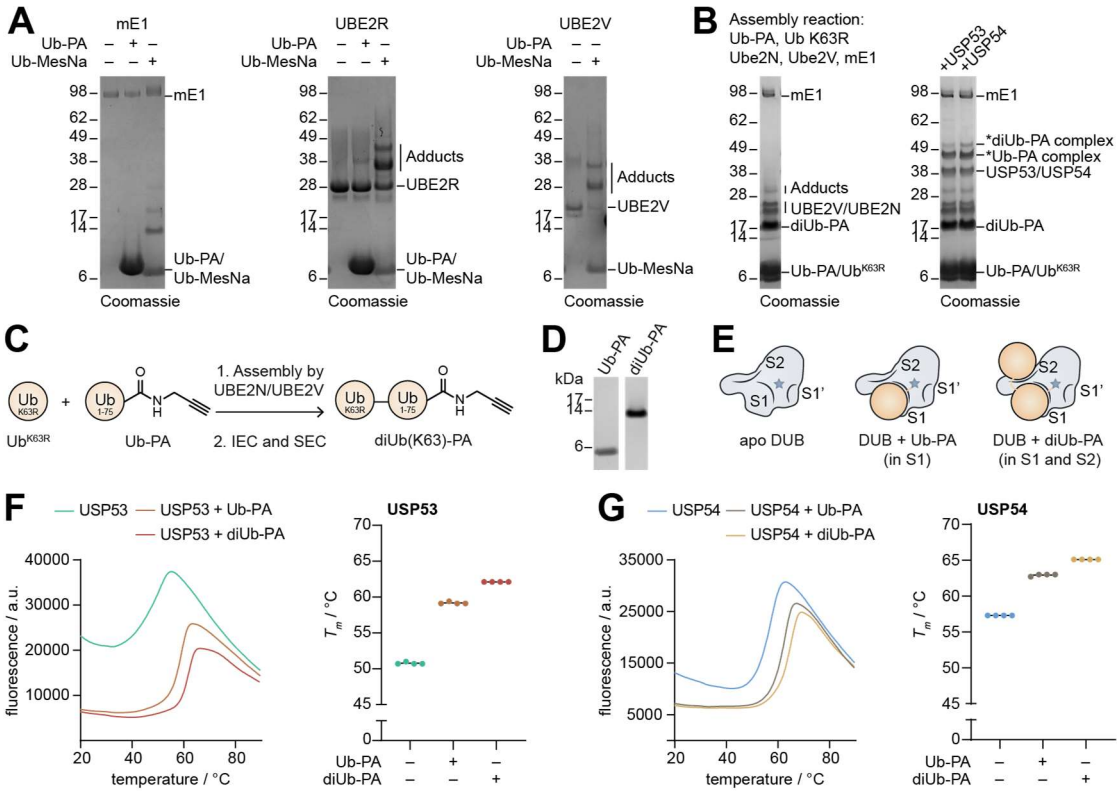

Figure 32: Effect of diUb(K63)-PA labeling on USP53 and USP54 stability. A) Ub-PA and Ub^{1-75}-MesNa were each incubated with ubiquitin chain assembly enzymes mE1, UBE2R or UBE2V. Their compatibilities were analyzed by SDS-PAGE and Coomassie-staining. B) The assembly of K63-linked diUb-PA was tested by mixing mE1, UBE2N, UBE2V and ATP with Ub-PA and Ub K63R as building blocks. Afterwards the complete reaction mixture was incubated with $USP53^{20-383}$ and $USP54^{21-369}$. Samples were analyzed by SDS-PAGE and Coomassie-staining. C) Scheme for the generation of diUb(K63)-PA using mE1 and the E2 enzymes UBE2N and UBE2V. D) Purified Ub-PA and diUb(K63)-PA were analyzed by SDS-PAGE and Coomassie-staining. E) Schematic for the binding modes of Ub-PA and diUb-PA to DUBs. E) $USP53^{20-368}$ was incubated with buffer, Ub-PA or diUb-PA. After the labeling reaction, the stability of USP53 was tested by thermal shift assay. F) The same assay as described in panel E was performed with $USP54^{21-369}$.

To obtain pure USP53 and USP54 in complex with Ub-PA or diUb-PA for crystallization trials, the purification scheme for USP53 and USP54 alone was adjusted and a labeling step integrated after the reverse Ni-NTA (Figure 33A). As the diUb probe is linked via a cleavable isopeptide bond, protein labeling competes with cleavage of the probe, more so for USP54 than USP53. To reduce this side-reaction, the effect of different temperatures and probe to DUB ratios was explored. Lowering the temperature to 4 °C minimized cleavage of diUb-PA and the subsequent formation of USP54~mUb-PA (Figure 33B). Additionally, a higher diUb-PA to DUB ratio led to less USP54~mUb-PA complex formation (Figure 33B). Having optimized the labeling conditions, a small-scale test purification according to the scheme in Figure 33A was performed for USP54. The flow-through of the reverse Ni-NTA purification was divided into three parts. One part was incubated with buffer, one with Ub-PA and one with diUb(K63)-PA. Partial labeling was visible after 10 min and labeling was almost complete after overnight incubation at 4 °C. Two protein bands were observed for USP54 alone as well as for the complexes due to the partial cleavage of USP54 during purification (Figure 33C). Impurities were removed and the respective proteins of different molecular weight were separated by

anion-exchange chromatography to give pure USP54 or USP54 complexes (Figure 33D). These results demonstrate that large amounts of Ub-PA and diUb(K63)-PA and subsequently also of the DUB complexes can be obtained in high purity.

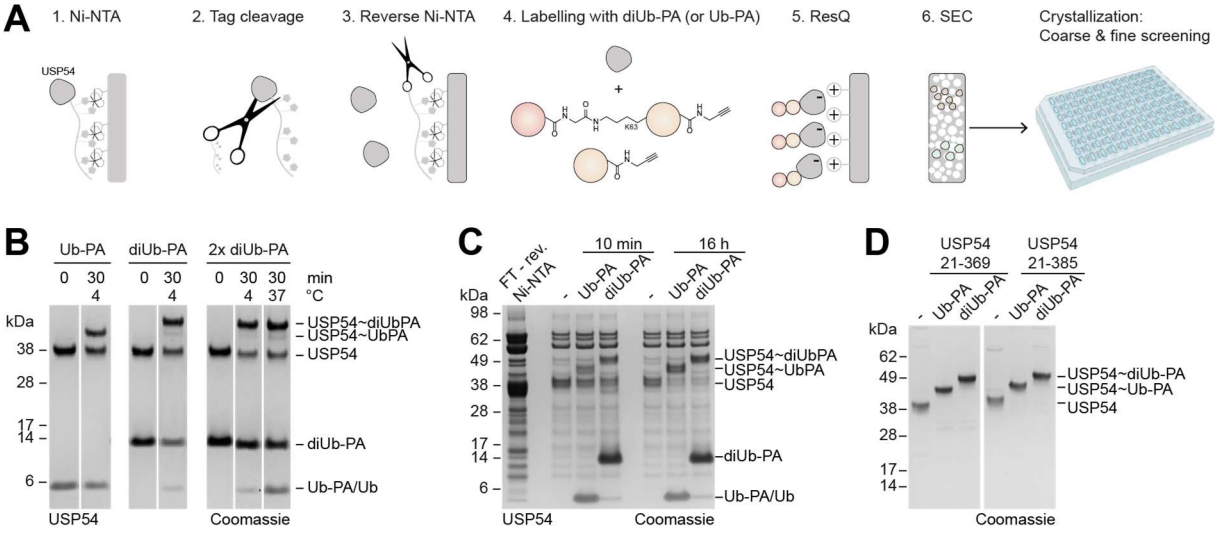

Figure 33: Complex purification for crystallization. A) Schematic depiction of the purification steps for USP53 and USP54 in complex with ubiquitin probes for crystallization. B) Probe labeling assay. Different conditions for labeling of USP54$^{21-369}$ with Ub-PA or diUb-PA were tested. Samples taken at indicated time points were analyzed by SDS-PAGE and Coomassie-staining. C) Test purification of USP54, USP54~Ub-PA and USP54~diUb-PA. The labeling efficiency and protein purity after ResQ purification were analyzed by SDS-PAGE and Coomassie-staining.

In general, after protein purification and complex generation, the sitting drop method was used for all coarse and fine screenings and drops were set up using a crystallization robot. Coarse screening to identify starting crystallization conditions for the purified protein complexes was performed with commercially available screening plates at 20 °C. Obtained crystals were cryo-protected when necessary, vitrified in liquid nitrogen and X-ray diffraction experiments were performed at 100 K. To obtain high amounts of USP53 and USP54, both proteins were expressed in large scale cultures of ~20-25 liters for each crystallization attempt. USP53 was purified and labeled according to the established protocol (Figure 33A). After labeling with Ub-PA, pure USP53$^{20-383}$~Ub-PA was obtained and concentrated to 6 mg/ml (Figure 34A). A T-shaped crystal grew from this protein solution at one condition, but resulted in poor diffraction quality when X-rayed (Figure 34A). The first large-scale attempt to purify USP53$^{20-383}$~diUb(K63)-PA yielded a mixture of the complex and impurities, including unlabeled USP53 and GST (Figure 34B). No crystals grew from this sample at a concentration of 5 mg/ml. A second purification attempt using an optimized USP53 construct and improved labeling conditions yielded pure USP53$^{20-368}$~diUb(K63)-PA (Figure 34B, Figure S4). The complex was only concentrated to 2.8 mg/ml due to incipient protein aggregation. However, as opposed to the apo-form of USP53, different crystallization conditions were identified for USP53~diUb(K63)-PA (Figure 34B, Figure S5). Fishing the resulting crystals for vitrification and X-ray crystallography proved difficult due to their small size and, in the case of some crystals, their soft surface. In order to obtain well diffracting crystals suitable for structure

determination, fine screening for USP53~mUb-PA and USP53~diUb-PA, which has not been carried out, will be necessary.

A slightly different approach was taken for coarse screening of crystallization conditions for USP54. As USP54$^{21-385}$ is partially C-terminally truncated during the first purification steps and to maximize final yields of uniform complexes with identical molecular weight, an additional IEX purification step was performed to separate the two USP54 proteins after the reverse Ni-NTA chromatography. Then, USP54$^{21-369}$ was labeled with diUb(K63)-PA and USP54$^{21-385}$ was labeled with Ub-PA. After a second IEX and a final SEC, pure USP54~mUb at a concentration of 6.5 mg/ml and pure USP54-diUb(K63)-PA were obtained (Figure 34C-D, Figure S4). In contrast to USP53~diUb(K63)-PA and apo USP54, USP54-diUb(K63)-PA was concentrated to 13.4 mg/ml without any visible aggregation. While no crystallization condition could be identified for USP54~mUb, USP54~diUb(K63)-PA crystals grew for different conditions (Figure 34D, Figure S5). X-ray diffraction of the crystals produced diffraction patterns varying between 4 and 15 Å resolution and showed that crystals in two different space groups, P3 and P222, were obtained. These groups corresponded to slightly twisted triangular and hexagonal prism shaped crystals, respectively (Figure 34D). The most promising crystal, which belonged to the space group P222 and diffracted to 4-5 Å resolution, was grown in the presence of PEG400, $CaCl_2$ and HEPES at pH 7.5.

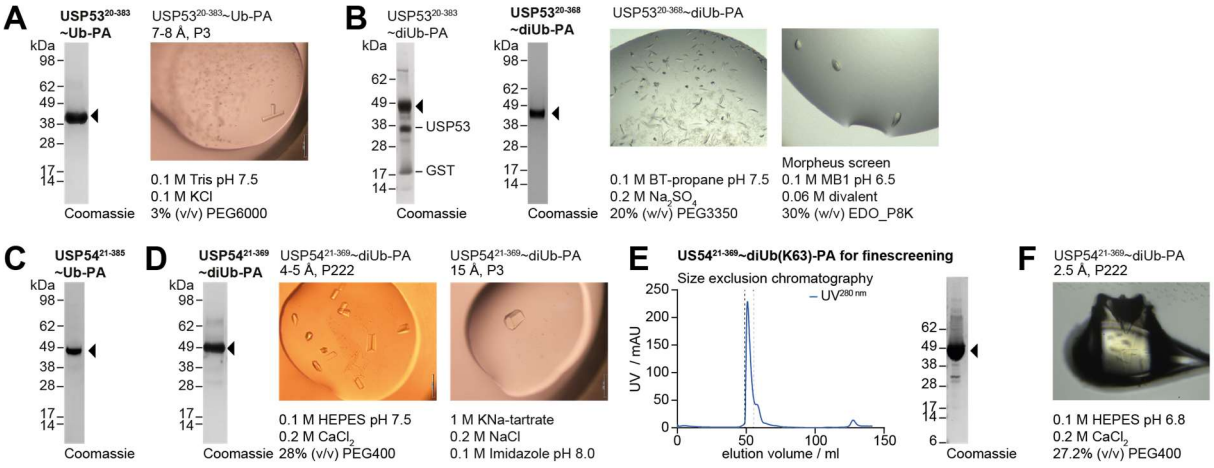

Figure 34. Differently ubiquitin-probe labeled USP53 and USP54 complexes used for crystallography. Samples of purified USP53$^{20-383}$~Ub-PA (A), USP53$^{20-383}$~diUb(K63)-PA, USP53$^{20-368}$~diUb(K63)-PA (B), USP54$^{21-385}$~Ub-PA (C) or USP54$^{21-369}$~diUb(K63)-PA (D) were analyzed by SDS-PAGE and Coomassie staining and used for crystallizations trials. Images of the obtained crystals are shown and the crystallization conditions are annotated. E) SEC chromatogram of USP54$^{21-369}$~diUb(K63)-PA. The dashed line indicates combined fractions which were analyzed by SDS-PAGE and Coomassie-staining and used for fine screening. F) An image of the USP54$^{21-369}$~diUb(K63)-PA crystal in a fishing loop. The crystal was obtained from the protein sample in panel D, diffracted to 2.5 Å and was used for structure determination.

For fine screening, USP54$^{21-369}$~diUb(K63)-PA was freshly prepared according to the scheme in Figure 33A after direct expression of USP54$^{21-369}$, a construct corresponding to the truncated USP54 species (Figure 34E). To improve the diffraction resolution, fine screening plates were prepared based on two initially identified conditions covering both space groups (Figure 34E).

Crystals from the fine screening plate based on the K/Na-tartrate condition showed improved diffraction patterns up to a resolution of 4 to 15 Å. However, crystals from the PEG400 fine screening plates generally diffracted better to resolutions in the range of 3 to 4 Å. Fortunately, one USP54~diUb(K63)-PA crystal, set up in a 1:1 drop ratio of a reservoir solution containing 0.1 M HEPES pH 6.8, 0.2 M $CaCl_2$ and 27.2 % (w/v) PEG400 and of the 13 mg/ml USP54~diUb(K63)-PA protein solution, gave a diffraction pattern extending to 2.5 Å resolution and was used for structure determination (Figure 34F).

Diffraction experiments for the USP54~diUb(K63)-PA crystals obtained during coarse screening revealed that the complex contained zinc ions. Therefore, a native and an anomalous dataset were recorded for the well diffracting USP54~diUb(K63)-PA crystal and both were used to solve the structure to a resolution of 2.5 Å (Table 15). Four copies of USP54~diUb-PA made up the asymmetric unit and were well covered by electron density (Figure 35).

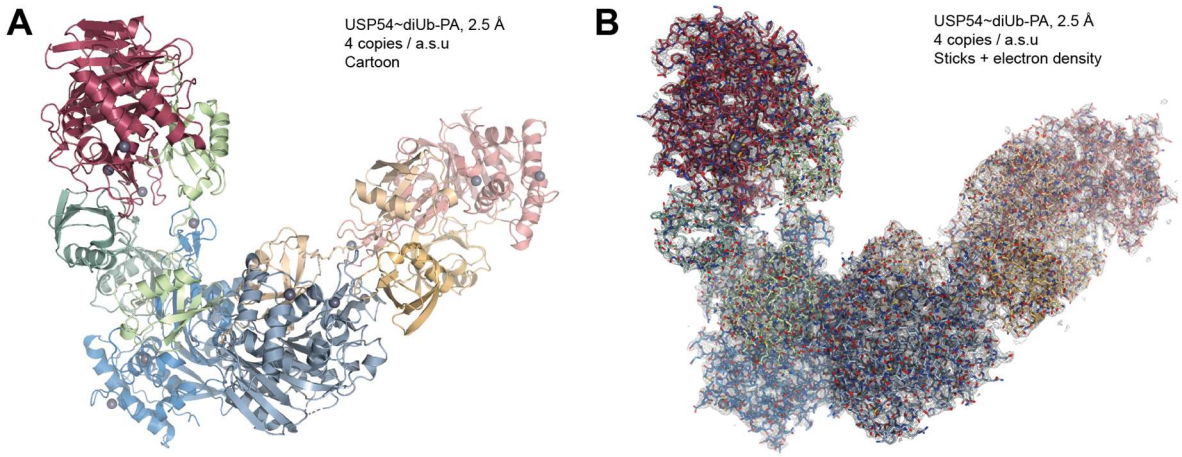

Figure 35: Asymmetric unit of USP54~diUb-Pa. A) Cartoon representation of the cell unit containing four copies of USP54~diUb-PA separated into 2 packages. B) Stick representation with overlayed electron density of the asymmetric unit of USP54~diUb-PA.

Table 15. Data collection and refinement statistics.

	USP54~diUb(K63)-PA (SAD data)	USP54~diUb(K63)-PA (native data, PDB code: 8C61)
Data collection		
Beamline	SLS – PX2	SLS – PX2
Wavelength	1.282 Å	1.000 Å
Space group	$P\,2_12_12_1$	$P\,2_12_12_1$
Cell dimensions		
a, *b*, *c* (Å)	122.58, 126.59, 144.22	122.74, 126.56, 144.17
α, β, γ (°)	90, 90, 90	90, 90, 90
Observed reflections	1,859,182 (122,127)	699,375 (71,819)
Unique reflections	69,709 (4,449)	78,247 (7,759)
Resolution (Å)	88.06 – 2.6 (2.66 – 2.6)	63.28 – 2.5 (2.59 – 2.5)
R_{merge}	0.091 (2.410)	0.062 (1.239)
R_{meas}	0.094 (2.498)	0.066 (1.313)
I/σ(I)	24.5 (2.2)	16.2 (1.7)
$CC_{1/2}$	1.000 (0.789)	0.998 (0.682)
Completeness (%)	100 (100)	100 (100)
Redundancy	26.7 (27.5)	6.6 (6.3)
Wilson *B* (Å^2)	74.4	74.8
Phasing		
Method	SAD	MR
Resolution (Å)	2.6	
Anom. completeness (%)	100 (100)	
Anom. multiplicity	13.8 (13.9)	
<FOM>	0.5179	
Refinement		
Copies / a.s.u.		4
Resolution (Å)		2.5 Å
No. reflections		78,226
R_{work} / R_{free} (%)		20.0 / 24.3
No. atoms		14,892
Protein		14,647
Ligand		32
Water		213
B factors (Å^2)		95.9
Protein (Å^2)		96.2
Ligand (Å^2)		88.8
Water (Å^2)		79.5
R.m.s.d.		
Bond lengths (Å)		0.004
Bond angles (°)		0.62
Ramachandran (favored / allowed / outlier) (%)		96.8 / 3.2 / 0
Clashscore		8.5
Rotamer outliers (%)		2.8

The dataset was collected from a single crystal. Values in parentheses are for highest-resolution shell. a.s.u., asymmetric unit. R.m.s.d., root mean square deviations.

Of the four copies in the asymmetric unit, two USP54~diUb-PA copies each arranged in a criss-cross formation and showed good alignment when superimposed (Figure S6, Figure 36A). In the arrangement of the two copies, the two ubiquitin moieties containing the warhead were bound to the S1 binding sites of two USP54 molecules, while the distal ubiquitin moieties occupied the S2 sites of the respective other USP54 molecule (Figure 36A). This formation rigidified the fingers domain of USP54. Multi-angle light scattering (MALS) experiments were performed to test whether this was due to crystal packing or an orientation adopted in solution. The determined molecular weights agreed with the calculated values of the monomeric complexes of USP54, USP54~Ub-PA and USP54~diUb-PA (Figure 36B). Consequently, the SEC-MALS results show that the USP54~diUb-PA complex exists in solution as a monomer with one diUb-PA molecule covering the S1 and S2 sites (Figure 36C).

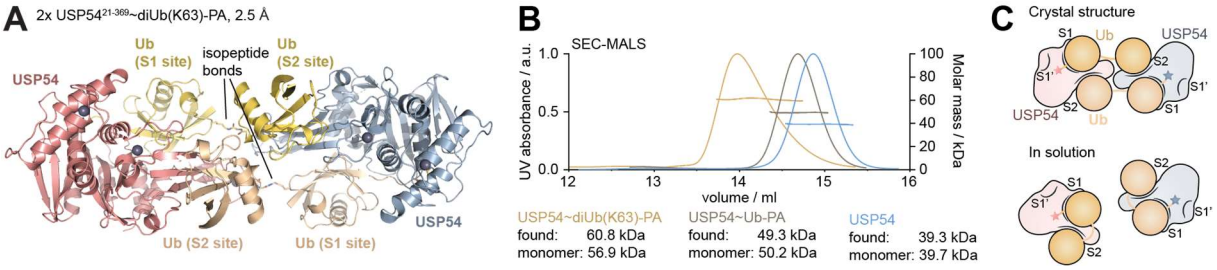

Figure 36: USP54~diUb-PA is dimeric in the crystal and monomeric in solution. A) Cartoon representation of two intertwined USP54~diUb-PA molecules. One USP54 is shown in grey, the other USP54 molecule is shown in red and isopeptide-linked ubiquitin moieties are shown in the same color, one in wheat and one in yellow. B) SEC-MALS measurement of USP54, USP54~Ub-PA and USP54~diUb-PA. C) Schematic representation of the ubiquitin binding modes of USP54 as found in the crystal structure and as assumed in solution.

4.2.2 USP54~diUb(K63)-PA structure

The USP54~diUb-PA structure in a matched topology illustrates that ubiquitin was bound to the S1 site formed by the front of the fingers and parts of the thumb and palm domains of USP54 (Figure 36A). The S2 site of USP54 is cryptically encoded at the backside of the fingers domain. Consistent with the binding of one diUb-PA molecule by USP54 in solution, the C-terminal residue of ubiquitin bound in the S2 site was in close proximity to the K63 side chain of the S1 ubiquitin in the USP54 crystal structure (Figure 37A). Superimposing the corresponding four copies of USP54~diUb~PA shows that they were oriented in the same way (Figure S6). USP54 shares the typical catalytic domain structure found in the USP family, which includes the palm, thumb and fingers domains, shown in red, grey and green, respectively (Figure 37B). In addition to the zinc atom coordinated at the tip of the fingers domain, which is present in many USP DUBs, the structure revealed two additional zinc finger motifs in the thumb domain of USP54 (Figure 37B). USP54 contains a canonical catalytic triad composed of cysteine, histidine and aspartate. In the structure, these residues were arranged in an active conformation and the warhead of the diUb-PA probe formed a covalent bond with the catalytic cysteine (Figure 37C). Mutation of the catalytic cysteine or histidine in USP54 and

in USP53 resulted in complete loss of their catalytic activities (Figure 37D-E). However, probe-binding was only partially disrupted for the catalytic histidine mutants, demonstrating the importance of the catalytic histidines of USP53 and of USP54 for the polarization of the catalytic cysteines for cleavage activity, but less for ubiquitin binding and probe reactivity (Figure 37F, Figure S7A).

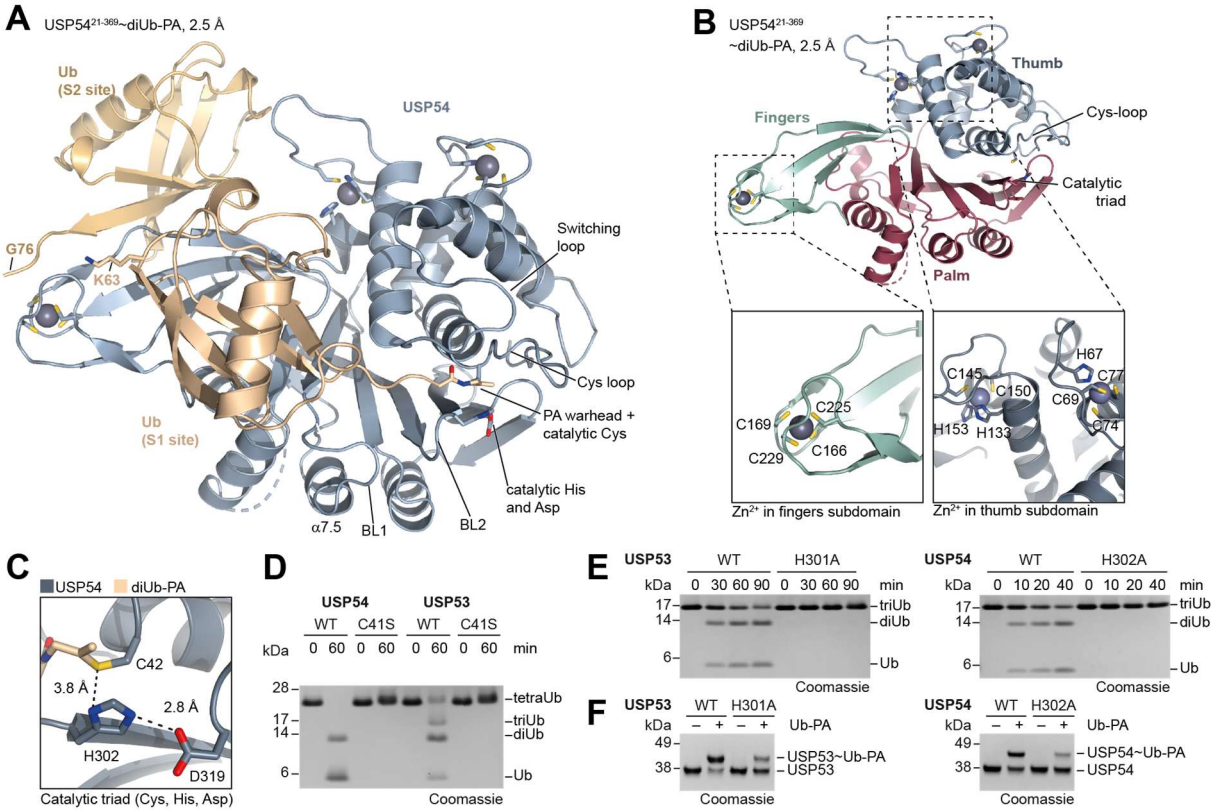

Figure 37: Crystal structure of USP54~diUb(K63)-PA. A) Cartoon representation of the matched structure of the catalytic domain of USP54 (grey) with ubiquitin (yellow) bound in its S1 and S2 sites. Important features are annotated. B) Cartoon representation of the catalytic domain of USP54 from the USP54~diUb(K63)-PA structure. The thumb domain is colored in grey, the fingers domain in green and the palm domain in red. Enlargements highlight the three zinc ions, which are shown as grey spheres and are present in the finger and thumb subdomains C) Zoom-in into the catalytic triad of USP54 consisting of C42, H302 and D319. D) Gel-based cleavage assays. USP53$^{20-383}$, USP54$^{21-369}$ and the respective catalytic cysteine mutants USP53$^{20-383}$ C41S and USP54$^{21-385}$ C42S were incubated with K63-linked tetraUb chains. Samples were taken at 0 and 60 min and analyzed by SDS-PAGE and Coomassie-staining. E) Gel-based cleavage assays. USP53$^{20-383}$, USP54$^{21-369}$ and the respective catalytic histidine mutants USP53$^{20-383}$ C41S and USP54$^{21-385}$ C42S were incubated with K63-linked triUb chains. Samples were taken after indicated reaction times and analyzed by SDS-PAGE and Coomassie-staining. F) The same proteins as in panel E were incubated with Ub-PA and labeling was analyzed by SDS-PAGE and Coomassie-staining.

A closer look at the blocking loops 1 and 2 of USP54 revealed a completely different picture compared to other USP DUBs. Blocking loop 1 (BL1) was less extended and instead an additional alpha-helix was identified, termed α7.5 due to its intermediate position between the alpha helices 7 and 8 as annotated for other DUBs (Figure 38A).[124] The blocking loop 2 (BL2), normally located just in front of the catalytic histidine and connecting two beta strands, was not present in USP54. Instead, the two beta strands were connected by a beta turn (Figure 38B). An overlay with USP2 and USP14 highlights these differences (Figure 38A), which are also reflected in the alignments of the corresponding sequences of USP54 and other USP DUBS

(Figure 38C-D). In particular, residues conserved in other USP DUBs are different in USP54 and its close homologue USP53. Unique residues found only in USP53 and USP54 are marked with black boxes in the alignment (Figure 38C-D). The sequence encoding the BL1 in other USP DUBs can be split into two parts for the corresponding sequence of USP54. The first part encodes the specially shaped and truncated BL1 and the second part encodes the additional alpha-helix (Figure 38C). Almost the entire sequence encoding for BL2 in other USP DUBs is missing in USP54, leaving only two residues that form a beta turn (Figure 38D). The sequence of USP53 aligns well with USP54, suggesting that BL1 and BL2 of USP53 also adopt a structure similar to the one found in USP54.

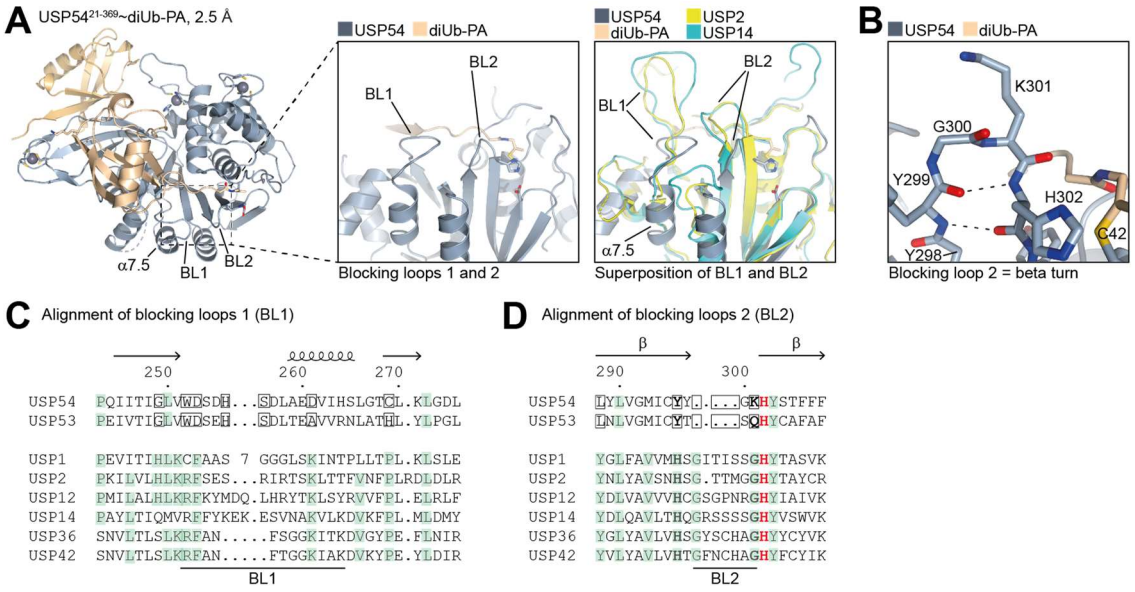

Figure 38: The blocking loops of USP54 have a unique architecture. A) Cartoon representation of USP54 in complex with diUb-PA for overview, with the additional alpha-helix and blocking loops annotated. Enlargement of the area of USP54 (grey) containing BL1 and BL2 (*left*). The same area is also shown overlaid with USP2 and USP14 (*right*). B-C) Alignment of the USP54 sequences encoding blocking loop 1 (B) and blocking loop 2 (C) with other USP DUB sequences. The structural annotation and amino acid numbers are from USP54. The BL1 and BL2 annotations are fitted to USP2.

Another unique feature found in USP54 was an elongated Cys-loop, here illustrated in comparison to USP2 and USP14 (Figure 39A). Generally, in USP DUBs, this Cys-loop is located before the catalytic cysteine in the S1' site and is flanked by two asparagine residues.[123] The positions of these asparagine residues in USP2 and USP12 align well with those in the USP54 structure (Figure 39A). The Cys-loop elongation is also reflected in the sequence of USP54 as well as of USP53, but not found for any other USP DUB (Figure 39B). Its importance for USP53 and USP54 activity was tested by exchanging their original loop sequence NEPGQNS with the sequence NLGNT which is found in many USP DUBs (Figure 39B). Cleavage of K63-linked triUb chains was abolished for the LGNT variants, while probe binding was minimally retained for USP53 LGNT and completely for USP54 LGNT (Figure 39C-D). One of the flanking asparagine residues in USP54 is positioned to act as an oxyanion hole, stabilizing the tetrahedral intermediates during isopeptide bond cleavage. Mutation of this

asparagine to alanine in USP54 and also in USP53 abolished catalytic activity while reactivity with ubiquitin probes was retained (Figure 39E-F, Figure S7B). These experiments demonstrated that the elongated Cys-loop is essential for the cleavage activity of USP53 and USP54. However, the mechanism for K63 linkage specificity could not be deduced from this experiment.

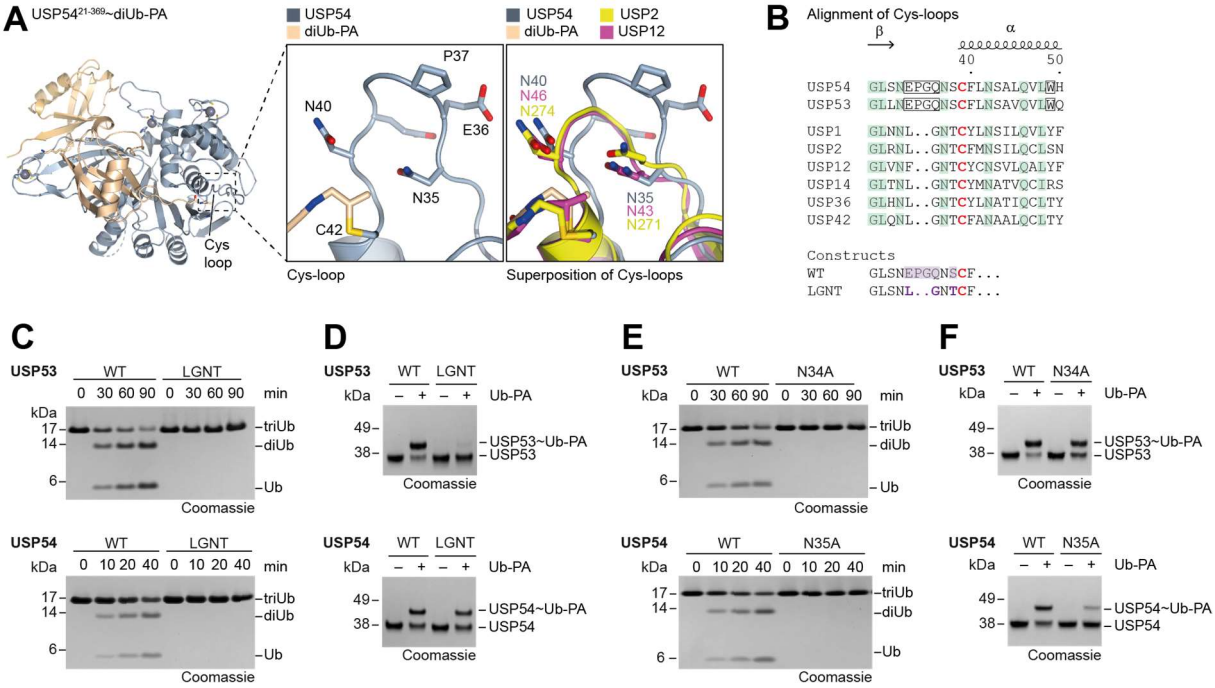

Figure 39: Analysis of the Cys-loop of USP54 and USP53. A) Close-up of the Cys-loop of USP54, alone (*left*) and overlayed with the Cys-loops of USP2 and USP12 (*right*). B) Sequence alignment of the Cys-loop in USP54 with its close homologue USP53 and other USP DUBs. LGNT constructs of USP53 and USP54 were generated to alter their loop sequences to match those in other USP DUBs. C) K63-linked triUb was incubated with USP53$^{20-383}$, USP54$^{21-369}$ and the respective LGNT mutants. Samples were taken at indicated time points and were analyzed by SDS-PAGE and Coomassie-staining. D) Ub-PA was incubated with the same proteins as in panel C and labeling was analyzed by SDS-PAGE and Coomassie staining. E) The same experiment as in panel C was performed with USP53$^{20-383}$ WT and N34A as well as with USP54$^{21-369}$ WT and N35A. F) The same experiment as in panel D was performed with the proteins used in panel E.

4.2.3 Ubiquitin binding in the S1 site of USP54

USP DUBs bind ubiquitin in their S1 sites through extensive interactions with the I44, I36 and F4 patches of ubiquitin and direct the scissile bond into the active site through recognition of the C-terminal tail of ubiquitin.[94] The ubiquitin in the S1 site of USP54 binds to the anterior part of the fingers domain and its C-terminus extends into the catalytic cleft between the thumb and palm domains (Figure 40A). Using the PISA web server, an interface area of 1088 A² was calculated for the interface of ubiquitin and the S1 site of USP54.[228] A closer look at interactions between ubiquitin and the S1 site of USP54 revealed a hydrogen bond between K6 of ubiquitin and D221 of USP54 as well as hydrophobic interactions between I44 of ubiquitin and Y184 of USP54 flanked by a hydrogen bond between R42 of ubiquitin and the hydroxy group of Y184 of USP54 (Figure 40A). To test the importance of these two prominent interactions for the cleavage activity of USP54 and also of its homologue USP53, K63-linked triUb chains with

mutations only in the middle ubiquitin were generated by Sarah Recknagel as part of her master thesis. A similar approach as described for the mixed ubiquitin chains was used and pure triubiquitin species obtained (Figure S8C). Mutation of the positively charged K6 to a negatively charged aspartate or of I44 to the smaller residue alanine in the middle ubiquitin strongly disrupted cleavage activity of USP53 (Figure 40B). The I44A mutation in the middle ubiquitin affected the cleavage activity of USP54 in a comparable manner and the K6E mutation resulted in a limited reduction of triUb cleavage by USP54 (Figure 40C). These results indicate, that ubiquitin is bound to the S1 site of USP54 as seen in the crystal structure, that USP53 is likely to bind ubiquitin in the S1 site in a very similar manner, and that the common strong interaction mediated by I44 of ubiquitin is important for ubiquitin recognition in the S1 sites of USP54 and USP53.

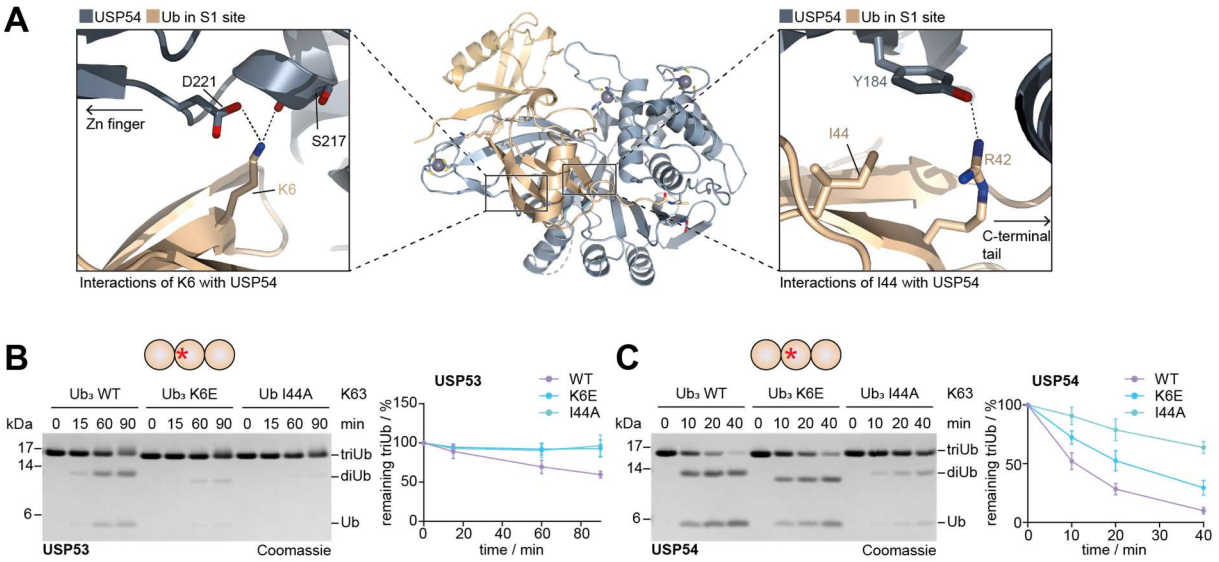

Figure 40: Interactions of Ubiquitin with the S1 site of USP54. A) Zoom-in into the interactions of USP54 with K6 (*left*) and the I44 patch (*right*) of the ubiquitin bound in the S1 site. B) K63-linked triUb chains containing specific mutations in the middle ubiquitin were assembled and tested by Sarah Recknagel. After incubation of the annotated triUb chains with USP5320-383 for indicated time points, samples were taken and analyzed by SDS-PAGE and Coomassie-staining. Cleavage activity of USP53 for wild-type and mutant triUb chains was quantified for three independent experiments by densitometry. Remaining triUb was plotted against incubation time. C) The same assay and analysis as in panel B was performed for USP54$^{21-369}$.

Interestingly, ubiquitin bound in the S1 site of USP54 was shifted by ~30° compared to ubiquitin bound by other USP DUBs, including USP7 and USP14, due to several changes in the interactions with ubiquitin (Figure 41A). First, in the USP54 structure, the F4 patch of ubiquitin is largely solvent-exposed. In other DUBs, shown here for USP2, the F4 patch is covered by a hydrophobic residue located at the front of the fingers domain and two amino acids ahead of a zinc-coordinating cysteine (Figure 41B). Second, the I36 patch of ubiquitin is largely solvent-exposed in USP54, as its BL1 assumes an unusual shape, orienting away from ubiquitin and forming the additional alpha-helix 7.5 (Figure 41C, Figure 38A). Normally, the I36 patch interacts with a hydrophobic residue in the BL1 of USP DUBs, for USP14 this is Y332 (Figure 41C). Third, extensive hydrogen bonds are typically formed with the backbone of the C terminal

tail of ubiquitin. Two of these, formed between USP7 and ubiquitin, are not formed between USP54 and the backbone of R72 and R74 in ubiquitin due to the shortened BL2 and the differently shaped BL1. In conclusion, the crystal structure of USP54 in complex with diUb-PA revealed a weakened S1 ubiquitin binding site due to changes in the USP54 sequence and structure.

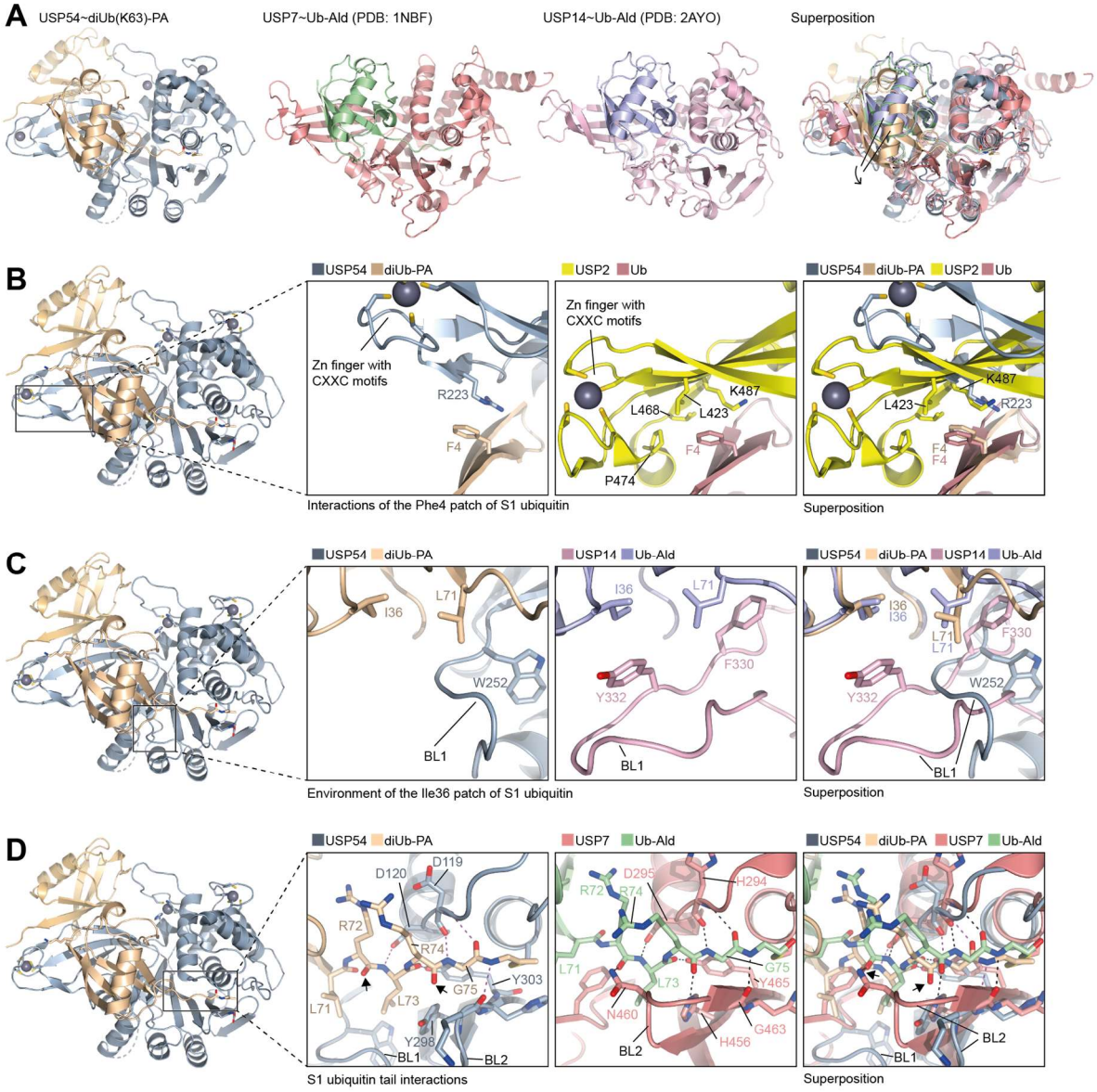

Figure 41: Comparison of S1 ubiquitin interactions of USP54, USP7, USP14 and USP2. A) Cartoon representation of USP54~diUb(K63)-PA (grey, yellow), USP7~Ub-Ald (red, green), USP14~Ub-Ald (pink, purple) and a superposition of all three structures. The shift of the S1 ubiquitin in USP54 is highlighted. B) Close-up of the interactions of the F4 patch in the S1 ubiquitin with USP54 (*left*) and USP2 (pdb: 2IBI, *middle*). The different engagement is illustrated in the overlay (*right*). C) Close-up of the environment of the Ile36 patch in the S1 ubiquitin with USP54 (*left*) and USP14 (pdb: 2AYO, *middle*) and a superposition (*right*). D) Close-up of the interactions of the C-terminal tail of the S1 ubiquitin with USP54 (*left*), USP7 (1NBF, *middle*) and a superposition (right). Differences in the hydrogen bond network are indicated by black arrows.

4.2.4 Ubiquitin binding in the S2 site of USP54

In vitro biochemical cleavage assays indicated the existence of an additional S2 binding site in USP54, which was then uncovered in the structure of USP54~diUb(K63)-PA (Figure 19, Figure 37). The interface area of the S2 site with ubiquitin was calculated by the PISA web server to be 840 A², comparable to the interface area of the S1 site with ubiquitin, indicating the importance of the S2 site for substrate recognition.[228] The extended and tight interface of ubiquitin with the S2 site in USP54 is visible in the surface representation of the structure and can be separated into two parts (Figure 42A). One is located at the back of the fingers domain of USP54 and the other is mediated by a loop in the thumb domain of USP54, stabilized by the additional zinc fingers (Figure 42A, D). The interface between the back of the fingers domain and ubiquitin in the USP54 structure is dominated by hydrophobic interactions. On the ubiquitin side, the I44 patch including I44, L8, V70 and H63 is mainly involved. The most central and prominent residue in the hydrophobic patch of the USP54 S2 site is F161 (Figure 42B). In USP53, this central residue in the S2 site is Y160, which is likely to form similar hydrophobic interactions with ubiquitin, while polar residues are typically found for other USP DUBs at this position (Figure 42C). The hydrophobic interaction core is flanked by a hydrogen bond between D174 in USP54 and R42 of ubiquitin (Figure 42B). The aspartate residue is also present in USP53 but not in any other USP DUB, as indicated by the black box in the sequence alignment (Figure 42C). A close-up of the thumb loop as part of the interface revealed the presence of hydrogen bonds between ubiquitin and USP54 in addition to the hydrophobic interaction between I144 of USP54 and F45 of ubiquitin (Figure 42D).

To validate the observed hydrophobic interactions between the S2 site and ubiquitin in the USP54 structure, the effect of mutating F161, as the central residue of the hydrophobic patch in USP54 to a potentially binding disruptive positively charged lysine, was tested. To this end, USP54 F161K alone and the corresponding Ub-PA and diUb(K63)~PA bound complexes were purified by Sarah Recknagel (Figure 42E). Stability measurements of USP54 F161K and the complexes showed that Ub-PA and diUb-PA binding stabilized USP54 F161K to the same extent (Figure 42F). These results suggest that the S1 site of USP54 F161K still binds Ub-PA and the proximal ubiquitin in diUb-PA, but that the F161K mutation prevents ubiquitin from binding to the S2 site as intended and hence no additional increase in melting temperature for diUb-PA binding compared to Ub-PA binding was observed (Figure 42G, Figure 32G). A Ub-RhoG cleavage assay provided additional evidence for unimpaired ubiquitin binding in the S1 site of USP54 F161K. A moderately increased catalytic efficiency for Ub-RhoG was determined for USP54 F161K compared to USP54 WT, probably due to prevention of unproductive binding of Ub-RhoG in the S2 site (Figure 42H).

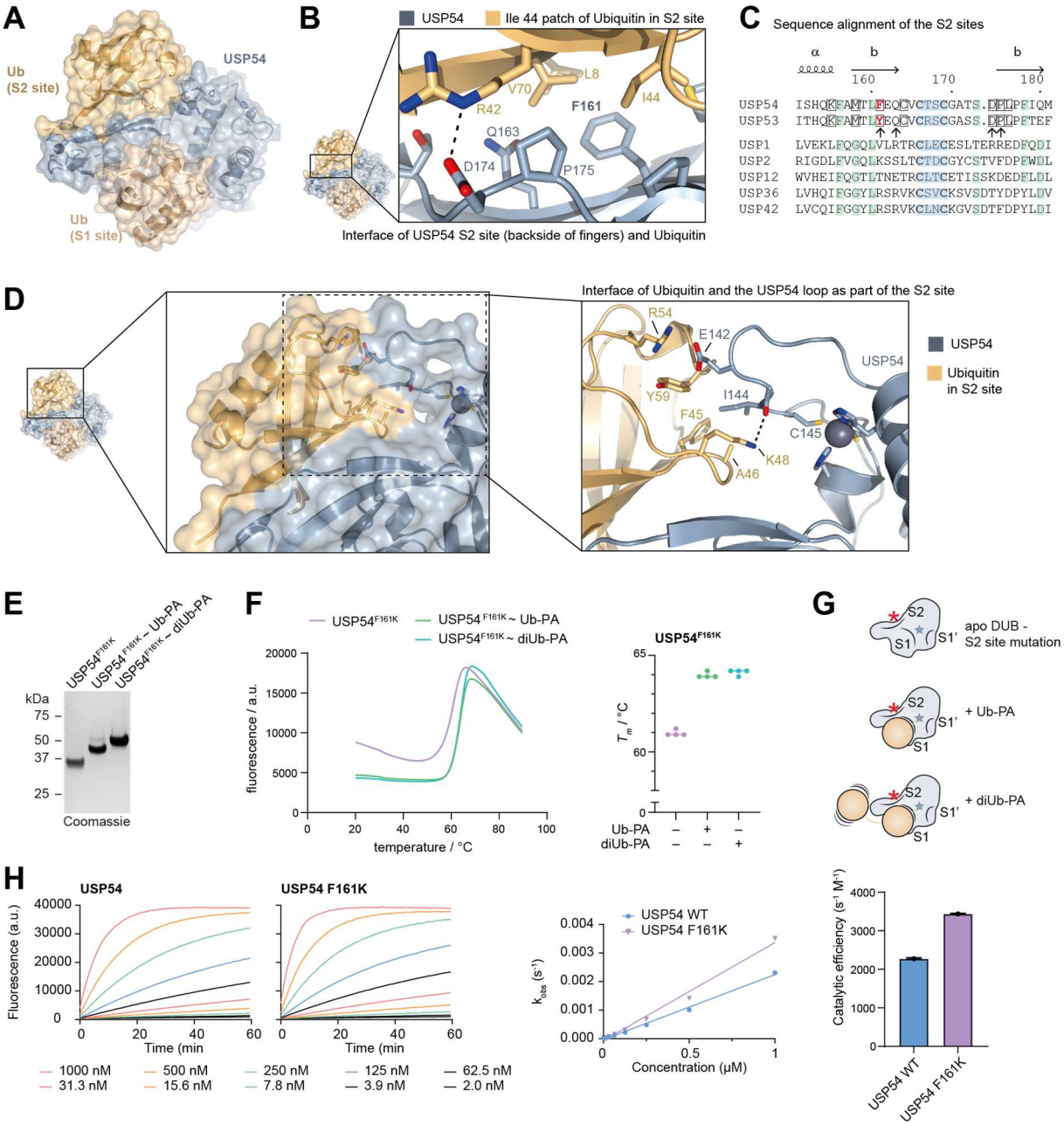

Figure 42: Interactions between ubiquitin and the S2 site of USP54. A) Cartoon and surface representation of USP54 in complex with diUb-PA. B) Close-up of the interactions between ubiquitin and the backside of the fingers as part of the S2 site. The dashed black line represents a hydrogen bond. C). Alignment of the sequences of the backside of the fingers domain of USP54 with sequences of other USP DUBs. D) Close-up of the interface between the thumb of USP54 as part of the S2 site and ubiquitin. A surface and a cartoon representation are shown. Residues mediating interactions are shown as sticks and the hydrogen bond is indicated by a black dashed line. E) Purified USP54 F161K, USP54 F161K~Ub-PA and USP54 F161K~diUb(K63)-PA were analyzed by SDS-PAGE and Coomassie-staining. F) The stability of the purified complexes from panel E were analyzed by TSA. Obtained melting temperatures are shown. G) Schematic representation of the probable binding modes of Ub-PA and diUb-PA by USP54 F161K. H) Ub-RhoG cleavage assay for different concentrations of USP54 and USP54 F161K. The obtained k_{obs} were fitted against the corresponding concentration and the catalytic efficiencies for Ub-RhoG were obtained as the slope after linear fitting. The experiments shown in panels E and F were performed by Sarah Recknagel.

Having shown that the F161K mutation in USP54 disrupts ubiquitin binding in the S2 site, its effect on the cleavage activity of USP54 on K63-linked polyubiquitin chains of different lengths was tested by quantitative gel-based cleavage assays. These assays were performed by

Sarah Recknagel as part of her master thesis. A decrease in cleavage activity on longer K63-linked tri- and tetraUb chains was observed for USP54 F161K (Figure 43A). Importantly, both USP54 F161K and USP54 WT cleaved K63-linked diUb to the same extent, confirming that binding and subsequent cleavage of ubiquitin chains in the S1 and S1' sites occur independently of binding events in the S2 site (Figure 43A). These findings indicate that hydrophobic interactions at the S2 site of USP54 are important for its increased cleavage activity on longer K63-linked ubiquitin chains. The picture was different for USP53. Mutation of the corresponding residue Y160 to a hydrophilic lysine reduced the cleavage activity of USP53 on K63-linked di-, tri- and tetraUb to similar levels, thus a strong decrease was observed for tri- and tetraUb (Figure 43B). These results highlight the importance of hydrophobic interactions at the S2 site of USP53 for its cleavage activity.

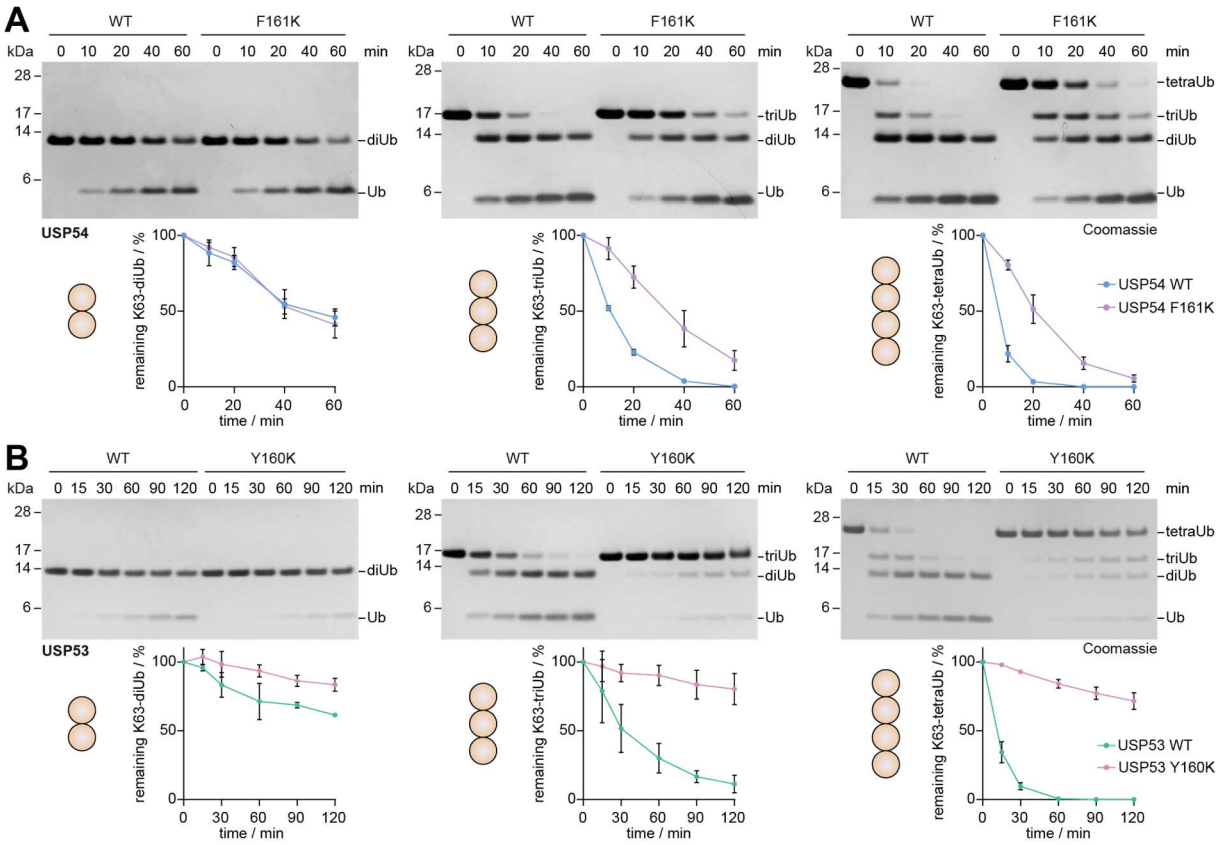

Figure 43: Effect of S2 site mutations on the cleavage activity on K63-linked polyubiquitin A) K63-linked di-, tri- and tetraUb were incubated with USP54 WT or USP54 F161K. Samples were taken at the indicated time points, separated by SDS-PAGE and protein bands visualized by Coomassie staining. Quantification of cleavage activity was performed for three replicates by densitometry of protein band intensities. The percentage of remaining initial substrate was plotted against the incubation time to visualize the cleavage activity. B) The same experiment and analysis as in panel A was performed with USP53$^{20-383}$ WT and USP53$^{20-383}$ Y160K. The substrates, assays and analysis presented in Figure 32 were performed by Sarah Recknagel as part of her master thesis in 2022.

In addition to the quantitative gel-based cleavage assays, the fluorescence polarization assays used to quantify the contribution of each ubiquitin binding site in USP53 and USP54 were also performed for the respective S2 site mutants. While Ub-KG-TAMRA was still processed by USP53 Y160K, albeit to a slightly lesser extent than by USP53 WT, and diUb-TAMRA cleavage

activity was comparable, a strong decrease in catalytic efficiency of USP53 Y160K for K63-linked triUb-TAMRA was observed compared to the wild-type protein (Figure 44A, C). These results support the notion that the S2 binding site is essential for efficient processing of longer K63-linked ubiquitin chains by USP53. The catalytic efficiencies of USP54 WT and USP54 F161K for Ub-KG-TAMRA and diUb-TAMRA were comparable, consistent with undisturbed binding in the S1 and S1' binding sites (Figure 44B-C). However, the catalytic efficiency of USP54 F161K for triUb-TAMRA did not show a 3-fold increase in comparison to diUb-TAMRA but rather a similar value (Figure 44B-C). Gel-based analysis of triUb-TAMRA cleavage by USP54 F161K revealed that this substrate was cleaved into equal proportions of fluorescent Ub-TAMRA and diUb-TAMRA at the first time points (Figure S9A). The results of both assays demonstrated that the F161K mutation in USP54 disrupts the binding of ubiquitin to the S2 site and thus also the preferential cleavage between the middle and proximal ubiquitin in triUb chains leading to a reduced cleavage activity on longer K63-linked ubiquitin chains. Based on the differential effect of the disruption of S2 site ubiquitin binding on USP53 and USP54 activity, these results again support the idea of two very distinct cleavage mechanisms for both proteins with different dependencies on their S2 sites.

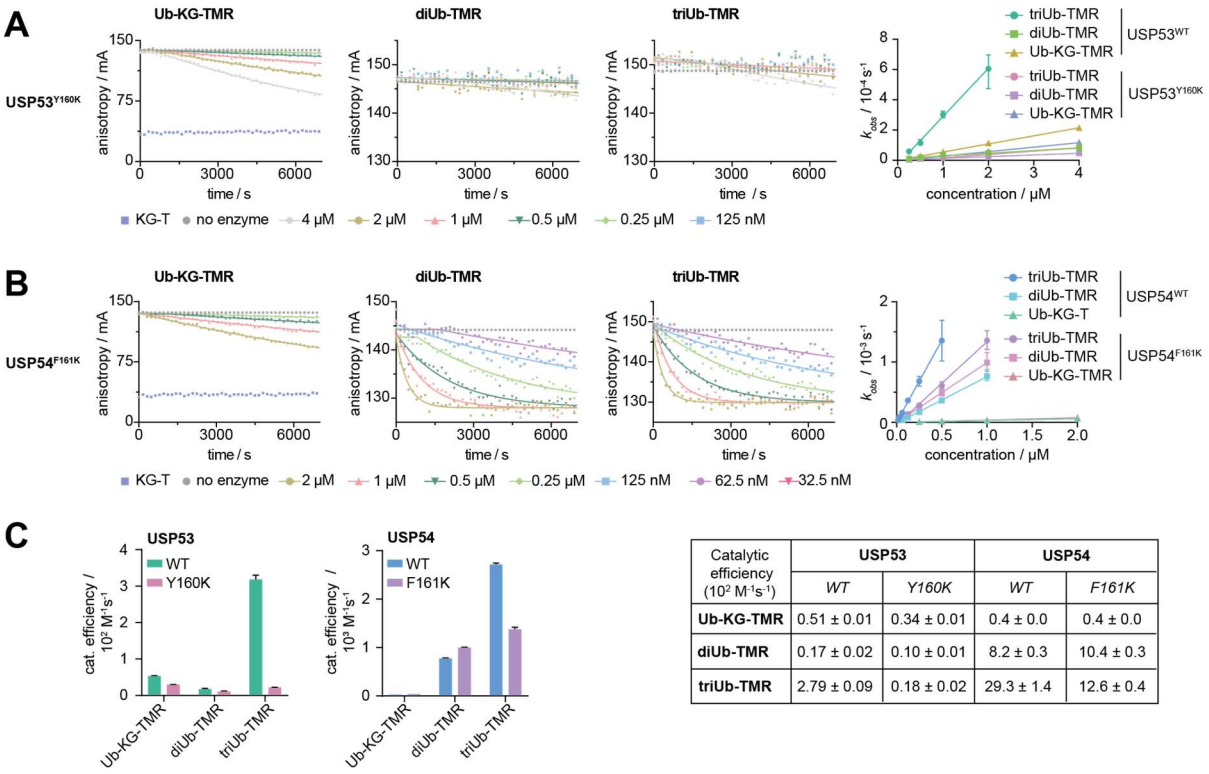

Catalytic efficiency (10^2 $M^{-1}s^{-1}$)	USP53		USP54	
	WT	*Y160K*	*WT*	*F161K*
Ub-KG-TMR	0.51 ± 0.01	0.34 ± 0.01	0.4 ± 0.0	0.4 ± 0.0
diUb-TMR	0.17 ± 0.02	0.10 ± 0.01	8.2 ± 0.3	10.4 ± 0.3
triUb-TMR	2.79 ± 0.09	0.18 ± 0.02	29.3 ± 1.4	12.6 ± 0.4

Figure 44: Fluorescence polarization assay for S2 site mutants. A-B) The fluorescence polarization was measured over time for each of the three substrates after addition of different concentrations of USP53$^{20-383}$ Y160K (A) or USP54$^{21-369}$ F161K (B). Observed rate constants (k_{obs}) were calculated using the function 'Plateau followed by one-phase decay' in GraphPad Prism and then plotted against the corresponding enzyme concentration. C) The catalytic efficiencies for each substrate were calculated as the slope of the linear regression line after linear fitting of k_{obs} plotted against the enzyme concentrations. The values for wild-type USP53 and USP54 were transferred from Figure 22 and displayed side by side with the calculated catalytic efficiencies of the S2 site mutants (*left*). Detailed values are given for each substrate in the table (*right*).

So far, the effect of mutations in the S2 site of USP54 on cleavage activity were tested. To validate the interface of ubiquitin with the S2 site in USP54 from the ubiquitin side as well, K63-linked triUb chains with additional mutations only in the distal ubiquitin of the triUb chains were generated and tested by Sarah Recknagel. The mutations, derived from the interface of ubiquitin with the back of the fingers domain of USP54, were designed to disrupt binding (Figure 42B). Ubiquitin with R42 mutated to negatively charged glutamate or ubiquitin with an I44A mutation were incorporated as the distal ubiquitin moiety into the K63-linked triUb chain. In addition, K63-linked triUb with H68R, V70A or F4R mutations in the distal ubiquitin were generated and tested. The masses of the mutated triUb chain substrates were validated by intact mass spectrometry (Figure S8B). Testing of these substrates against wild-type K63-linked triUb (Figure S8A), followed by quantification, revealed reduced cleavage activities of USP53 and of USP54, with the strongest effect for the R42E and I44A mutations and less pronounced for the H68R and V70A mutations (Figure 45A-B, Figure S9B). The F4R mutation served as a control and as expected had no effect on the cleavage activities of USP53 and USP54 (Figure S9B). Overall, these experiments demonstrate the importance of the I44 patch in ubiquitin for the interaction with the S2 sites of USP53 and USP54.

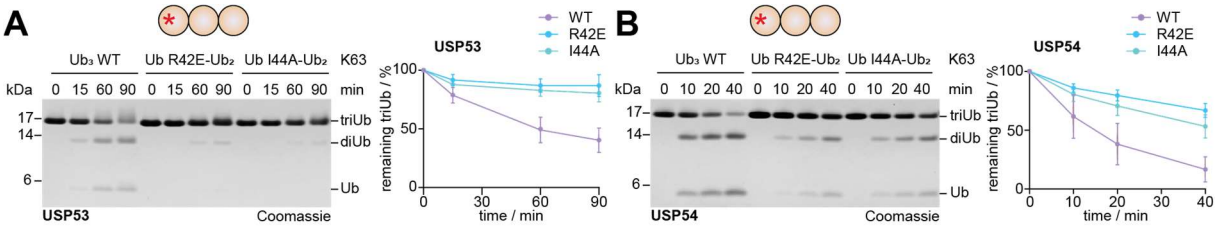

Figure 45: Gel-based cleavage assay of triUb substrates with mutations in the distal ubiquitin. A) WT K63-linked triUb or K63-linked triUb with an additional mutation in the distal ubiquitin moieties were incubated with USP53. Samples were taken after indicated time points and analyzed as described in Figure 32. B) The same assay as in panel A was performed for USP54$^{21-369}$. Sarah Recknagel performed the experiments illustrated in this figure.

In summary, the structure of USP54 in complex with diUb(K63)-PA revealed a fold that is characteristic for USP DUBs, but also many unique features. The biochemical characterization that followed the structural determination validated the quality of the USP54 structure and also the importance of the identified structural features including the S2 sites and the unique Cys-loops of USP54 and of USP53.

4.3 Analysis of ubiquitin binding in the S1' sites of USP53 and USP54

The structure of USP54 in complex with diUb(K63)-PA revealed how ubiquitin is bound in the S1 and S2 sites but not in the S1' site. This is particularly relevant for USP54, as ubiquitin binding in the S1' site greatly enhances its cleavage activity. Therefore, the next aim of the structural characterization part, was to visualize the interfaces of the S1' sites of USP53 and USP54 with ubiquitin using X-ray crystallography. In DUBs, the S1' site can be part of the catalytic domain. Other options are that the S1' site is formed by additional domains outside of the catalytic domain or by insertions into the catalytic domain.[94] In USP54, the S1' site is part of the catalytic domain as the functional experiments were performed with the catalytic domain that does not contain any insertions (4.1).[123] With the ultimate goal of obtaining a crystal structure of either USP53 or USP54 with a ubiquitin bound in the S1' site, several ubiquitin substrates and ubiquitin probes with different internal warheads were generated and tested (Figure 46). Following the reactivity tests, co-crystallization experiments were carried out using K63-linked triUb together with inactive USP53 and USP54 (Figure 46B).

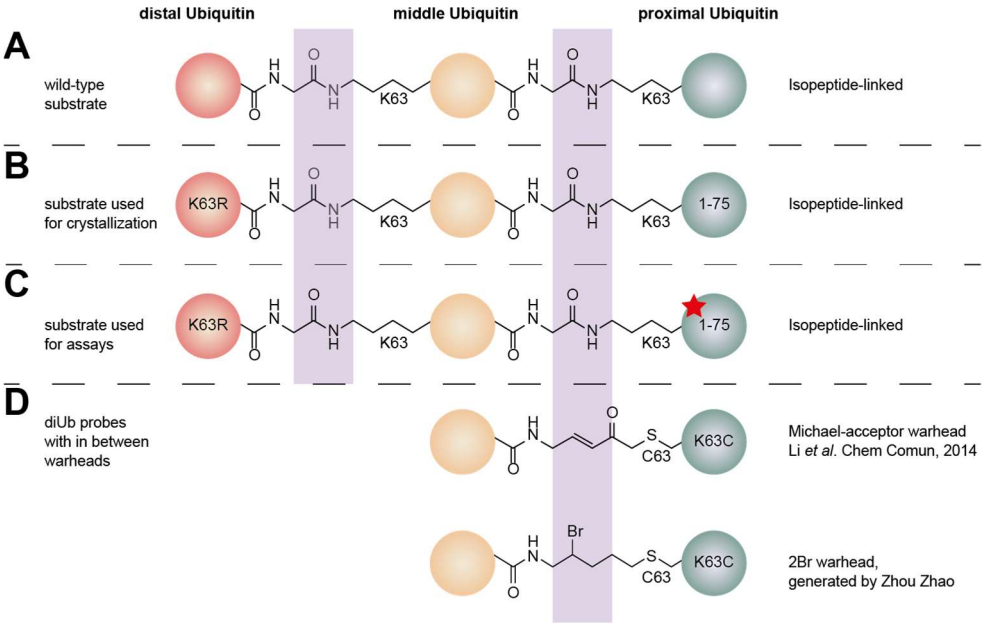

Figure 46: Overview of the used substrates and probes with in between warheads to analyze S1' site interactions with ubiquitin. A) Representation of the wild-type isopeptide linkages connecting the three ubiquitin molecules. B) Representation of the used K63-linked triUb substrate for crystallization trials. C) Representation of a K63-linked triUb substrate containing a proximal ubiquitin with additional mutations illustrated by a red star D) Representation of two diUb probes with different in between warheads. The distal ubiquitin is shown in red, the middle ubiquitin in yellow and the proximal ubiquitin in green. These are designed to bind to the S2 site, S1 site and S1' site of USP53 and USP54, respectively. The isopeptide bonds or the corresponding chemical structures in the probes that are positioned where the isopeptide bond would be are highlighted with a purple background.

4.3.1 Exploratory cleavage assays to analyze ubiquitin binding in the S1' sites

In the absence of a structure for USP53 or USP54 with ubiquitin bound in their S1' sites, information on ubiquitin binding in the S1' site was first sought by using K63-linked triUb chains with additional mutations in the proximal ubiquitin (Figure 46C). The mutations were chosen

based on the two common interactions patches F4 and I44 of ubiquitin. K63-linked triUb chains, that contain a proximal ubiquitin with an F4A mutation, an F4R mutation to disrupt possible hydrophobic interactions or an I44A mutation were generated by Sarah Recknagel. However, when tested, these three K63-linked triUb substrates were cleaved by USP53 and USP54 to the same extent as wild-type triUb chains (Figure 47A-B). The K63 linkage-specific DUB AMSH* interacts with Q62 and E64 of ubiquitin in its S1' site.[118] Therefore, K63-linked triUb containing a proximal ubiquitin with Q62A and E64A mutations was generated by Jan André Hane, to test for the possibility of a similar interaction mode in USP54. However, no difference in USP54 cleavage activity was observed (Figure 47C). These experiments suggest that F4, I44, Q62 and E64 are unlikely to be the major residues in ubiquitin that interact with the S1' sites of USP53 or USP54. However, they may still be important as part of an interaction network that is not addressed here, as it is not known yet how ubiquitin is bound in the S1' sites of USP53 and USP54.

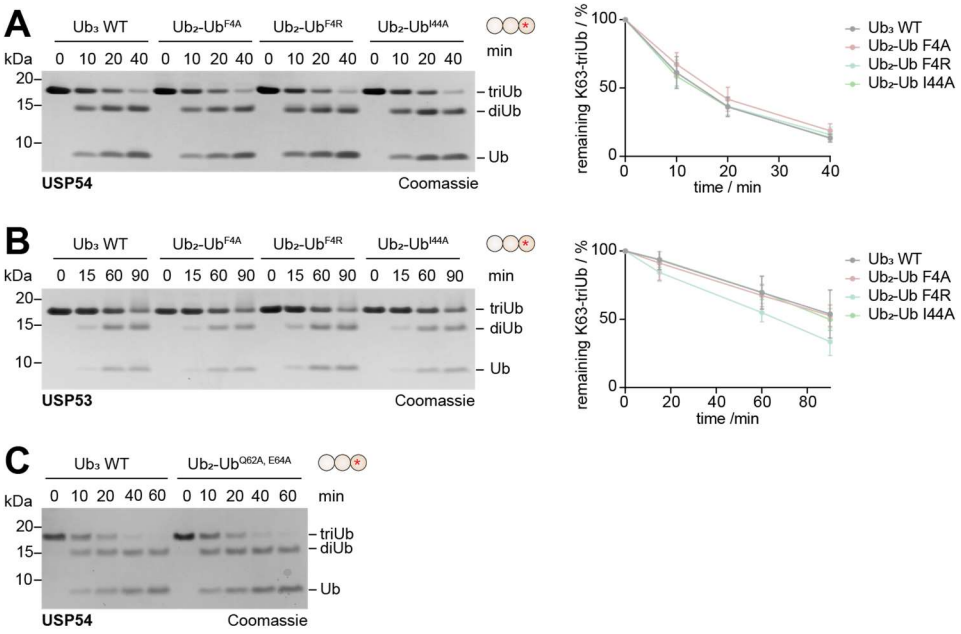

Figure 47: Gel-based cleavage assays to assess S1' site binding. A) Wild-type K63-linked triUb chains or K63-linked triUb chains containing specific mutations in the proximal ubiquitin were incubated with USP54$^{21-369}$ for indicated time points and analyzed by SDS-PAGE and Coomassie-staining. The cleavage activity was quantified by densitometry of protein band intensities for three independent experiments. To visualize the cleavage activities for each triUb substrate, the percentage of remaining triUb was plotted against the incubation time. B) The same assay and analysis as in panel A was performed for USP53$^{20-383}$. C) The same assay as in panel A was performed but K63-linked triUb chains with a double mutation in the proximal ubiquitin were used as substrates to test cleavage activity of USP54$^{21-369}$. The experiments in panel A and B were performed by Sarah Recknagel and the experiment in panel C was performed by Jan André Hane.

4.3.2 Crystallization trial of inactive USP53 and USP54 with K63-linked triUb

A common strategy for crystallizing linkage-specific DUBs is to use inactive enzymes that trap ubiquitin substrates instead of cleaving them. USP30, rendered inactive by mutation of the catalytic cysteine to alanine, was successfully co-crystallized with its substrate, K6-linked diubiquitin.[116] To assess the binding of inactive USP54 and USP53 to ubiquitin, a fluorescence

polarization binding assay was performed using Ub-KG-TAMRA and triUb-TAMRA (Figure 48A). For both enzymes, two different constructs were tested in which the cysteine was mutated to either alanine or to serine. However, even at very high DUB concentrations of up to 100 µM, the binding affinities for Ub-KG-TAMRA as well as for the more suitable substrate K63-linked triUb-TAMRA could not be reliably determined as the binding curves did not reach a plateau indicating low ubiquitin binding affinities of inactive USP53 and USP54 (Figure 48A). An initial flattening of the binding curve was observed for USP53 C41S and USP54 C42S, in contrast to USP53 C41A and USP54 C42A for K63-linked triUb. On this basis, large scale purifications of USP53$^{20-383}$ C41S and of USP54$^{21-369}$ C42S were performed and used for co-crystallization experiments. After SEC, pure proteins were obtained (Figure 48B). The substrate, K63-linked triUb, was generated as described for the mass-based cleavage assay substrates and then added in small excess to USP53 C41S and USP54 C42S (Figure 28B). The protein mixtures were concentrated to 8 mg/ml and then used to set up crystallization droplets in many different conditions. The achieved high concentration indicated the binding of triUb to the DUBs, as apo USP53 and USP54 cannot normally be concentrated to this level. However, no crystals of USP53 or USP54 in complex with K63-linked triUb were obtained. All grown crystals likely corresponded to K63-linked triUb crystals, as the conditions and crystal shapes matched those previously reported for ubiquitin chains.[242]

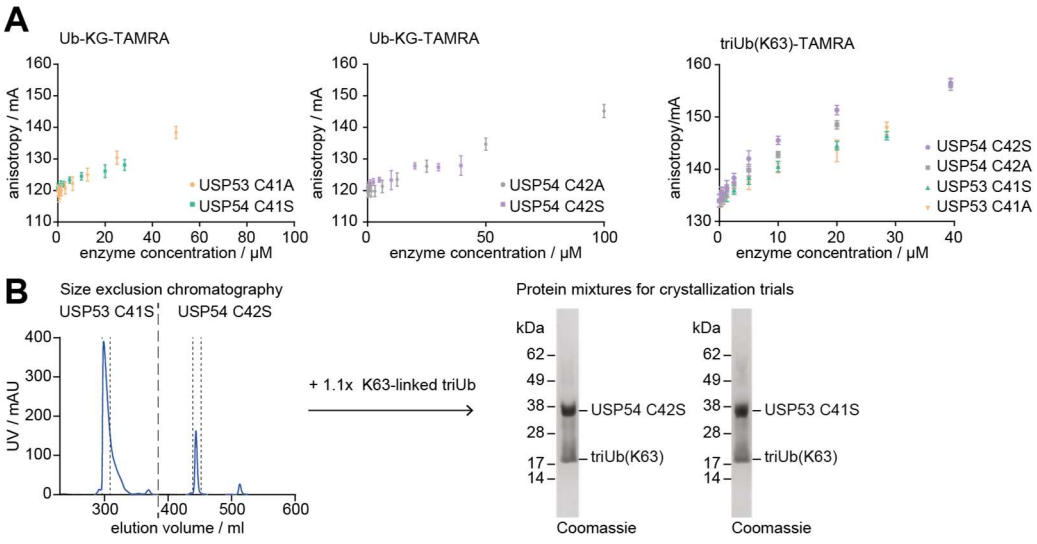

Figure 48: Co-crystallization trial of inactive USP53 and USP54 with K63-linked triUb A) Fluorescence polarization binding assay. Ub-KG-TAMRA or K63-linked triUb-TAMRA were incubated with different concentrations of USP54 C42S, USP54 C41S, USP53 C41S and USP53 C41A. The anisotropy was measured and plotted against the corresponding enzyme concentration. B) The UV_{280nm} chromatograph of the final SEC run of USP53$^{20-383}$ C41S (*left peak*) and USP54$^{21-385}$ C42S (*right peak*). The dashed lines indicate the combined fractions after SEC. After addition of K63-linked triUb chains, the protein mixtures used for crystallization trials were analyzed by SDS-PAGE and Coomassie-staining.

4.3.3 Generation and testing of diUb probes

Co-crystallization attempts of inactive USP53 and USP54 with K63-linked triUb failed to provide crystals with ubiquitin bound in the S1 and S1' sites. Taking a different approach,

diubiquitin probes with in-between warheads were generated and tested for their ability to bind to USP53 and USP54 as a prerequisite for the generation of covalent complexes for purification and crystallization.

In a first attempt, diubiquitin probes with a Michael acceptor (MA) incorporated into the linkage between the ubiquitin moieties (diUb-MA) were generated according to reported methodology (Figure 49A).[217] In these probes, the length of the linker corresponds to the length of native isopeptide bonds and specific linkages can be mimicked (Figure 46A, D). The first step involved conjugation of Ub-MesNa and the linker molecule by aminolysis. The linker molecule was provided by Dr. Zhou Zhao. The ketal protecting the carbonyl group of the Michael acceptor was removed at pH 1.0-1.3 by the addition of perchloric acid instead of the previously reported TFA-H_2O-p-TsOH mixture (Figure 49B). The resulting ubiquitin with a C-terminal α-bromo-vinylketone was reacted with the cysteines of Ub K63C and Ub K63C to yield diUb probes mimicking K63 and K48 linkages, respectively (Figure 49A). Following purification, three mass peaks were identified for diUb(K48)-MA. The left and right peak corresponded to the correct species (Figure 49B). However, a third peak without an assigned mass was visible in the deconvolution spectra of diUb(K48)-MA. This peak likely corresponds to 17144 Da, as found as the sole species for diUb(K63)-MA (Figure 49B). It differs by 18 Da from the correct probe mass and could correspond to a diUb probe with an adducted water to the warhead or an oxidized thioether bond (Figure 49B). It is possible that the two probes form the higher molecular weight species to a different extent due to differences in solvent accessibility of the warheads, which can be influenced by the topologies of the linkages. The diUb-MA probes were then tested for their reactivity with different DUBs, together with Ub-PA. The non-specific DUB USP2 was efficiently labeled by all three probes, demonstrating the functionality of the generated diUb-MA probes (Figure 49D). This finding indicates that the warhead of the higher molecular weight species is intact, suggesting that oxidation is taking place. While incubation with Ub-PA resulted in limited labeling, OTUB1* reacted completely with diUb(K48)-MA but not with diUb (K63)-MA, matching exactly its K48 linkage specificity profile (Figure 49D). Surprisingly, USP53 and USP54 were labeled to the same extent by Ub-PA and diUb(K48)-MA, but almost not by diUb(K63)-MA. Several reasons could explain this labeling behavior: i) A low amount of functional diUb(K63)-MA probe could lead to reduced reactivity. ii) The S1 and S2 binding sites in USP53 and USP54 could bind diUb(K63)-MA in an unproductive conformation, not occurring for diUb(K48)-MA. iii) The chemical differences in the Michael acceptor linker compared to an isopeptide bond may sterically hinder the binding of diUb(K63)-MA. Due to limited success in obtaining large amounts of diUb(K63)-MA and mainly of the complexes, no crystallization attempts were made. USP53 is capable of cleaving K48, K63 and ubiquitin-substrate linkages, so a USP53~diUb(K48)-MA structure may be of interest. The next step towards that, would be to test how diUb(K48)-MA binding to USP53

affects its stability. USP54 specifically cleaves K63 linkages, so only a USP54~diUb(K63)-MA structure would be of interest. To obtain this complex in large quantities suitable for crystallization experiments, the diUb(K63)-MA generation procedure and labeling efficiency would need to be improved.

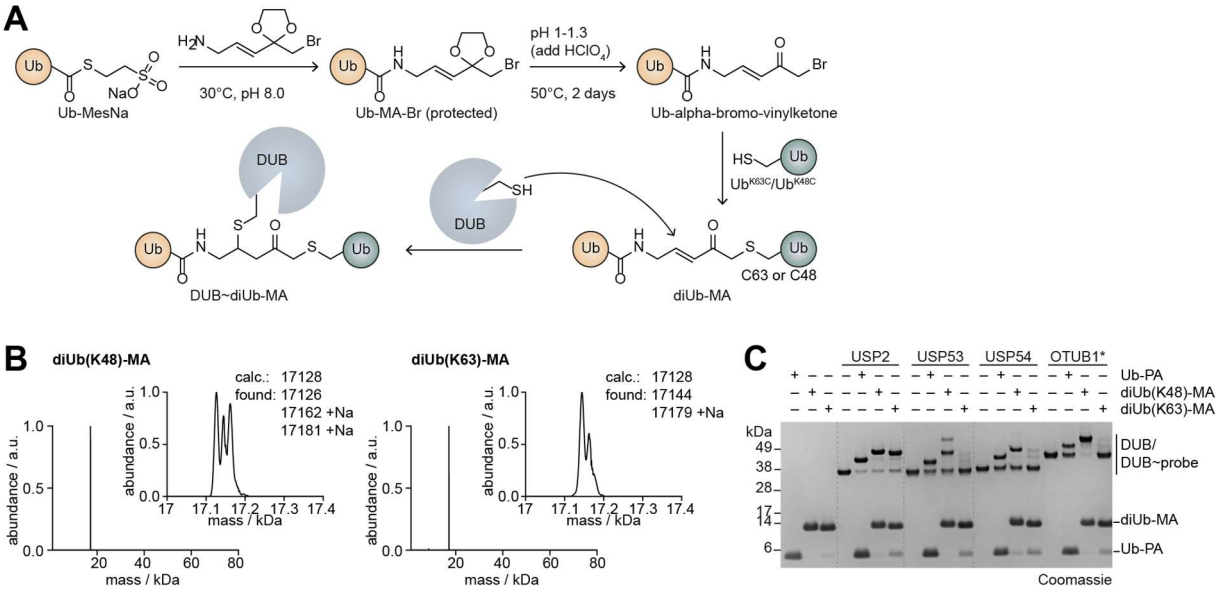

Figure 49: DiUb probes with an in between Michael-acceptor warhead. A) Generation of the diUb-MA probes and schematic depiction of the conjugation reaction mechanism. B) Deconvoluted mass spectra of purified diUb(K63)-MA and diUb(K48)-MA probes. C) Ub-PA and the two generated diUb-MA probes were incubated with USP2, USP53, USP54 and OTUB1*. Labeling was analyzed by SDS-PAGE and Coomassie-staining.

In the diUb-MA probes, the carbonyl group of the α,β-unsaturated ketone is shifted relative to the carbonyl group in a natural isopeptide bond (Figure 46A, D). Based on commonly used monoubiquitin probes with haloalkane warheads, Dr. Zhou Zhao designed and generated a diubiquitin probe with an in-between alkyl bromide warhead, while retaining the isopeptide linkage length (Figure 50A). Notably, the isopeptide bond was replaced by an alkyl bromide placed at the exact position of the isopeptide carbonyl (Figure 46A, D). The reaction of Ub^{1-75}-hydrazide with the amino group of a novel small molecule resulted in the formation of a peptide bond to give Ub-2Br-ene. Using a thiol-ene reaction, Ub-2Br-ene was further reacted with a second ubiquitin containing a K63C mutation to yield the K63 linkage mimicking diUb-2Br probe (Figure 50A). After purification, the final diUb(K63)-2Br probe was obtained by Dr. Zhou Zhao with a purity of 40%. Impurities were identified as hydrolyzed species and disulfide-linked diUb formed by two Ub K63C ubiquitin moieties (Figure 50B). The novel diUb-2Br probe and Ub-PA were used comparatively in gel-based reactivity assays. USP2 reacted with Ub-PA and to some extent with the diUb-2Br probe suggesting that nucleophilic attack on the alkyl bromide is possible but inhibited as the active site must accommodate the bulky size of the bromide as the leaving group (Figure 50C). OTUB1* is a K48 linkage-specific DUB and did not react with the diUb(K63)-2Br probe fitting that the probe mimics a K63 linkage. USP53 and USP54 are K63 linkage-specific and reacted with Ub-PA but not with

diUb(K63)-2Br (Figure 50C). This may be because the proximal ubiquitin moiety blocks the catalytic active sites of USP53 and USP54, leaving insufficient space for the bromide as a leaving group, or because both proteins are not sufficiently reactive. Therefore, the diUb-2Br probe is not suitable for generating complexes of USP53 and USP54 with ubiquitin bound in their S1 and S1' sites, which could be used for crystallization.

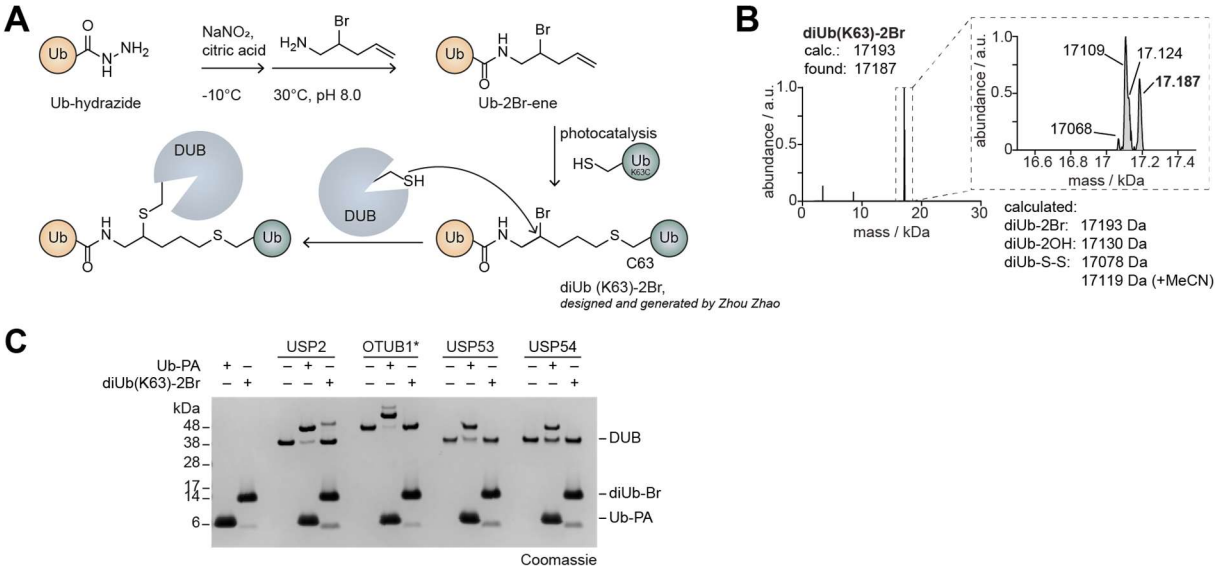

Figure 50: K63 linkage mimicking diUb probe with an in-between alkyl bromide warhead. A) Schematic depiction of the generation of the diUb-2Br probe, designed and generated by Zhou Zhao. B) Deconvoluted mass spectra of diUb(K63)-2Br. C) Ub-PA and diUb(K63)-2Br probes were incubated with USP2, OTUB1*, USP53$^{20-383}$ and USP54$^{21-369}$. Labeling was analyzed by SDS-PAGE and Coomassie-staining.

4.4 Analysis of USP53 related disease mutations

Recent reports have associated homozygous or compound heterozygous *USP53* mutations with pediatric cholestasis.[135-137,246] As an overview, a list of reported mutations in *USP53*, categorized into missense, frameshift, nonsense and splice site mutations, was compiled (Table S1). All missense mutations resulting in single amino acid changes were marked on the amino acid sequence of USP53 (Figure 51A). Interestingly, all but one clustered in the catalytic domain. Determining the structural positions of the mutated residues in USP53 would make it possible to speculate on their role in the protein's function. For this purpose, a homology model of the catalytic domain of USP53 based on the USP54~diUb-PA structure was generated using the SWISS-MODEL server (Figure 51B). The side chains of residues mutated in cholestasis patients are shown as sticks and are highlighted in red (Figure 51B). The C228S, H132S and H132Y mutations disrupt zinc binding in two zinc fingers, one located at the tip of the fingers domain, the other in the thumb domain of USP53. Residue G293 is part of a beta sheet in the core of the protein and mutation to the larger residue valine is likely to disrupt the fold of USP53. Residues G31, V49, R99 and C303 are located close to the catalytic center and may be important for the catalytic activity, either by mediating important interactions or by correctly positioning structural elements necessary for catalytic activity. Residue R99, mutated to serine in one patient, was found to be in a prominent position, central to mediating a network of interactions with the switching loop and the extended Cys-loop present only in USP53 and USP54 (Figure 51C). This interaction network is very similar for R100 in USP54 (Figure 51C). To test its importance for catalytic activity, USP53 R99S and the corresponding USP54 R100A mutant were expressed and purified with yields similar to wild-type USP53 and USP54. The mutations abolished cleavage activity on both K63-linked triUb and Ub-RhoG (Figure 51D-E). However, both mutant proteins still reacted with Ub-VS, and TSA assays showed that they were as stable as the wild-type proteins (Figure 51F-G). These results indicate that USP53 R99S and USP54 R100A are correctly folded, as ubiquitin binding in the S1 site requires correct folding of the enzymes.

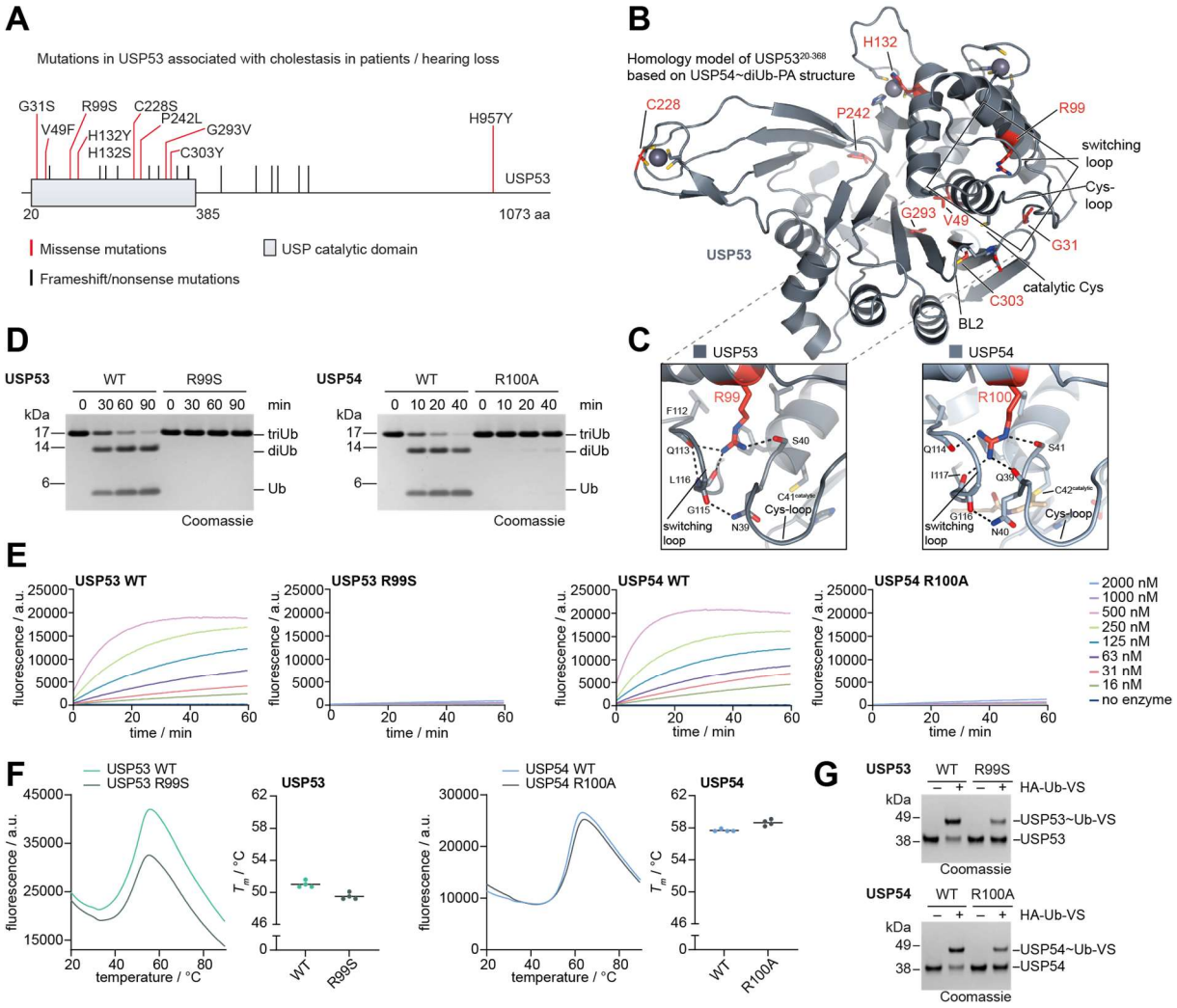

Figure 51: Analysis of cholestasis mutations in USP53. A) Compilation of reported mutations in *USP53* which lead to missense, frameshift or nonsense mutations at the protein level. The location of missense mutations is indicated by red lines which are annotated while the frameshift and nonsense mutations are indicated by black lines. B) The missense mutations were mapped onto a homology model of the catalytic domain of USP53. Close-up of the interactions of residue R99 in USP53. Hydrogen bonds are indicated by dashed black lines C) Close-up of the corresponding residue R100 in USP54. D-G) USP53$^{20-383}$, USP53$^{20-383}$ R99S, USP54$^{21-369}$ and USP54$^{21-369}$ R100A were used in K63-linked triUb cleavage assays (D), in probe reactivity assays with the probe Ub-VS (E), in fluorescence-based Ub-RhoG cleavage assay (F) and their stability was assessed with a TSA to determine their melting temperatures (G). In panels D and G, samples were taken after indicated incubation times and analyzed by SDS-PAGE and Coomassie-staining.

The same suite of assays was performed for USP53 G31S, USP53 C303Y and USP53 H132Y, and repeated for R99S, in comparison to USP53 WT by Nafizul Kazi and Jan André Hane, thus covering two residues that are close to the catalytic residues and a zinc-coordinating residue (Figure 52). Activity-based assays using K63-linked triubiquitin revealed that the G31S and H132Y mutations rendered USP53 inactive and the C303Y mutation rendered USP53 nearly inactive (Figure 52A). For the activated substrate Ub-RhoG, USP53 C303Y and USP53 H132Y for Ub-RhoG retained slight catalytic activity (Figure 52C-D). As observed for USP53 R99S, the three additional tested mutated proteins were still able to react with a Ub-VS probe and showed comparable melting temperatures, again indicating a proper protein fold (Figure 52E). The mutation of the zinc-coordinating residue H132 to tyrosine resulted in the strongest

decrease in stability and probe binding, indicating an importance of the zinc finger for the structural stabilization of USP53 which in turn is probably important for the activity.

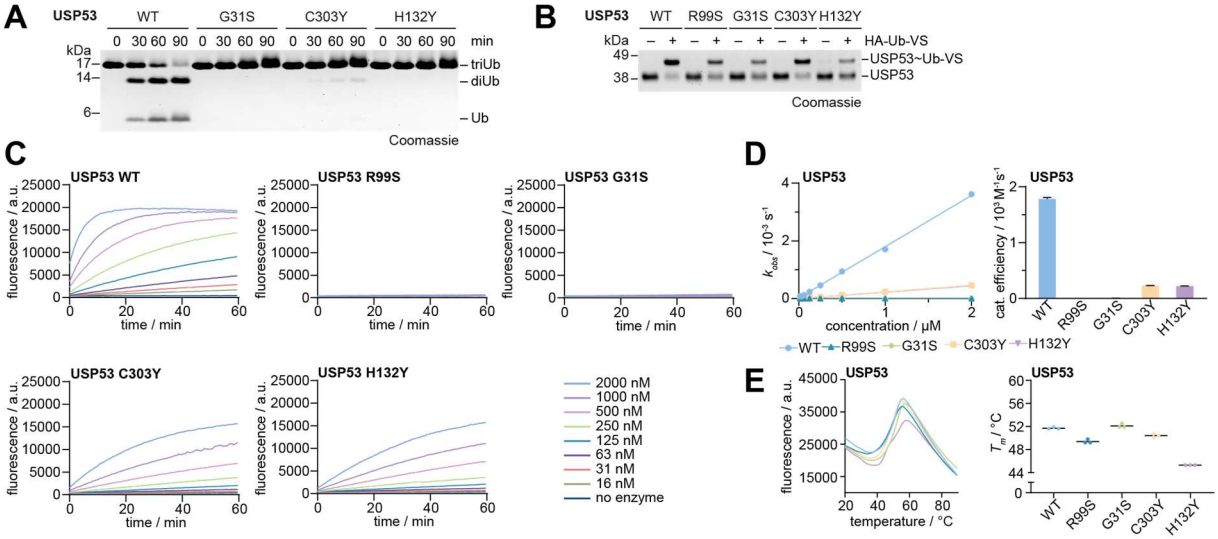

Figure 52: Analysis of cholestasis mutations G31S, C303Y and H132Y mutations in USP53. A-E) USP53$^{20-383}$, USP53$^{20-383}$ R99S, USP53$^{20-383}$ G31S, USP53$^{20-383}$ C303Y and USP53$^{20-383}$ H132Y were used K63-linked triUb cleavage assays (A), in probe reactivity assays with the probe HA-Ub-VS (B), in fluorescence-based Ub-RhoG cleavage assay (C-D) and their stability was assessed with a TSA to determine their melting temperatures (E). In panels A and B, samples were taken after indicated incubation times and analyzed by SDS-PAGE and Coomassie-staining. Nafizul Kazi purified the mutant proteins USP53$^{20-383}$ G31S, USP53$^{20-383}$ C303Y and USP53$^{20-383}$ H132Y and Jan André Hane performed the corresponding activity and stability assays.

Concluding, residues R99, G31, H132 and C303 in USP53 are essential for its catalytic activity. This suggests that the interaction network mediated by R99 maintains the switching loop and the Cys-loop in a specific position necessary for activity. A likely explanation for the effect of the G31S and C303Y mutations on catalytic activity is that these mutations disrupt the arrangement of the catalytic active site due to their close localization.

In conclusion, these findings link the cholestasis phenotype to the cleavage activity of USP53 and are an important step towards understanding the mechanisms behind the observed phenotype in patients.

5 Discussion

The activity of deubiquitinating enzymes determines the final ubiquitination status of substrates and thus regulates their cellular functions by influencing their stability, activity, localization and interactions.[19,26] DUB dysfunction or dysregulation contributes to various diseases, making DUBs potential therapeutic targets.[94,104] USP7 is an extensively studied DUB that is overexpressed in a number of cancers.[247] It deubiquitinates and stabilizes the ligase MDM2, which in turn leads to ubiquitination and destabilization of p53, an important tumor suppressor.[248] Consequently, USP7 inhibition may represent a valid anti-cancer strategy. In general, the development of DUB inhibitors is an emerging therapeutic strategy and first DUB inhibitors are currently tested in clinical trials.[249-251] Conversely, DUB inhibition would be an ineffective treatment for OTULIN-related autoinflammatory syndrome (ORAS) for which the loss of the activity of the DUB OTULIN has been identified as the underlying cause.[252,253] Functional OTULIN specifically disassembles linear ubiquitin chains and thereby prevents tumor necrosis factor (TNF)-associated systemic inflammation in humans.[119,253] In this case, understanding the function of OTULIN informs the treatment of ORAS patients who benefit from the off-label treatment with antibodies targeting TNF or from hematopoietic stem cell transplantation.[252,253] The latter two examples highlight the need to understand the activity, substrates, and cellular functions of DUBs, in order to conceive and develop treatments for DUB-related diseases. Yet, many of the approximately 100 human DUBs remain poorly characterized.[254] USP53 and USP54 are two particularly neglected DUBs, although the first related signaling pathways and potential substrates have been reported in recent years.[131,132,153,154] Both have been associated with cancer, and USP53 with cholestasis and hearing loss, but a molecular understanding of their activities, functions, and disease association remains elusive.[131,160,246] The results obtained in this work revise the annotation of USP53 and USP4 from inactive DUBs to active DUBs. Comprehensive analysis of USP53 and USP54 activities and structures led to the discovery of two distinct mechanisms of K63-linked polyubiquitin chain length decoding, with one mechanism establishing K63 linkage-directed *en bloc* deubiquitination as a novel DUB activity. In addition, loss of USP53 activity was identified as a likely cause of the observed cholestasis phenotype, highlighting the importance of the catalytic activity of DUBs in the context of disease.

5.1 USP53 and USP54 are active DUBs with unique and distinct mechanisms

Prior to cleavage, DUBs and Ubl proteases must recognize and bind their specific substrates. A major specificity determinant is the recognition and binding of the respective modifier through the S1 site.[95,98,107] Canonical USP DUBs contain a dominant S1 binding site and show limited interactions with ubiquitin in any other binding site and therefore tend to cleave differently linked ubiquitin chains or ubiquitin substrate linkages to a similar extent (Figure 53).[110,111] As an example, USP8 cleaved all isopeptide bonds when incubated *in vitro* with GFP modified with K48- or K63-linked ubiquitin chains (Figure 26B). Interestingly, the shared structural fold of the USP family exhibits a high plasticity of the S1 site, allowing also the recognition of other Ubls instead of or in addition to ubiquitin, mediated by specific sequence variations.[123] USPL1 belongs to the USP DUB family but specifically recognizes and cleaves SUMO.[99,236] USP18 is specific for ISG15, while USP5, USP14 and USP21 cleave ubiquitin and ISG15.[96-99] USP16 and USP36 exhibit cross-reactivity with three modifiers, including ubiquitin and the two Ubls ISG15 and Fubi.[99,109,255] Until recently, the protein database uniprot annotated both USP53 and USP54 as inactive enzymes without conclusive experimental confirmation.[256] The idea that they might cleave Ubls was appealing, especially in light of the first published experiments in which no activity on ubiquitin was observed.[128,129] This study used an *in vitro* approach to test the potential activity and modifier specificity of USP53 and USP54. Experiments using a custom-made probe panel and a purchased fluorogenic substrate panel based on ubiquitin and several Ubls excluded C-terminal hydrolase activity of USP53 and USP54 on any of the tested Ubls. Instead, both enzymes were found to be active DUBs with unique cleavage mechanisms (Figure 14, Figure 15, Figure 17, Figure 53). Accordingly, during the experimental phase of this thesis, the identification of PLK4 as a potential substrate for USP54 led to the change of the uniprot annotation of USP54 to an active enzyme.[132,256] Furthermore, the reactivity of endogenous USP54 with Ub-PA was detected by mass spectrometry by Dr. Rachel O'Dea, which is consistent with the DUB activity discovered here. USP53 was not detected.[109,257] Earlier proteomics studies as well as a more recent comprehensive profiling study aiming to identify the landscape of active deubiquitinating enzymes failed to detect monoubiquitin probe reactivity of either protein.[166,203,211] In contrast, two independent DUB profiling studies that identified ZUFSP as a novel DUB, also detected USP54 and one even USP53 as ubiquitin probe reactive by mass spectrometry.[114,115] Given their low cellular protein levels, it is likely that previous approaches missed the ubiquitin probe reactivity of USP53 and USP54 due to the used enrichment methodologies or proteomics detection limits.[63] Fittingly, both proteins display limited reactivity with commonly used monoubiquitin probes, as demonstrated by *in vitro* labeling of USP53 and USP54 with Ub-PA or Ub-VS (Figure 50, Figure 51, Figure 52). Subsequent experiments revealed that the catalytic efficiencies of USP53 and

USP54 for the monubiquitin substrate Ub-KG-TAMRA are at least a 1,000-fold lower than those of UCHL1, USP2, USP16, or USP36 (Figure 22).[99] The low levels of activity on monoubiquitin substrates of USP54 is consistent with the weakened S1 ubiquitin binding that was observed in the USP54~diUb PA structure, which is likely also true for USP53 (Figure 41, Figure 51B). This hypothesis is supported by the observation that USP30 with its weakened S1 site binding of ubiquitin, has only a ~10-fold higher catalytic efficiency for Ub-KG-TAMRA than USP53 and USP54.[116] In general, USP53 and USP54 share unique sequence and structural features (see section 5.2), specifically recognize K63 linkages in ubiquitin chains, and prefer longer ubiquitin chains due to the presence of S2 sites that were established using fluorescently labeled K63-linked triUb chains as substrate (Figure 19). However, when comparing their activities, USP54 shows a higher catalytic activity on Ub-KG-TAMRA (Figure 22) and particularly on K63-linked polyubiquitin chains compared to USP53 (Figure 18), and indeed, two markedly different activity mechanisms were discovered for USP53 and USP54 (Figure 53). This discovery was made possible by generating and assaying custom substrates including specifically ubiquitinated GFP species and triubiquitin chains with mixed K48/K63 linkages (see section 5.3).

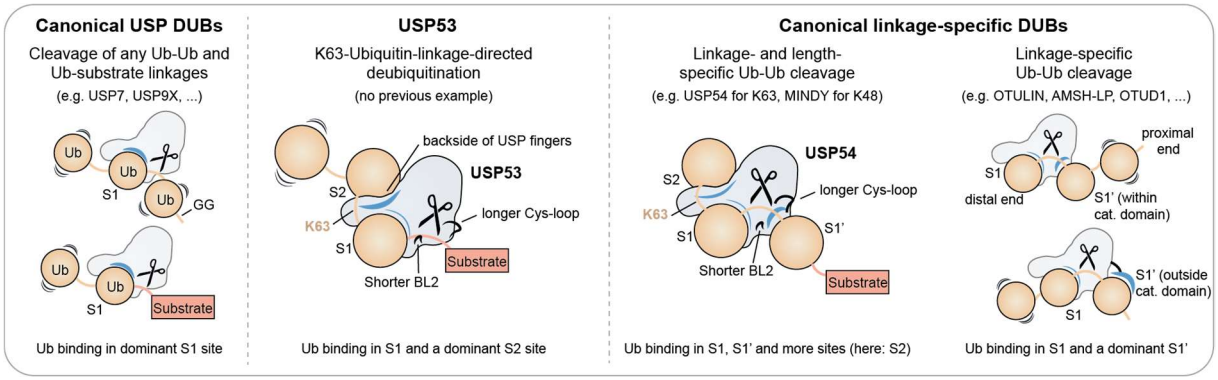

Figure 53: Ubiquitin recognition and processing by DUBs. Canonical USP DUBs depend mainly on ubiquitin binding through a dominant S1 site and cleave different ubiquitin linkages to a similar extent (*left*). USP53 exhibits a unique K63 linkage-directed deubiquitination activity. The binding of K63-linked ubiquitin moieties in the S1 and S2 sites of USP53 facilitates the cleavage of different isopeptide bonds via a promiscuous catalytic center (*middle*). USP54 belongs to the group of canonical linkage-specific DUBs and exhibits K63 linkage and length-dependent cleavage activity. Ubiquitin binding in the S1' site and the additional S2 site specific for K63 linkages facilitate the linkage specificity and the length preference, respectively (*right*).

USP53 features a K63 linkage-directed deubiquitination activity which is mediated through a promiscuous catalytic center under the control of a K63 linkage-specific S2 site (Figure 53). Correspondingly, occupation of the S1 and S2 sites of USP53 by K63-linked ubiquitin enhances the cleavage of K63 or K48 linkages in homotypic or mixed triubiquitin, respectively (Figure 29) and of the ubiquitin-substrate bond in the GFP substrate modified with K63-linked polyubiquitin (Figure 27A-B). Remarkably, although K63-linked ubiquitin chains of at least three ubiquitin moieties are internally cleaved by USP53 (Figure 18A), *en bloc* cleavage of the entire K63-linked ubiquitin chain from GFP is favored over endo cleavage within the chain

(Figure 27A-B). An S2 site is also critical in the SARS-CoV-1 protease PLpro for the recognition of K48-linked polyubiquitin.[122] However, while a K48 linkage-directed deubiquitination activity has been proposed for PLpro, it was concluded that the enzyme prefers cleavage within K48-linked polyubiquitin. This marks an even further difference to the mechanism of USP53 apart from the different linkage preference.[122,208] Although ubiquitin binding in the S1' site appears to be negligible for USP53 activity, binding of other cellular substrates in the S1' site may contribute to the preferred *en bloc* activity and has not yet been the focus of investigation. *En bloc* cleavage activity has also been observed for PSMD14 and USP14, two proteasome associated DUBs. However, their activity differs from the linkage-directed deubiquitination activity of USP53 in that cleavage occurs irrespective of the linkage type.[258,259] At high concentrations and longer incubation times, USP53 inefficiently cleaves K48- and K11-linked diUb chains (Figure 16A), longer K48-linked ubiquitin chains (Figure 18E), and GFP modified with K48-linked polyubiquitin albeit without the *en bloc* cleavage preference (Figure 27A-B). Mutation of the S2 site of USP53 reduced the activity also on K63-linked polyubiquitin to similar low levels, highlighting the importance of the S2 site for USP53 activity (Figure 43B). To summarize, the promiscuous catalytic active center of USP53 can cleave ubiquitin linkages, except M1 linkages, to a limited extend without occupation of the S2 site with K63-linked ubiquitin. A comparable specificity extension at higher concentrations has been observed *in vitro* for CYLD, a USP DUB that is generally specific for M1/K63 linkages.[117] Lastly, the poor activity of USP53 on K63-linked diUb substrates can be explained by unproductive binding of these substrates in the S1 and S2 sites, not leading to cleavage (Figure 16A, Figure 22A-B).

USP54 features a K63 linkage- and length-specific ubiquitination activity. The activity and the linkage specificity of USP54 depend on additional ubiquitin binding in the S1' site. This cleavage activity is reflected in the following observations. First, the cleavage activity of USP54 is increased 20-fold for K63-linked diubiquitin compared to the monoubiquitin substrate Ub-KG-TAMRA (Figure 22D). Second, USP54 trims GFP modified with K63-linked polyubiquitin to monoubiquitinated GFP and not to unmodified GFP (Figure 27C). Third, USP54 cleaves only the K63 linkage in mixed K48/K63-linked or M1/K63-linked triubiquitin (Figure 30, Figure 31C-D). The two DUBs AMSH and CYLD also specifically recognize K63 linkages through S1 and S1' site binding.[117,118] However, they do not contain an S2 site. The one present in USP54 mediates its length preference as occupation of the K63 linkage-specific S2 site in addition to the S1 and S1' sites increases USP54 activity 4-fold (Figure 22D). Additionally, mutation of the S2 site only abrogates the increase in cleavage activity on longer K63-linked ubiquitin substrates, but not on shorter substrates of up to two moieties (Figure 42H, Figure 43A, Figure 44C). Mechanisms for K48 linkage- and length-specificity in DUBs have been understood at the molecular level for MINDY DUBs and for the SARS-CoV-1

enzyme PLpro, which are mediated by additional S2', S3', and S4' sites and by an additional S2 site, respectively.[113,122,207] The DUB OTUD2 also has S2, S1 and S1' sites, but the S2 and S1' sites are specific for K11 linkages.[120] For ZUFSP, a K63 linkage and length-specific cleavage activity has been demonstrated. However, the underlying molecular mechanism remains to be elucidated. In addition, the S1' site of ZUFSP formed by tandem UBDs differs from USP54, as the UBDs are outside of the catalytic domain and do not specifically bind K63-linked polyubiquitin.[114,115,181,260] Lastly, while USP54 shows exquisite specificity, especially for a USP DUB, marginal cleavage of K11 and K48 linkages at elevated protein levels and of extended K48-linked polyubiquitin chains can be detected (Figure 16A, Figure 18F).
In summary, the two discovered mechanisms for USP53 and USP54 highlight how polyubiquitin processing by DUBs is fine-tuned in a linkage- and length-dependent manner.

5.2 Implications from the structure of USP54~diUb-PA

The differences in the mechanisms of USP53 and USP54 compared to other DUBs are also reflected in their sequences and structures, which will be discussed and correlated in more detail in this section. USP53 and USP54 differ in amino acid sequence at several positions that are otherwise highly conserved among USP family members, including two short insertions and one deletion (Table S2).[123] The obtained structure of USP54 in complex with K63-linked diUb-PA allows to map and assess the relevance of these differences. It is striking that the divergent amino acids, shown in light pink, cluster around the catalytic active center and the ubiquitin tail binding cleft (Figure 54A). M118 in USP54 is such a residue and replaces the commonly observed glycine. In the structure, USP54 M118 loops over the C-terminal tail of ubiquitin and forms a hydrophobic contact with K301, which is located in BL2 and in turn contacts BL1 (Figure 54B). Structural analysis of ubiquitin binding in the S1 site of USP54 revealed a shift of the S1 ubiquitin and a strongly altered BL1 and BL2 architecture compared to other USP DUBs which is also reflected in the sequence (Figure 38, Figure 41, Figure 54). These changes lead to a weakened S1 ubiquitin binding in USP54 which is illustrated by the comparison of the interaction areas of the S1 sites of USP54 and other USP DUBs with ubiquitin as calculated by the PISA webserver from available crystal structures.[228] While the interaction area of the S1 site of USP54 with ubiquitin is 1088 Å^2, this value is much higher for the highly active DUBs USP2 and USP7 with areas of 1909 Å^2 and 1719 Å^2, respectively.[124,261] Even compared to CYLD and USP30, which show specialized cleavage activities and also have divergent sequences, partly at the same positions as USP54, the interaction area of the S1 site of USP54 with ubiquitin is significantly smaller than theirs with 1652 Å^2 and 1243-1253 Å^2, respectively.[116,117,123] These values are consistent with the low ubiquitin binding and low catalytic efficiencies for single ubiquitin substrates by USP54 and USP53 (Figure 22, Figure

48A) and are consistent with the proposed two distinct mechanisms, both of which rely on additional ubiquitin binding in other sites for efficient cleavage activity.

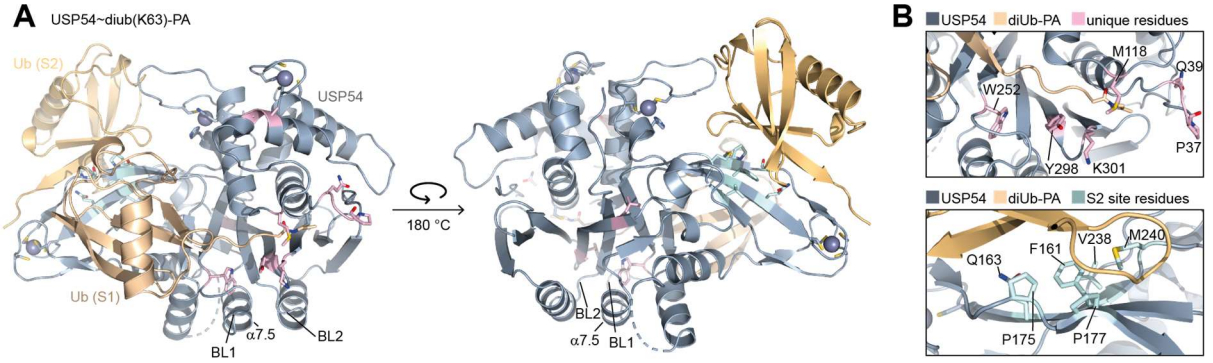

Figure 54: Mapping of unique residues in USP54 derived from the sequence and of important S2 site residues derived from the structure. A) Cartoon representation of USP54 in complex with K63-linked diUb-PA. Unique sequences in USP54 compared to otherwise highly conserved sequences in USP DUBs are highlighted in light pink. Residues important for mediating ubiquitin interactions in the S2 site of USP54 are highlighted in light cyan. B) Close-up of the highlighted residues around the catalytic center and the S2 site in USP54.

As an unexpected feature of USP54, three coordinated zinc atoms were observed in the structure, including one commonly seen in USP DUBs at the tip of the fingers domain, and two additional zinc atoms in the thumb domain. All three zinc atoms have previously only been structurally characterized in yeast Ubp8 as part of the SAGA complex.[262,263] In the recently reported structure of USP36, in addition to the zinc atom in the fingers domain, a second zinc atom was observed, corresponding to the zinc atom in the thumb domain of USP54 closer to the N-terminus. Based on sequence considerations, these two zinc atoms are probably also present in USP42, USP17, USP27X, USP51, and all three zinc atoms in USP22, the human homolog of yeast Ubp8.[109,263] For USP54, the two additional zinc atoms in the thumb domain are probably important for stabilizing its structural fold and its catalytic activity. The sequence similarity and homology modeling of the catalytic domain of USP53 based on the structure of USP54 suggest that USP53 adopts a comparable fold including the altered blocking loops and the three zinc atoms (Figure 51B). USP53 H132 was found to be mutated in a patient with cholestasis and corresponds to USP54 H133, the residue that coordinates a zinc atom in the thumb domain and is close to the loop that forms part of the S2 binding site.[246] Introducing the mutation into USP53 rendered it inactive and reduced its thermal stability, confirming the importance of the residue and indicating the importance of the zinc atoms also in USP53 for the structural fold and perhaps for the integrity of the S2 site which is particularly important for USP53 activity (Figure 43).

The structure of USP54 revealed the S2 site (Figure 37A) and the residues important for ubiquitin binding in the S2 site which could not have been identified by sequence analysis alone.[123] Shown in pale cyan (Figure 54B), the residues mediate hydrophobic interactions with the I44 patch of ubiquitin, a common interaction site of ubiquitin that is also important for ubiquitin recognition in the S1 site of USP DUBs.[19] A central aromatic residue (F161 in USP54

and Y160 in USP53) and a charged residue (D174 in USP54 and D173 in USP53) stand out, which are not found at this position in any other USP DUB. Subsequent validation activity assays proved that the observed interactions between ubiquitin and the S2 site in USP54, as well as the corresponding interactions in USP53 are indeed relevant for the length-dependent cleavage mechanisms of both proteins.

In linkage-specific DUBs, the additional binding of ubiquitin in the S1' site directs only the correct lysine residue towards the catalytic center, thereby determining the linkage type that can be cleaved.[95] The structure of USP54 in complex with K63-linked diUb revealed how ubiquitin is bound in the S1 and the S2 site. However, the small interaction area of USP54 with ubiquitin in the S1 site, the high specificity for K63 linkages and the strong increase in catalytic efficiency for K63-linked diUb in comparison to Ub-KG-TAMRA, suggest additional and specific binding of ubiquitin by USP54 in its S1' site. While the interactions between ubiquitin and the S1' site of USP54 remain to be elucidated, the crystal structures of CYLD, USP30, and AMSH in complex with ubiquitin in the S1' site have been obtained. CYLD shows a striking difference to previously determined USP structures as an additional ß-sheet forms the majority of the S1' site and interacts with F4 of ubiquitin (Figure 55). The interaction area of the S1' site of CYLD with ubiquitin is 587-671 $Å^2$.[117] Although USP30 does not contains such an insertion, its S1' site interaction area with ubiquitin is with 535 $Å^2$ similar to CYLD and also contacts F4 of ubiquitin.[116] For USP54 however, no prominent structural element that could form the S1' site is present and mutation of F4 in the proximal ubiquitin of K63-linked triUb did not affect USP54 cleavage activity (Figure 37A, Figure 47A, Figure 55). The same was true for mutation of I44 or of Q62/E64 in the proximal ubiquitin of K63-linked triUb (Figure 47A,C). The two latter are important ubiquitin residues that mediate interactions with the S1' site of AMSH, a K63 linkage-specific metalloprotease.[118] These results suggest a binding mode of ubiquitin in the S1' site of USP54 that is distinct from other linkage-specific DUBs. An untargeted approach to identify relevant residues for the interaction between USP54 and ubiquitin in the S1' site would be to perform targeted alanine scanning for USP54 and also for the proximal ubiquitin in a triUb substrate, although synergistic effects could be missed. To elucidate all relevant interactions mediated by the S1' site of USP54, a structure of USP54 with ubiquitin bound in the S1' site is of great importance. This structure will also provide information on the high specificity of USP54 for K63 linkages. An attempt to crystallize inactive USP54 in complex with K63-linked triubiquitin proved unsuccessful (Figure 48). Although the achieved high protein concentration of 8 mg/ml suggested ubiquitin binding, the general low binding affinity of USP54 for ubiquitin probably hampered crystal formation. Instead, the generation and use of a diUb or triUb-based probe with an in-between warhead mimicking the K63 linkage could facilitate stable complex formation and crystallization to obtain the structure of USP54 with ubiquitin bound in the S1' site. No binding of diUb probes with an in-between MA or an alkyl bromide warhead to USP54

was observed, different to the unspecific DUB USP2 that readily reacted with the probes (Figure 49, Figure 50). To accommodate the specific binding mode of USP54, a successful probe will likely need to contain a reactive warhead that is positioned in the exactly correct position and is small enough to avoid steric hindrance.

The structure of USP54 in complex with K63-linked diUb-PA revealed a unique Cys-loop in a prominent position, which is likely part of the S1' site of USP54. Truncation of the Cys-loop to match the sequence of most USP DUBs rendered USP54 and also USP53 inactive, demonstrating that the unique additional four amino acids that are part of the Cys-loop are essential for their catalytic activity. Binding of K63-linked diubiquitin across the active site of USP54 could bring the Cys-loop into an active conformation, which the truncated loop may not be able to access. This hypothesis can be evaluated through the acquisition and the subsequent comparison of the apo structure of USP54 and a structure of USP54 in which ubiquitin is bound in the S1' site. It is noteworthy that truncation of the Cys-loop and mutation of the catalytic histidine or of the oxyanion hole forming asparagine did not disrupt but only reduced the reactivity of USP53 and USP54 with Ub-VS and Ub-PA probes. This finding aligns with the observation, that USP2 has ISG15 probe reactivity but lacks ISG15 cleavage activity. Consequently, while probe-binding has been found to reflect and report enzyme activities and changes in these activities upon stimuli or inhibitor treatment, probe reactivity and cleavage activity cannot be viewed at the same level.[99,200,264,265]

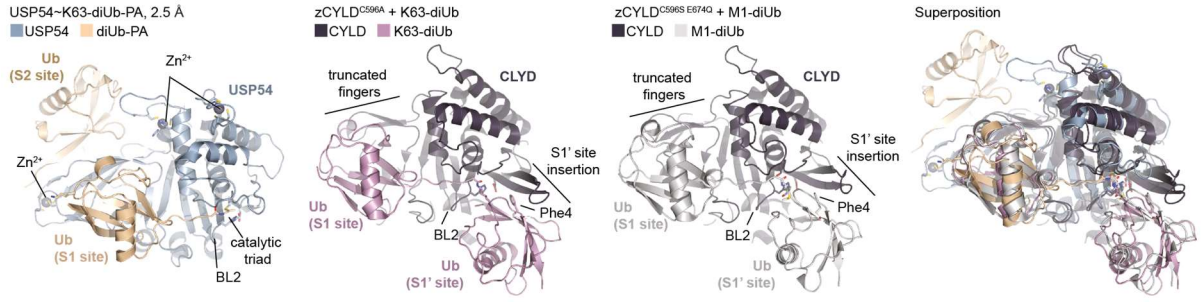

Figure 55: Cartoon representation of USP54~diUb(K63)-PA obtained in this study, CYLD in complex with K63-linked diubiquitin (PDB: 3wxg) or with M1-linked diubiquitin (PDB: 3wxf). To illustrate the differences in structural elements for ubiquitin recognition, a superposition of all three structures is shown.

The reduced interaction area of USP54 with ubiquitin in the S1 site suggests a similarly low area in the homologue USP53. However, USP53 has a K63 linkage-directed cleavage mechanism with a promiscuous catalytic active center suggesting that the activation mechanism for this novel DUB activity must be different from that of USP54 and much more dependent on ubiquitin binding in the S2 site. Therefore, once identified, mutation of the S1' interface mediating residues of USP54 should not affect USP53 activity to the same extent. In conclusion, the unique structural fold of USP54, and by extension of USP53, is essential for their catalytic activities and supports the proposed cleavage mechanisms.

5.3 Tool development to study DUB activity

To enable the discovery of the cleavage mechanisms of USP53 and USP54, a number of broadly applicable custom ubiquitin probes and ubiquitin substrates were developed. Generally, reported ubiquitin assembly reactions were used.[183] However, to account for substrate specificities such as the linkage-type, the length, or other modifications, two variations of commonly used assembly protocols for K63 and K48 linkages between ubiquitin moieties proved essential. One previously reported variation is the use of ubiquitin variants, that can either not be conjugated or not be modified.[183] The second variation involves mixing wild-type and truncated ubiquitin at specific ratios. Ratios of 1:6 and of up to 1:10 were tested and validated so that the wanted conjugation reaction is strongly favored over other possible conjugation reactions. In most cases, combinations of both variations were used in assembly reactions, allowing for easy generation of advanced ubiquitin substrates in large quantities to enable cleavage assays. These included proximally fluorescently labeled K63-linked ubiquitin chains of varying length, ranging from two to four ubiquitin moieties. The advantage of labeled over unlabeled ubiquitin chains is that they report on preferred cleavage events, which is useful for studying length-specific enzymes, and that cleavage activities can be readily quantified, for example by fluorescence polarization experiments. However, before using fluorescently labeled substrates in DUB cleavage assays, it is important to first compare the cleavage of labeled and unlabeled substrates for each new enzyme to ensure that the fluorophore itself does not affect the enzyme activity, as was the case with FlAsH for USP54 (Figure 19C). Another application of the mutation/ratio assembly method was the generation of heterotypic mixed K48/K63- or M1/K63-linked triubiquitin chains and homotypic K63-linked triubiquitin chains with mutations only in ubiquitin at a specific position. An inherent advantage of these substrates is that each ubiquitin moiety contains a different molecular mass, allowing cleavage events to be monitored and assigned by mass spectrometry.

Typically, panels of free ubiquitin chains are widely used to assess DUB activities and linkage specificities.[116,241] However, in cells, endogenous substrates of DUBs are typically protein-bound ubiquitin chains.[24,266] The newly generated pure K48- or K63-polyubiquitinated GFP substrates were instrumental for the discovery of the linkage-directed cleavage mechanism of USP53 (Figure 27A, B). In contrast to free ubiquitin chains, they have the great advantage that cleavage activities on isopeptide bonds in-between ubiquitin chains and isopeptide bond between ubiquitin and substrates can be differentiated. The recently reported chemical biology method LACE served as a starting point to first obtain mono-ubiquitinated GFP.[196] After upscaling of the LACE reaction, the purification of the resulting GFP-mUb product was successfully established. Polyubiquitinated GFP was obtained by enzymatic conjugation of single ubiquitin moieties or preassembled K63-linked and K48-linked ubiquitin chains of

different length to GFP-mUb, followed by purification. The findings for USP53 implicate that the activities and specificities of DUBs should also be evaluated in this more complex setting when both ubiquitin-ubiquitin and ubiquitin-substrate bonds are present in the same substrate, as this could lead to the discovery of further DUBs with linkage-directed cleavage mechanisms. The same lab that introduced LACE engineered a chimeric E1 which together with Ubc9 is able to directly conjugate ubiquitin to the LACE tag of a model protein.[197] This site-specific protein ubiquitination technique allows also the one-step addition of complex, previously assembled ubiquitin chains including heterotypic ubiquitin chains to any substrate with an incorporated LACE tag. This reaction broadens the range of complex ubiquitinated substrate proteins that can be generated to further test the length- and linkage-specificity of DUBs, but no purification protocols have been established to date.[197] Recent findings have revealed that not only the linkage but also the chain length of ubiquitin chains and more complex ubiquitin modifications are specifically recognized and play a crucial role in cellular signaling.[58,60] This highlights the necessity for the development of advanced tools for analyzing DUB cleavage. For instance, the debranching activities of ATXN3 and MINDY were discovered by establishing and utilizing purified branched and unbranched K48-and K63-linked ubiquitin chains as substrates.[172]

5.4 Outlook

In this work, the activity and cleavage mechanisms of the catalytic domains of USP53 and USP54 have been thoroughly characterized using established and newly developed substrates. For both proteins, the N-terminal catalytic domains are part of much larger proteins. The extended C-terminal domains are predicted to be unstructured[267,268] and may regulate the catalytic activities of USP53 and USP54, as observed for USP7 and USP5.[269,270] However, it is most likely that the C-terminal domains determine the cellular localization or mediate interactions with binding partners.[110,165] Recently, the first interaction partners of USP53 and USP54 have been reported. However, their effect on the activities remains widely unknown.[129,132,165] It will be a critical next step to relate the findings presented here in these contexts. Apart from the catalytic activity, the specificity profiles of the catalytic domains of USP53 and USP54 may differ from the complete proteins. The full-length versions of USP53 and USP54 were resistant to purification after expression in insect cells and could not be analyzed. Thus, the study of full-length USP53 and USP54, either obtained from mammalian cells or in a cellular environment, is an important avenue for a complete molecular characterization of the activities. The identified distinct K63 linkage-dependent decoding mechanisms of USP53 and USP54 will guide further research on USP53 and USP54 by influencing the design of future experiments to uncover their substrates and cellular roles,

especially in a disease context. An important part will also be to connect the chain length-dependent activities of USP53 and USP54 on K63-linked polyubiquitin with cellular signaling events, as K63-linked ubiquitin chains of 2-4 moieties exist and are specifically recognized on substrate proteins in cells.[59,266] Based on the discovered cleavage mechanism of USP53, Dr. Kai Gallant performed a diGly ubiquitinome profiling for USP53. From this experiment, the tricellular junction complex proteins MARVELD2 and LSR were identified as substrates of USP53.[257] Additionally, he showed that USP53 depletion in CaCo-2 cells increased K63-linked but not K48-linked polyubiquitination on MARVELD2 which is consistent with the K63 linkage-directed *en bloc* cleavage activity of the catalytic domain of USP53 observed *in vitro.*[257] This study, together with the two identified substrates MARVELD2 and LSR, links for the first time the cholestasis phenotype to the cleavage activity of USP53.[257] Both substrates are essential for the maintenance of functional tricellular junctions of epithelial cells and their associated patient phenotypes fit the USP53 related phenotypes.[129,135,136,271-273]

For USP54, a functional and mechanistic characterization of its relevance to disease is lacking. The findings on the specificity of USP54 presented in this thesis allow for a new angle in the study of proposed cellular substrates. One potential avenue could be to investigate the regulation of PLK4 cellular function by long K63-linked ubiquitin chains. This, in turn, could shed light on the cellular relevance of the proposed deubiquitination activity of USP54 and on gastric cancer progression.[132] In the context of DUBs as therapeutic targets, the reannotation of USP54 as an active DUB and studies associating USP54 overexpression in various cancers with tumor progression, suggest a role for its catalytic activity in pathological function.[132,159,160] This makes USP54 a potential drug target and serves as a basis for the development of USP54 inhibitors, their evaluation in vivo and in the long term in the clinic. In addition, specific USP54 inhibitors could be used to study USP54 activity in a cellular context.

6 References

1 Berg, J. M., Tymoczko, J. L., Gatto, G. J. & Stryer, L. *Stryer Biochemie*. (Springer Spektrum, 2018).

2 Lander, E. S. *et al.* Initial sequencing and analysis of the human genome. *Nature* **409**, 860-921, doi:10.1038/35057062 (2001).

3 Venter, J. C. *et al.* The sequence of the human genome. *Science* **291**, 1304-1351, doi:10.1126/science.1058040 (2001).

4 Nurk, S. *et al.* The complete sequence of a human genome. *Science* **376**, 44-53, doi:10.1126/science.abj6987 (2022).

5 Djebali, S. *et al.* Landscape of transcription in human cells. *Nature* **489**, 101-108, doi:10.1038/nature11233 (2012).

6 Mattick, J. S. & Makunin, I. V. Non-coding RNA. *Hum Mol Genet* **15 Spec No 1**, R17-29, doi:10.1093/hmg/ddl046 (2006).

7 Aebersold, R. *et al.* How many human proteoforms are there? *Nat Chem Biol* **14**, 206-214, doi:10.1038/nchembio.2576 (2018).

8 Nilsen, T. W. & Graveley, B. R. Expansion of the eukaryotic proteome by alternative splicing. *Nature* **463**, 457-463, doi:10.1038/nature08909 (2010).

9 Wang, E. T. *et al.* Alternative isoform regulation in human tissue transcriptomes. *Nature* **456**, 470-476, doi:10.1038/nature07509 (2008).

10 Kim, M. S. *et al.* A draft map of the human proteome. *Nature* **509**, 575-581, doi:10.1038/nature13302 (2014).

11 Morris, R., Black, K. A. & Stollar, E. J. Uncovering protein function: from classification to complexes. *Essays Biochem* **66**, 255-285, doi:10.1042/EBC20200108 (2022).

12 Lee, J. M., Hammaren, H. M., Savitski, M. M. & Baek, S. H. Control of protein stability by post-translational modifications. *Nat Commun* **14**, 201, doi:10.1038/s41467-023-35795-8 (2023).

13 Doll, S. & Burlingame, A. L. Mass spectrometry-based detection and assignment of protein posttranslational modifications. *ACS Chem Biol* **10**, 63-71, doi:10.1021/cb500904b (2015).

14 Burnum-Johnson, K. E. *et al.* New Views of Old Proteins: Clarifying the Enigmatic Proteome. *Mol Cell Proteomics* **21**, 100254, doi:10.1016/j.mcpro.2022.100254 (2022).

15 Hofmann, R. M. & Pickart, C. M. Noncanonical MMS2-encoded ubiquitin-conjugating enzyme functions in assembly of novel polyubiquitin chains for DNA repair. *Cell* **96**, 645-653, doi:10.1016/s0092-8674(00)80575-9 (1999).

16 Rahman, S. & Wolberger, C. Breaking the K48-chain: linking ubiquitin beyond protein degradation. *Nat Struct Mol Biol* **31**, 216-218, doi:10.1038/s41594-024-01221-w (2024).

17 Werner, A., Manford, A. G. & Rape, M. Ubiquitin-Dependent Regulation of Stem Cell Biology. *Trends Cell Biol* **27**, 568-579, doi:10.1016/j.tcb.2017.04.002 (2017).

18 Vijay-Kumar, S., Bugg, C. E. & Cook, W. J. Structure of ubiquitin refined at 1.8 A resolution. *J Mol Biol* **194**, 531-544, doi:10.1016/0022-2836(87)90679-6 (1987).

19 Komander, D. & Rape, M. The ubiquitin code. *Annu Rev Biochem* **81**, 203-229, doi:10.1146/annurev-biochem-060310-170328 (2012).

20 Swatek, K. N. & Komander, D. Ubiquitin modifications. *Cell Res* **26**, 399-422, doi:10.1038/cr.2016.39 (2016).

21 Mukhopadhyay, D. & Riezman, H. Proteasome-independent functions of ubiquitin in endocytosis and signaling. *Science* **315**, 201-205, doi:10.1126/science.1127085 (2007).

22 Husnjak, K. & Dikic, I. Ubiquitin-binding proteins: decoders of ubiquitin-mediated cellular functions. *Annu Rev Biochem* **81**, 291-322, doi:10.1146/annurev-biochem-051810-094654 (2012).

23 Clague, M. J., Urbé, S. & Komander, D. Breaking the chains: deubiquitylating enzyme specificity begets function. *Nat Rev Mol Cell Biol* **20**, 338-352, doi:10.1038/s41580-019-0099-1 (2019).

24 Kim, W. *et al.* Systematic and quantitative assessment of the ubiquitin-modified proteome. *Mol Cell* **44**, 325-340, doi:10.1016/j.molcel.2011.08.025 (2011).

25 Peng, J. *et al.* A proteomics approach to understanding protein ubiquitination. *Nat Biotechnol* **21**, 921-926, doi:10.1038/nbt849 (2003).

26 Yau, R. & Rape, M. The increasing complexity of the ubiquitin code. *Nat Cell Biol* **18**, 579-586, doi:10.1038/ncb3358 (2016).

27 van der Veen, A. G. & Ploegh, H. L. Ubiquitin-like proteins. *Annu Rev Biochem* **81**, 323-357, doi:10.1146/annurev-biochem-093010-153308 (2012).

28 Cappadocia, L. & Lima, C. D. Ubiquitin-like Protein Conjugation: Structures, Chemistry, and Mechanism. *Chem Rev* **118**, 889-918, doi:10.1021/acs.chemrev.6b00737 (2018).

29 Schulman, B. A. & Harper, J. W. Ubiquitin-like protein activation by E1 enzymes: the apex for downstream signalling pathways. *Nat Rev Mol Cell Biol* **10**, 319-331, doi:10.1038/nrm2673 (2009).

30 Barbour, H. *et al.* An inventory of crosstalk between ubiquitination and other post-translational modifications in orchestrating cellular processes. *iScience* **26**, 106276, doi:10.1016/j.isci.2023.106276 (2023).

31 Fan, J. B. *et al.* Identification and characterization of a novel ISG15-ubiquitin mixed chain and its role in regulating protein homeostasis. *Sci Rep* **5**, 12704, doi:10.1038/srep12704 (2015).

32 Wauer, T. *et al.* Ubiquitin Ser65 phosphorylation affects ubiquitin structure, chain assembly and hydrolysis. *EMBO J* **34**, 307-325, doi:10.15252/embj.201489847 (2015).

33 Ohtake, F. *et al.* Ubiquitin acetylation inhibits polyubiquitin chain elongation. *EMBO Rep* **16**, 192-201, doi:10.15252/embr.201439152 (2015).

34 Hershko, A., Heller, H., Elias, S. & Ciechanover, A. Components of ubiquitin-protein ligase system. Resolution, affinity purification, and role in protein breakdown. *J Biol Chem* **258**, 8206-8214 (1983).

35 Kerscher, O., Felberbaum, R. & Hochstrasser, M. Modification of proteins by ubiquitin and ubiquitin-like proteins. *Annu Rev Cell Dev Biol* **22**, 159-180, doi:10.1146/annurev.cellbio.22.010605.093503 (2006).

36 Jin, J., Li, X., Gygi, S. P. & Harper, J. W. Dual E1 activation systems for ubiquitin differentially regulate E2 enzyme charging. *Nature* **447**, 1135-1138, doi:10.1038/nature05902 (2007).

37 Pelzer, C. *et al.* UBE1L2, a novel E1 enzyme specific for ubiquitin. *J Biol Chem* **282**, 23010-23014, doi:10.1074/jbc.C700111200 (2007).

38 Ciechanover, A., Heller, H., Katz-Etzion, R. & Hershko, A. Activation of the heat-stable polypeptide of the ATP-dependent proteolytic system. *Proc Natl Acad Sci U S A* **78**, 761-765, doi:10.1073/pnas.78.2.761 (1981).

39 Li, W. *et al.* Genome-wide and functional annotation of human E3 ubiquitin ligases identifies MULAN, a mitochondrial E3 that regulates the organelle's dynamics and signaling. *PLoS One* **3**, e1487, doi:10.1371/journal.pone.0001487 (2008).

40 Stewart, M. D., Ritterhoff, T., Klevit, R. E. & Brzovic, P. S. E2 enzymes: more than just middle men. *Cell Res* **26**, 423-440, doi:10.1038/cr.2016.35 (2016).

41 Hann, Z. S. *et al.* Structural basis for adenylation and thioester bond formation in the ubiquitin E1. *Proc Natl Acad Sci U S A* **116**, 15475-15484, doi:10.1073/pnas.1905488116 (2019).

42 Eletr, Z. M., Huang, D. T., Duda, D. M., Schulman, B. A. & Kuhlman, B. E2 conjugating enzymes must disengage from their E1 enzymes before E3-dependent ubiquitin and ubiquitin-like transfer. *Nat Struct Mol Biol* **12**, 933-934, doi:10.1038/nsmb984 (2005).

43 Pickart, C. M. & Rose, I. A. Functional heterogeneity of ubiquitin carrier proteins. *J Biol Chem* **260**, 1573-1581 (1985).

44 Wenzel, D. M., Lissounov, A., Brzovic, P. S. & Klevit, R. E. UBCH7 reactivity profile reveals parkin and HHARI to be RING/HECT hybrids. *Nature* **474**, 105-108, doi:10.1038/nature09966 (2011).

45 Branigan, E., Plechanovova, A., Jaffray, E. G., Naismith, J. H. & Hay, R. T. Structural basis for the RING-catalyzed synthesis of K63-linked ubiquitin chains. *Nat Struct Mol Biol* **22**, 597-602, doi:10.1038/nsmb.3052 (2015).

46 Pruneda, J. N. *et al.* Structure of an E3:E2~Ub complex reveals an allosteric mechanism shared among RING/U-box ligases. *Mol Cell* **47**, 933-942, doi:10.1016/j.molcel.2012.07.001 (2012).

47 Zheng, N. & Shabek, N. Ubiquitin Ligases: Structure, Function, and Regulation. *Annu Rev Biochem* **86**, 129-157, doi:10.1146/annurev-biochem-060815-014922 (2017).

48 Morreale, F. E. & Walden, H. Types of Ubiquitin Ligases. *Cell* **165**, 248-248 e241, doi:10.1016/j.cell.2016.03.003 (2016).

49 Deshaies, R. J. & Joazeiro, C. A. RING domain E3 ubiquitin ligases. *Annu Rev Biochem* **78**, 399-434, doi:10.1146/annurev.biochem.78.101807.093809 (2009).

50 Skaar, J. R., Pagan, J. K. & Pagano, M. Mechanisms and function of substrate recruitment by F-box proteins. *Nat Rev Mol Cell Biol* **14**, 369-381, doi:10.1038/nrm3582 (2013).

51 Buetow, L. & Huang, D. T. Structural insights into the catalysis and regulation of E3 ubiquitin ligases. *Nat Rev Mol Cell Biol* **17**, 626-642, doi:10.1038/nrm.2016.91 (2016).

52 Huang, L. *et al.* Structure of an E6AP-UbcH7 complex: insights into ubiquitination by the E2-E3 enzyme cascade. *Science* **286**, 1321-1326, doi:10.1126/science.286.5443.1321 (1999).

53 D'Amico, F., Mukhopadhyay, R., Ovaa, H. & Mulder, M. P. C. Targeting TRIM Proteins: A Quest towards Drugging an Emerging Protein Class. *Chembiochem* **22**, 2011-2031, doi:10.1002/cbic.202000787 (2021).

54 Hehl, L. A. *et al.* Structural snapshots along K48-linked ubiquitin chain formation by the HECT E3 UBR5. *Nature Chemical Biology* **20**, 190-200, doi:10.1038/s41589-023-01414-2 (2024).

55 Christensen, D. E., Brzovic, P. S. & Klevit, R. E. E2-BRCA1 RING interactions dictate synthesis of mono- or specific polyubiquitin chain linkages. *Nat Struct Mol Biol* **14**, 941-948, doi:10.1038/nsmb1295 (2007).

56 Wickliffe, K. E., Lorenz, S., Wemmer, D. E., Kuriyan, J. & Rape, M. The mechanism of linkage-specific ubiquitin chain elongation by a single-subunit E2. *Cell* **144**, 769-781, doi:10.1016/j.cell.2011.01.035 (2011).

57 Varadan, R. *et al.* Solution conformation of Lys63-linked di-ubiquitin chain provides clues to functional diversity of polyubiquitin signaling. *J Biol Chem* **279**, 7055-7063, doi:10.1074/jbc.M309184200 (2004).

58 Haakonsen, D. L. & Rape, M. Branching Out: Improved Signaling by Heterotypic Ubiquitin Chains. *Trends Cell Biol* **29**, 704-716, doi:10.1016/j.tcb.2019.06.003 (2019).

59 Waltho, A. *et al.* K48- and K63-linked ubiquitin chain interactome reveals branch- and length-specific ubiquitin interactors. *Life Sci Alliance* **7**, doi:10.26508/lsa.202402740 (2024).

60 Lutz, J., Hollmuller, E., Scheffner, M., Marx, A. & Stengel, F. The Length of a Ubiquitin Chain: A General Factor for Selective Recognition by Ubiquitin-Binding Proteins. *Angew Chem Int Ed Engl* **59**, 12371-12375, doi:10.1002/anie.202003058 (2020).

61 Ziv, I. *et al.* A perturbed ubiquitin landscape distinguishes between ubiquitin in trafficking and in proteolysis. *Mol Cell Proteomics* **10**, M111.009753, doi:10.1074/mcp.M111.009753 (2011).

62 Joo, H. Y. *et al.* Regulation of cell cycle progression and gene expression by H2A deubiquitination. *Nature* **449**, 1068-1072, doi:10.1038/nature06256 (2007).

63 Clague, M. J., Heride, C. & Urbe, S. The demographics of the ubiquitin system. *Trends Cell Biol* **25**, 417-426, doi:10.1016/j.tcb.2015.03.002 (2015).

64 Ulrich, H. D. & Walden, H. Ubiquitin signalling in DNA replication and repair. *Nat Rev Mol Cell Biol* **11**, 479-489, doi:10.1038/nrm2921 (2010).

65 Kaiser, S. E. *et al.* Protein standard absolute quantification (PSAQ) method for the measurement of cellular ubiquitin pools. *Nat Methods* **8**, 691-696, doi:10.1038/nmeth.1649 (2011).

66 Crowe, S. O., Rana, A., Deol, K. K., Ge, Y. & Strieter, E. R. Ubiquitin Chain Enrichment Middle-Down Mass Spectrometry Enables Characterization of Branched Ubiquitin Chains in Cellulo. *Anal Chem* **89**, 4428-4434, doi:10.1021/acs.analchem.6b03675 (2017).

67 Swatek, K. N. *et al.* Insights into ubiquitin chain architecture using Ub-clipping. *Nature* **572**, 533-537, doi:10.1038/s41586-019-1482-y (2019).

68 Hershko, A., Ciechanover, A. & Rose, I. A. Resolution of the ATP-dependent proteolytic system from reticulocytes: a component that interacts with ATP. *Proc Natl Acad Sci U S A* **76**, 3107-3110, doi:10.1073/pnas.76.7.3107 (1979).

69 Meyer, H. J. & Rape, M. Enhanced protein degradation by branched ubiquitin chains. *Cell* **157**, 910-921, doi:10.1016/j.cell.2014.03.037 (2014).

70 Thrower, J. S., Hoffman, L., Rechsteiner, M. & Pickart, C. M. Recognition of the polyubiquitin proteolytic signal. *Embo j* **19**, 94-102, doi:10.1093/emboj/19.1.94 (2000).

71 Braten, O. *et al.* Numerous proteins with unique characteristics are degraded by the 26S proteasome following monoubiquitination. *Proc Natl Acad Sci U S A* **113**, E4639-4647, doi:10.1073/pnas.1608644113 (2016).

72 Lu, Y., Lee, B. H., King, R. W., Finley, D. & Kirschner, M. W. Substrate degradation by the proteasome: a single-molecule kinetic analysis. *Science* **348**, 1250834, doi:10.1126/science.1250834 (2015).

73 Saeki, Y. *et al.* Lysine 63-linked polyubiquitin chain may serve as a targeting signal for the 26S proteasome. *Embo j* **28**, 359-371, doi:10.1038/emboj.2008.305 (2009).

74 Erpapazoglou, Z., Walker, O. & Haguenauer-Tsapis, R. Versatile roles of k63-linked ubiquitin chains in trafficking. *Cells* **3**, 1027-1088, doi:10.3390/cells3041027 (2014).

75 Chen, Z. J. & Sun, L. J. Nonproteolytic Functions of Ubiquitin in Cell Signaling. *Molecular Cell* **33**, 275-286, doi:10.1016/j.molcel.2009.01.014 (2009).

76 Ohtake, F., Tsuchiya, H., Saeki, Y. & Tanaka, K. K63 ubiquitylation triggers proteasomal degradation by seeding branched ubiquitin chains. *Proc Natl Acad Sci U S A* **115**, E1401-e1408, doi:10.1073/pnas.1716673115 (2018).

77 Boname, J. M. *et al.* Efficient internalization of MHC I requires lysine-11 and lysine-63 mixed linkage polyubiquitin chains. *Traffic* **11**, 210-220, doi:10.1111/j.1600-0854.2009.01011.x (2010).

78 Emmerich, C. H. *et al.* Activation of the canonical IKK complex by K63/M1-linked hybrid ubiquitin chains. *Proc Natl Acad Sci U S A* **110**, 15247-15252, doi:10.1073/pnas.1314715110 (2013).

79 Ohtake, F., Saeki, Y., Ishido, S., Kanno, J. & Tanaka, K. The K48-K63 Branched Ubiquitin Chain Regulates NF-κB Signaling. *Mol Cell* **64**, 251-266, doi:10.1016/j.molcel.2016.09.014 (2016).

80 Pao, K. C. *et al.* Activity-based E3 ligase profiling uncovers an E3 ligase with esterification activity. *Nature* **556**, 381-385, doi:10.1038/s41586-018-0026-1 (2018).

81 Kelsall, I. R., Zhang, J., Knebel, A., Arthur, J. S. C. & Cohen, P. The E3 ligase HOIL-1 catalyses ester bond formation between ubiquitin and components of the Myddosome in mammalian cells. *Proc Natl Acad Sci U S A* **116**, 13293-13298, doi:10.1073/pnas.1905873116 (2019).

82 Qiu, J. *et al.* Ubiquitination independent of E1 and E2 enzymes by bacterial effectors. *Nature* **533**, 120-124, doi:10.1038/nature17657 (2016).

83 Otten, E. G. *et al.* Ubiquitylation of lipopolysaccharide by RNF213 during bacterial infection. *Nature* **594**, 111-116, doi:10.1038/s41586-021-03566-4 (2021).

84 Zhu, K. *et al.* DELTEX E3 ligases ubiquitylate ADP-ribosyl modification on protein substrates. *Sci Adv* **8**, eadd4253, doi:10.1126/sciadv.add4253 (2022).

85 Kelsall, I. R. *et al.* HOIL-1 ubiquitin ligase activity targets unbranched glucosaccharides and is required to prevent polyglucosan accumulation. *EMBO J* **41**, e109700, doi:10.15252/embj.2021109700 (2022).

86 Sakamaki, J. I. *et al.* Ubiquitination of phosphatidylethanolamine in organellar membranes. *Mol Cell* **82**, 3677-3692 e3611, doi:10.1016/j.molcel.2022.08.008 (2022).

87 Lechtenberg, B. C. & Komander, D. Just how big is the ubiquitin system? *Nat Struct Mol Biol* **31**, 210-213, doi:10.1038/s41594-023-01208-z (2024).

88 Prus, G., Satpathy, S., Weinert, B. T., Narita, T. & Choudhary, C. Global, site-resolved analysis of ubiquitylation occupancy and turnover rate reveals systems properties. *Cell* **187**, 2875-2892 e2821, doi:10.1016/j.cell.2024.03.024 (2024).

89 de Poot, S. A. H., Tian, G. & Finley, D. Meddling with Fate: The Proteasomal Deubiquitinating Enzymes. *J Mol Biol* **429**, 3525-3545, doi:10.1016/j.jmb.2017.09.015 (2017).

90 Reyes-Turcu, F. E. *et al.* The ubiquitin binding domain ZnF UBP recognizes the C-terminal diglycine motif of unanchored ubiquitin. *Cell* **124**, 1197-1208, doi:10.1016/j.cell.2006.02.038 (2006).

91 Grou, C. P., Pinto, M. P., Mendes, A. V., Domingues, P. & Azevedo, J. E. The de novo synthesis of ubiquitin: identification of deubiquitinases acting on ubiquitin precursors. *Sci Rep* **5**, 12836, doi:10.1038/srep12836 (2015).

92 Heideker, J. & Wertz, I. E. DUBs, the regulation of cell identity and disease. *Biochem J* **465**, 1-26, doi:10.1042/bj20140496 (2015).

93 Ma, A. & Malynn, B. A. A20: linking a complex regulator of ubiquitylation to immunity and human disease. *Nat Rev Immunol* **12**, 774-785, doi:10.1038/nri3313 (2012).

94 Lange, S. M., Armstrong, L. A. & Kulathu, Y. Deubiquitinases: From mechanisms to their inhibition by small molecules. *Mol Cell* **82**, 15-29, doi:10.1016/j.molcel.2021.10.027 (2022).

95 Mevissen, T. E. T. & Komander, D. Mechanisms of Deubiquitinase Specificity and Regulation. *Annu Rev Biochem* **86**, 159-192, doi:10.1146/annurev-biochem-061516-044916 (2017).

96 Basters, A. *et al.* Structural basis of the specificity of USP18 toward ISG15. *Nat Struct Mol Biol* **24**, 270-278, doi:10.1038/nsmb.3371 (2017).

97 Wang, T. *et al.* Expedient Synthesis of Ubiquitin-like Protein ISG15 Tools through Chemo-Enzymatic Ligation Catalyzed by a Viral Protease Lb(pro). *Angew Chem Int Ed Engl* **61**, e202206205, doi:10.1002/anie.202206205 (2022).

98 Ye, Y. *et al.* Polyubiquitin binding and cross-reactivity in the USP domain deubiquitinase USP21. *EMBO Rep* **12**, 350-357, doi:10.1038/embor.2011.17 (2011).

99 Zhao, Z., O'Dea, R., Wendrich, K., Kazi, N. & Gersch, M. Native Semisynthesis of Isopeptide-Linked Substrates for Specificity Analysis of Deubiquitinases and Ubl Proteases. *J Am Chem Soc* **145**, 20801-20812, doi:10.1021/jacs.3c04062 (2023).

100 Walden, M., Masandi, S. K., Pawłowski, K. & Zeqiraj, E. Pseudo-DUBs as allosteric activators and molecular scaffolds of protein complexes. *Biochem Soc Trans* **46**, 453-466, doi:10.1042/bst20160268 (2018).

101 De Cesare, V. *et al.* Deubiquitinating enzyme amino acid profiling reveals a class of ubiquitin esterases. *Proc Natl Acad Sci U S A* **118**, doi:10.1073/pnas.2006947118 (2021).

102 Amerik, A. Y. & Hochstrasser, M. Mechanism and function of deubiquitinating enzymes. *Biochim Biophys Acta* **1695**, 189-207, doi:10.1016/j.bbamcr.2004.10.003 (2004).

103 Nijman, S. M. B. *et al.* A Genomic and Functional Inventory of Deubiquitinating Enzymes. *Cell* **123**, 773-786, doi:10.1016/j.cell.2005.11.007 (2005).

104 Snyder, N. A. & Silva, G. M. Deubiquitinating enzymes (DUBs): Regulation, homeostasis, and oxidative stress response. *J Biol Chem* **297**, 101077, doi:10.1016/j.jbc.2021.101077 (2021).

105 Komander, D., Clague, M. J. & Urbe, S. Breaking the chains: structure and function of the deubiquitinases. *Nat Rev Mol Cell Biol* **10**, 550-563, doi:10.1038/nrm2731 (2009).

106 Schechter, I. & Berger, A. On the size of the active site in proteases. I. Papain. *Biochem Biophys Res Commun* **27**, 157-162, doi:10.1016/s0006-291x(67)80055-x (1967).

107 Drag, M. *et al.* Positional-scanning fluorigenic substrate libraries reveal unexpected specificity determinants of DUBs (deubiquitinating enzymes). *Biochem J* **415**, 367-375, doi:10.1042/BJ20080779 (2008).

108 Ronau, J. A., Beckmann, J. F. & Hochstrasser, M. Substrate specificity of the ubiquitin and Ubl proteases. *Cell Res* **26**, 441-456, doi:10.1038/cr.2016.38 (2016).

109 O'Dea, R. *et al.* Molecular basis for ubiquitin/Fubi cross-reactivity in USP16 and USP36. *Nat Chem Biol* **19**, 1394-1405, doi:10.1038/s41589-023-01388-1 (2023).

110 Faesen, A. C. *et al.* The differential modulation of USP activity by internal regulatory domains, interactors and eight ubiquitin chain types. *Chem Biol* **18**, 1550-1561, doi:10.1016/j.chembiol.2011.10.017 (2011).

111 Ritorto, M. S. *et al.* Screening of DUB activity and specificity by MALDI-TOF mass spectrometry. *Nat Commun* **5**, 4763, doi:10.1038/ncomms5763 (2014).

112 Morgan, M. T. *et al.* Structural basis for histone H2B deubiquitination by the SAGA DUB module. *Science* **351**, 725-728, doi:10.1126/science.aac5681 (2016).

113 Abdul Rehman, S. A. *et al.* Mechanism of activation and regulation of deubiquitinase activity in MINDY1 and MINDY2. *Mol Cell* **81**, 4176-4190 e4176, doi:10.1016/j.molcel.2021.08.024 (2021).

114 Hewings, D. S. *et al.* Reactive-site-centric chemoproteomics identifies a distinct class of deubiquitinase enzymes. *Nat Commun* **9**, 1162, doi:10.1038/s41467-018-03511-6 (2018).

115 Kwasna, D. *et al.* Discovery and Characterization of ZUFSP/ZUP1, a Distinct Deubiquitinase Class Important for Genome Stability. *Mol Cell* **70**, 150-164.e156, doi:10.1016/j.molcel.2018.02.023 (2018).

116 Gersch, M. *et al.* Mechanism and regulation of the Lys6-selective deubiquitinase USP30. *Nat Struct Mol Biol* **24**, 920-930, doi:10.1038/nsmb.3475 (2017).

117 Sato, Y. *et al.* Structures of CYLD USP with Met1- or Lys63-linked diubiquitin reveal mechanisms for dual specificity. *Nat Struct Mol Biol* **22**, 222-229, doi:10.1038/nsmb.2970 (2015).

118 Sato, Y. *et al.* Structural basis for specific cleavage of Lys 63-linked polyubiquitin chains. *Nature* **455**, 358-362, doi:10.1038/nature07254 (2008).

119 Keusekotten, K. *et al.* OTULIN antagonizes LUBAC signaling by specifically hydrolyzing Met1-linked polyubiquitin. *Cell* **153**, 1312-1326, doi:10.1016/j.cell.2013.05.014 (2013).

120 Mevissen, T. E. *et al.* OTU deubiquitinases reveal mechanisms of linkage specificity and enable ubiquitin chain restriction analysis. *Cell* **154**, 169-184, doi:10.1016/j.cell.2013.05.046 (2013).

121 Berk, J. M. *et al.* A deubiquitylase with an unusually high-affinity ubiquitin-binding domain from the scrub typhus pathogen Orientia tsutsugamushi. *Nat Commun* **11**, 2343, doi:10.1038/s41467-020-15985-4 (2020).

122 Bekes, M. *et al.* Recognition of Lys48-Linked Di-ubiquitin and Deubiquitinating Activities of the SARS Coronavirus Papain-like Protease. *Mol Cell* **62**, 572-585, doi:10.1016/j.molcel.2016.04.016 (2016).

123 Ye, Y., Scheel, H., Hofmann, K. & Komander, D. Dissection of USP catalytic domains reveals five common insertion points. *Mol Biosyst* **5**, 1797-1808, doi:10.1039/b907669g (2009).

124 Hu, M. *et al.* Crystal structure of a UBP-family deubiquitinating enzyme in isolation and in complex with ubiquitin aldehyde. *Cell* **111**, 1041-1054, doi:10.1016/s0092-8674(02)01199-6 (2002).

125 UniProt, C. UniProt: the Universal Protein Knowledgebase in 2023. *Nucleic Acids Res* **51**, D523-D531, doi:10.1093/nar/gkac1052 (2023).

126 Rigden, D. J., Liu, H., Hayes, S. D., Urbe, S. & Clague, M. J. Ab initio protein modelling reveals novel human MIT domains. *FEBS Lett* **583**, 872-878, doi:10.1016/j.febslet.2009.02.012 (2009).

127 Thul, P. J. *et al.* A subcellular map of the human proteome. *Science* **356**, doi:10.1126/science.aal3321 (2017).

128 Quesada, V. *et al.* Cloning and enzymatic analysis of 22 novel human ubiquitin-specific proteases. *Biochem Biophys Res Commun* **314**, 54-62, doi:10.1016/j.bbrc.2003.12.050 (2004).

129 Kazmierczak, M. *et al.* Progressive Hearing Loss in Mice Carrying a Mutation in Usp53. *J Neurosci* **35**, 15582-15598, doi:10.1523/JNEUROSCI.1965-15.2015 (2015).

130 Yao, Y. *et al.* USP53 plays an antitumor role in hepatocellular carcinoma through deubiquitination of cytochrome c. *Oncogenesis* **11**, 31, doi:10.1038/s41389-022-00404-8 (2022).

131 Liu, Y., Tang, W. & Yao, F. USP53 Exerts Tumor-Promoting Effects in Triple-Negative Breast Cancer by Deubiquitinating CRKL. *Cancers (Basel)* **15**, doi:10.3390/cancers15205033 (2023).

132 Zhang, C. *et al.* Centrosomal protein 120 promotes centrosome amplification and gastric cancer progression via USP54-mediated deubiquitination of PLK4. *iScience* **26**, 105745, doi:10.1016/j.isci.2022.105745 (2023).

133 Liu, X. *et al.* Endothelial Dickkopf-1 Promotes Smooth Muscle Cell-derived Foam Cell Formation via USP53-mediated Deubiquitination of SR-A During Atherosclerosis. *Int J Biol Sci* **20**, 2943-2964, doi:10.7150/ijbs.91957 (2024).

134 Alhebbi, H. *et al.* New paradigms of USP53 disease: normal GGT cholestasis, BRIC, cholangiopathy, and responsiveness to rifampicin. *J Hum Genet* **66**, 151-159, doi:10.1038/s10038-020-0811-1 (2021).

135 Maddirevula, S. *et al.* Identification of novel loci for pediatric cholestatic liver disease defined by KIF12, PPM1F, USP53, LSR, and WDR83OS pathogenic variants. *Genet Med* **21**, 1164-1172, doi:10.1038/s41436-018-0288-x (2019).

136 Zhang, J. *et al.* Low-GGT intrahepatic cholestasis associated with biallelic USP53 variants: Clinical, histological and ultrastructural characterization. *Liver Int* **40**, 1142-1150, doi:10.1111/liv.14422 (2020).

137 Bull, L. N. *et al.* Cholestasis Due to USP53 Deficiency. *J Pediatr Gastroenterol Nutr* **72**, 667-673, doi:10.1097/MPG.0000000000002926 (2021).

138 Shatokhina, O. *et al.* A Two-Year Clinical Description of a Patient with a Rare Type of Low-GGT Cholestasis Caused by a Novel Variant of USP53. *Genes (Basel)* **12**, doi:10.3390/genes12101618 (2021).

139 Sambrotta, M. *et al.* Mutations in TJP2 cause progressive cholestatic liver disease. *Nat Genet* **46**, 326-328, doi:10.1038/ng.2918 (2014).

140 Shagrani, M. *et al.* Genetic profiling of children with advanced cholestatic liver disease. *Clin Genet* **92**, 52-61, doi:10.1111/cge.12959 (2017).

141 Hariri, H., Kose, O., Bezdjian, A., Daniel, S. J. & St-Arnaud, R. USP53 Regulates Bone Homeostasis by Controlling Rankl Expression in Osteoblasts and Bone Marrow Adipocytes. *J Bone Miner Res* **38**, 578-596, doi:10.1002/jbmr.4778 (2023).

142 Samanta, A., Parveen, N., Sen Sarma, M., Poddar, U. & Srivastava, A. Cholestatic Liver Disease due to Novel USP53 Mutations: A Case Series of Three Indian Children. *J Clin Exp Hepatol* **14**, doi:10.1016/j.jceh.2023.10.001 (2024).

143 Kanwal, A. *et al.* Genome Sequencing of Consanguineous Family Implicates Ubiquitin-Specific Protease 53 (*USP53*) Variant in Psychosis/Schizophrenia: Wild-Type Expression in Murine Hippocampal CA 1-3 and Granular Dentate with AMPA Synapse Interactions. *Genes-Basel* **14**, doi:10.3390/genes14101921 (2023).

144 Tibbetts, R. S. *et al.* A role for ATR in the DNA damage-induced phosphorylation of p53. *Genes Dev* **13**, 152-157, doi:10.1101/gad.13.2.152 (1999).

145 Ma, Z. Y. *et al.* Recurrent gain-of-function USP8 mutations in Cushing's disease. *Cell Res* **25**, 306-317, doi:10.1038/cr.2015.20 (2015).

146 Bowen, S. *et al.* Mutations in the CYLD gene in Brooke-Spiegler syndrome, familial cylindromatosis, and multiple familial trichoepithelioma: lack of genotype-phenotype correlation. *J Invest Dermatol* **124**, 919-920, doi:10.1111/j.0022-202X.2005.23688.x (2005).

147 Odqvist, L. *et al.* Genetic variations in A20 DUB domain provide a genetic link to citrullination and neutrophil extracellular traps in systemic lupus erythematosus. *Ann Rheum Dis* **78**, 1363-1370, doi:10.1136/annrheumdis-2019-215434 (2019).
148 Park, T. Crk and CrkL as Therapeutic Targets for Cancer Treatment. *Cells* **10**, doi:10.3390/cells10040739 (2021).
149 Zhao, X., Wu, X., Wang, H., Yu, H. & Wang, J. USP53 promotes apoptosis and inhibits glycolysis in lung adenocarcinoma through FKBP51-AKT1 signaling. *Mol Carcinog* **59**, 1000-1011, doi:10.1002/mc.23230 (2020).
150 Cheng, W. *et al.* USP53 activated by H3K27 acetylation regulates cell viability, apoptosis and metabolism in esophageal carcinoma via the AMPK signaling pathway. *Carcinogenesis* **43**, 349-359, doi:10.1093/carcin/bgab123 (2022).
151 Gui, D. *et al.* Ubiquitin-specific peptidase 53 inhibits the occurrence and development of clear cell renal cell carcinoma through NF-kappaB pathway inactivation. *Cancer Med* **10**, 3674-3688, doi:10.1002/cam4.3911 (2021).
152 Meng, X. *et al.* USP53 Affects the Proliferation and Apoptosis of Breast Cancer Cells by Regulating the Ubiquitination Level of ZMYND11. *Biol Proced Online* **26**, 24, doi:10.1186/s12575-024-00251-4 (2024).
153 Li, Q. *et al.* Ubiquitin-specific peptidase 53 promotes chronic constriction injury-induced neuropathic pain through the RhoA/ROCK pathway. *Acta Neurobiol Exp (Wars)* **82**, 468-476, doi:10.55782/ane-2022-045 (2022).
154 Baek, D. *et al.* Ubiquitin-specific protease 53 promotes osteogenic differentiation of human bone marrow-derived mesenchymal stem cells. *Cell Death Dis* **12**, 238, doi:10.1038/s41419-021-03517-x (2021).
155 Hariri, H., Addison, W. N. & St-Arnaud, R. Ubiquitin specific peptidase Usp53 regulates osteoblast versus adipocyte lineage commitment. *Sci Rep* **11**, 8418, doi:10.1038/s41598-021-87608-x (2021).
156 Brave, H. & MacLoughlin, R. State of the Art Review of Cell Therapy in the Treatment of Lung Disease, and the Potential for Aerosol Delivery. *Int J Mol Sci* **21**, doi:10.3390/ijms21176435 (2020).
157 Kurban, M. *et al.* Copy Number Variations on Chromosome 4q26-27 Are Associated with Cantu Syndrome. *Dermatology* **223**, 316-320, doi:10.1159/000333800 (2011).
158 Bolton, J. *et al.* Molecular Biomarkers for Weight Control in Obese Individuals Subjected to a Multiphase Dietary Intervention. *J Clin Endocrinol Metab* **102**, 2751-2761, doi:10.1210/jc.2016-3997 (2017).
159 Zhou, C. *et al.* USP54 is a potential therapeutic target in castration-resistant prostate cancer. *BMC Urol* **24**, 32, doi:10.1186/s12894-024-01418-7 (2024).
160 Fraile, J. M., Campos-Iglesias, D., Rodríguez, F., Español, Y. & Freije, J. M. The deubiquitinase USP54 is overexpressed in colorectal cancer stem cells and promotes intestinal tumorigenesis. *Oncotarget* **7**, 74427-74434, doi:10.18632/oncotarget.12769 (2016).
161 Sercin, O. *et al.* Transient PLK4 overexpression accelerates tumorigenesis in p53-deficient epidermis. *Nat Cell Biol* **18**, 100-110, doi:10.1038/ncb3270 (2016).
162 Firat-Karalar, E. N., Rauniyar, N., Yates, J. R., 3rd & Stearns, T. Proximity interactions among centrosome components identify regulators of centriole duplication. *Curr Biol* **24**, 664-670, doi:10.1016/j.cub.2014.01.067 (2014).
163 Wu, Q. *Mechanisms of centriole duplication and spindle assembly in human cells*, (2019).
164 Kasahara, K. *et al.* EGF receptor kinase suppresses ciliogenesis through activation of USP8 deubiquitinase. *Nat Commun* **9**, 758, doi:10.1038/s41467-018-03117-y (2018).
165 Wijdeven, R. H. *et al. Chapter 5: USP54 is a novel regulator of cytoskeletal dynamics*, (2017).
166 Ekkebus, R. *et al.* On terminal alkynes that can react with active-site cysteine nucleophiles in proteases. *J Am Chem Soc* **135**, 2867-2870, doi:10.1021/ja309802n (2013).

167 Magin, R. S. *et al.* Small molecules as tools for functional assessment of deubiquitinating enzyme function. *Cell Chem Biol* **28**, 1090-1100, doi:10.1016/j.chembiol.2021.04.021 (2021).

168 Schauer, N. J., Magin, R. S., Liu, X., Doherty, L. M. & Buhrlage, S. J. Advances in Discovering Deubiquitinating Enzyme (DUB) Inhibitors. *J Med Chem* **63**, 2731-2750, doi:10.1021/acs.jmedchem.9b01138 (2020).

169 Mattern, M., Sutherland, J., Kadimisetty, K., Barrio, R. & Rodriguez, M. S. Using Ubiquitin Binders to Decipher the Ubiquitin Code. *Trends Biochem Sci* **44**, 599-615, doi:10.1016/j.tibs.2019.01.011 (2019).

170 Conole, D. *et al.* Discovery of a Potent Deubiquitinase (DUB) Small-Molecule Activity-Based Probe Enables Broad Spectrum DUB Activity Profiling in Living Cells. *Angew Chem Int Ed Engl* **62**, e202311190, doi:10.1002/anie.202311190 (2023).

171 Gorka, M., Magnussen, H. M. & Kulathu, Y. Chemical biology tools to study Deubiquitinases and Ubl proteases. *Semin Cell Dev Biol* **132**, 86-96, doi:10.1016/j.semcdb.2022.02.006 (2022).

172 Lange, S. M. *et al.* VCP/p97-associated proteins are binders and debranching enzymes of K48-K63-branched ubiquitin chains. *Nat Struct Mol Biol* **31**, 1872-1887, doi:10.1038/s41594-024-01354-y (2024).

173 Dang, L. C., Melandri, F. D. & Stein, R. L. Kinetic and Mechanistic Studies on the Hydrolysis of Ubiquitin C-Terminal 7-Amido-4-Methylcoumarin by Deubiquitinating Enzymes. *Biochemistry* **37**, 1868-1879, doi:10.1021/bi9723360 (1998).

174 Hassiepen, U. *et al.* A sensitive fluorescence intensity assay for deubiquitinating proteases using ubiquitin-rhodamine110-glycine as substrate. *Anal Biochem* **371**, 201-207, doi:10.1016/j.ab.2007.07.034 (2007).

175 Turnbull, A. P. *et al.* Molecular basis of USP7 inhibition by selective small-molecule inhibitors. *Nature* **550**, 481-486, doi:10.1038/nature24451 (2017).

176 Wrigley, J. D. *et al.* Identification and Characterization of Dual Inhibitors of the USP25/28 Deubiquitinating Enzyme Subfamily. *ACS Chemical Biology* **12**, 3113-3125, doi:10.1021/acschembio.7b00334 (2017).

177 Klemm, T. *et al.* Mechanism and inhibition of the papain-like protease, PLpro, of SARS-CoV-2. *Embo j* **39**, e106275, doi:10.15252/embj.2020106275 (2020).

178 Lee, B. H., Finley, D. & King, R. W. A High-Throughput Screening Method for Identification of Inhibitors of the Deubiquitinating Enzyme USP14. *Curr Protoc Chem Biol* **4**, 311-330, doi:10.1002/9780470559277.ch120078 (2012).

179 Tirat, A. *et al.* Synthesis and characterization of fluorescent ubiquitin derivatives as highly sensitive substrates for the deubiquitinating enzymes UCH-L3 and USP-2. *Anal Biochem* **343**, 244-255, doi:10.1016/j.ab.2005.04.023 (2005).

180 Geurink, P. P., El Oualid, F., Jonker, A., Hameed, D. S. & Ovaa, H. A general chemical ligation approach towards isopeptide-linked ubiquitin and ubiquitin-like assay reagents. *Chembiochem* **13**, 293-297, doi:10.1002/cbic.201100706 (2012).

181 Haahr, P. *et al.* ZUFSP Deubiquitylates K63-Linked Polyubiquitin Chains to Promote Genome Stability. *Mol Cell* **70**, 165-174.e166, doi:10.1016/j.molcel.2018.02.024 (2018).

182 Hibbert, R. G. & Sixma, T. K. Intrinsic flexibility of ubiquitin on proliferating cell nuclear antigen (PCNA) in translesion synthesis. *J Biol Chem* **287**, 39216-39223, doi:10.1074/jbc.M112.389890 (2012).

183 Michel, M. A., Komander, D. & Elliott, P. R. Enzymatic Assembly of Ubiquitin Chains. *Methods Mol Biol* **1844**, 73-84, doi:10.1007/978-1-4939-8706-1_6 (2018).

184 Mulder, M. P. C., Witting, K. F. & Ovaa, H. Cracking the Ubiquitin Code: The Ubiquitin Toolbox. *Curr Issues Mol Biol* **37**, 1-20, doi:10.21775/cimb.037.001 (2020).

185 El Oualid, F. *et al.* Chemical synthesis of ubiquitin, ubiquitin-based probes, and diubiquitin. *Angew Chem Int Ed Engl* **49**, 10149-10153, doi:10.1002/anie.201005995 (2010).

186 Yang, R., Pasunooti, K. K., Li, F., Liu, X. W. & Liu, C. F. Synthesis of K48-linked diubiquitin using dual native chemical ligation at lysine. *Chem Commun (Camb)* **46**, 7199-7201, doi:10.1039/c0cc01382j (2010).
187 Ye, Y. *et al.* Semi-synthesis of K27-linked-mixed-triubiquitin chains through a combination of enzymatic reaction with CAACU strategy. *Tetrahedron Letters* **71**, 153000, doi:10.1016/j.tetlet.2021.153000 (2021).
188 Padala, P. *et al.* The Crystal Structure and Conformations of an Unbranched Mixed Tri-Ubiquitin Chain Containing K48 and K63 Linkages. *J Mol Biol* **429**, 3801-3813, doi:10.1016/j.jmb.2017.10.027 (2017).
189 Pérez Berrocal, D. A., van der Heden van Noort, G. J. & Mulder, M. P. C. Chemical Synthesis of Non-hydrolyzable Ubiquitin(-Like) Hybrid Chains. *Methods Mol Biol* **2602**, 41-49, doi:10.1007/978-1-0716-2859-1_3 (2023).
190 Valkevich, E. M. *et al.* Forging isopeptide bonds using thiol-ene chemistry: site-specific coupling of ubiquitin molecules for studying the activity of isopeptidases. *J Am Chem Soc* **134**, 6916-6919, doi:10.1021/ja300500a (2012).
191 Fottner, M. *et al.* A modular toolbox to generate complex polymeric ubiquitin architectures using orthogonal sortase enzymes. *Nature Communications* **12**, 6515, doi:10.1038/s41467-021-26812-9 (2021).
192 Stanley, M. & Virdee, S. Genetically Directed Production of Recombinant, Isosteric and Nonhydrolysable Ubiquitin Conjugates. *Chembiochem* **17**, 1472-1480, doi:10.1002/cbic.201600138 (2016).
193 Mali, S. M., Singh, S. K., Eid, E. & Brik, A. Ubiquitin Signaling: Chemistry Comes to the Rescue. *J Am Chem Soc* **139**, 4971-4986, doi:10.1021/jacs.7b00089 (2017).
194 Virdee, S. *et al.* Traceless and Site-Specific Ubiquitination of Recombinant Proteins. *Journal of the American Chemical Society* **133**, 10708-10711, doi:10.1021/ja202799r (2011).
195 Fottner, M. *et al.* Site-specific ubiquitylation and SUMOylation using genetic-code expansion and sortase. *Nat Chem Biol* **15**, 276-284, doi:10.1038/s41589-019-0227-4 (2019).
196 Hofmann, R., Akimoto, G., Wucherpfennig, T. G., Zeymer, C. & Bode, J. W. Lysine acylation using conjugating enzymes for site-specific modification and ubiquitination of recombinant proteins. *Nat Chem* **12**, 1008-1015, doi:10.1038/s41557-020-0528-y (2020).
197 Akimoto, G., Fernandes, A. P. & Bode, J. W. Site-Specific Protein Ubiquitylation Using an Engineered, Chimeric E1 Activating Enzyme and E2 SUMO Conjugating Enzyme Ubc9. *ACS Cent Sci* **8**, 275-281, doi:10.1021/acscentsci.1c01490 (2022).
198 Borodovsky, A. *et al.* A novel active site-directed probe specific for deubiquitylating enzymes reveals proteasome association of USP14. *Embo j* **20**, 5187-5196, doi:10.1093/emboj/20.18.5187 (2001).
199 Geurink, P. P. *et al.* in *Methods in Enzymology* Vol. 618 (ed Mark Hochstrasser) 357-387 (Academic Press, 2019).
200 Naik, E. & Dixit, V. M. Usp9X Is Required for Lymphocyte Activation and Homeostasis through Its Control of ZAP70 Ubiquitination and PKCbeta Kinase Activity. *J Immunol* **196**, 3438-3451, doi:10.4049/jimmunol.1403165 (2016).
201 Sui, X. *et al.* Development and application of ubiquitin-based chemical probes. *Chem Sci* **11**, 12633-12646, doi:10.1039/d0sc03295f (2020).
202 de Jong, A. *et al.* Ubiquitin-based probes prepared by total synthesis to profile the activity of deubiquitinating enzymes. *Chembiochem* **13**, 2251-2258, doi:10.1002/cbic.201200497 (2012).
203 Borodovsky, A. *et al.* Chemistry-based functional proteomics reveals novel members of the deubiquitinating enzyme family. *Chem Biol* **9**, 1149-1159, doi:10.1016/s1074-5521(02)00248-x (2002).
204 Perler, F. B. & Adam, E. Protein splicing and its applications. *Current Opinion in Biotechnology* **11**, 377-383, doi:10.1016/S0958-1669(00)00113-0 (2000).

205 Hewings, D. S., Flygare, J. A., Bogyo, M. & Wertz, I. E. Activity-based probes for the ubiquitin conjugation-deconjugation machinery: new chemistries, new tools, and new insights. *Febs j* **284**, 1555-1576, doi:10.1111/febs.14039 (2017).
206 Lam, Y. A., Xu, W., DeMartino, G. N. & Cohen, R. E. Editing of ubiquitin conjugates by an isopeptidase in the 26S proteasome. *Nature* **385**, 737-740, doi:10.1038/385737a0 (1997).
207 Abdul Rehman, S. A. *et al.* MINDY-1 Is a Member of an Evolutionarily Conserved and Structurally Distinct New Family of Deubiquitinating Enzymes. *Mol Cell* **63**, 146-155, doi:10.1016/j.molcel.2016.05.009 (2016).
208 Bekes, M. *et al.* SARS hCoV papain-like protease is a unique Lys48 linkage-specific di-distributive deubiquitinating enzyme. *Biochem J* **468**, 215-226, doi:10.1042/BJ20141170 (2015).
209 Dharadhar, S., Clerici, M., van Dijk, W. J., Fish, A. & Sixma, T. K. A conserved two-step binding for the UAF1 regulator to the USP12 deubiquitinating enzyme. *J Struct Biol* **196**, 437-447, doi:10.1016/j.jsb.2016.09.011 (2016).
210 Love, K. R., Pandya, R. K., Spooner, E. & Ploegh, H. L. Ubiquitin C-terminal electrophiles are activity-based probes for identification and mechanistic study of ubiquitin conjugating machinery. *ACS Chem Biol* **4**, 275-287, doi:10.1021/cb9000348 (2009).
211 Pinto-Fernandez, A. *et al.* Comprehensive Landscape of Active Deubiquitinating Enzymes Profiled by Advanced Chemoproteomics. *Front Chem* **7**, 592, doi:10.3389/fchem.2019.00592 (2019).
212 Rut, W. *et al.* Engineered unnatural ubiquitin for optimal detection of deubiquitinating enzymes. *Chem Sci* **11**, 6058-6069, doi:10.1039/d0sc01347a (2020).
213 Flierman, D. *et al.* Non-hydrolyzable Diubiquitin Probes Reveal Linkage-Specific Reactivity of Deubiquitylating Enzymes Mediated by S2 Pockets. *Cell Chem Biol* **23**, 472-482, doi:10.1016/j.chembiol.2016.03.009 (2016).
214 McGouran, J. F., Gaertner, S. R., Altun, M., Kramer, H. B. & Kessler, B. M. Deubiquitinating enzyme specificity for ubiquitin chain topology profiled by di-ubiquitin activity probes. *Chem Biol* **20**, 1447-1455, doi:10.1016/j.chembiol.2013.10.012 (2013).
215 Mulder, M. P. C., El Oualid, F., ter Beek, J. & Ovaa, H. A Native Chemical Ligation Handle that Enables the Synthesis of Advanced Activity-Based Probes: Diubiquitin as a Case Study. *ChemBioChem* **15**, 946-949, doi:10.1002/cbic.201402012 (2014).
216 Weber, A. *et al.* A Linear Diubiquitin-Based Probe for Efficient and Selective Detection of the Deubiquitinating Enzyme OTULIN. *Cell Chem Biol* **24**, 1299-1313.e1297, doi:10.1016/j.chembiol.2017.08.006 (2017).
217 Li, G., Liang, Q., Gong, P., Tencer, A. H. & Zhuang, Z. Activity-based diubiquitin probes for elucidating the linkage specificity of deubiquitinating enzymes. *Chem Commun (Camb)* **50**, 216-218, doi:10.1039/c3cc47382a (2014).
218 Mevissen, T. E. T. *et al.* Molecular basis of Lys11-polyubiquitin specificity in the deubiquitinase Cezanne. *Nature* **538**, 402-405, doi:10.1038/nature19836 (2016).
219 Haj-Yahya, N. *et al.* Dehydroalanine-based diubiquitin activity probes. *Org Lett* **16**, 540-543, doi:10.1021/ol403416w (2014).
220 Basar, M. A., Beck, D. B. & Werner, A. Deubiquitylases in developmental ubiquitin signaling and congenital diseases. *Cell Death Differ* **28**, 538-556, doi:10.1038/s41418-020-00697-5 (2021).
221 Sacco, J. J., Coulson, J. M., Clague, M. J. & Urbe, S. Emerging roles of deubiquitinases in cancer-associated pathways. *IUBMB Life* **62**, 140-157, doi:10.1002/iub.300 (2010).
222 Emsley, P., Lohkamp, B., Scott, W. G. & Cowtan, K. Features and development of Coot. *Acta Crystallogr D Biol Crystallogr* **66**, 486-501, doi:10.1107/S0907444910007493 (2010).
223 Skubak, P. *et al.* A new MR-SAD algorithm for the automatic building of protein models from low-resolution X-ray data and a poor starting model. *IUCrJ* **5**, 166-171, doi:10.1107/S2052252517017961 (2018).

224 Beilsten-Edmands, J. *et al.* Scaling diffraction data in the DIALS software package: algorithms and new approaches for multi-crystal scaling. *Acta Crystallogr D Struct Biol* **76**, 385-399, doi:10.1107/S2059798320003198 (2020).

225 Schneider, C. A., Rasband, W. S. & Eliceiri, K. W. NIH Image to ImageJ: 25 years of image analysis. *Nat Methods* **9**, 671-675, doi:10.1038/nmeth.2089 (2012).

226 McCoy, A. J. *et al.* Phaser crystallographic software. *J Appl Crystallogr* **40**, 658-674, doi:10.1107/S0021889807021206 (2007).

227 Liebschner, D. *et al.* Macromolecular structure determination using X-rays, neutrons and electrons: recent developments in Phenix. *Acta Crystallogr D Struct Biol* **75**, 861-877, doi:10.1107/S2059798319011471 (2019).

228 Krissinel, E. & Henrick, K. Inference of macromolecular assemblies from crystalline state. *J Mol Biol* **372**, 774-797, doi:10.1016/j.jmb.2007.05.022 (2007).

229 Waterhouse, A. *et al.* SWISS-MODEL: homology modelling of protein structures and complexes. *Nucleic Acids Res* **46**, W296-W303, doi:10.1093/nar/gky427 (2018).

230 Gasteiger, E. *et al.* in *John M. Walker (ed): The proteomics protocols handbook* 571-608 (Humana Press Totowa, NJ, USA:, 2005).

231 Pickart, C. M. & Raasi, S. Controlled synthesis of polyubiquitin chains. *Methods Enzymol* **399**, 21-36, doi:10.1016/S0076-6879(05)99002-2 (2005).

232 Gersch, M. *et al.* Distinct USP25 and USP28 Oligomerization States Regulate Deubiquitinating Activity. *Mol Cell* **74**, 436-451 e437, doi:10.1016/j.molcel.2019.02.030 (2019).

233 Evans, P. R. & Murshudov, G. N. How good are my data and what is the resolution? *Acta Crystallogr D Biol Crystallogr* **69**, 1204-1214, doi:10.1107/S0907444913000061 (2013).

234 Emsley, P., Lohkamp, B., Scott, W. G. & Cowtan, K. Features and development of Coot. *Acta Crystallogr D Struct Biol* **66**, 486-501, doi:10.1107/S0907444910007493 (2010).

235 Adams, P. D. *et al.* The Phenix software for automated determination of macromolecular structures. *Methods* **55**, 94-106, doi:10.1016/j.ymeth.2011.07.005 (2011).

236 Schulz, S. *et al.* Ubiquitin-specific protease-like 1 (USPL1) is a SUMO isopeptidase with essential, non-catalytic functions. *EMBO Rep* **13**, 930-938, doi:10.1038/embor.2012.125 (2012).

237 Pugh, D. J. *et al.* DWNN, a novel ubiquitin-like domain, implicates RBBP6 in mRNA processing and ubiquitin-like pathways. *BMC Struct Biol* **6**, 1, doi:10.1186/1472-6807-6-1 (2006).

238 Li, S. J. & Hochstrasser, M. A new protease required for cell-cycle progression in yeast. *Nature* **398**, 246-251, doi:10.1038/18457 (1999).

239 Virdee, S., Ye, Y., Nguyen, D. P., Komander, D. & Chin, J. W. Engineered diubiquitin synthesis reveals Lys29-isopeptide specificity of an OTU deubiquitinase. *Nat Chem Biol* **6**, 750-757, doi:10.1038/nchembio.426 (2010).

240 McGouran, J. F. *et al.* Fluorescence-based active site probes for profiling deubiquitinating enzymes. *Org Biomol Chem* **10**, 3379-3383, doi:10.1039/c2ob25258a (2012).

241 Paudel, P. *et al.* Crystal structure and activity-based labeling reveal the mechanisms for linkage-specific substrate recognition by deubiquitinase USP9X. *Proc Natl Acad Sci U S A* **116**, 7288-7297, doi:10.1073/pnas.1815027116 (2019).

242 Komander, D. *et al.* Molecular discrimination of structurally equivalent Lys 63-linked and linear polyubiquitin chains. *EMBO Rep* **10**, 466-473, doi:10.1038/embor.2009.55 (2009).

243 Maurer, S. K. *et al.* Ubiquitin-specific protease 11 structure in complex with an engineered substrate mimetic reveals a molecular feature for deubiquitination selectivity. *J Biol Chem* **299**, 105300, doi:10.1016/j.jbc.2023.105300 (2023).

244 Morrow, M. E. *et al.* Active site alanine mutations convert deubiquitinases into high-affinity ubiquitin-binding proteins. *EMBO Rep* **19**, doi:10.15252/embr.201745680 (2018).

245 Rennie, M. L., Arkinson, C., Chaugule, V. K., Toth, R. & Walden, H. Structural basis of FANCD2 deubiquitination by USP1-UAF1. *Nat Struct Mol Biol* **28**, 356-364, doi:10.1038/s41594-021-00576-8 (2021).

246 Zheng, Y. C. *et al.* Diagnostic yield and novel candidate genes by next generation sequencing in 166 children with intrahepatic cholestasis. *Hepatology International*, doi:10.1007/s12072-023-10553-6 (2023).

247 Pozhidaeva, A. & Bezsonova, I. USP7: Structure, substrate specificity, and inhibition. *DNA Repair (Amst)* **76**, 30-39, doi:10.1016/j.dnarep.2019.02.005 (2019).

248 Li, M., Brooks, C. L., Kon, N. & Gu, W. A dynamic role of HAUSP in the p53-Mdm2 pathway. *Mol Cell* **13**, 879-886, doi:10.1016/s1097-2765(04)00157-1 (2004).

249 Wertz, I. E. & Wang, X. From Discovery to Bedside: Targeting the Ubiquitin System. *Cell Chem Biol* **26**, 156-177, doi:10.1016/j.chembiol.2018.10.022 (2019).

250 Ge, F. *et al.* Deubiquitinating enzymes: Promising targets for drug resistance. *Drug Discov Today* **27**, 2603-2613, doi:10.1016/j.drudis.2022.06.009 (2022).

251 Rowinsky, E. K. *et al.* Phase 1 study of the protein deubiquitinase inhibitor VLX1570 in patients with relapsed and/or refractory multiple myeloma. *Invest New Drugs* **38**, 1448-1453, doi:10.1007/s10637-020-00915-4 (2020).

252 Damgaard, R. B. *et al.* OTULIN deficiency in ORAS causes cell type-specific LUBAC degradation, dysregulated TNF signalling and cell death. *EMBO Mol Med* **11**, doi:10.15252/emmm.201809324 (2019).

253 Damgaard, R. B. *et al.* The Deubiquitinase OTULIN Is an Essential Negative Regulator of Inflammation and Autoimmunity. *Cell* **166**, 1215-1230 e1220, doi:10.1016/j.cell.2016.07.019 (2016).

254 Hanpude, P., Bhattacharya, S., Dey, A. K. & Maiti, T. K. Deubiquitinating enzymes in cellular signaling and disease regulation. *IUBMB Life* **67**, 544-555, doi:10.1002/iub.1402 (2015).

255 Gan, J. *et al.* USP16 is an ISG15 cross-reactive deubiquitinase that targets pro-ISG15 and ISGylated proteins involved in metabolism. *Proc Natl Acad Sci U S A* **120**, e2315163120, doi:10.1073/pnas.2315163120 (2023).

256 Bairoch, A. *et al.* The universal protein resource (UniProt). *Nucleic Acids Research* **33**, D154-D159, doi:10.1093/nar/gki070 (2005).

257 Wendrich, K. *et al.* Discovery and mechanism of K63-linkage-directed deubiquitinase activity in USP53. *Nat Chem Biol*, doi:10.1038/s41589-024-01777-0 (2024).

258 Lee, B. H. *et al.* USP14 deubiquitinates proteasome-bound substrates that are ubiquitinated at multiple sites. *Nature* **532**, 398-401, doi:10.1038/nature17433 (2016).

259 Jonsson, E., Htet, Z. M., Bard, J. A. M., Dong, K. C. & Martin, A. Ubiquitin modulates 26S proteasome conformational dynamics and promotes substrate degradation. *Sci Adv* **8**, eadd9520, doi:10.1126/sciadv.add9520 (2022).

260 Hermanns, T. *et al.* A family of unconventional deubiquitinases with modular chain specificity determinants. *Nat Commun* **9**, 799, doi:10.1038/s41467-018-03148-5 (2018).

261 Walker, J. R. *et al.* Covalent Ubiquitin-USP2 Complex. doi:10.2210/pdb2ibi/pdb (2006).

262 Köhler, A., Zimmerman, E., Schneider, M., Hurt, E. & Zheng, N. Structural basis for assembly and activation of the heterotetrameric SAGA histone H2B deubiquitinase module. *Cell* **141**, 606-617, doi:10.1016/j.cell.2010.04.026 (2010).

263 Samara, N. L. *et al.* Structural insights into the assembly and function of the SAGA deubiquitinating module. *Science* **328**, 1025-1029, doi:10.1126/science.1190049 (2010).

264 Wang, T. *et al.* Evidence for bidentate substrate binding as the basis for the K48 linkage specificity of otubain 1. *J Mol Biol* **386**, 1011-1023, doi:10.1016/j.jmb.2008.12.085 (2009).

265 Grethe, C. *et al.* Structural basis for specific inhibition of the deubiquitinase UCHL1. *Nat Commun* **13**, 5950, doi:10.1038/s41467-022-33559-4 (2022).

266 Tsuchiya, H. *et al.* Ub-ProT reveals global length and composition of protein ubiquitylation in cells. *Nat Commun* **9**, 524, doi:10.1038/s41467-018-02869-x (2018).

267 Jumper, J. *et al.* Highly accurate protein structure prediction with AlphaFold. *Nature* **596**, 583-589, doi:10.1038/s41586-021-03819-2 (2021).

268 Varadi, M. *et al.* AlphaFold Protein Structure Database: massively expanding the structural coverage of protein-sequence space with high-accuracy models. *Nucleic Acids Res* **50**, D439-D444, doi:10.1093/nar/gkab1061 (2022).

269 Avvakumov, G. V. *et al.* Two ZnF-UBP domains in isopeptidase T (USP5). *Biochemistry* **51**, 1188-1198, doi:10.1021/bi200854q (2012).

270 Faesen, A. C. *et al.* Mechanism of USP7/HAUSP activation by its C-terminal ubiquitin-like domain and allosteric regulation by GMP-synthetase. *Mol Cell* **44**, 147-159, doi:10.1016/j.molcel.2011.06.034 (2011).

271 Masuda, S. *et al.* LSR defines cell corners for tricellular tight junction formation in epithelial cells. *J Cell Sci* **124**, 548-555, doi:10.1242/jcs.072058 (2011).

272 Riazuddin, S. *et al.* Tricellulin is a tight-junction protein necessary for hearing. *Am J Hum Genet* **79**, 1040-1051, doi:10.1086/510022 (2006).

273 Ikenouchi, J. *et al.* Tricellulin constitutes a novel barrier at tricellular contacts of epithelial cells. *J Cell Biol* **171**, 939-945, doi:10.1083/jcb.200510043 (2005).

274 Cheema, H. *et al.* Genomic testing in 1019 individuals from 349 Pakistani families results in high diagnostic yield and clinical utility. *NPJ Genom Med* **5**, 44, doi:10.1038/s41525-020-00150-z (2020).

275 Ates, B. B. *et al.* A novel homozygous mutation in the USP53 gene as the cause of benign recurrent intrahepatic cholestasis in children: a case report. *Turkish J Pediatr* **65**, 1012-1017, doi:10.24953/turkjped.2023.367 (2023).

276 Cheema, H. A. *et al.* The mutational landscape of genetic cholestatic diseases in Pakistani children. *J Pak Med Assoc* **73**, 1610-1621, doi:10.47391/Jpma.7069 (2023).

277 Porta, G. *et al.* Progressive Familial Intrahepatic Cholestasis Associated With USP53 Gene Mutation in a Brazilian Child. *J Pediatr Gastroenterol Nutr* **72**, 674-676, doi:10.1097/MPG.0000000000003110 (2021).

278 Gezdirici, A., Sengul, Ö. K., Dogan, M., Özgüven, B. Y. & Akbulut, E. Biallelic Novel Splicing Variant Disrupting the Gene Function that Causes Cholestasis Phenotype and Review of the Literature. *Mol Syndromol* **13**, 471-484, doi:10.1159/000523937 (2023).

279 Vij, M. & Sankaranarayanan, S. Biallelic Mutations in Ubiquitin-Specific Peptidase 53 (USP53) Causing Progressive Intrahepatic Cholestasis. Report of a Case With Review of Literature. *Pediatr Devel Pathol* **25**, 207-212, doi:10.1177/10935266211051175 (2022).

280 Ahn, S., Choi, J. & Jeong, S. H. The First Korean Adult Case of Progressive Familial Intrahepatic Cholestasis Type 7 with Novel Splicing Variants by Next Generation Sequencing. *Yonsei Med J* **64**, 745-749, doi:10.3349/ymj.2023.0161 (2023).

7 Appendix

7.1 Supplementary figures

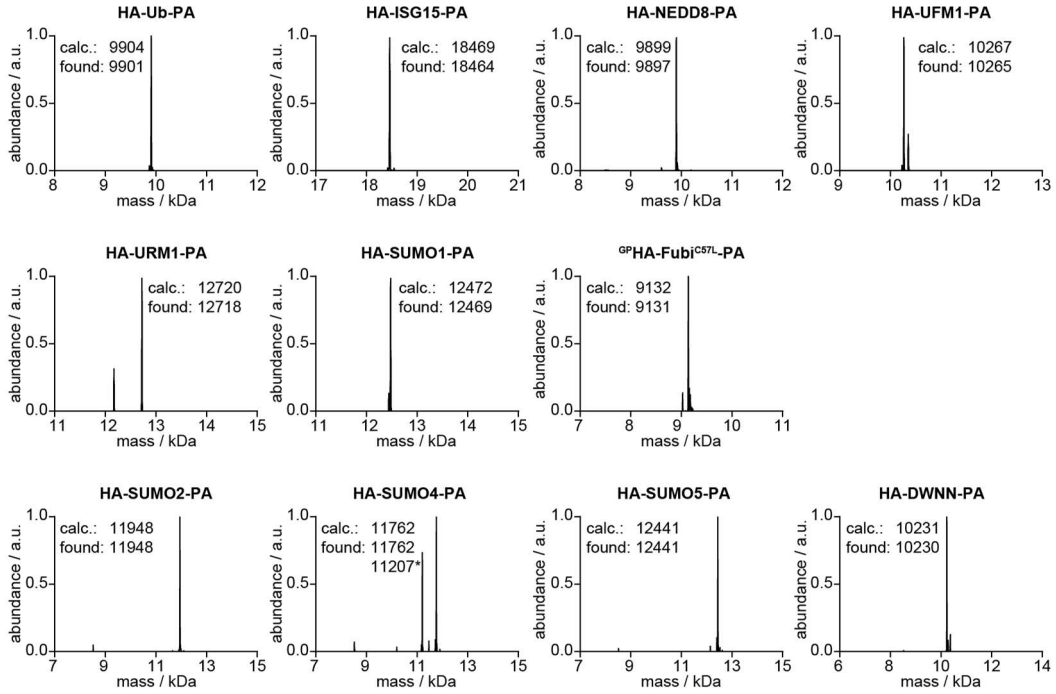

Figure S1: Deconvoluted mass spectra of HA-Ub-PA and HA-Ubl-PA probes. The measured mass of 11207 Dalton (Da) for HA-SUMO4-PA, marked with an asterisk, corresponds to a functional construct, shortened by four amino acids at the N-terminus. Masses are given in Dalton.

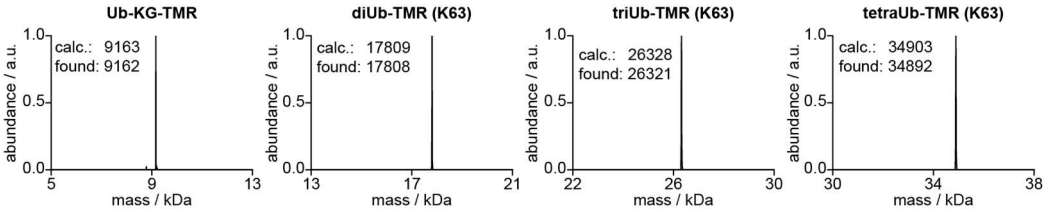

Figure S2: Deconvoluted mass spectra of substrates used in fluorescence polarization and gel-based cleavage assays. Masses are given in Dalton.

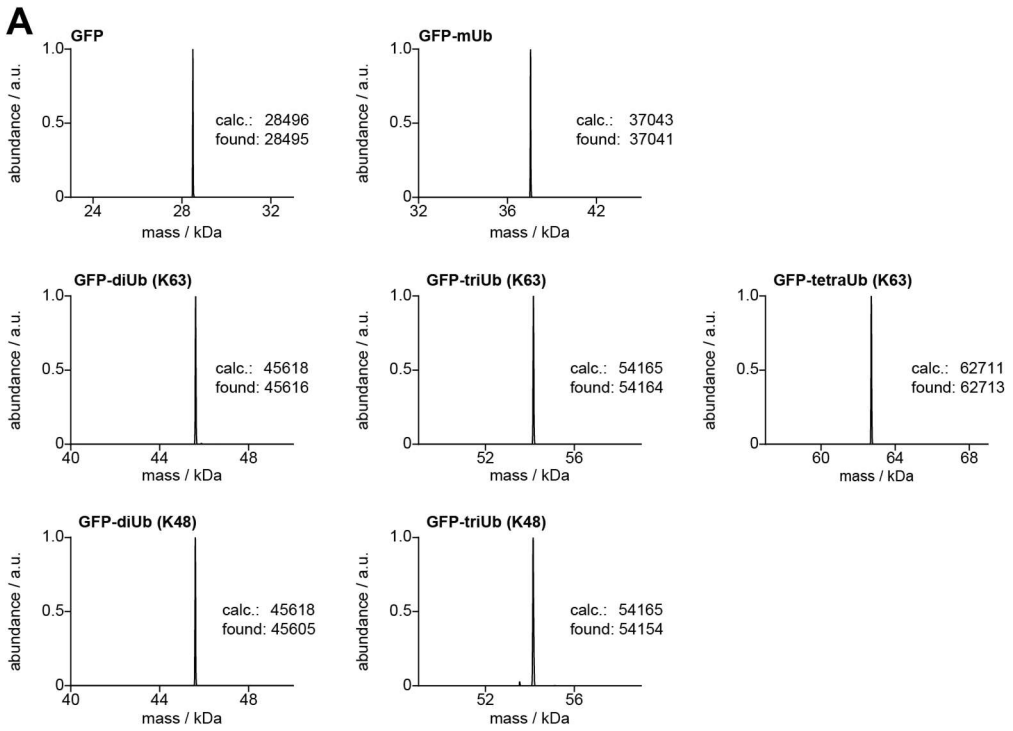

Figure S3: Deconvoluted mass spectra of GFP and ubiquitinated GFP-species. Masses are given in Dalton.

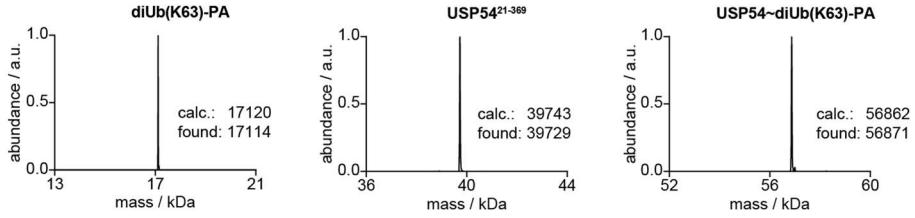

Figure S4: Deconvoluted mass spectra of the diUb(K63)-PA probe, purified unlabeled USP54$^{21-369}$ and the resulting complex USP54~diUb(K63)-PA after labeling used for crystallization. Masses are given in Dalton.

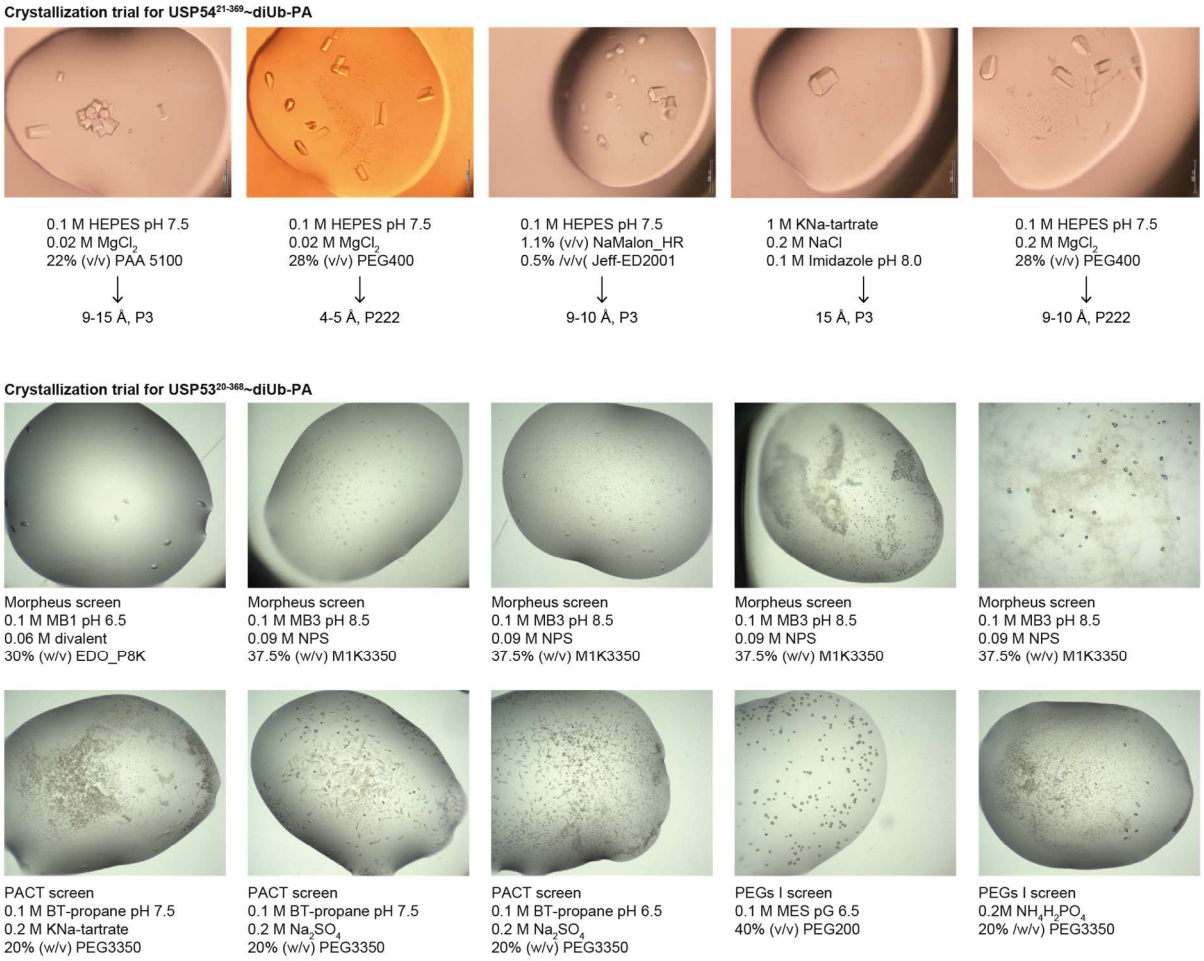

Figure S5: Images of crystals of USP54$^{21-369}$~diUb-PA and USP53$^{20-368}$~diUb-PA. The respective crystallization conditions and diffraction resolutions are commented.

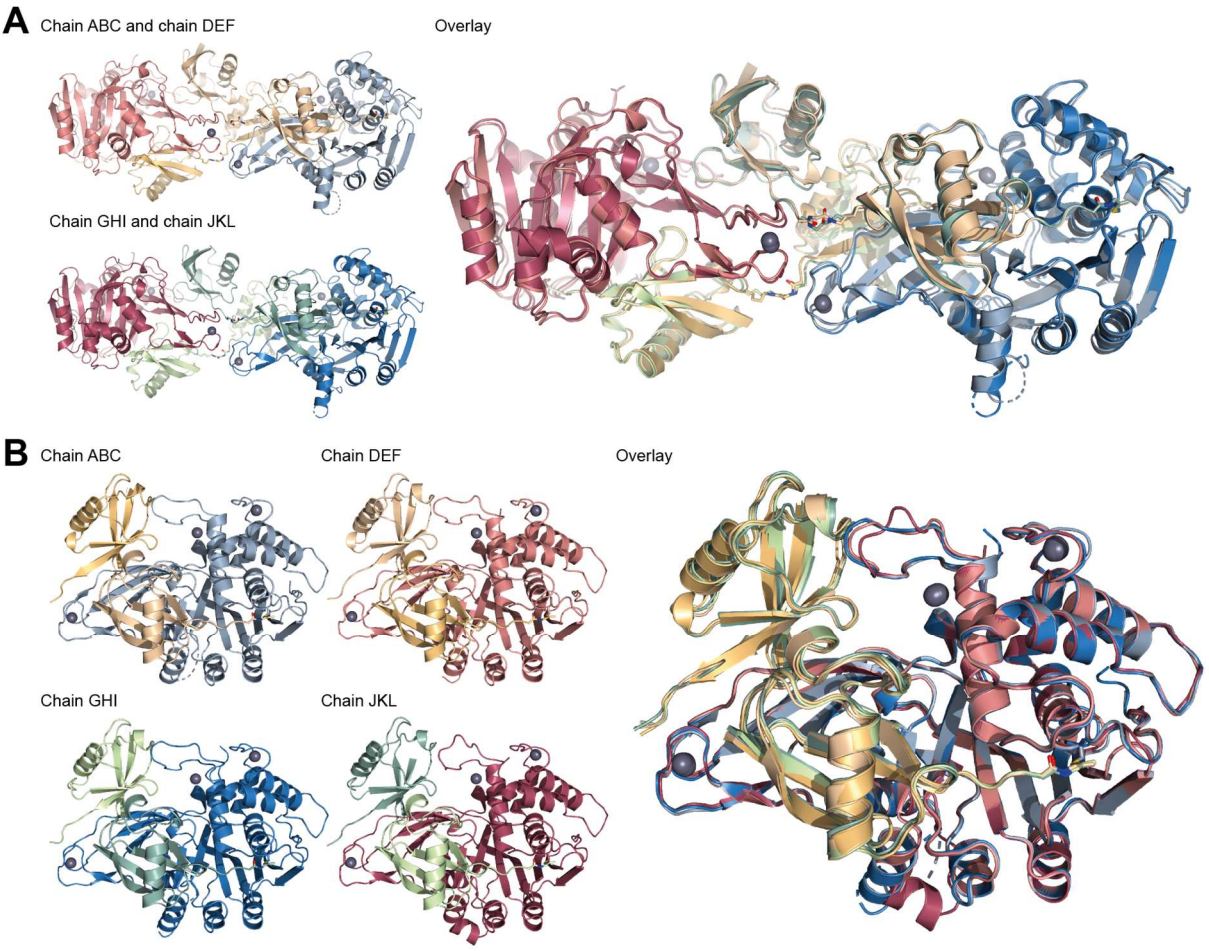

Figure S6: Crystal structure of USP54~diUb-PA in different conformations. A) The conformation of 2x USP54~diUb-PA, as observed in the crystal structure and formed by chains A-F and chains G-L, is shown as two cartoons and a superposition B) The hypothetical conformation of USP54~diUb-PA molecules in solution, formed by chains ABC, DEF, GHI, JKL in the crystal structure, are shown as cartoons and superimposed.

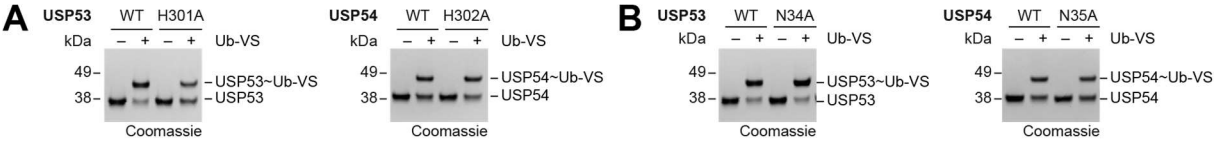

Figure S7: Probe labeling assays using Ub-VS. A-B) Ub-VS was incubated with USP53$^{20-383}$ WT, H301A and N34A as well as with USP54$^{21-369}$ WT, H302A and N35A. Reactivity was assessed by SDS-PAGE and Coomassie-staining.

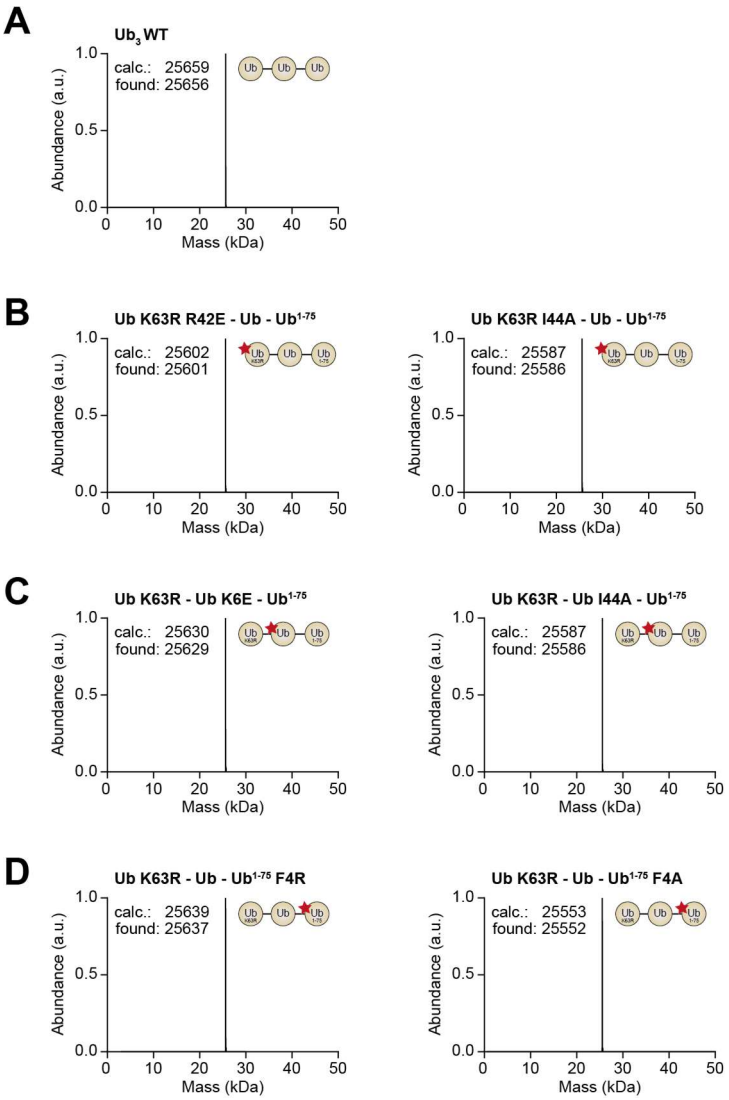

Figure S8: Deconvoluted mass spectra of K63-linked triUb species. A) Deconvoluted mass spectra of wild-type K63-linked triUb. B-D) Deconvoluted mass spectra of K63-linked triUb chains containing a K63R mutation in the distal ubiquitin moiety and in which the proximal ubiquitin is truncated by removal of a glycine residue at the C-terminus. Additional specific mutations were incorporated into the distal ubiquitin (B), middle ubiquitin (C) and proximal ubiquitin (D).

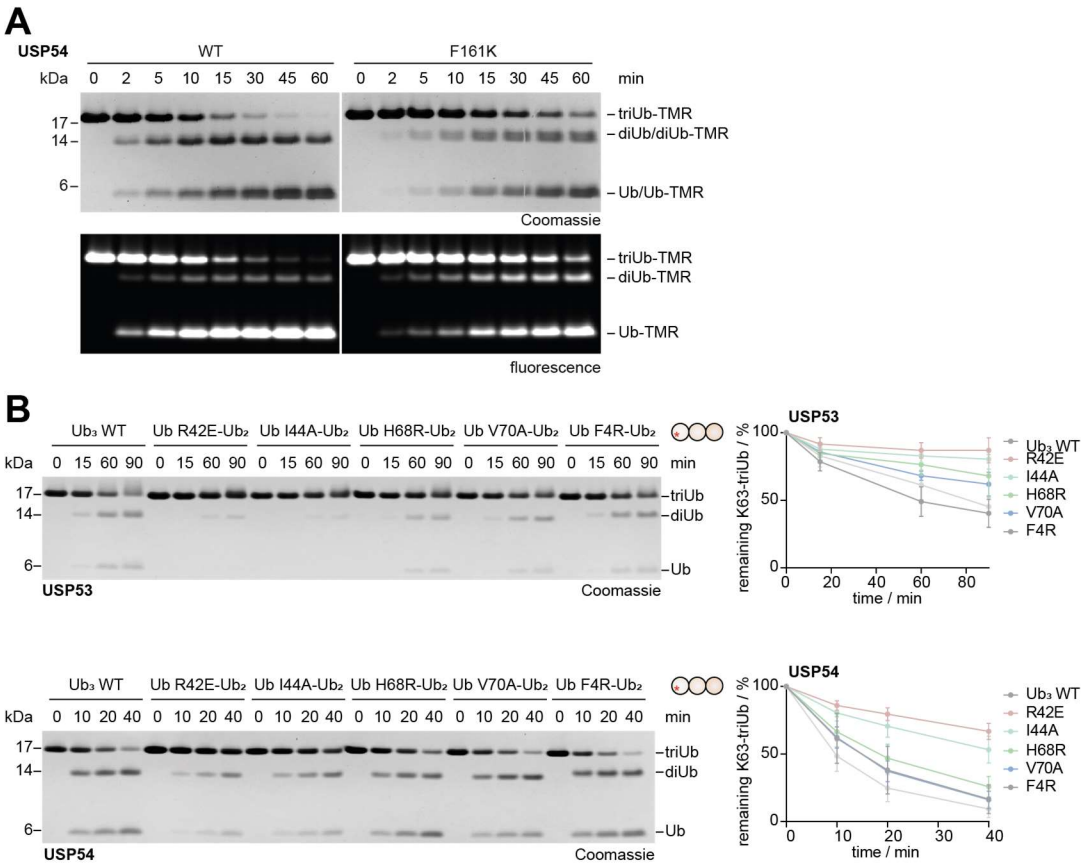

Figure S9: Gel-based cleavage assays. A) USP54$^{21-369}$ WT and F161K were incubated with K63-linked triUb-TAMRA for indicated time points. Samples were analyzed by SDS-PAGE and visualized by fluorescence scanning and Coomassie-staining. B) K63-linked triUb chains containing specific mutations in the distal ubiquitin moiety were incubated with USP53$^{20-383}$ or USP54$^{20-369}$ for indicated time points. Cleavage was analyzed by SDS-PAGE and Coomassie-staining. Cleavage activity was quantified by densitometry of the triUb bands and visualized by plotting the remaining percentage of initial triUb substrate against the incubation time.

7.2 Supplementary tables

Table S1. Patient mutations in USP53 associated with familial intrahepatic cholestasis

Mutation (Genetic)	Mutation (Protein)	Reference	Comment
Missense			
c.91G > A	p.Gly31Ser	Zheng *et al.*, 2023 [246]	Near active site
c.145G>T	p.Val49Phe	Samanta *et al.*, 2024 [142]	Near active site
c.297G>T	p.Arg99Ser	Zhang *et al.*, 2020 [136]	Near active site
c.395A>G	p.His132Arg	Zhang *et al.*, 2020 [136]	Zn^{2+} coordinating
c.394C > T	p.His132Tyr	Zheng *et al.*, 2023 [246]	Zn^{2+} coordinating
c.682T>C	p.Cys228Arg	Samanta *et al.*, 2024 [142]	Zn^{2+} coordinating
c.725C>T	p.Pro242Leu	Bull *et al.*, 2021 [137]	Within domain
c.878G>T	p.Gly293Val	Zhang *et al.*, 2020 [136]	Within domain
c.908G>A	p.Cys303Tyr	Samanta *et al.*, 2024 [142]	Near active site
c.2869C>T	p.His957Tyr	Samanta *et al.*, 2024 [142]	Outside cat. domain
Nonsense			
c.169C>T	p.Arg57*	Zhang *et al.*, 2020 [136]	
c.169C>T	p.Arg57*	Cheema *et al.*, 2020 [274]	
c.1012C>T	p.Arg338*	Zhang *et al.*, 2020 [136]	
c.1426C>T	p.Arg476*	Zhang *et al.*, 2020 [136]	
c.1558C>T	p.Arg520*	Zhang *et al.*, 2020 [136]	
		Ates *et al.*, 2023 [275]	
c.1744C>T9	p.Arg582*	Alhebbi *et al.*, 2021 [134]	
c.145-11_167del	p: ?	Bull *et al.*, 2021 [137]	Intron/Exon boundary
Deletion of exon 1	p: ?	Bull *et al.*, 2021 [137]	+*MYOZ2* deletion
Deletion of exon 14/15	p:?	Cheema *et al.*, 2023 [276]	
Frameshift			
c.475_476delCT	p.Leu159fs	Cheema *et al.*, 2020 [274]	
c.510delA	p.Ser171Argfs*62	Bull *et al.*, 2021 [137]	
c.581delA	p.Arg195Glufs*38	Zhang *et al.*, 2020 [136]	
c.774_774delG	p.Thr259Profs*8	Cheema *et al.*, 2023 [276]	
c.831_832insAG	p:Val279Glufs*16	Zhang *et al.*, 2020 [136]	
c.951delT	p.Phe317Leufs*6	Maddirevula *et al.*, 2019 [135]	
		Cheema *et al.*, 2020 [274]	
		Alhebbi *et al.*, 2021 [134]	
c.1017_1057del	p.Cys339Trpfs*7	Shatokina *et al.*, 2021 [138]	
c.1214dupA	p.Asn405fs	Cheema *et al.*, 2020 [274]	
c.1687_1688delinsC	p.Ser563Profs*25	Porta *et al.*, 2021 [277]	

Mutation (Genetic)	Mutation (Protein)	Reference	Comment
Splice site			
c.238-1G>C	p:?	Gezdirici *et al.*, 2023 [278]	
c.569+2T>C	P:?	Zhang *et al.*, 2020 [136]	
c.822+1delG	p:?	Cheema *et al.*, 2020 [274]	
		Vij *et al.*, 2022 [279]	
c.972+3_972+6del	p:?	Ahn *et al.*, 2023 [280]	

Table S2: Sequence differences of USP53 and USP54 in strongly conserved regions of the catalytic domains or unique insertions in comparison to other USP DUB family members. The location, the conserved residues and examples for exceptions in other USPs are listed.

Location	USP53/USP54	USPs	Exceptions
Box 1 - insertion	PG 36-37/37-38	-	-
Box 1, 3 aa before cat. cysteine	Q 38/39	G	CYLD: Y
Box 2	ES 104-105 / KT 105-106	-	-
Box 2	M 117/118	Q	USP30:E
Box 4, second CXX motif	CXXXC	CXXC	USP5,7,10,13,14,15,15,28: del
Box 4	W 251/252	R	CYLD: del
Box 5, behind Ub tail cleft	L 289/290	Y	USP30: F, CYLD: M
Box 5, 9 aa before cat. histidine	Y 297/298	H	CYLD: I
Box 5, 1 aa before cat. histidine	Q 300 / K 301	G	CYLD: S

Eidesstattliche Versicherung (Affidavit)

Wendrich, Kim Solveig
Name, Vorname
(Surname, first name)

216583
Matrikel-Nr.
(Enrolment number)

Belehrung:

Wer vorsätzlich gegen eine die Täuschung über Prüfungsleistungen betreffende Regelung einer Hochschulprüfungsordnung verstößt, handelt ordnungswidrig. Die Ordnungswidrigkeit kann mit einer Geldbuße von bis zu 50.000,00 € geahndet werden. Zuständige Verwaltungsbehörde für die Verfolgung und Ahndung von Ordnungswidrigkeiten ist der Kanzler/die Kanzlerin der Technischen Universität Dortmund. Im Falle eines mehrfachen oder sonstigen schwerwiegenden Täuschungsversuches kann der Prüfling zudem exmatrikuliert werden, § 63 Abs. 5 Hochschulgesetz NRW.

Die Abgabe einer falschen Versicherung an Eides statt ist strafbar.

Wer vorsätzlich eine falsche Versicherung an Eides statt abgibt, kann mit einer Freiheitsstrafe bis zu drei Jahren oder mit Geldstrafe bestraft werden, § 156 StGB. Die fahrlässige Abgabe einer falschen Versicherung an Eides statt kann mit einer Freiheitsstrafe bis zu einem Jahr oder Geldstrafe bestraft werden, § 161 StGB.

Die oben stehende Belehrung habe ich zur Kenntnis genommen:

Official notification:

Any person who intentionally breaches any regulation of university examination regulations relating to deception in examination performance is acting improperly. This offence can be punished with a fine of up to EUR 50,000.00. The competent administrative authority for the pursuit and prosecution of offences of this type is the chancellor of the TU Dortmund University. In the case of multiple or other serious attempts at deception, the candidate can also be unenrolled, Section 63, paragraph 5 of the Universities Act of North Rhine-Westphalia.

The submission of a false affidavit is punishable.

Any person who intentionally submits a false affidavit can be punished with a prison sentence of up to three years or a fine, Section 156 of the Criminal Code. The negligent submission of a false affidavit can be punished with a prison sentence of up to one year or a fine, Section 161 of the Criminal Code.

I have taken note of the above official notification.

Ort, Datum
(Place, date)

Unterschrift
(Signature)

Titel der Dissertation:
(Title of the thesis):

Discovery of USP53 and USP54 deubiquitinase activities

Ich versichere hiermit an Eides statt, dass ich die vorliegende Dissertation mit dem Titel selbstständig und ohne unzulässige fremde Hilfe angefertigt habe. Ich habe keine anderen als die angegebenen Quellen und Hilfs- mittel benutzt sowie wörtliche und sinngemäße Zitate kenntlich gemacht.
Die Arbeit hat in gegenwärtiger oder in einer anderen Fassung weder der TU Dortmund noch einer anderen Hochschule im Zusammenhang mit einer staatlichen oder akademischen Prüfung vorgelegen.

I hereby swear that I have completed the present dissertation independently and without inadmissible external support. I have not used any sources or tools other than those indicated and have identified literal and analogous quotations.

The thesis in its current version or another version has not been presented to the TU Dortmund University or another university in connection with a state or academic examination.*

*Please be aware that solely the German version of the affidavit ("Eidesstattliche Versicherung") for the PhD thesis is the official and legally binding version.

Ort, Datum
(Place, date)

Unterschrift
(Signature)